



Doctoral Thesis - SK186601

**MIXED MATRIX HOLLOW FIBER MEMBRANE
POLYSULFONE-ZEOLITE TEMPLATED CARBON :
FABRICATION, CHARACTERIZATION AND GAS
SEPARATION STUDY**

Rika Wijiyanti
01211660010002

PROMOTORS
Nurul Widiastuti, S.Si., M.Si., Ph.D.
Dr. Zulhairun Abd. Karim

DOCTORAL PROGRAM
CHEMISTRY
DEPARTMENT OF CHEMISTRY
FACULTY OF SCIENCE
INSTITUT TEKNOLOGI SEPULUH NOPEMBER
SURABAYA
2019

APPROVAL SHEET OF DOCTORAL THESIS

This thesis is presented for achieving the Degree of
Doctor (Dr) of

Institut Teknologi Sepuluh Nopember

By :

Rika Wijiyanti

NRP : 01211660010002

Date of Examination : 28 August 2019

Graduation Period : September 2019

Approved by :

Promotors :

1. Nurul Widiastuti, S.Si., M.Si., Ph.D
NIP : 1971042519941202001

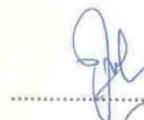


2. Dr. Zulhairun Abdul Karim
Staff Number : 13831



Examiners :

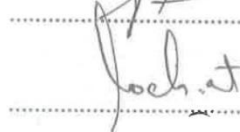
1. Ass. Prof. Dr. Juhana Jaafar
Staff Number : 10122



2. Dr. Ir. Sumarno, M.Eng.
NIP : 196406081991021001



3. Drs. Lukman Atmaja, M.Si., Ph.D
NIP : 196108161989031001



Head of Chemistry Department
Faculty of Science


Prof. Dr. Didik Prasetyoko, S.Si., M.Sc.
NIP : 197106161997031002

MIXED MATRIX HOLLOW FIBER MEMBRANE POLYSULFON-ZEOLITE TEMPLATED CARBON : FABRICATION, CHARACTERIZATION AND GAS SEPARATION STUDY

Name : Rika Wijiyanti
NRP : 01211660010002
Promotor : Nurul Widiastuti, S.Si., M.Si., Ph.D
Co-Promotor : Dr. Zulhairun Abd. Karim

ABSTRACT

This study introduces a structurally engineered carbon, named as zeolite templated carbon (ZTC), as a new filler membrane for superior gas separation performance. It is produced by carbon filling inside zeolite-Y template to combine the advantage of each materials and eliminate both weakness. The open and no rigid pore structure of ZTC would facilitate its compatibility with polymer matrix. In addition, the ZTC could reach a higher specific surface area with almost micropore content compared to zeolite and carbon alone. It was noticed that large surface area could improve the gas permeance, while the ordered pore structure increased the membrane selectivity. As a result, this filler could improve the overall separation performance of the mixed matrix membrane (MMM). This thesis aims to investigate the feasibility of separating gas using ZTC filler in order to find high performance material.

Zeolite-Y as a ZTC template, was prepared by hydrothermal method. In this study, two different ZTCs with distinct pore properties were used. The ZTC was synthesized by impregnation method with sucrose as carbon precursor, named as ZTC-1. Meanwhile, the ZTC prepared by combination of impregnation and chemical vapor deposition (CVD) is referred as ZTC-2. Polysulfone polymer was used as a matrix membrane. The MMM was fabricated into hollow fiber module via dry-wet spinning method. The obtained fiber was sealed with PDMS by dip-coating method. For other treatment, the fiber was subjected to the heating treatment above PSF's T_g. The membrane performance was tested using single gas (CO₂, O₂, H₂, N₂ and CH₄) and mixed-gas (CO₂/CH₄ and H₂/CH₄).

The result demonstrated that structural ordering of ZTC from two step routes is higher than the ZTC from the single carbon deposition. Also, in this case, the surface area of ZTC-2 is larger with higher micropore content. Having a very high surface area with almost no mesopores is more favourable in gas separation membrane, because mesopores results in a lower selectivity. Furthermore, the selectivity enhancement of MMM with acceptable permeance was obtained at lower ZTC-1 loading, while the increased in ZTC-1 loading lead to the poorer selectivity with much higher permeance due to the presence of severe unselective barrier between the ZTC-1 and matrix. Compared to PSF membrane, PSF/ZTC-1 0.4 wt% recorded the highest selectivity improvement for CO₂/CH₄ (290%), CO₂/N₂ (219%), O₂/N₂ (117%) and H₂/CH₄ (272%), but marginal decrement was

observed on the permeances (P_{CO_2} , P_{O_2} and P_{H_2}). When binary gas (CO_2/CH_4 and H_2/CH_4) was separated by the membranes, significant differences were observed in the separation performance due to competitive sorption and the effect of non-ideal gas behavior in the mixed-gas system. By performing PDMS coating, the MMM selectivity of CO_2/CH_4 , O_2/N_2 , CO_2/N_2 and H_2/CH_4 was improved up to 46.42 (780%), 6.06 (215%), 35.14 (481%) and 92.57 (491%), respectively, compared to that of uncoated MMM, while the decrease in permeance was minimal when 0.25 wt% ZTC-1 was loaded. When the fibers were heated, the selectivity of CO_2/CH_4 , O_2/N_2 and CO_2/N_2 at 0.25 wt% loading was found to be enhanced up to 652%, 246% and 458%, respectively, with very low permeances which lead to undesirable resistance to gas transport. Furthermore, a remarkable enhancement in permeance (about 112%) and selectivity were observed for coated MMM filled with ZTC-2. Compared to ZTC-1 filled MMM, PSF/ZTC-2 recorded higher CO_2/CH_4 , O_2/N_2 , CO_2/N_2 and H_2/CH_4 selectivity of 59.75, 7.32, 38.25 and 159.42, respectively, with CO_2 , O_2 and H_2 permeances of 81.86, 15.66 and 218.40 GPU, respectively. When the zeolite carbon composite (ZCC) or ZTC material prior template removal was loaded within PSF, the separation performance was lower compared to neat PSF. It can be concluded that permeance and selectivity enhancement could be achieved even at low loading (0.25 wt%) and the ZTC filler could be a promising candidate for a new mixed matrix membrane for CO_2 , O_2 and H_2 separation.

Key words : mixed-matrix membranes, zeolite templated carbon, zeolite carbon composite, polysulfone, hollow fiber, gas separation

PREFACE

We are grateful to Almighty Allah SWT for the gracious mercy and tremendous blessing that allows me to complete this dissertation entitled “Mixed Matrix Hollow Fiber Membrane Polysulfone - Zeolite Templated Carbon : Fabrication, Characterization and Gas Separation Study”.

I would like to thank the Directorate General of Higher Education, Ministry of Research, Technology and Higher Education of Republik Indonesia for the research funding during my study under PMDSU scholarship.

I would like to express my sincere gratitude to my supervisor, Nurul Widiastuti Ph.D for her valuable comments, discussions and assistance to the completion of my study. I also would like to express my deep gratitude to my co-promotor, Dr. Zulhairun Abdul Karim for the valuable discussion and suggestion for the improvement of my research. This dissertation could not be completed without their guidance, patience and encouragement.

I also would like to extend my thank to Prof. Mardi Santoso as head of Postgraduate Program in Chemistry Department and Prof. Didik Prasetyoko as head of Chemistry Department for their enduring guidance and support.

Moreover, I would like to say thanks to Dr. Djoko Hartanto, Prof. Fauzi Ismail and Assoc. Prof. Simon Smart for allowing me to conduct research on Material and Energy Laboratory of Chemistry ITS, Energy Laboratorium of ITS, Advanced Membrane Technology Laboratory (AMTEC) of Universiti Teknologi Malaysia, and The Films and Inorganic Membrane Laboratory (FIMLab) of University of Queensland, Australia, respectively.

This work would be finally dedicated to my beloved husband, Rendy Febrianto, in appreciation of his loving support, understanding and encouragement during my study. Great attitude also for my father Hermanu Setijanto, my mother Risminingsih and my sister esti Ristanti for their loving support from the beginning.

Last but not least, the author gratitudes all the support and assistance from my great team (Afifah and Zarah) during my study.

TABLE OF CONTENT

| | |
|---|-----|
| COVER | i |
| APPROVAL SHEET | ii |
| ABSTRACT | iii |
| PREFACE | v |
| TABLE OF CONTENT | vii |
| LIST OF FIGURES | x |
| LIST OF TABLES | xv |
| CHAPTER 1 INTRODUCTION | 1 |
| 1.1 Background | 1 |
| 1.2 Problems | 6 |
| 1.3 Research Objectives | 7 |
| 1.4 Originality | 8 |
| CHAPTER 2 LITERATURE REVIEW | 9 |
| 2.1 Gas Separation Technology | 9 |
| 2.1.1 Overview of Gas Separation Membrane | 9 |
| 2.1.2 Development of Membrane Technology | 9 |
| 2.2 Mixed Matrix Membranes (MMMs) | 14 |
| 2.3 Membrane Materials in MMMs | 17 |
| 2.3.1 Polymer Selection | 18 |
| 2.3.2 Inorganic Materials | 27 |
| 2.4 Post-treatment for Defect Free of MMMs | 39 |
| CHAPTER 3 RESEARCH METHODOLOGY | 49 |
| 3.1 Materials | 49 |
| 3.2 Preparation of Zeolite Templated Carbon (ZTC) | 50 |
| 3.3 Membrane Preparation | 51 |
| 3.4 Heat Treatment of Fibers | 52 |
| 3.5 Membrane Surface Coating | 53 |
| 3.6 Permeation Test | 53 |
| 3.7 Material Characterizations | 57 |

| | | |
|---|--|-----|
| 3.7.1 | X-Ray Diffraction (XRD) | 57 |
| 3.7.2 | Braunauer-Emmett-Teller (BET) | 58 |
| 3.7.3 | High Resolution Transmission Electron Microscopy (HR TEM)..... | 58 |
| 3.7.4 | Scanning Electron Microscopy (SEM) | 58 |
| 3.7.5 | Atomic Force Microscopy (AFM) | 59 |
| 3.7.6 | Fourier Transforms Infrared Spectroscopy (FTIR)..... | 59 |
| 3.7.7 | Thermogravimetric Analysis (TGA)..... | 59 |
| 3.7.8 | Differential Scanning Calorimetry (DSC) | 59 |
| 3.8 | Filler Interparticle Spacing and Size of Polymer Molecule | 59 |
| 3.9 | Summary the Sample Designation | 60 |
| CHAPTER 4 SYNTHESIS AND CHARACTERISTICS OF ZEOLITE TEMPLATED CARBON AS MEMBRANE FILLER | | |
| 63 | | |
| 4.1 | Characteristics of Zeolite Templated Carbons (ZTCs) | 63 |
| 4.2 | Summary | 77 |
| CHAPTER 5 MIXED MATRIX MEMBRANE CHARACTERISTICS AND ITS PERFORMANCE FOR GAS SEPARATION | | |
| 79 | | |
| 5.1 | Characteristics of MMM | 79 |
| 5.2 | Gas separation performance of MMM | 92 |
| 5.3 | Summary | 96 |
| CHAPTER 6 MEMBRANE MODIFICATION BY SURFACE COATING AND HEATING TREATMENT | | |
| 99 | | |
| 6.1 | The Improvement of MMM Performance by Coating Surface | 100 |
| 6.2 | The Improvement of MMM Performance by Heating Treatment | 109 |
| 6.3 | Summary | 117 |
| CHAPTER 7 GAS SEPARATION PROPERTIES OF POLYSULFONE BASED MMMs | | |
| 119 | | |
| 7.1 | Characteristics of Polysulfone (PSF) Based MMMs | 119 |
| 7.2 | Comparison of ZTC and ZCC as a Filler Toward The Improvement of MMM Performance | 128 |
| 7.3 | Summary | 132 |
| Table 7.5 Gas Separation Performance of Coated MMM Containing Different Filler Types | | 133 |

| | |
|---|-----|
| CHAPTER 8 CONCLUSIONS AND RECOMMENDATIONS | 135 |
| 8.1 Conclusions..... | 135 |
| 8.1.1 Synthesis and Characteristics of Zeolite Templated Carbon (ZTC) as Membrane Filler | 135 |
| 8.1.2 Mixed Matrix Membranes Embedded with ZTC-1 for Gas Separation | 136 |
| 8.1.3 Membrane Post-treatment using Heat Treatment and Surface Coating | 137 |
| 8.1.4 Gas Separation Properties of Polysulfone Based MMMs | 139 |
| 8.2 Recommendations..... | 140 |
| REFERENCES..... | 143 |

LIST OF FIGURES

| | |
|---|----|
| Figure 2.1 Milestones of membrane development in the industrial application (Sridhar <i>et al.</i> , 2014) | 10 |
| Figure 2.2 Upper bound curves correlation for polymer membranes (Robeson, 2008) | 14 |
| Figure 2.3 Schematic of mixed matrix membrane | 15 |
| Figure 2.4 Schematic diagram of the transport mechanism of MMMs with (a) conventional and (b) high aspect ratio permeable fillers (Adapted from Ansaloni & Deng (2016)) | 16 |
| Figure 2.5 SEM images of unmodified (left) and modified MCM-48/PSF membrane (Adapted from Jomekian, Mansoori, et al. (2011))..... | 17 |
| Figure 2.6 Robeson’s upper bound analysis of MMM derivatives from polysulfones, polyimides, PIMs, PTMSP and Pebax..... | 17 |
| Figure 2.7 The evaluation CO ₂ /CH ₄ , O ₂ /N ₂ , CO ₂ /N ₂ and H ₂ /CH ₄ separation performance for PSF membrane | 19 |
| Figure 2.8 Cross section of PSF membranes prepared by (a) dry and (b) wet inversion process. Adapted from Pinnau and Koros (1991)..... | 22 |
| Figure 2.9 Cross section of PSF membranes prepared by dry/wet process. Adapted from Pinnau and Koros (1991)..... | 23 |
| Figure 2.10 The cross section images of PSF membrane at different PSF concentration (a) 20 wt%, (b) 25 wt% and (c) 30 wt% (Ismail <i>et al.</i> , 2017) | 24 |
| Figure 2.11 The cross section images of PSF membrane at (a) 19%, (b) 21% and (c) 23% PSF concentration (Sidek and Nora, 2011)..... | 24 |
| Figure 2.12 The SEM images of PSF membrane made from a dope solution containing of (a) 30 wt% PSF, 70 wt% NMP and (b) 30 wt% PSF, 60 wt% NMP 10 wt% ethanol (Aroon <i>et al.</i> , 2010)..... | 26 |
| Figure 2.13 The cross sectional image of PSF membrane containing of 30 wt% PSF, 10 wt% EtOH, 45 wt% NMP and 15 wt% THF (Aroon <i>et al.</i> , 2010) | 27 |
| Figure 2.14 The performance of PSF membrane made by dry/wet phase inversion process (Julian and Wenten, 2012) | 27 |
| Figure 2.15 Illustration of Zeolite Templated Carbon (ZTC) Synthesis : (a) Structure of Zeolite-Y Template, (b) Structure of Zeolite/Carbon Composite. A Black Framework Represents Impregnated Carbon and (c) Framework Structure of the ZTC After Template Removal (Nishihara <i>et al.</i> , 2008) | 30 |
| Figure 2.16 HRTEM images of ZTC prepared through impregnation-CVD method (adapted from Ma <i>et al.</i> (2002)) | 32 |

| | |
|--|----|
| Figure 2.17 Pore size distribution of ZTC prepared using (a) impregnation (Guan <i>et al.</i> , 2009); (b) impregnation-CVD method (Nishihara <i>et al.</i> , 2009). | 32 |
| Figure 2.18 An Idealized Model for ZTC (a) Containing Carbon and Hydrogen Atoms and (b) Containing Some Functional Groups. Large Red Spheres Indicate O Atoms (Nishihara <i>et al.</i> , 2008)..... | 34 |
| Figure 2.19 The illustration of CO ₂ interaction with zeolite surface | 35 |
| Figure 2.20 The cross section images of PSF/SAPO-34 at 20 wt% (left) and 30 wt% (right) (Junaidi <i>et al.</i> , 2014) | 39 |
| Figure 2.21 The SEM images of (a) cross section and (b) surface of PI/PES/zeolite heated at 280 °C, 2h (Kusworo <i>et al.</i> , 2013) | 41 |
| Figure 2.22 The SEM images of Matrimid/PSF/zeolite β (a) before and (b) after heated at 200°C, 2h (Ferreira and Trierweiler, 2009) | 41 |
| Figure 2.23 The cross section SEM images of (a, b, c) : PES/zeolite 3A, 4A and 5A MMMs with immediate cooling, respectively; (d, e, f) : PES/zeolite 3A, 4A and 5A MMMs with natural cooling, respectively (Ferreira and Trierweiler, 2009)..... | 42 |
| Figure 2.24 The illustration of asymmetric composite membrane partially coated by silicon rubber polymer (Marchese <i>et al.</i> , 1995) | 43 |
| Figure 2.25 SEM images of surface (left) and cross section (right) of 20 wt% MCM-48/PSF MMM coated by 30 wt% PDMS solution (Jomekian, Mansoori, <i>et al.</i> , 2011) | 44 |
| Figure 2.26 The cross section images of (a) uncoated, (b) coated polyimide/zeolite MMMs and surface images of (c) uncoated, (d) coated polyimide/zeolite MMMs (Agustin and Sakti, 2010) | 45 |
| Figure 3.1 Schematic diagram of dry-wet spinning system to prepare the hollow fiber membranes for gas separation : (1) N ₂ gas cylinder, (2) dope reservoir, (3) gear pump, (4) spinneret, (5) bore fluid syringe pump, (6) bore fluid reservoir, (7) coagulation bath, (8) washing bath, (9) collection bath and (10) collection drum..... | 53 |
| Figure 3.2 Single gas permeation testing rig..... | 55 |
| Figure 3.3 Mixed-gas permeation testing rig | 55 |
| Figure 4.1 XRD spectra of (a) synthesized zeolite-Y, (b) ZCC-1 and (c) ZTC-1 (zeolite-Y standard is indicated by triangle symbol)..... | 65 |
| Figure 4.2 The possibility filling of sucrose molecules into the pore window of zeolite-Y | 65 |
| Figure 4.3 Raman spectra of ZTC-1 | 66 |
| Figure 4.4 XRD spectra of ZCC-2 and ZTC-2 | 67 |
| Figure 4.5 The possibility filling of FA molecules into the pore window of zeolite-Y | 67 |
| Figure 4.6 SEM images of (a) zeolite-Y, (b) ZCC-1 and (c) ZTC-1 | 68 |

| | |
|---|----|
| Figure 4.7 Particle size histogram of (a) zeolite-Y, (b) ZCC-1 and (c) ZTC-1 obtained from the SEM data | 69 |
| Figure 4.8 TEM images from zeolite-Y (a), ZCC-1 (b), The EDX mapping for ZCC-1 (c) and the concentration of elements represent of zeolite and carbon particles | 70 |
| Figure 4.9 The TEM images of ZTC-1 (a), the HRTEM images for the ZTC with randomly distributed mesopores structure, the region indicated by an arrow is the carbon layers deposited in the external surface of zeolite-Y (b) the partial ordered micropores (i) and little mesopores (ii) in the inner surface of zeolite-Y (c) | 71 |
| Figure 4.10 SEM images of (a) ZCC-2 and (b) ZTC-2 | 72 |
| Figure 4.11 Particle size histogram of (a) ZCC-2 and (b) ZTC-2 | 73 |
| Figure 4.12 The EDX mapping for ZCC-2 (c) and the content of elements represent of zeolite and carbon particles | 73 |
| Figure 4.13 Nitrogen adsorption-desorption isotherms of (a) zeolite-Y, (b) ZCC-1 (c) ZCC-2, (d) ZTC-1 and (e) ZTC-2 (solid and dot line : adsorption and desorption branch, respectively) | 75 |
| Figure 4.15 Pore size distributions of (a) zeolite-Y, ZCC-1, ZTC-1, (b) ZCC-2 and (c) ZTC-2 obtained by the 2D-NLDFT method..... | 76 |
| Figure 4.16 Illustration of carbon deposition at different routes (a) sucrose impregnation (ZTC-1) (b) FA-impregnation and propylene CVD (ZTC- 2) | 78 |
| Figure 5.1 XRD spectra of PSF/ZTC mixed matrix membrane with (a) 0, (b) 0.25, (c) 0.4, (d) 0.5, (e) 0.7 and (f) 1 wt% ZTC-1 loadings..... | 80 |
| Figure 5.2 Raman spectra of (a) selected MMMs (Inset : I_D/I_G peak intensity ratio vs ZTC-1 loading) and (b) selected MMMs between 1200-2000 cm^{-1} . | 81 |
| Figure 5.3 SEM micrographs of cross section of (a) neat PSF and PSF/ZTC-1 MMM with (b) 0.25 wt%, (c) 0.4 wt%, (d) 0.5 wt%, (e) 0.7 wt% and (f) 1 wt% ZTC-1 loadings | 83 |
| Figure 5.4 SEM micrographs of surface of (a) neat PSF and PSF/ZTC-1 MMM with (b) 0.25 wt%, (c) 0.4 wt%, (d) 0.5 wt%, (e) 0.7 wt% and (f) 1 wt% ZTC-1 contents | 84 |
| Figure 5.5 FESEM images of cross section morphology of neat PSF membrane at different magnification (a) 700x, (b) 2000x and (c) 5000x revealing the average dense selective layer of ~189 nm | 85 |
| Figure 5.6 Surface FESEM images of PSF/ZTC-1 with (a) 0.25 wt%, (b) 0.5 wt% and (c) 1 wt% ZTC-1 loadings..... | 87 |
| Figure 5.7 AFM images of the surface of PSF/ZTC-1 MMM : (a) 0, (b) 0.25, (c) 0.4, (d) 0.5, (e) 0.7 and (f) 1 wt% ZTC-1 loadings..... | 89 |
| Figure 5.8 FTIR spectra of (a) neat PSF and ZTC-1 (b) all prepared MMMs | 90 |
| Figure 5.9 Thermal Decomposition Curve of PSF/ZTC-1 MMMs..... | 92 |

| | |
|--|-----|
| Figure 5.10 Gas permeability and selectivity of (a) CO ₂ /CH ₄ , (b) CO ₂ /N ₂ , (c) O ₂ /N ₂ and (d) H ₂ /CH ₄ of all prepared membranes | 94 |
| Figure 6.1 SEM images of (1) cross section and (2) surface of (a) 0.25 wt% ZTC/PSF, (b) 0.4 wt% ZTC/PSF and (c) 0.5 wt% ZTC/PSF MMMs with 3 wt% PDMS solution | 101 |
| Figure 6.2 SEM EDX surface marking for (a) 0.25 wt% ZTC/PSF, (b) 0.4 wt% ZTC/PSF and (c) 0.5 wt% ZTC/PSF MMMs, respectively (1) and their representative mapping (2) | 102 |
| Figure 6.3 Gas separation performance of PSF/ZTC-1 MMMs for CO ₂ /CH ₄ , CO ₂ /N ₂ , O ₂ /N ₂ and H ₂ /CH ₄ gas pairs with respect to Robeson trade-off line, compared with the data on other PSF-based MMMs from literatures. The detail citations are listed in Table 6.4..... | 106 |
| Figure 6.4 SEM micrograph of the cross-sectional view of the (a) 0.25 wt%, (b) 0.4 wt% and (c) 0.5 wt% ZTC-1 loaded MMMs after heat treated at 200°C | 110 |
| Figure 6.5 Surface morphology of the (a) 0.25 wt%, (b) 0.4 wt% and (c) 0.5 wt% ZTC-1 loaded MMMs with heat treatment at 200°C | 111 |
| Figure 6.6 The permeance and selectivity of membrane as a function of ZTC-1 loading after heat treated at 200 °C for 30 min. | 112 |
| Figure 6.7 SEM micrograph of the cross-sectional view of the (a) 0.25 wt%, (b) 0.4 wt% and (c) 0.5 wt% ZTC-1 loaded MMMs after heat treated at 200°C | 113 |
| Figure 6.8 Surface morphology of the (a) 0.25 wt%, (b) 0.4 wt% and (c) 0.5 wt% ZTC-1 loaded MMMs with heat treatment at 200°C | 114 |
| Figure 6.9 The permeance and selectivity of membrane as a function of ZTC-1 loading after heat treated at 200 °C for 120 min. | 115 |
| Figure 6.10 SEM images of (a) cross sectional and (b) surface of 0.25 wt% ZTC-1 heat treated at 200 °C for 4 h..... | 116 |
| Figure 7.1 XRD patterns of (a) neat PSF, (b) PSF/ZTC-2, (c) PSF/ZCC-2 and (d) PSF/ZCC-1 at 0.25 wt% filler loading | 120 |
| Figure 7.2 Cross section view of PSF membrane incorporating (a) ZTC-2, (b) ZCC-2 and (c) ZCC-1 particles at (i) low and (ii) high magnification..... | 122 |
| Figure 7.3 Surface view of PSF membrane incorporating (a) ZTC-2, (b) ZCC-2 and (c) ZCC-1 particles | 123 |
| Figure 7.4 Cross sectional X-ray mapping of (a) PSF/ZCC-2 and (b) PSF/ZCC-1 MMMs containing 0.25 wt% ZCC (blue, yellow and red represent to Al, Si and C elements, respectively) | 124 |
| Figure 7.5 FTIR patterns of (a) ZCC-2, (b) neat PSF with PSF/ZCC-2, (c) neat PSF with PSF/ZCC-2 between 1200-500 cm ⁻¹ and (d) PSF/ZTC-2... .. | 126 |
| Figure 7.6 Thermogravimetric analysis for different MMMs..... | 128 |

| | |
|--|-----|
| Figure 7.7 Gas permeation results for coated PSF-based MMM containing different filler types..... | 130 |
| Figure 7.8 Gas separation performance of the MMM at 0.25 wt% filler loading with respect to Robeson trade-off line, compared with the data on other MMMs in the references. Detailed citations of MMMs are listed in Table 6.4 | 131 |

LIST OF TABLES

| | |
|---|-----|
| Table 2.1 Some application of gas separation membrane..... | 10 |
| Table 2.2 Separation Performances of Polymeric Membranes for Gas Separation | 11 |
| Table 2.3 Separation Performances of Inorganic Membranes for Gas Separation | 12 |
| Table 2.4 Separation Performances of MMMs for Gas Separation..... | 13 |
| Table 2.5 The Features of Some Polymers (Adapted from Castro-muñoz (2018)) | 21 |
| Table 2.6 The Supported Properties of Polysulfone for Matrix Polymer in MMMs (Roland 2014; Teoh et al. 2016)..... | 22 |
| Table 2.7 Characteristics of Gas Molecules Used for Gas Separation (Castro- muñoz, 2018)..... | 22 |
| Table 2.8 ZTC Properties Prepared Using Different Methods | 30 |
| Table 2.9 The Properties of Inorganic Fillers | 36 |
| Table 2.10 Separation Performance of MMMs Incorporated Various of Particles | 38 |
| Table 2.11 The Effect of Heat Treatment on the Gas Separation Properties of MMMs..... | 46 |
| Table 2.12 The Solubility of Gases With PDMS (Jomekian, et al. 2011)..... | 47 |
| Table 2.13 The Effects of Surface Coating Parameter on the Gas Separation Properties of MMMs | 47 |
| Table 3.1 Critical Properties and Omega Values (Wang <i>et al.</i> , 2002)..... | 57 |
| Table 3.2 Sample Designation of Membrane..... | 61 |
| Table 4.1 Textural Properties of Zeolite-Y Template, ZCC and ZTC..... | 77 |
| Table 5.1 XRD Parameters for Pure PSF and PSF Based Membrane Filled with ZTC-1 | 80 |
| Table 5.2 Surface Roughness Parameters of PSF/ZTC-1 MMMs..... | 87 |
| Table 5.3 The Thermal Behavior of PSF/ZTC-1 MMMs..... | 91 |
| Table 5.4 Binary Gas Permeance and Selectivity | 96 |
| Table 5.5 Fugacity Coefficients for Single Gases and Mixed-Gases at Equivalent Feed Pressure and Temperature of 25 °C..... | 96 |
| Table 5.6 Gas Permeation Properties of All Fabricated Membranes..... | 98 |
| Table 5.7 The Comparisons of Gas Separation Performances of PSF Based MMMs Loaded with Several Type of Fillers | 98 |
| Table 6.1 EDX Surface Mapping Result for the Coated MMMs | 102 |
| Table 6.2 Gas Separation Performance of Coated MMMs..... | 107 |
| Table 6.3 Filler Interparticle Spacing and Size of PSF Molecule, Assuming Uniform Dispersion of Filler | 107 |

| | |
|--|-----|
| Table 6.4 Gas Separation Performances of Coated PSF Based MMMs from Previous Work | 108 |
| Table 6.5 The Glass Transition Temperature of MMMs at Various Heating Period | 111 |
| Table 6.6 Single Gas Permeation Data of 0.25 wt% ZTC Loaded MMM Heat Treated at 200° C for 240 Min | 116 |
| Table 7.1 XRD Parameters for Neat PSF and PSF Based MMMs | 120 |
| Table 7.2 SEM-EDX Cross Sectional Elemental Analysis Results for 0.25 wt% Filler Embedding MMMs | 123 |
| Table 7.3 Summary of Thermal Properties for Neat PSF and MMMs Filled with Different Fillers | 127 |
| Table 7.4 Filler Interparticle Spacing and Size of PSF Molecule, Assuming Uniform Dispersion of Filler | 132 |
| Table 7.5 Gas Separation Performance of Coated MMM Containing Different Filler Types | 133 |

CHAPTER 1

INTRODUCTION

1.1 Background

Gas separation process using membrane technology is a dynamic and rapidly growing field due to low capital and operating costs, low requirements and ease of operation for various separation involving air separation, natural gas purification and refinery hydrogen recovery (Suleman et al. 2016; Bastani et al. 2013). Currently, most of commercialized membrane is made from polymeric membrane. Although the membranes have the advantages of desirable mechanical properties and the flexibility processing capability, their performance rarely exceeds the trade off between permeability and selectivity as indicated by the Robeson plot (selectivity must be sacrificed for permeability and vice versa). Furthermore, such membrane has demerits such as low thermal and chemical stability. To overcome the Robeson upper bound line, researchers have used inorganic membranes for gas separation providing better permeability and selectivity as well as high stability under severe operating condition. Although the performance of inorganic membranes appears to be attractive, fabrication of such membranes is expensive, fragile and easy to crack (Nejad *et al.*, 2016). Therefore, a composite membrane known as mixed matrix membranes (MMMs) is developed to overcome these limitations.

MMMs are made by incorporating inorganic particles into the polymer matrix which might be bonded via van der Waals force, hydrogen or covalent bonds (Vinoba *et al.*, 2017). MMMs combine the advantages of both inorganic and polymer materials, in which high separation capabilities and stability of inorganic material as well as desired mechanical and economical properties of polymer can be fully utilised in the whole membrane. The inorganic materials as dispersed phase possess unique structure, the capability of separating gases, surface chemistry and mechanical strength (Nejad *et al.*, 2016). Furthermore, they provide the longer and tortuous pathway of non-adsorbable molecules to permeate across the polymer matrix. As a result, the separation performances of composite

membranes become better with the adding of particles. Furthermore, the particles also act as a heat adsorbing material in the matrix and provide a barrier effect causing delayed decomposition (Zulhairun *et al.*, 2017). Therefore, the thermal stability of MMMs can be improved. Such improvement was found in Zulhairun and co-workers study (Zulhairun, Ng, *et al.*, 2014). They reported that the adding of cloisite 15A within the polysulfone matrix increased the selectivity in CO₂/CH₄ and thermal stability up to 46.72% and 16.82%, respectively. The enhanced permeability and selectivity in H₂/CH₄ separation of PBNPI membrane (204% and 19% respectively) as well as thermal stability (2.72%) were also investigated by Weng *et al.* (2009) using the dispersed MWCNT. Furthermore, Zornoza, Esekhi, *et al.* (2011) investigated the permeability and selectivity improvement in O₂/N₂ separation up to 43% and 47%, respectively for PSF based membrane by incorporating of HZS. The presence of selective adsorption and diffusion properties of particles has allow to enlarge permeability and selectivity of neat polymer membranes, thus achieving the objective of the simultaneous performance improvement in MMM (Bastani *et al.* 2013; Yeo *et al.* 2012; Ansaloni & Deng 2016).

The selection of suitable polymer matrix and inorganic filler is important in developing the MMM performance. The morphology of an ideal membrane would ensure the gas transport mainly through the superior inorganic phase rather than the polymer phase (Dong *et al.*, 2013). The less permeable glassy polymer tends to be more suitable due to its rigid chain structure, in which a higher portion of the overall transport will be dominated by the inorganic phase. Polysulfone (PSF) as a glassy polymer is a good choice for continuous phase due to its permeability and high intrinsic selectivity combined with good mechanical strength and thermal properties as well as easy processability (Zornoza, Téllez, *et al.* 2011; Zulhairun, Ismail, *et al.* 2014). On the other hand, the effect of inorganic particles on the gas separation characteristics depends on the particle size, porous structure and the sorption capability of the particles (Dong *et al.* 2013; Magueijo *et al.* 2013). The ideal filler used in MMMs should possess inorganic particles size of 0.3-5 µm to prevent severe agglomeration (Ferreira and Trierweiler, 2009), high surface area and superior adsorptivity which contribute to high sorption capacity (Zornoza,

Téllez, *et al.*, 2011), high porosity and well pore size distribution to ensure high gas permeability and selectivity of the membrane (Dong et al. 2013; Foley 2014).

Numerous inorganic materials have been identified as filler in membrane application such as zeolites, carbon molecular sieves (CMS), activated carbons (AC), metal organic frameworks (MOF) and carbon nanotubes (CNT). A well defined pore structure of zeolites results in an accurate size and excellent shape discrimination, leading to superior selectivity. The presence of channels and cavities of zeolite regarded as void volume is beneficial to enhance the sorption and diffusion properties, leading to high permeability. However, the rigid pore structure of zeolite have resulted in the complexity to obtain continuous and defect free structure (P S Goh *et al.*, 2011). The formation of sieve in a cage morphology of MMMs with zeolite filler was reported by Husain & Koros (2007) and Junaidi et al. (2015). Activated carbon (AC) with high surface area and high pore volume is one of the promising membrane filler. But, a wide range and poor pore size distribution leads to poor gas diffusion and selectivity (Konwar and De, 2013). Anson et al. (2004) reported that a wider pore size distribution of AC showed lower CO₂ permeability and CO₂/CH₄ permselectivity compared to narrower pore size distribution. In addition, CMS possesses better affinity toward glassy polymers, especially polysulfone, because of its similar properties, high surface area as and porosity (Moore et al. 2004; Goh et al. 2011). CMS is well distributed inside the polyethersulfone and good affinity to Matrimid matrix, as reported by Farnam et al. (2016). It might be due to its weight force balance to the buoyant force, thus allowing better distribution of particles within the polymer (Bakhtiari *et al.*, 2011). However, the dead-end (not interconnected) of CMS does not greatly aid the transport of molecules since the molecules can not diffuse through the particles or may only do so to a small extent (Duval *et al.*, 1993). Another class of porous carbon which possess tremendous research made from CNTs due to their large surface area and good control of pore dimensions (Nejad *et al.*, 2016). They naturally tend to form bundles, however, which restrict the formation of a good dispersion inside the matrix, as reported by Ge et al. (2011). Their vertical alignment behaves as pinholes, leading to a high permeability with loss selectivity (P S Goh *et al.*, 2011). Other porous material, metal organic framework

(MOF), possess uniform pore distribution, large surface area as well as controlled porosity and affinity (Dong *et al.*, 2013). Although MMMs containing MOF appear to be attractive, they lead to a low thermal stability of membrane due to the presence of linker and strong interaction between particles tends to form the cavity structure leading to a decline gas performance (Perez *et al.*, 2009). Existing fillers have therefore not yet demonstrated ideal gas separation performances. Challenge regarding MMM fabrication remain, such as the formation of pinholes at the polymer and filler interface, the unfavorable pore structure and orientation of filler.

This study proposed filler which made from the combination of zeolite and carbon known as zeolite templated carbon (ZTC) to overcome above issue. The ZTC is a structurally engineered carbon having the negative replica of zeolite template with controlled porosity and large surface area, produced by depositing carbon precursor inside the pore of zeolite template. Therefore, carbon with open and no rigid pore structure can be achieved to improve the compatibility with polymer matrix, reducing the filler-polymer interfacial defects inside the membrane matrix. By looking its textural properties, the successful of ZTC synthesis possess higher specific surface area reached to 4000 m²/g and almost 95% of micropore content with the pore size of 1.2 nm (Nishihara and Kyotani, 2012). Such properties can be controlled by the manipulation of its synthesis method and condition. Moreover, the ZTC could enhance the storage capacity for gases such as hydrogen (Guan *et al.* 2009; Konwar & De 2013) and carbon dioxide (Song *et al.*, 2013). The results exhibited a satisfactory performance of ZTC as adsorbent materials. On the basis of these characteristics, ZTC is suitable not only for gas adsorbent, but also for separation purpose as filler material. However, there have been no reported studies regarding the use of this material as a membrane filler.

The addition of ZTC inside glassy polymer (PSF) still creates voids at the interface that act as alternative pathway for gas molecules due to the rigid polymer chain structure. This problem can be avoided by thermal annealing above the glass transition temperature of polymer which could minimize or even remove the voids or pinholes (Dong *et al.*, 2013). By heating treatment, the membrane is expected

that the polymer chains will be more flexible, thus easily surrounding the particle surface (Ferreira & Trierweiler 2009). After heating, the membrane become denser in the surface layer and the thermal soaking period is being a factor to transform defect into fully dense structure. Ferreira & Trierweiler (2009) observed that the longer time of thermal treatment seriously affect the membrane structure denser and increase the selectivity. Another attempt to treat defects or pinholes in the active layer is by surface coating of highly permeable silicone rubber polymer, thus gas molecules will pass through the ZTC pores and polymer matrix (Ying *et al.*, 2006). The hydrophobic silicon rubber will attach to the surface of hydrophobic ZTC, thus it helps to tighten the surface structure. In addition to the void formation, the other challenge of MMM is to get good dispersion of inorganic particles within polymer matrix. Good particle dispersion can prevent the aggregate particles, in which the aggregation occurs in high amount particle loading as observed by Junaidi *et al.* (2014). These aggregation can form voids between the particles and such voids provide extra channels to allow the transport of gas, leading to low selectivity. The fabrication strategy to solve this issue is by introducing prime protocol (Dong *et al.*, 2013). In this prime process, a small amount of polymer is added into the particle suspension solution and the particles will be surrounded by a thin layer of polymer, thus reducing agglomeration of particles (Mahajan and Koros, 2002b). Then, the remaining polymer is added into the prime solution. Another strategy to obtain good particle dispersion is by preparing of high concentration polymer solution to reduce particle sedimentation. The suppression of sedimentation is achieved because a high viscosity could hinder the particle mobility, thereby decreasing the particle sedimentation rate (Chung *et al.*, 2007). In this study, MMMs were fabricated with different amount of ZTC loading by prime protocol process and the obtained membranes were post-treated with thermal annealing and surface coating. Furthermore, ZTC particles with distinct pore properties have been synthesized by different methods of carbon filling.

1.2 Problems

The development of membrane technology for gas separation rapidly increased. Since the advanced technology and requirements become more demanding, new membrane materials are needed to satisfy the separation performance. Currently, mixed matrix membranes (MMMs) have been developed for these application (Vinoba *et al.*, 2017). By combining molecular sieves in the polymer matrix, the MMMs inherit the superior characteristics of these particles and possess the advantages of polymer in the bulk membrane, thus achieving the simultaneous performance improvement and surpassing the trade-off line. The selective adsorption and diffusion properties of inorganic particles has allow to improve permeability and selectivity of polymer membrane.

Inorganic filler selection plays important role in preparing MMM. Magueijo *et al.* (2013) stated that the effect of fillers on the separation characteristics of MMM strongly depends on their pore size. A good pore structure with a pore size below 2 nm is highly desirable because of the resulting size-selective nature (Vinoba *et al.*, 2017). Several inorganic materials containing zeolite and carbon such as activated carbon (AC), carbon molecular sieve (CMS), activated carbon (AC) and carbon nanotube (CNT) has been incorporated within polymer matrix. Although these fillers seem more promising, there are still some challenges to be addressed including the compatibility problem between the polymer and filler as well as their porous structure. Regarding to these issue, it is reasonable to find more suitable filler with good properties and better compatibility to polymer matrix in order to produce outstanding separation performance of MMMs. Zeolite templated carbon (ZTC) appears to be an attractive option as new filler for this application due to its superior properties such as high pore volume, regular pore structure and large surface area. No one given the attention on ZTC as filler for MMM even it was widely used as adsorbent for several gases. This material is unique as it has structure similar to zeolite in the form of carbon, but with no rigid pore structure to improve the compatibility with polymer matrix. The effect of ZTC on the gas separation of MMMs was studied by varying the amount of ZTC loading since these membrane has not been available in the literature. A different ZTC and its carbon derived material (ZTC prior template removal) with distinct

properties were used and their effect on the gas permeation performance will be analysed.

In addition to filler material, the problem of polymer matrix is to ensure good interaction between these two phases. The use of PSF glassy polymer weakens the adhesion with the particles due to its rigid chain structure. As a consequence, the ZTC incorporated with PSF matrix still contains voids at the interface that reduce the gas transport resistance. The strategies to deal with this issue are heating treatment and surface coating. Introducing these strategies could potentially reduce or even remove the various defects. The effect of thermal soaking time for attaining less defective polymer zeolite membrane structure was conducted, while the surface coating was performed by dip-coating with PDMS coating solution.

1.3 Research Objectives

Based on the problems discussed above, the overall goal of this research is to investigate the feasibility of gas separation using ZTC filler inside the PSF matrix including enhance membrane performance by post treated the membrane using surface coating and heat treatment. The specific goals are organized as follow :

1. To synthesize and characterize zeolite templated carbon (ZTC) as filler in mixed matrix hollow fiber membrane
2. To prepare mixed matrix hollow fiber membrane and investigate the effect of filler loading towards the membrane structural, morphological, thermal stability and gas permeation performance
3. To investigate the influence of heat treatment and surface coating on the membrane morphological, thermal stability and gas separation performance
4. To study the effects of ZTC with distinct pore properties on the membrane structural, morphological, thermal stability and gas permeation performance

The obtained membrane is expected to be a promising candidate for a new membrane which can be applied for natural gas separation, oxygen-nitrogen separation and hydrogen separation.

1.4 Originality

Mixed matrix membrane containing a continuous matrix filled with inorganic filler such as zeolites, activated carbons, carbon nanotubes, carbon molecular sieve and metal organic frameworks have been extensively studied for various gas separation such as air separation, hydrogen recovery and natural gas separation. However, existing filler still have some challenges to be addressed such as the incompatibility problem between polymer and filler as well as their porous structure. A new carbon material receiving great interest is named as zeolite templated carbon (ZTC) due to its suitable characteristics including high pore volume with no rigid pore structure, large surface area, narrow pore size distribution and the gas adsorption capability. These material is suitable for some applications such as gas sorbents, batteries, capacitors and catalysis. Its unique properties and good polymer compatibility render the ZTC not only suitable for these application, but also for MMMs filler in gas separation. Therefore, ZTC is proposed to be the next promising candidate filler for a new membrane. The originality of this research that contributes to the application development is incorporating ZTC as filler for outstanding separation performance of MMM, yet to be found. Furthermore, the understanding of gas transport mechanism of the prepared membrane will support the scientific approach.

CHAPTER 2

LITERATURE REVIEW

2.1 Gas Separation Technology

2.1.1 Overview of Gas Separation Membrane

In order to develop more effective, economic and environmentally friendly method for gas separation process, a number of means for gas separation have been investigated from conventional process to membrane technology. The membrane gas separation is rapidly growing over the past 35 years due to some advantages over conventional methods (Baker and Low, 2014). The conventional methods including pressure swing adsorption, cryogenic distillation and amine absorption seems to be high energy consumption, high cost with negative impact on the environment (Yeo *et al.*, 2012). Membrane technology has been promisingly used as a method to get some gases with high purity, low energy requirements, low cost, easy of operation (no moving parts, no phase change), continuous process and unnecessary regeneration process (Sridhar *et al.* 2014; Adewole *et al.* 2013). According to Ismail *et al.* (2015), a concept of membrane is it acts as selective barrier between two gases and separation occurs by controlling the diffusion rate. The desirable membrane should possess several properties such as high permeability, high selectivity, sufficient mechanical, high thermal and chemical stability under certain operation condition (Compañ *et al.* 2010; Zulhairun & Ismail 2014).

2.1.2 Development of Membrane Technology

The feasibility of membrane process on gas separation has been known for more than a century, but the commercial membrane was available in 1980s (A. F. Ismail *et al.*, 2015). Figure 2.1 shows the membrane development for industrial process that occurred in the last 35 years. The first large scale of gas separation membrane was applied for hydrogen separation purpose. Since its first industrial development in the 1980s, the membrane-based technology has been used into expanded gas separation applications. However, the membranes are bounded by

their performance and they suffer severe deformation in corrosive and aggressive operating condition since most of commercialized membrane are made from polymer membrane (Nejad *et al.*, 2016).

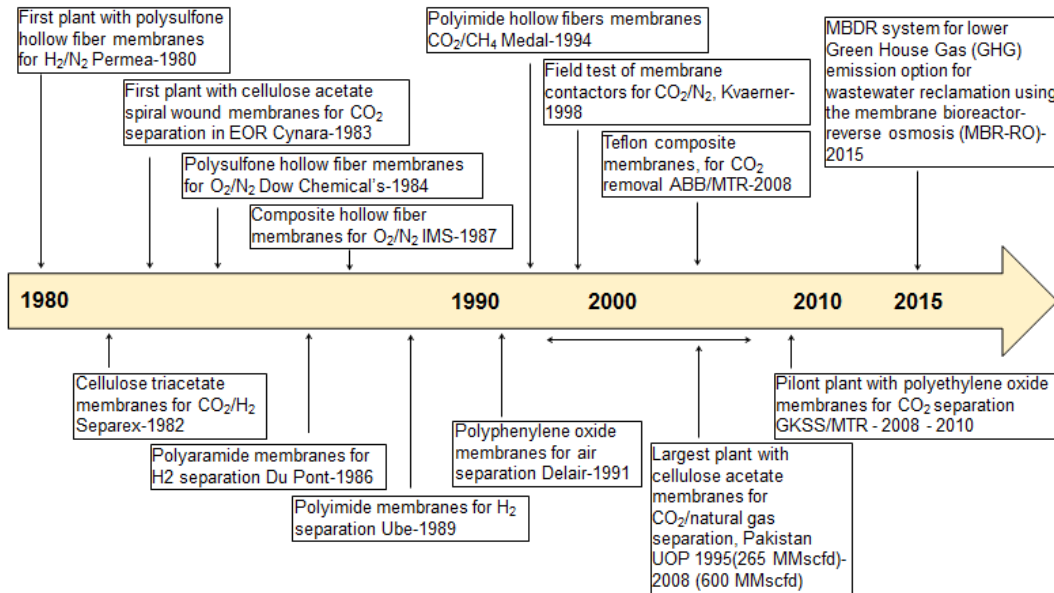


Figure 2.1 Milestones of membrane development in the industrial application (Sridhar *et al.*, 2014)

Table 2.1 Some application of gas separation membrane

| Gas separation | Application |
|----------------------------------|---|
| O ₂ /N ₂ | Nitrogen generation Oxygen enrichment |
| CO ₂ /N ₂ | Post-combustion CO ₂ capture |
| CO ₂ /CH ₄ | Acid gas treatment Landfill gas upgrading Enhanced oil recovery |
| H ₂ -hydrocarbons | Refinery hydrogen recovery |

Furthermore, polymer membranes are only able to operate in small volume of gas and possess limitation in chemical and physical stability as well as CO₂-induced plasticization or swelling at high operating pressure. Also, the permeability and selectivity are hindered by a trade off relationship (high permeability must be sacrificed with low selectivity, and vice-versa) (Robeson, 2008). The performances of some polymeric membrane are shown in Table 2.2. The improvement of the polymeric membrane has been attempted by modification

of polymers such as introducing chemical linkers, cross-linking, depositing an ultrathin and dense polymer or thermally rearranged polymers. Unfortunately, the performance of polymeric membranes has reached in steady state and hard to achieve significant improvement, as shown in Table 2.2 (Yeo *et al.*, 2012). On the other hand, inorganic membranes offer better separation properties and can withstand at harsh operating condition.

Table 2.2 Separation Performances of Polymeric Membranes for Gas Separation

| Membrane | Operating condition | | Gas test* | Separation properties (best performance) | | References |
|------------------------------------|---------------------|--------|----------------------------------|---|-------------|------------------------------|
| | P (bar) | T (°C) | | Permeability | Selectivity | |
| Matrimid / PSF | 5 | 25 | O ₂ /N ₂ | P _{O₂} = 3.65 ^b | 7.76 | (Ding <i>et al.</i> , 2008) |
| Matrimid / PES | 5 | 25 | O ₂ /N ₂ | P _{O₂} = 13.17 ^b | 7.79 | (Ding <i>et al.</i> , 2013) |
| 6FDA-mPDA / 6FDA-durene15000 /2500 | 3 | 20 | CO ₂ /CH ₄ | P _{CO₂} = 6.8 ^a | 48.57 | (Heck <i>et al.</i> , 2016) |
| | | | O ₂ /N ₂ | P _{O₂} = 2.2 ^a | 6.11 | |
| Hyflon [®] AD 60 | 3 | 22 | CO ₂ /CH ₄ | P _{CO₂} = 1,330 ^b | 18 | (Fang <i>et al.</i> , 2016) |
| Poly(PFMD D-co-PFMD) | 3 | 22 | CO ₂ /CH ₄ | P _{CO₂} = 78 ^b | 28 | |
| Teflon [®] AF 2700 | 3 | 22 | CO ₂ /CH ₄ | P _{CO₂} = 13,000 ^b | 5.7 | |
| PVDF/RTIL | 2 | 35 | CO ₂ /N ₂ | P _{CO₂} = 1778 ^a | 41.1 | (Chen <i>et al.</i> , 2012) |
| Polyaniline/ polybenzimidazole | 1.5 | 30 | CO ₂ /N ₂ | P _{CO₂} = 1.07 ^a | 86 | (Jan <i>et al.</i> , 2016) |
| | 1.5 | 30 | CO ₂ /CH ₄ | P _{CO₂} = 1.07 ^a | 104 | |
| | 1.5 | 30 | O ₂ /N ₂ | P _{O₂} = 0.129 ^a | 10.4 | |
| PSF | 8 | 25 | CO ₂ /CH ₄ | P _{CO₂} = 8.23 ^b | 31.65 | (Aroon <i>et al.</i> , 2010) |

^aunit in barrer

^bunit in GPU

*single gas permeation testing

The separation properties of inorganic membranes is shown in Table 2.3. It can be seen that the membrane performance showed higher selectivity without compromising the permeability than those of neat polymer membrane. The membranes might offer the excellent performance transcending Robeson's upper bound. However, the complexity of synthesis cause the material cost higher than

polymer membrane. Another challenges of inorganic membrane are reproducibility issue and the difficulty to obtain defect-free membranes at large scale due to its fragile nature (Dong *et al.*, 2013).

Table 2.3 Separation Performances of Inorganic Membranes for Gas Separation

| Membrane | Operating condition | | Gas testing | Separation properties (best performance) | | Reference |
|----------------------------|---------------------|--------|---|--|-------------|--------------------------------------|
| | P (bar) | T (°C) | | Permeability (GPU) | Selectivity | |
| Carbon | 3.5 | 30 | CO ₂ /N ₂ | P _{CO2} = 134.5 ^a | 13.2 | (He <i>et al.</i> , 2011) |
| Zeolite-T/carbon composite | 1 | 25 | CO ₂ /N ₂ | P _{CO2} = 24.81 ^b | 51.6 | (Yin <i>et al.</i> , 2013) |
| | 1 | 25 | CO ₂ /CH ₄ | P _{CO2} = 24.81 ^b | 97.3 | |
| | 1 | 25 | CO ₂ /N ₂ [*] | P _{CO2} = 23.8 ^b | 67.1 | |
| | 1 | 25 | CO ₂ /CH ₄ [*] | P _{CO2} = 23.88 ^b | 143 | |
| Zeolite-T | 1 | 30 | CO ₂ /CH ₄ | P _{CO2} = 21 ^b | 70.8 | (Mirfendereski <i>et al.</i> , 2008) |
| Carbon | 1 | 25 | CO ₂ /CH ₄ | P _{CO2} = 13.9 ^b | 197 | (Yoshimune and Haraya, 2013a) |
| | 1 | 25 | O ₂ /N ₂ | P _{O2} = 2.9 ^b | 12.1 | |
| | 1 | 25 | H ₂ /CH ₄ | P _{H2} = 95.54 ^b | 1354 | |
| | 1 | 25 | CO ₂ /N ₂ | P _{CO2} = 13.9 ^b | 58 | |
| | 1 | 25 | CO ₂ /CH ₄ [*] | P _{CO2} = 15.16 ^b | 199 | |
| Mesoporous silica / Torlon | 3 | 35 | CO ₂ /N ₂ | P _{CO2} = 100 ^b | 16.7 | (Jang <i>et al.</i> , 2011) |
| | 3 | 35 | CO ₂ /CH ₄ | P _{CO2} = 100 ^b | 12 | |
| | 7 | 35 | CO ₂ /CH ₄ [*] | P _{CO2} = 57 ^b | 9 | |

^aunit in barrer

^bunit in GPU

*biner gas permeation testing

Recent efforts have been made by combining polymer and inorganic materials to form mixed matrix membranes (MMMs) for improving the separation performance and the robustness of the membranes. The improvement of MMMs performance compared to polymeric membranes can be seen in Table 2.4 and it should be exceed the Robeson upper bound line (Figure 2.2).

Table 2.4 Separation Performances of MMMs for Gas Separation

| Polymer | Filler loading | Thermal degradation (°C) | | Gas testing* | Separation properties (best performance) | | Ref. |
|--------------|------------------|--------------------------|--------|----------------------------------|--|--|---------------------------------------|
| | | Polymer | MMM | | Neat polymer | MMM | |
| PBNPI | MWCNT | 529.7 | 544.1 | CO ₂ /CH ₄ | $\alpha = 3.73$; P _{CO2} = 2.61 ^a | $\alpha = 3.37$; P _{CO2} = 6 ^a | (Weng <i>et al.</i> , 2009) |
| Matrimid | Activated carbon | 420 | 440 | CO ₂ /CH ₄ | $\alpha = 36.8$; P _{CO2} = 12.3 ^a | $\alpha = 37.4$; P _{CO2} = 39.5 ^a | (Weigelt <i>et al.</i> , 2018) |
| | | | | O ₂ /N ₂ | $\alpha = 8.11$; P _{O2} = 2.41 ^a | $\alpha = 5.48$; P _{O2} = 8.22 ^a | |
| Elvaloy 4170 | f-MWNT | - | - | CO ₂ /CH ₄ | $\alpha = 7.48$; P _{CO2} = 104.25 ^a | $\alpha = 6.10$; P _{CO2} = 105.67 ^a | (Ranjbaran <i>et al.</i> , 2015) |
| PES | CMS | 500 | 510 | CO ₂ /CH ₄ | $\alpha = 3.57$; P _{CO2} = 25.7 ^b | $\alpha = 11.15$; P _{CO2} = 68 ^b | (Farnam <i>et al.</i> , 2016) |
| PSF | Cloisite 15A | 364.5 | 425.8 | CO ₂ /CH ₄ | $\alpha = 27.44$; P _{CO2} = 60.09 ^b | $\alpha = 40.26$; P _{CO2} = 56.25 ^b | (Zulhairun, Ng, <i>et al.</i> , 2014) |
| PSF | ZIF-8 | - | - | CO ₂ /CH ₄ | $\alpha = 19.83$; P _{CO2} = 21.27 ^b | $\alpha = 34.09$; P _{CO2} = 21.16 ^b | (Abdul <i>et al.</i> , 2015) |
| PSF | Zeolite-T | - | - | CO ₂ /CH ₄ | $\alpha = 2.63$; P _{CO2} = 12.33 ^b | $\alpha = 3.37$; P _{CO2} = 78.9 ^b | (Mohamad <i>et al.</i> , 2016) |
| PSF | SAPO-34 | 500 | 490 | CO ₂ /CH ₄ | $\alpha = 17.3$; P _{CO2} = 22.01 ^b | $\alpha = 28.2$; P _{CO2} = 314.02 ^b | (Junaidi <i>et al.</i> , 2014) |
| | | | | CO ₂ /N ₂ | $\alpha = 16.5$; P _{N2} = 1.33 ^b | $\alpha = 26.1$; P _{CO2} = 12.03 ^b | |
| PES | MWCNT | 488.58 | 502.05 | O ₂ /N ₂ | $\alpha = 2.56$; P _{O2} = 2.13 ^b | $\alpha = 10.65$; P _{CO2} = 3.19 ^b | (Ismail <i>et al.</i> , 2011) |
| | | | | CO ₂ /CH ₄ | $\alpha = 51.26$; P _{CO2} = 10.98 ^b | $\alpha = 250.13$; P _{CO2} = 6.79 ^b | |
| PEI | f-MWNT | 549 | 559 | O ₂ /N ₂ | $\alpha = 4.06$; P _{O2} = 1.22 ^b | $\alpha = 3.75$; P _{O2} = 2.29 ^b | (P. S. Goh <i>et al.</i> , 2011) |
| PSF | CMS | 495 | 516 | O ₂ /N ₂ | $\alpha = 5.50$; P _{O2} = 1.58 ^a | $\alpha = 5.97$; P _{O2} = 7.96 ^a | (Ismail <i>et al.</i> , 2009) |

^aunit in barrer

^bunit in GPU

*single gas permeation testing

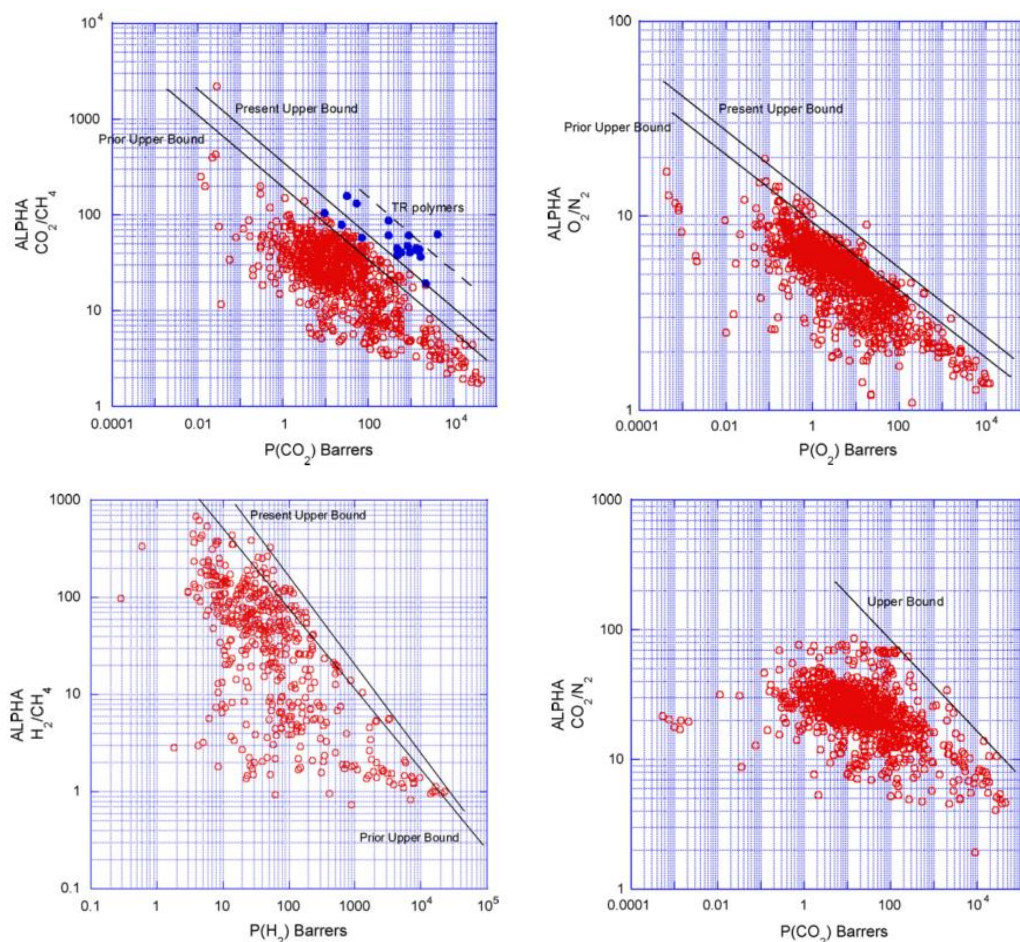


Figure 2.2 Upper bound curves correlation for polymer membranes (Robeson, 2008)

2.2 Mixed Matrix Membranes (MMMs)

Today, MMMs have been identified as very promising candidates membrane for gas separation. MMMs have synergistic characteristics of each phase, in which high separation performance of the inorganic particles as dispersed phase and the ease of processability of the polymer as the membrane matrix. Also, the MMMs provide improved thermal and mechanical properties, thus it can withstand aggressive and harsh operating condition (Dechnik *et al.*, 2017). For instance, the thermal stability of MMMs using TiO_2 -PSF has been investigated to be higher than those of neat PSF. This can be due to a higher thermal stability of TiO_2 than PSF. The particles would provide a barrier effect hindering the flow of degradation product from the bulk polymer into gas phase and good filler-polymer interfacial interaction leading to the increase of degradation's activation energy (Marosfoi *et al.* 2006; Ismail *et al.* 2011). As a

result, a good thermal stability can be achieved for MMMs. The schematic of mixed matrix membrane is shown in Figure 2.3.

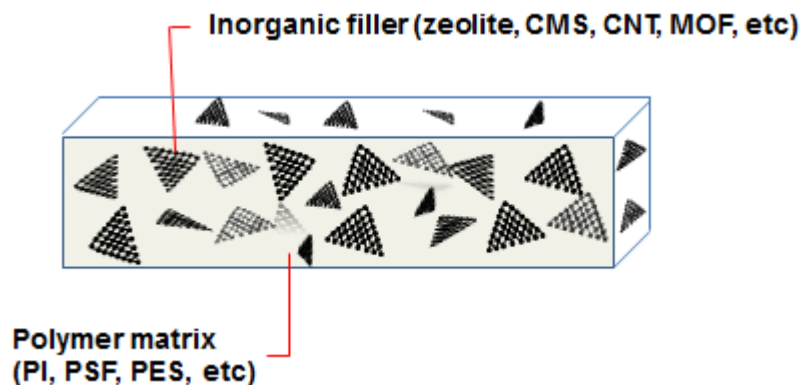


Figure 2.3 Schematic of mixed matrix membrane

Furthermore, the presence of porous fillers in the polymers results in the increase of free volume due to the particles cavities and the loosen polymer packing in the polymer-filler interface. However, good interaction between polymer and filler should hinder the chain motion and rotation to increase polymer chain rigidity. The additional free volume and the increase in chain rigidity resulted in the simultaneous enhancement of permeability and selectivity for the MMMs. The rigidified polyethersulfone (PES) chains around the zeolite-4A surface was observe to enhance the O_2/N_2 selectivity, but lower permeability (Li *et al.*, 2005). While, the incorporation of ZIF-7 into PBI resulted in increasing permeability, but lower selectivity due to larger fractional free volume (Zhang *et al.*, 2012).

Also, the inorganic particles are able to separate gases based on the molecular weight, size of molecules or surface interaction, which can be described as Knudsen diffusion, molecular sieving or surface adsorption mechanism, respectively. The presence of particles could create tortuous pattern of matrix for gas diffusion pathways. Figure 2.4 shows the representation of the mechanism transport of MMMs by asumming molecular sieving effect on the particles for CO_2/CH_4 separation. The species with larger kinetic size (CH_4) is unable to pass through the inorganic phase due to its pore size, resulting longer and tortuous diffusion pathway for CH_4 within the polymer phase. While, species with smaller

kinetic diameter (CO_2) can pass through the inorganic phase, thus high selectivity of MMMs can be achieved. Furthermore, if the gas diffusion through the dispersed phase is larger compared to polymer phase, the gas flow across the MMMs will increase, thus achieving simultaneous improvement of permeability and selectivity for MMMs.

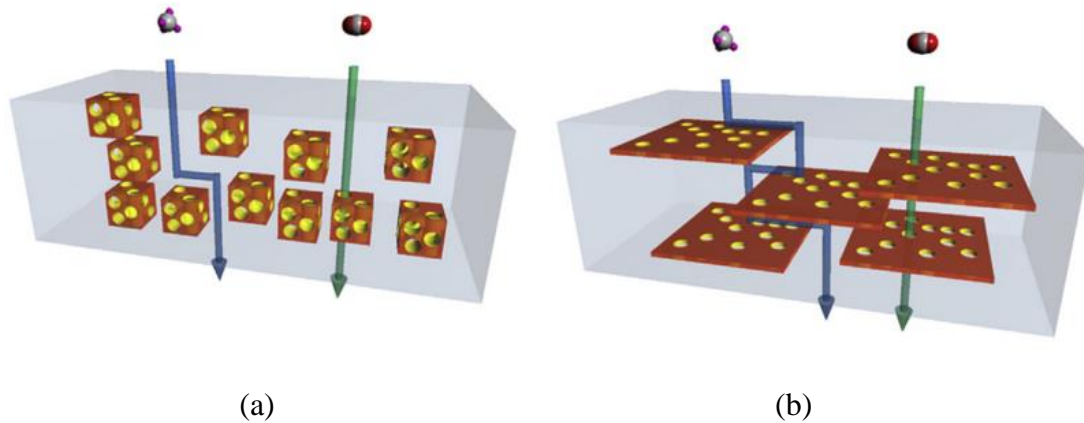


Figure 2.4 Schematic diagram of the transport mechanism of MMMs with (a) conventional and (b) high aspect ratio permeable fillers (Adapted from Ansaloni & Deng (2016))

As summarized in Table 2.4, it demonstrated that the incorporation of inorganic fillers including zeolites, CNTs, CMS contributes to improve the performance of polymer membrane. However, there are some literatures that the permeability and selectivity are still hindered by trade-off curve after the addition of inorganic filler, as shown in Figure 2.6. Furthermore, it could be solved by guaranteeing the good control of polymer-filler interactions, the particle distribution inside the polymer matrix and the membrane morphology. These can be controlled by careful manipulation of the synthesis conditions and the modifications or functionalizations of the surface chemistry of fillers, thus resulted in superior performance of MMMs. Jomekian et. (2011) reported the surface modification of MCM-48 filler using dimethyldichlorosilane (DMDCS). The modified MCM-48 particles showed better dispersion in PSF matrix and there were no distinct voids between two phases, as shown in Figure 2.5. Furthermore, the presence of modified MCM-48 was believed to be responsible for the substantial improvement of permeability for all gases.

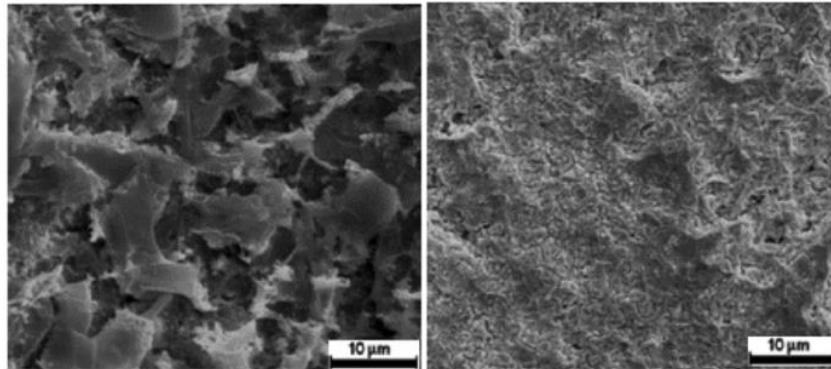


Figure 2.5 SEM images of unmodified (left) and modified MCM-48/PSF membrane (Adapted from Jomekian, Mansoori, et al. (2011))

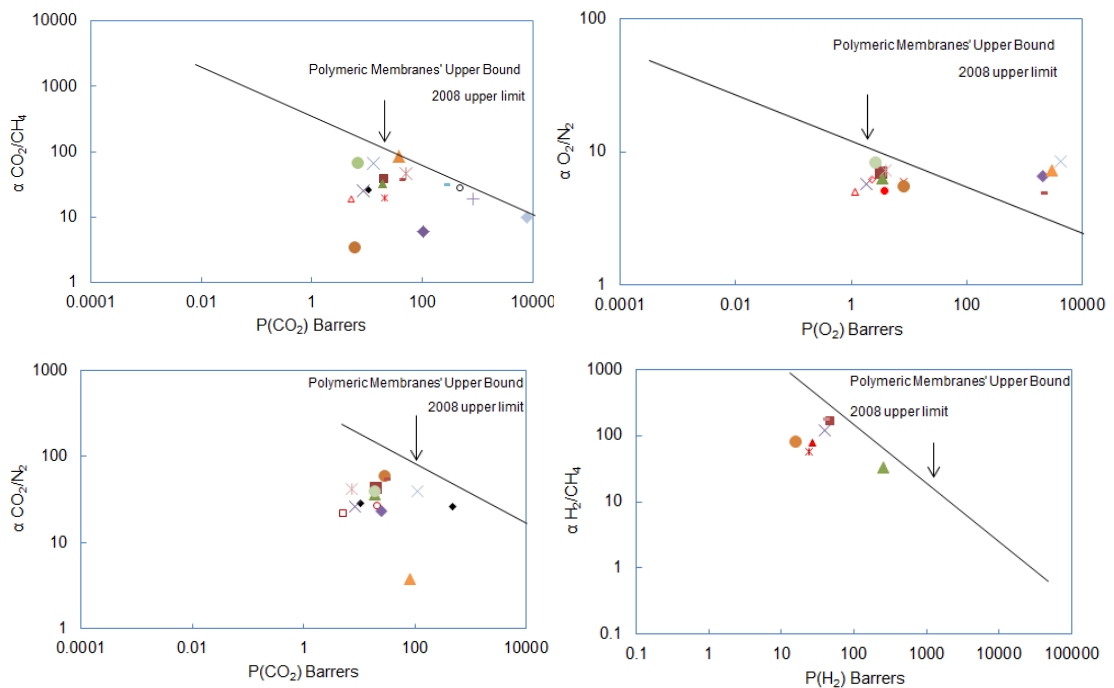


Figure 2.6 Robeson's upper bound analysis of MMM derivatives from polysulfones, polyimides, PIMs, PTMSP and pebax

2.3 Membrane Materials in MMMs

Material selection for both polymer matrix and inorganic phase is also a major aspect in the development of MMMs. This section reviews the polymer and filler structure related to their potential application as membrane material for gas separation.

2.3.1 Polymer Selection

The gas separation performance of polymer phase is controlled by its intrinsic properties. The intrinsic properties of polymer are determined by the structure of polymer materials. Table 2.5 shows the characteristics polymers commonly used for gas separation membrane. It shows that PSF has low permeabilities with acceptable selectivity values. Furthermore, the low permeability of polymer is preferable for the preparation of MMMs since the majority of gas diffusion would occur within the particles (Chung *et al.*, 2007). This is due to the rotational of polymer segments that restricted by the steric hindrance along the polymer backbone, thus resulting in a rigid structure. This properties are associated with glassy polymers. The other properties of polysulfone which make the polymer suitable for matrix material in MMMs are summarized in Table 2.6. The features make polysulfone material suitable not only for gas separation, but also for hemodialysis (Wenten *et al.*, 2016) and ultrafiltration (Daufin *et al.*, 2001). Also, polysulfone has a polar characteristic due to the availability of sulfone group. As a result, it exhibits higher solubility or chemical affinity to the gas penetrants having a quadrupolar moment (Bastani *et al.* 2013; Reif 2006; Zornoza *et al.* 2009). In this case, the gas properties have to be taken into account, as shown in Table 2.7.

The performances of PSF membrane with respect to Robeson trade-off line are shown in Figure 2.7. The point of PSF membranes approach the upper bound line for all separation and these values are higher than the intrinsic selectivity values as shown in Table 2.5. However, achieving higher selectivity with similar permeability is the main issue faced by the polymer membrane, including PSF to exceed Robeson's upper bound. Many researchers tried to solve the problem by changing the synthesis and processing conditions and membrane formulation.

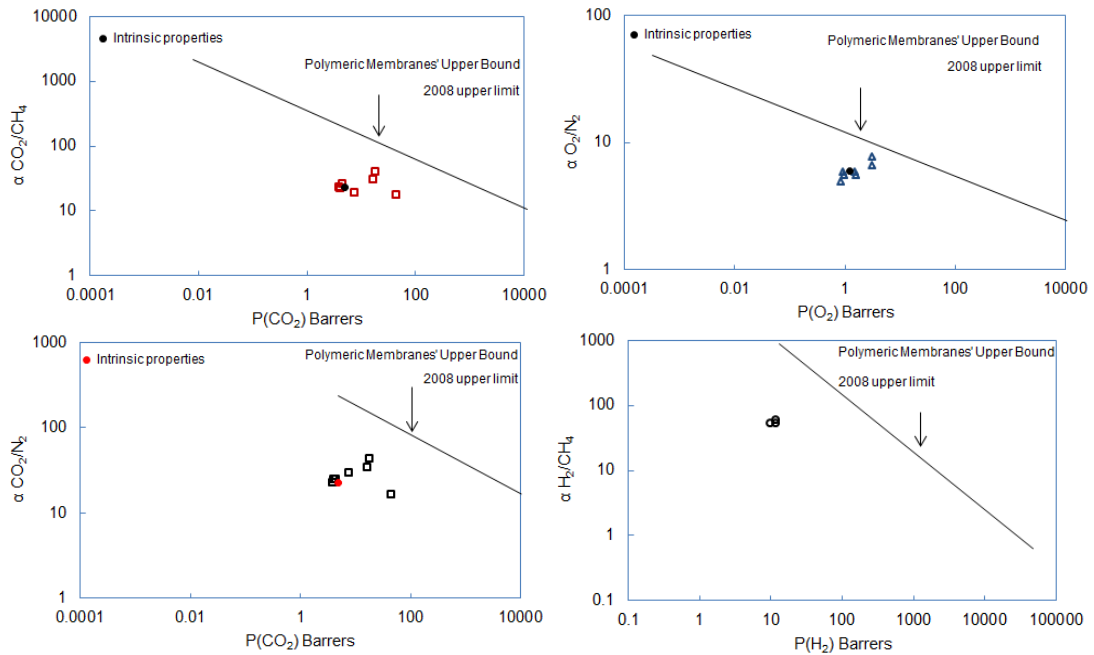


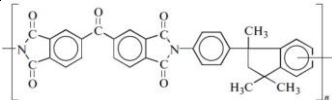
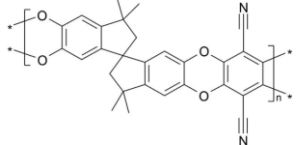
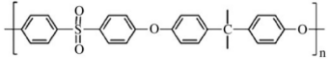
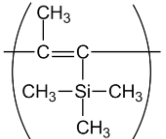
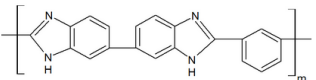
Figure 2.7 The evaluation CO_2/CH_4 , O_2/N_2 , CO_2/N_2 and H_2/CH_4 separation performance for PSF membrane

The structure of PSF membrane used for gas separation can be categorized into dense, asymmetric and composite. The fabrication process of these membranes is different. There are three types of phase inversion process in order to form dense and asymmetric membranes; dry, wet and dry/wet inversion process (Julian and Wenten, 2012). Pinnau and Koros (1991) investigated PSF membrane made by dry and wet process. The PSF membrane obtained by dry process consists a very thick dense skin layer of about $17.5 \mu m$ supported by sponge-like and macrovoid structure, as shown in Figure 2.8(a). The gas permeation rate of this membrane was very low due to the thickness of selective layer. Conversely, PSF membrane made by wet process consists of sponge-like structure containing of macrovoids with too many defects on the skin layer, as observed in Figure 2.8(b). As a result, the gas transport was dominated by pore flow through skin layer defects leading to a high O_2 fluxes (600 GPU) and low O_2/N_2 selectivity (0.91). Sidek & Nora (2011) also prepared PSF membrane by wet inversion phase and resulted membrane with finger-like structure and macrovoids at the bottom, promoting a high flux and loss selectivity.

Regarding to these issues, Pinnau and Koros (1991) proposed a new technique by combining of evaporation and quench steps (dry/wet phase) to form PSF membrane with defect-free and ultrathin skin layers. The dry/wet phase inversion with evaporation time 60 s resulted in a thin dense skin layer (0.1 μm) supported by tightly packed nodular transition layer (0.3 μm) and highly porous substructure, as shown in Figure 2.9. The O_2/N_2 selectivity was found to be enhanced up to 5.2 with O_2 flux of 22 GPU. Kiadehi et al. (2015) also reported that PSF membrane made by dry/wet inversion phase with 30 s evaporation consisted of dense selective layer and finger-like structure. The O_2 flux and O_2/N_2 selectivity obtained were 17.7 GPU and 1.61, respectively. The results showed that membrane structure depends on the prolonged evaporation period, which results in the deformation and fusion of structures.

In addition, the composite membrane can be prepared by surface coating the other polymer onto the matrix polymer for certain time. The coating material should possess high flux, thus it would not provide additional resistance to gas transport. Chong et al. (2018) prepared hollow fiber PSF membrane with surface coating using polydimethylsiloxane (PDMS) and poly(ether block amide) (PEBAX). PDMS coating is able to fix membrane surface defects by eliminating the non-selective pores, thus improving O_2/N_2 selectivity as well as O_2 permeance. Unlike PDMS, PEBAX contains both polyamides glassy and polyether rubbery fragments, achieving simultaneous improvement between permeance and selectivity (Roslan *et al.*, 2018). They reported that PSF membrane coated with PEBAX showed lower O_2 permeance and O_2/N_2 selectivity. This findings showed that PEBAX coating seems not effective to form good integrity coating layer on the hollow fiber form, but it is effective to be used for flat sheet membrane. Magueijo et al. (2013) also found that PSF hollow fiber membranes coated with PDMS via dip coating method were able to improve ideal selectivity of CO_2/CH_4 , O_2/N_2 , CO_2/O_2 and CH_4/N_2 with acceptable permeances. Marchese et al. (1995) prepared PSF flat sheet membrane with PDMS via dip coating onto the surface of PSF and the permselectivity for H_2/N_2 and H_2/CH_4 improved, while the permeabilities decreased since the surface pores are plugged and the surface thickness increased.

Table 2.5 The Features of Some Polymers (Adapted from Castro-muñoz (2018))

| Polymer | Chemical Structure | T _g (°C) | Permeability (Barrer) | | | | | Selectivity | | | | | FV | ρ (g/cm ³) | |
|---|---|---------------------|-----------------------|----------------|----------------|-----------------|-----------------|--------------------------------|---------------------------------|----------------------------------|---------------------------------|--------------------------------|-------|------------------------|---------------------------------|
| | | | O ₂ | H ₂ | N ₂ | CO ₂ | CH ₄ | O ₂ /N ₂ | CO ₂ /N ₂ | CO ₂ /CH ₄ | H ₂ /CO ₂ | H ₂ /N ₂ | | | H ₂ /CH ₄ |
| Matrimid |  | 302-310 | 2.1 | 27.16 | 0.28 | 7.68 | 0.22 | 6.4 | 30 | 34.91 | 3.88 | 97 | 83.33 | 0.17 | 1.2 |
| Polymers of intrinsic microporosity (PIM-1) |  | 399-415 | 370 | 1300 | 92 | 2300 | 125 | 4.0 | 25 | 18 | 0.57 | 14 | 10 | 0.24 | 0.94 |
| Polysulfone (PSF) |  | 185 | 1.2 | 16.4* | 0.20 | 4.9 | 0.21 | 6.0 | 22.4 | 23.3 | 1.53 | 20 | 34.4 | 0.13 | 1.19 |
| Poly[1-trimethylsilyl)-1-propyne] (PTMSP) |  | >250 | 7200 | 4200 | 6890 | 37000 | 18400 | 1.7 | 10.7 | 4.46 | 0.53 | 2.5 | 0.995 | 0.34 | 0.83 |
| Polybenzimidazole (PBI) |  | 435 | 0.009 | 0.6 | 0.0048 | 0.16 | 0.0018 | 2.0 | 3.5 | 88.88 | 3.75 | 125 | 333.3 | 0.11 | 1.311 |

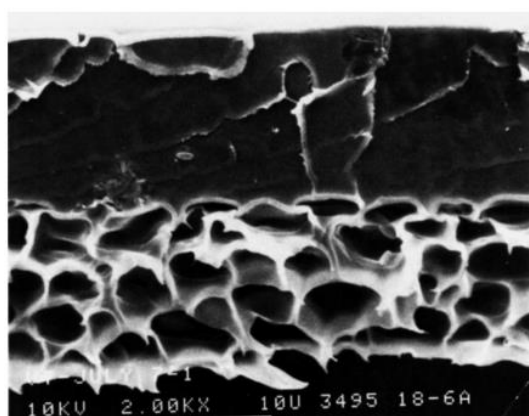
*Permeance in GPU units; T_g : glass transition temperature; FV : Free volume; ρ : density

Table 2.6 The Supported Properties of Polysulfone for Matrix Polymer in MMMs (Roland 2014; Teoh et al. 2016)

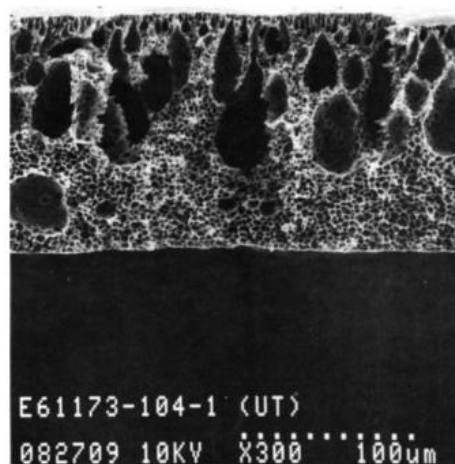
| Characteristics | Description |
|-------------------------------------|---|
| Mechanical strength | PSF can maintain high strength due to the presence of ether linkage, allowing flexibility to the backbone chain |
| Resistance to chemical environments | PSF exhibits a stable resistance to oxidizing agent, acid solution, alkali, aliphatic hydrocarbons, parafin since the sulphur atom is in the highest state of oxidation and tends to draw electrons from the adjacent benzene rings |
| Thermal stability | PSF exhibits no structural change up to 500°C due to the presence of aromatic nature of diphenylene sulphone |
| Glass transition temperature (Tg) | The existance of the backbone aromatic structure leads to intermediate value of Tg (190-230°C) due to the existence of sulfone group and the rigid backbone structure |
| Amorphous | PSF is amorphous and non-crystallizable polymer, leading to low shrinkage and high dimensional stability upon usage |

Table 2.7 Characteristics of Gas Molecules Used for Gas Separation (Castro-muñoz, 2018)

| Molecule | Kinetic diameter (Å) | Polarizability (Å ³) | Dipole Moment (D) | Quadropole Moment (D Å) |
|-----------------|----------------------|----------------------------------|-------------------|-------------------------|
| CO ₂ | 3.30 | 2.650 | 0.000 | 4.30 |
| CH ₄ | 3.76 | 2.600 | 0.000 | 0.02 |
| H ₂ | 2.89 | 0.80 | 0.000 | 0.66 |
| O ₂ | 3.47 | 1.600 | 0.000 | 0.39 |
| N ₂ | 3.64 | 1.760 | 0.000 | 1.52 |



(a)



(b)

Figure 2.8 Cross section of PSF membranes prepared by (a) dry and (b) wet inversion process. Adapted from Pinnau and Koros (1991)

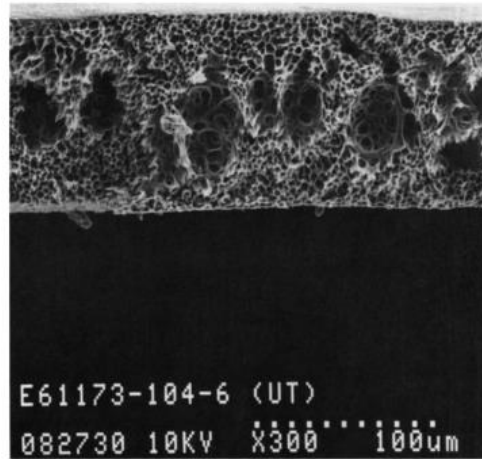


Figure 2.9 Cross section of PSF membranes prepared by dry/wet process. Adapted from Pinnau and Koros (1991)

As previously discussed, asymmetric membrane is preferable structure for gas separation due to its higher gas productivity. The concentration of polymer in a solution plays significant role to produce ultrathin and defect-free on asymmetric membranes. It was found that higher polymer concentration lead to a higher skin layer thickness and decreased larger macrovoids within the membrane (Ismail *et al.*, 2017). This properties result in higher selectivity but less productivity. Ismail *et al.* (2017) investigated the effect of polymer concentration on the overall membrane morphology. All fabricated PSF membranes in Figure 2.10 showed a dense surface layer and porous support. The SEM images revealed that addition of PSF concentration from 20 wt% to 30 wt% altered from a thin skin layer with large finger like macrovoids to a denser skin layer with tear drop macrovoids structure. The development of thin skin layer is occurred due to the spontaneous demixing of solvent and non solvent during the phase inversion. Meanwhile, the formation of large finger like macrovoids in the porous sublayer is due to a faster diffusion of non solvent rate into low concentrated polymer phase than those of solvent diffusion outward (Junaidi *et al.*, 2014). Similar asymmetric properties was also reported by Sidek & Nora (2011). The increased of polymer concentration resulted in a denser and thicker skin layer since a higher viscosity of solution hindered the diffusion exchange between NMP and water in the sublayer, thus leading to the rapid phase separation in the skin layer and the slow solvent

precipitation in the sublayer. Generally, a higher PSF concentration is more favourable to promote more selective but lower productive membrane.

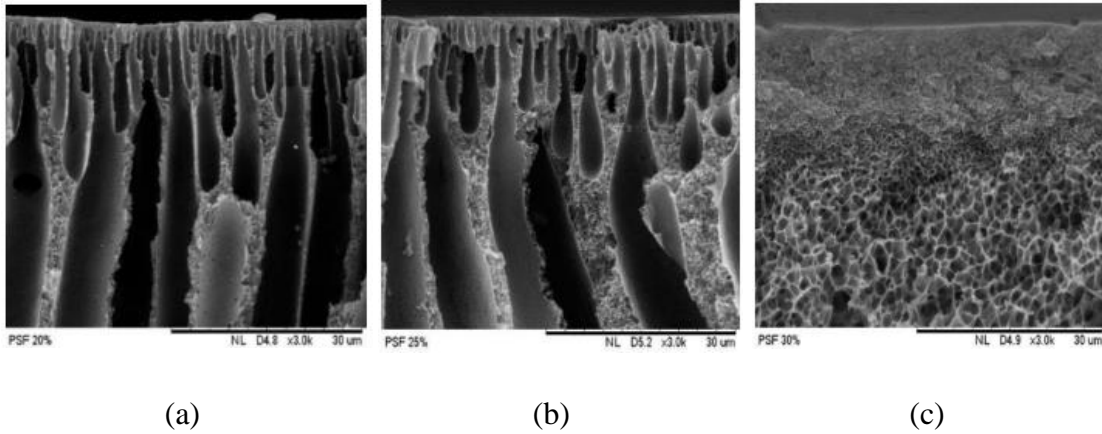


Figure 2.10 The cross section images of PSF membrane at different PSF concentration (a) 20 wt%, (b) 25 wt% and (c) 30 wt% (Ismail *et al.*, 2017)

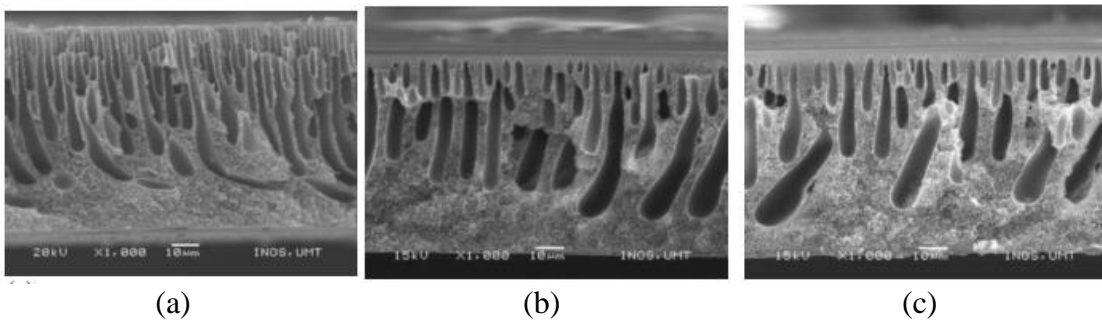


Figure 2.11 The cross section images of PSF membrane at (a) 19%, (b) 21% and (c) 23% PSF concentration (Sidek and Nora, 2011)

However, a highly concentrated solutions (50,000-100,000 cP) are preferable in hollow fiber form to get stable spinning than that of flat sheet form (1,000-2,000 cP) (Pesek and Koros, 1993). Furthermore, high concentrated polymer (> 30 wt%) are preferable to obtain pressure resistance membranes since hollow fiber is self supporting during operation. In addition to the polymer concentration, the optimization of solution components, such as non solvent and volatile solvent in the dope solution is necessary.

In order to produce high flux and defect-free membranes, it is necessary to add a non solvent additive into the dope solution. The non solvent has changed the binodal curve and brought it nearer to polymer-solvent axis, leading to an increase

permeability and selectivity. Aroon et al. (2010) investigated the effects of non solvent on the morphology and performance of PSF gas separation membrane. Figure 2.12(a) exhibits that the PSF membrane with no ethanol possesses a sublayer with finger-like macrovoids structure. This finger-like structure possibly ends at the surface layer and thus leading to the formation of pinholes at the membrane surface. Conversely, Figure 2.12(b) reveals that the membrane has a nodular structure at the sub layer when PSF membrane was made from the ethanol containing dope, reducing the possible formation of pinholes at the membrane surface. Furthermore, the presence of ethanol reduces the surface layer thickness from 560 nm to 340 nm. When ethanol is introduced into the polymer solution, the solidification can rapidly occur in the surface layer and results the membrane with thinner skin layer and uniform structure (Wang *et al.*, 1995). It can be explained that the ethanol in the dope solution would bring the initial composition of solution closer to the precipitation point. As a result, the CO₂ permeance and CO₂/CH₄ selectivity enhanced up to 98% and 100%, respectively when ethanol was employed.

Although the presence of ethanol can improve the CO₂ permeance (7.26 to 14.35 GPU) and CO₂/CH₄ permselectivity from 4.43 to 8.86, this selectivity value is still lower than the intrinsic value of 23.3. This indicated the presence of some defects in the surface membrane. Further improvement needs to be made by using a mixture of volatile and non volatile solvent along with non solvent. A volatile solvent should have a good miscibility with water as coagulant to reduce the solvent volatility (Julian and Wenten, 2012). Tetrahydrofuran (THF) is one of high volatile solvent that are a good water miscible solvent and a strong solvent for PSF. The addition of THF leads to a delayed demixing process during the evaporation step, making the formation of porous membrane in the sublayer and denser membrane structure. Since THF reduced the interaction of solvent and non solvent, the membrane with sponge-like sublayer was formed instead of finger like macrovoids (Junaidi *et al.*, 2014). Figure 2.13 shows that the selective layer thickness of PSF membrane are higher (500 nm) than those of the membrane prepared without THF (Figure 2.12b). The membrane with the less tendency to form finger-like macrovoids structure with thicker skin layer allows the obtained

membrane with less defects and pinholes. The addition of THF increases the CO_2/CH_4 selectivity (12.45 as compared to 8.86) due to a defect free surface layer, while decreasing the CO_2 permeance (4.11 GPU or 2.06 barrer) due to a thicker skin layer. These values are much lower than the intrinsic value in Table 2.5.

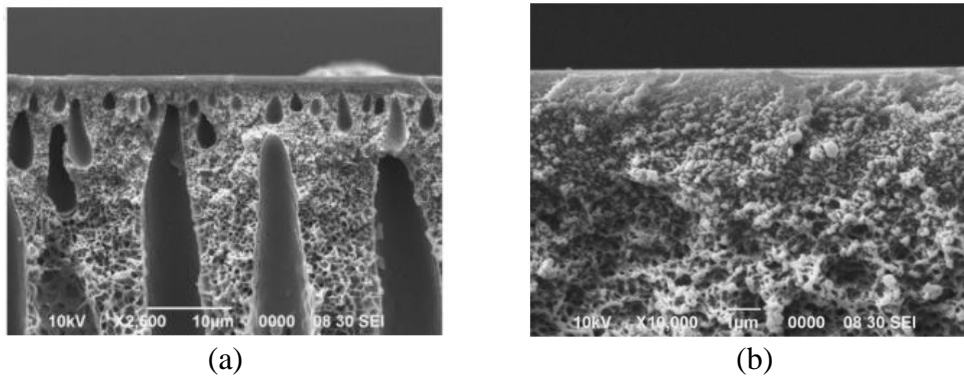


Figure 2.12 The SEM images of PSF membrane made from a dope solution containing of (a) 30 wt% PSF, 70 wt% NMP and (b) 30 wt% PSF, 60 wt% NMP 10 wt% ethanol (Aroon *et al.*, 2010)

However, Pesek & Koros (1993) investigated that a larger amount of ethanol is needed in order to bring near to its boundary due to a stronger NMP solvent for PSF. They suggested that dimethylacetamide (DMAc) is the most convenient candidate as less volatile solvent in order to optimize the skin thickness and to form a defect free membrane structure. Zulhairun, et al. (2014) prepared asymmetric membrane via dry/wet process containing of 30 wt% PSF, 35 wt% DMAc, 30 wt% THF and 5 wt% EtOH. The obtained PSF membrane shows a dense skin layer (250 nm in thickness) containing tear drop macrovoids sublayer. The enhanced performances were found to be enhanced with CO_2 permeance of 19.88 GPU (4.97 barrer) and CO_2/CH_4 selectivity of 23.12. The properties of these PSF membrane are very similar to those in Table 2.5 when DMAc was used as the less volatile solvent. The performance of PSF membrane containing of PSF/DMAc/THF/EtOH exceeded Robeson's upper bound for CO_2/CH_4 separation when proper manufacturing variables were applied, as shown in Figure 2.14.

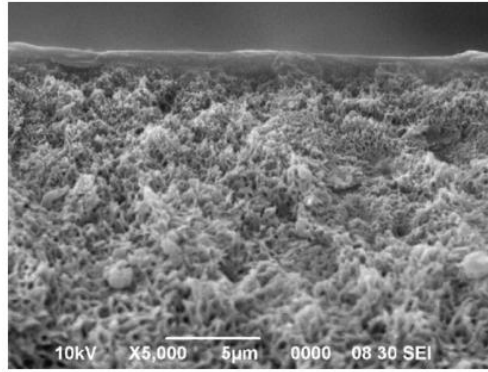


Figure 2.13 The cross sectional image of PSF membrane containing of 30 wt% PSF, 10 wt% EtOH, 45 wt% NMP and 15 wt% THF (Aroon *et al.*, 2010)

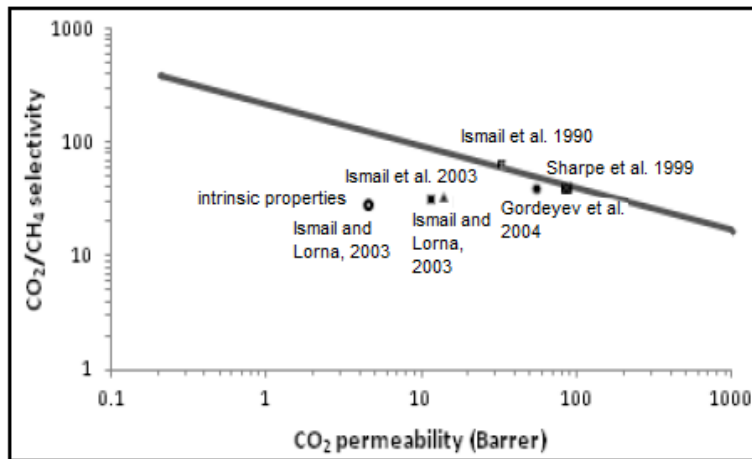


Figure 2.14 The performance of PSF membrane made by dry/wet phase inversion process (Julian and Wenten, 2012)

2.3.2 Inorganic Materials

The incorporation of inorganic fillers inside polymer matrix can significantly alter the gas transport properties of neat polymer itself. For MMMs fabrication, inorganic fillers used can be porous or nonporous materials. When porous inorganic applied, separating gases is based on the different size or shape (molecular sieving effect). In case of larger pore size of particles than the molecule size, adsorption and selective surface flow mechanism is also to be considered (Bastani *et al.*, 2013). The obtaining membrane is represented by higher permeance and selectivity of desired molecules. While, dense inorganic fillers lead to low diffusion of larger molecules and increase of matrix tortuous pattern. The resulting membrane is characterized by high selectivity, but low

permeability (Yeo *et al.*, 2012). The use of fillers for gas separation MMMs is dominated by porous inorganic materials (Dong *et al.*, 2013).

The effect of inorganic particles on the MMMs properties depends to their structure and the type of particles (Aroon and Ismail, 2010). Most inorganic fillers is selected based on their gas sorption behavior rather than their transport behavior. It can be attributed as (1) more adsorbable gas decreases the concentration gradient of less adsorbable component, and (2) more adsorbable gas reduces the diffusion rate of more mobile gas (Dong *et al.*, 2013). High specific surface area, well defined microporous structure and porosity as well as superior adsorptivity are good characteristics of filler candidate for the gas separation MMMs (Dong *et al.* 2013; A K Zulhairun *et al.* 2017; P S Goh *et al.* 2011). Filler material with controlled properties via various forms of surface functionalization offers great prospects to facilitate the selective binding or adsorption of target species. Therefore, the flexible surface functionalization of filler is suitable for this application (Magueijo *et al.* 2013; Zornoza, Téllez, *et al.* 2011).

Several porous inorganic have been applied for membrane filler such as activated carbon (Weigelt *et al.*, 2018), zeolite (Mohamad *et al.*, 2016), carbon molecular sieve (Farnam *et al.*, 2016), metal organic framework (Zulhairun *et al.*, 2015) and carbon nanotube (Ahmad *et al.*, 2014). Several inorganic particles used in MMMs is briefly reviewed in Table 2.9 and the separation performances of polysulfone based MMMs are presented in Table 2.10. However, the existing of such potential fillers have not reached the expectation of current gas separation performance. This is due to several factors such as incomplete separation performance, unfavourable orientation fillers and the issue of polymer filler interaction. New type of fillers are expected to emerge because there are still many structure of filler waiting to be considered. Among the existing fillers, a new class of porous carbon, namely zeolite templated carbon (ZTC) have potential for surpassing Robeson's upper bound owing to its unique properties which is suitable with the filler characteristics. A deep insight of the ZTC structure is indispensable before exploring its application. The detail explanation of ZTC structure related to its potential application as filler membrane will be discussed in the following section.

2.3.2.1 Zeolite Templated Carbon (ZTC)

Porous carbons which have well defined micropore structure is a great demand for some application. Therefore, some efforts to control pore structure have been proposed. Among of them, great attention has been paid to the zeolite templated carbon (ZTC). ZTC possess a unique structure and it totally different with traditional porous carbons. ZTC is synthesized through the controlled pyrolysis of a carbon precursor loaded in the nanochannels of zeolite template. Compared with traditional porous carbon, ZTC posses large surface area (up to 4000 m²/g), well porosity (up to 95%), uniform pores structure as well as easy functionalization (Nishihara & Kyotani 2012; Song et al. 2013; Yabushita et al. 2016). Therefore, structural control of ZTC has attracted a great deal of interest for industrial application such as gas adsorbents (Guan *et al.*, 2009), capacitors (Moon *et al.*, 2015), batteries (Stadie *et al.*, 2017) and catalysts (Yabushita *et al.*, 2016).

The synthesis procedure of the ZTC is shown in Figure 2.15. First, carbon precursor is introduced in the channel of zeolite template, polymerized and carbonized. Then, the zeolite network of composite sample is removed by washing with HF and/or HCl solution to obtain the ZTC. As a consequence, the shape of zeolite template is replicated by the ZTC. Carbon must be uniformly infiltrated into the zeolite nanochannels to ensure the successful synthesis of ZTC. It can be controlled by suitable choice of zeolite template, carbon precursor and the method of carbon filling (Nishihara and Kyotani, 2012). The quality of the resulting ZTC was reported from the previous study, as summarized in Table 2.8.

Zeolites are porous aluminosilicate materials with regular intracrystalline cavities and channels structure. The minimum channel diameter of zeolite is ranging from 0.3 - 1 nm (Wahab *et al.*, 2004). For preparing templated carbon, the pore entrance of zeolite should be large in order to avoid pore blocking upon the carbon filling. The pore entrance contains a ring of O-Si-O chain and its size depends on the number of O atom inside the ring (Nishihara and Kyotani, 2012). The pore entrance of zeolite-Y with 12-membered ring is properly enough to introduce carbon inside the zeolite micro-channels than those of 8-membered rings. In addition, zeolite should have three dimensionally connected framework

to retain structure regularity of the zeolite, as shown in Figure 2.15(c). Enzel and Bien (Enzel and Bein, 1992) investigated that pyrolysis of polyacrylonitrile in the spatial limitation channels of zeolite-Y prevents the formation of graphite structure. Zeolite-Y is a fine choice of template material because of having oxygen 12-membered ring and having three-dimensionally connected pores.

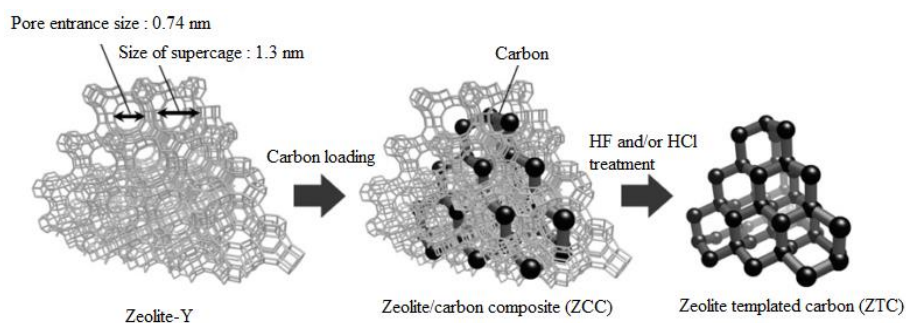


Figure 2.15 Illustration of Zeolite Templated Carbon (ZTC) Synthesis : (a) Structure of Zeolite-Y Template, (b) Structure of Zeolite/Carbon Composite. A Black Framework Represents Impregnated Carbon and (c) Framework Structure of the ZTC After Template Removal (Nishihara *et al.*, 2008)

To synthesize the ZTC, the carbon precursor in the form of a liquid polymer or a hydrocarbon vapor is introduced into the micropores of zeolite template by the methods of impregnation or chemical vapor deposition (CVD) or impregnation-CVD. Impregnation is a simplest and easiest method and no need complicated equipments for synthesize the ZTC. In this method, zeolite channels is filled with liquid monomers and polymerized. A large amount of polymer formed inside pore template is decomposed upon the carbonization process and followed by template removal. However, the resulting carbon is not robust enough to retain structure regularity of zeolite after the zeolite removal and results in lower surface area of ZTC. The quality of resulting ZTC depends on the synthesis parameter such as carbonization temperature and dwelling time, heating ramp profile and flow rate of N_2 (Konwar and De, 2013). For CVD method, hydrocarbon vapor as carbon source is deposited into the zeolite pores below its decomposition temperature. It allows a larger amount of carbon to pass through the zeolite pores compared to those of impregnation method, thus the resulting ZTC frameworks can be stronger with larger surface area. Furthermore, carbon source should be small, thus it can penetrate to the narrow zeolite channels.

Propylene is small hydrocarbon and suitable as CVD source to synthesize high quality of ZTC (Geng et al. 2015; Nishihara et al. 2009). Also, parameter such as temperature, time and concentration of CVD source also significantly determine the properties of the ZTC (Nishihara and Kyotani, 2012). However, the CVD process is difficult for a large scale due to its productivity and a potential danger of explosion at high temperature (Shi *et al.*, 2015). Thirdly, two step method involves of liquid monomer impregnation and followed by further CVD process. This method is possible to obtain ZTC with high ordered pore structure having an extremely high surface area, as shown by HRTEM image in Figure 2.16 (Ma *et al.*, 2002a).

Table 2.8 ZTC Properties Prepared Using Different Methods

| Materials | | Preparation method | BET surface area (m ² /g) | Total pore volume (cm ³ /g) | Micropore volume (cm ³ /g) | Ref. |
|---------------------------|-----------------------------|----------------------------|--------------------------------------|--|---------------------------------------|-----------------------------------|
| Zeolite type | Carbon source | | | | | |
| Zeolite-NH ₄ Y | Sucrose | Carbonisation/impregnation | 684 – 1033 | 0.4 - 0.676 | 0.21 - 0.293 | (Sarkar and Bhattacharyya, 2012) |
| Zeolite-10X | Acetylene | CVD | 1303 – 3331 | 0.88 - 1.94 | 0.33 – 1 | (Cai, Li, <i>et al.</i> , 2014) |
| Zeolite-NH ₄ Y | Furfuryl alcohol | Carbonisation/impregnation | 632 – 1886 | 0.303 - 1.314 | 0.011 - 0.513 | (Konwar and De, 2013) |
| Zeolite NaX | Acetylene | CVD | 1941 – 2973 | 1.29 - 1.46 | 0.73 - 1.18 | (Choi <i>et al.</i> , 2015) |
| Zeolite-Y | Furfuryl alcohol | Carbonisation/impregnation | 1245 – 2135 | 0.33 - 0.57 | 0.65 - 1.4 | (Song <i>et al.</i> , 2013) |
| Zeolite-NH ₄ Y | Sucrose | Carbonisation/impregnation | 1500 | 1.30 | 0.78 | (Guan <i>et al.</i> , 2009) |
| Zeolite-Y | Furfuryl alcohol, Propylene | Impregnation-CVD | 1610 – 3800 | 0.77 - 1.70 | 0.60 - 1.58 | (Nishihara <i>et al.</i> , 2009) |
| Zeolite-NaY | Furfuryl alcohol, Propylene | Impregnation-CVD | 3751 | 1.512 | 1.154 | (Geng <i>et al.</i> , 2015) |
| Zeolite-β | Acetylene | CVD | 757 – 1127 | 0.58 - 0.75 | 0.16 - 0.29 | (Antoniou <i>et al.</i> , 2014) |
| Zeolite-NaY | Glucose | Carbonisation/impregnation | 1173 – 1562 | 1.15 - 1.78 | 0.46 - 0.58 | (Shi <i>et al.</i> , 2015) |
| Zeolite-USY | Sucrose | Carbonisation/impregnation | 1038 - 1218 | 0.731 - 1.068 | 0.414 - 0.498 | (Cai, Yang, <i>et al.</i> , 2014) |
| Zeolite-Y | Sucrose | Carbonisation | 1254 | 0.95 | 0.09 | (Gunawan, 2018) |

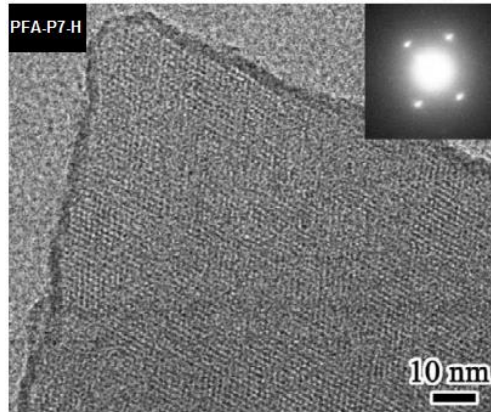


Figure 2.16 HRTEM images of ZTC prepared through impregnation-CVD method (adapted from Ma et al. (2002))

The pore size distribution of ZTC calculated by the density functional theory (DFT) method is shown in Figure 2.17. The ZTC prepared using impregnation method (Figure 2.17a) showed the major contribution of pores with the size above 1 nm and the sharp peak about 1.2 nm. Figure 2.17b represents the pore size distribution of ZTC synthesized via impregnation-CVD method. It confirmed that ZTC's possess a very sharp and intense peak at around 1.2 nm. Though all ZTC's have similar intense peak, the ZTC synthesized from impregnation method has a broader distribution due to its poor structure regularity.

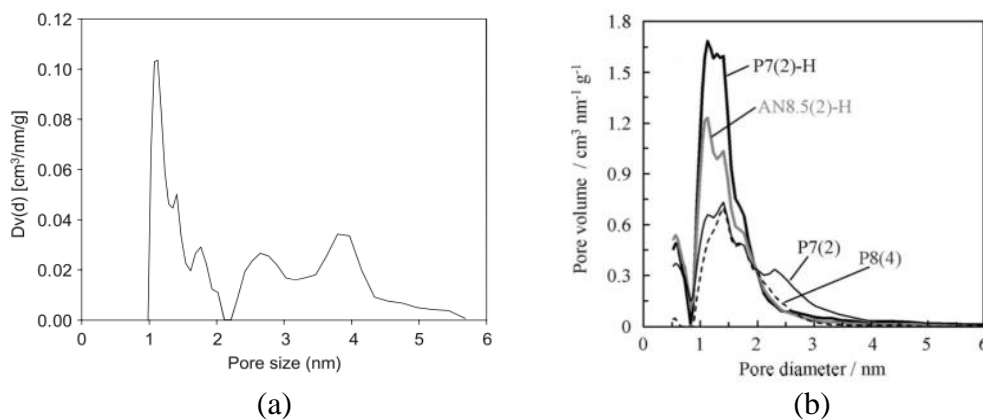


Figure 2.17 Pore size distribution of ZTC prepared using (a) impregnation (Guan et al., 2009); (b) impregnation-CVD method (Nishihara et al., 2009)

There are a lot of literatures reporting about this material. However, there is a few literature discussing the structure of ZTC deeply. Nishihara et al. (2008)

have proposed a molecular model for ZTC using molecular orbital theory combined with analysis results, as illustrated in Figure 2.18. The ZTC is comprised by single curved graphene sheets assembled into a three dimensionally regular network. The existence of such curved graphene sheets is possible because the sheets is forced into the spherical cavities (1.3 nm) of the zeolite-Y supercage and the pore entrance of 0.74 nm. By calculation on the model, the inner diameter of curved graphene is ranging from 0.9-1.3 nm and the pore size is in the range of 1-1.7 nm. Thus, the ZTC is being unique among any other nanoporous carbons, in which stacked graphene sheets constitute the pore walls. As shown in Figure 2.18(a), all the radical edge sites of ZTC easily react with water in the air or HF solution and then saturated by oxygen or hydrogen species (Nishihara *et al.*, 2008). After the addition of large quantity of oxygen atoms, Figure 2.18(b) shows that the edge sites of the ZTC are stable and occupied by different functional groups (66 mol% ether, 15 mol% phenol, 15 mol% acid anhydride and 4 mol% carbonyl group).

Such properties render the ZTC not only suitable for application such as gas adsorbents, capacitors, batteries and catalysts, but also for gas separation membrane. Large surface area of the ZTC may increase the adsorption capacity of gases, leading to high gas permeability (Konwar & De 2013; Zornoza, Téllez, et al. 2011). The ZTC have been also evidently proven to be very effective for CO₂ and H₂ gases (Ma et al. 2002b; Sarkar & Bhattacharyya 2012; Balahmar et al. 2016), thus it can enhance the gas separation capacity (Foley, 2014). The heat adsorption of CO₂ on a carbon material is low, thus resulting in a high gas diffusion of CO₂ (Ma et al. 2012). Meanwhile, the interaction between hydrogen and carbon material is based on the van der Waals force and the thermal motion energy of hydrogen was in accordance with the van der Waals force at low temperature (Jin *et al.*, 2007). Also, the electronegativity between hydrogen and carbon has a low range, thus the bonding has a weak dipole moment, leading to a higher gas permeability. A well defined porous array and porosity will ensure high gas permeability and selectivity (Dong et al. 2013; Anson et al. 2004). In addition, the tuneable properties of ZTC can control the surface area, pore volume and pore size distribution via its synthesis conditions.

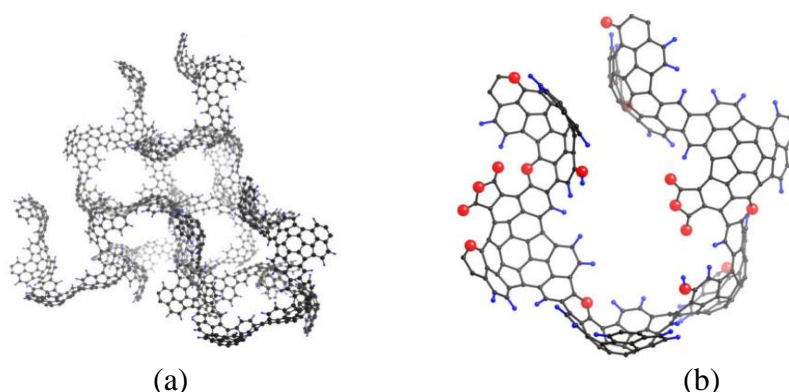


Figure 2.18 An Idealized Model for ZTC (a) Containing Carbon and Hydrogen Atoms and (b) Containing Some Functional Groups. Large Red Spheres Indicate O Atoms (Nishihara *et al.*, 2008)

Another interesting material coming from single synthesis route of ZTC is zeolite carbon composite (ZCC), a preceding material before template removal (Figure 2.15(b)). The ZCC substantially differs from the zeolite carbon composite normally used, in which this composite contains a zeolite with its pores filled by carbon. Zeolite has been found to be advantageous for separating CO₂ from gas mixtures. The adsorption capacity of CO₂ depends on the pore size, surface basicity of zeolite and the electric fields caused by the existence of unexchangeable cations in the zeolite frameworks. The presence of zeolite in base form (Na) will enhance the affinity of CO₂ molecules. Due to a higher quadrupole moment of CO₂, the oxygen sites of CO₂ makes stronger interaction with Na cations on the zeolite surface in Figure 2.19, thus CO₂ gas will be attracted into zeolite pores by van der Waals force (Deng *et al.*, 2012). This characteristic is predicted to improve selectivity and adsorption capacity for CO₂. Meanwhile, carbon that obtained from carbonization possesses high adsorption capacity of CO₂ at ambient pressure and the heat of adsorption of CO₂ on carbon is lower than those of zeolite (Ma *et al.*, 2012). Thus, the presence of carbon inside the zeolite channels may results in high gas diffusion of CO₂. These characteristics of ZCC are predicted to be suitable as membrane filler. However, none of the literatures paid attention to utilizing this material in the application of gas separation.

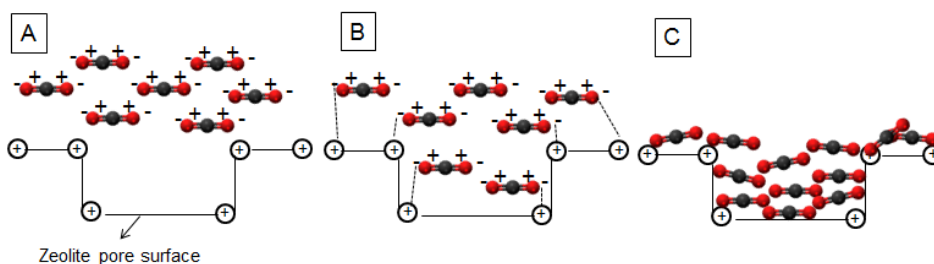


Figure 2.19 The illustration of CO₂ interaction with zeolite surface

In this work, porous carbon with sucrose as precursor in the presence of zeolite-Y by a simple impregnation technique is prepared. Sucrose is a kind of small organic molecules, a green chemical and low cost. The as-synthesized ZTC will be used to fabricate asymmetric polysulfone hollow fiber membranes. The other ZTC prepared using impregnation-CVD method as well as ZCC with distinct pore properties will also be used to compare their effects on the gas permeation performance.

Table 2.9 The Properties of Inorganic Fillers

| Inorganic material | Structure | Potential properties as filler | Drawbacks | Ref. |
|-------------------------|--|---|--|---|
| Zeolite | <ul style="list-style-type: none"> The uniform pore structure and channel diameter in the range of 3-10 Å The interconnected cavities by pore openings | <ul style="list-style-type: none"> The size and shape selective ability with the presence of molecular-sized cavities and pores The capability to selectively adsorb gases by polarity | <ul style="list-style-type: none"> The rigid nature makes the difficulty to form continuous and defect free membrane The presence of water in the separation process tends to blockage the pores due to the hydrophilic surface properties The hydrophilic in nature needs further modification to improve interfacial adhesion and gas selectivity | (Shekhawat et al. 2003; Yeo et al. 2012; P S Goh et al. 2011) |
| Activated carbon | <ul style="list-style-type: none"> Large pore size and pore volume High surface area (>500 m²/g) | <ul style="list-style-type: none"> High surface area ensures higher sorption capacity of gases | <ul style="list-style-type: none"> Wider and poorly pore size distribution leads to low gas diffusion and selectivity | (Konwar & De 2013; Zulkhairun et al. 2017; Dong et al. 2013) |
| Carbon molecular sieve | <ul style="list-style-type: none"> High porosity and surface area Good pore size distribution (<1 nm) Having large opening with narrow necks | <ul style="list-style-type: none"> Superior adsorptivity for some specific gases High porosity and fine pore size distribution lead to high selectivity The gas transport through porosity of permeable CMS also allows gas permeation The constrictions of aperture help to transport gas molecules, due to the dispersive and repulsive interaction between gas and carbon atoms Good affinity to glassy polymer without introducing further process | <ul style="list-style-type: none"> The lack of transport improvement due to a dead-end porous structure | (Yeo et al. 2012; P S Goh et al. 2011; Duval et al. 1993; Vinoba et al. 2017) |
| Metal organic framework | <ul style="list-style-type: none"> Consist of transition metal and transition metal oxide connected by organic ligands | <ul style="list-style-type: none"> High surface area contributes to high sorption capacity High porosity ensures high selectivity | <ul style="list-style-type: none"> The presence of inorganic linkers leads to low thermal and chemical stability of membrane | (P S Goh et al. 2011; Perez et al. 2009; Dong et al. |

| | | | | |
|------------------|---|---|---|---|
| | <ul style="list-style-type: none"> • High surface area (>1000 m²/g) • Controlled porosity | <ul style="list-style-type: none"> • High affinity for certain gas and with polymer chains due to the presence of organic linkers • The flexible structure allows the addition of functional groups to modify pore size and chemical properties | <ul style="list-style-type: none"> • Strong interaction between the walls of particles and polymer creates interfacial stress, leading to cavity structure and polymer veins (plastic deformation) • Strong contact between two phase is not strong enough to break the agglomeration | 2013) |
| Carbon nanotubes | <ul style="list-style-type: none"> • High surface area • Made of graphitic sheets and rolled into a tube • Having a tubular structure with nano scale diameter and high length/diameter ratio • The SWNTs inside diameter of 0.4-1 nm and length up to centimeters • The MWNTs inside diameter of 5-10 nm, length of 20-500 μm, thickness of 50-90 μm and inter tube distance of 0.35 nm | <ul style="list-style-type: none"> • High surface area enhance a high sorption capacity of gas • The nanotube inner cores acts as channel for transport of light gases, resulting in high gas permeability | <ul style="list-style-type: none"> • Tend to form bundles in nature due to the strong inter tube Van der Walls and restricts a good dispersion within the matrix • The vertically aligner of CNT behaves like pinholes, allowing rapid transport without selectivity | (Cong et al. 2007; Nejad et al. 2016; Ismail et al. 2008) |

Table 2.10 Separation Performance of MMMs Incorporated Various of Particles

| Polymer | Filler loading | Operating condition | | Gas testing | Separation performance | | Ref. |
|---------|--------------------------|---------------------|---------|--|---|--|---------------------------------|
| | | T (°C) | P (bar) | | Neat | MMM | |
| PSF | Carbon nanofiber (1 wt%) | RT | 4 | CO ₂ /CH ₄ O ₂ /N ₂ | $\alpha = 3.73$; P _{CO₂} = 0.71 $\alpha = 1.61$; P _{O₂} = 0.31 | $\alpha = 12.17$; P _{CO₂} = 4.87 $\alpha = 3.86$; P _{O₂} = 2.24 | (Kiadehi <i>et al.</i> , 2015) |
| PSF | Carbon xerogel (5 wt%) | RT | 5 | CO ₂ /CH ₄ O ₂ /N ₂ | $\alpha = 1.02$; P _{CO₂} = 187* $\alpha = 1$; P _{O₂} = 135 | $\alpha = 1.2$; P _{CO₂} = 262 $\alpha = 1.13$; P _{O₂} = 175 | (Magueijo <i>et al.</i> , 2013) |
| PSF | CMS (20 wt%) | - | - | O ₂ /N ₂ | $\alpha = 5.50$; P _{O₂} = 1.58 | $\alpha = 5.97$; P _{O₂} = 7.96 | (Ismail <i>et al.</i> , 2009) |
| PSF | SWCNTs (5 wt%) | 35 | 4 | CO ₂ /CH ₄ | $\alpha = 23.55$; P _{CO₂} = 3.90 | $\alpha = 18.82$; P _{CO₂} = 5.12 | (Kim <i>et al.</i> , 2007) |
| | | | | O ₂ /N ₂ | P _{O₂} = 0.84 ; $\alpha = 4.94$ | P _{O₂} = 1.16 ; $\alpha = 5.04$ | |
| PSF | Zeolite SAPO-34 (10 wt%) | RT | 3.48 | CO ₂ /CH ₄ | $\alpha = 17.3$; P _{CO₂} = 22.01* | $\alpha = 28.2$; P _{CO₂} = 314.02* | (Junaidi <i>et al.</i> , 2014) |
| PSF | Zeolite T (3 wt%) | RT | 2 | CO ₂ /CH ₄ | $\alpha = 2.63$; P _{CO₂} = 12.33* | $\alpha = 3.37$; P _{CO₂} = 78.90* | (Mohamad <i>et al.</i> , 2016) |
| PSF | MIL-101 (24 wt%) | - | - | CO ₂ /CH ₄ | $\alpha = 20$; P _{CO₂} = 5 | $\alpha = 25$; P _{CO₂} = 35 | (Jeazet <i>et al.</i> , 2013) |
| PSF | ZIF-8 (0.5 wt%) | | | CO ₂ /CH ₄ | $\alpha = 21.27$; P _{CO₂} = 19.83* | $\alpha = 23.16$; P _{CO₂} = 29.19* | (Abdul <i>et al.</i> , 2015) |

*Unit in GPU
Other, in barrer

2.4 Post-treatment for Defect Free of MMMs

In addition to the appropriate membrane materials and the dope solution components, the other MMM challenges are to guarantee interfacial defect free between polymer and particle and to obtain better dispersion of inorganic particle inside the polymer matrix. The strategy in the fabrication of MMM is necessary to overcome these challenges, ensuring the membrane integrity and separation performance (Dong *et al.*, 2013).

Increasing the amount of inorganic particle loading is often hindered by the formation of particle agglomeration. These agglomeration can induce some voids within the particle agglomeration which can not be penetrated by polymer chain. As a consequence, such voids will provide the extra pathway for gas molecules to transport through, leading to the selectivity decrement of the membrane (Dong *et al.*, 2013). Junaidi *et al.* (2014) reported that well dispersion of SAPO-34 particles within polysulfone matrix was obtained for zeolite loading less than 10 wt% with selectivity improvement of CO₂/CH₄ and O₂/N₂ up to 63% and 58%, respectively. However, large aggregation (> 2 μm in diameter) at higher SAPO-34 content (20 - 30 wt%) were observed in Figure 2.20, leading to the selectivity decrement up to 83% for both separation as a result of agglomeration.

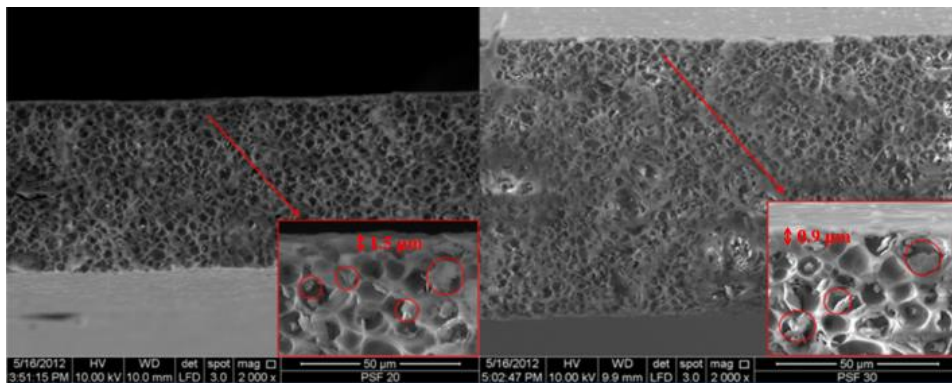


Figure 2.20 The cross section images of PSF/SAPO-34 at 20 wt% (left) and 30 wt% (right) (Junaidi *et al.*, 2014)

The common approach to prevent aggregation is prime process (Mahajan and Koros, 2000a). Priming the inorganic particles involves adsorbing a layer of polymer into the particle surface. In this process, the particles are dispersed in solvent and then sonicated, followed by the addition of a small portion of

polymer. Then, the remaining polymer is added gradually into the primed solution (Bastani *et al.*, 2013). Mahajan & Koros (2000) observed that primed zeolite were found to be different with the unprimed zeolite and they were much easier to disperse in toluene solvent. Vu *et al.* (2003) was reported that MMM exhibited increasing selectivity up to 45% in CO₂/CH₄ selectivity when prime process was employed.

The polymer particle interface is another challenge in the fabrication of MMMs. Low adhesion between two phase results in the unselective voids in some area of selective layer, leading to a less resistant for gas molecules pathway (A. F. Ismail, *et al.* 2008). The formation of voids may be due to the difference in characteristic and density between polymer and matrix (Chung *et al.*, 2007). Thermal treatment is an effective way to minimize or even remove the surface defects (Dong *et al.*, 2013). The membrane is subjected to heat treatment above the glass transition temperature of polymer. At temperature above T_g of polymer, the polymer chain is in the rubber state and become more flexible and mobile, thus caused in enhancing adherence of particles to the polymer (A. F. Ismail, *et al.* 2008). Kusworo *et al.* (2013) prepared PEI/PES/zeolite membrane and then subjected to thermal annealing above T_g and the SEM images of the membrane are shown in Figure 2.21. The SEM image reveals that zeolite well adhered with polymer matrix, leading to high selectivity. Also, the defects on the membrane surface could be suppressed, as shown in Figure 2.21b. After heat treatment, MMM become more compact in the surface layer and provide a high degree of size and shape discrimination between gas species. This is consistent with decreasing the CO₂ permeance of 56% and increasing CO₂/CH₄ selectivity. Ferreira and Trierweiler (2009) also investigated the effects of thermal annealing on the morphology of matrimid/PSF/zeolite β membrane and the obtained result are shown in Figure 2.22. The outer layer in Figure 2.22(a) is porous and most of zeolites seems to be loosely attached to the polymer. When the heat treatment is applied, the zeolite/polymer interface and the polymer structure appears to be better condition.

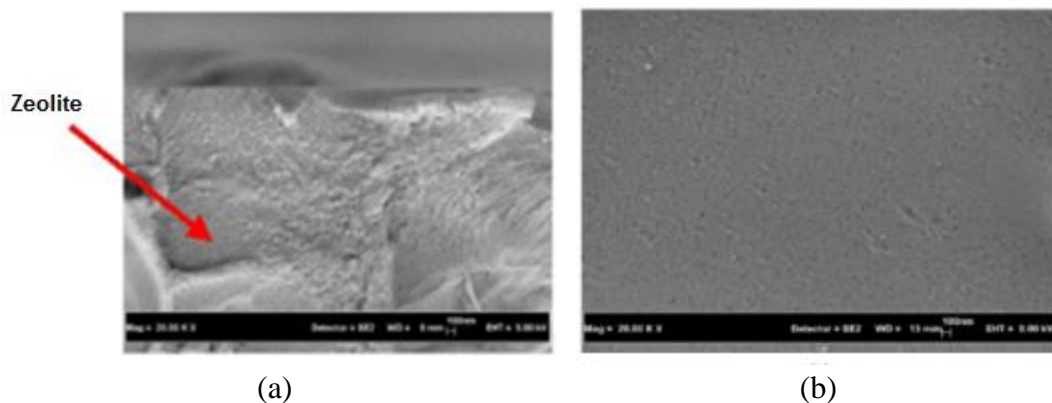


Figure 2.21 The SEM images of (a) cross section and (b) surface of PI/PES/zeolite heated at 280 °C, 2h (Kusworo *et al.*, 2013)

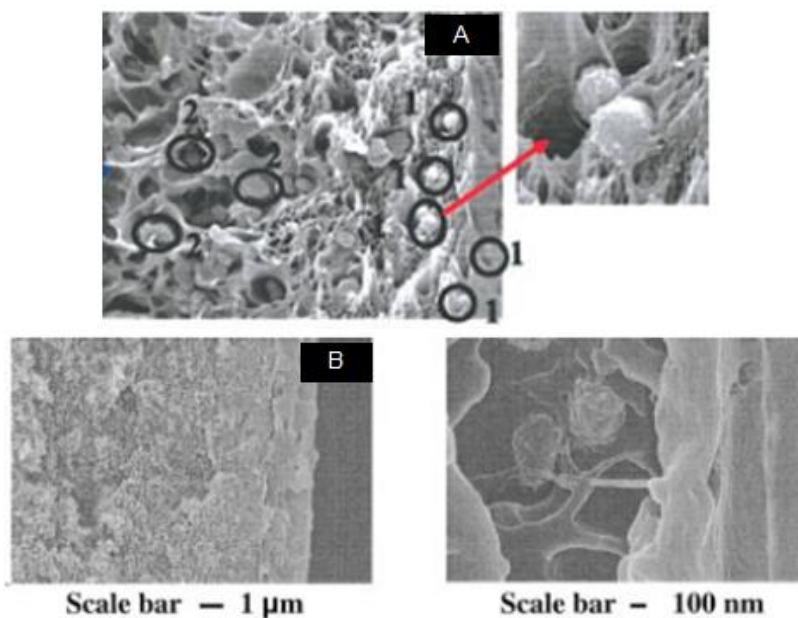


Figure 2.22 The SEM images of Matrimid/PSF/zeolite β (a) before and (b) after heated at 200°C, 2h (Ferreira and Trierweiler, 2009)

Furthermore, immediate and natural cooling after thermal annealing result in different performance of MMMs. Li *et al.* (2005) tried to compare the effects of different cooling of PES/zeolite-A MMM on its morphology and the performance of O₂/N₂ and H₂/N₂ separation. The representative SEM images are presented in Figure 2.23. The interaction between polymer and zeolite of MMM made from natural cooling better improved than those with immediate cooling. The use of immediate cooling causes the polymer chains suddenly frozen since the polymer chains are still in the random condition. This results in a higher free volume in the

polymer matrix and higher permeability with loss in selectivity. Conversely, natural cooling makes the polymer chains harden and shrink slowly and gradually with decreasing of temperature. This leads to high selectivity and low permeability with better adherence of polymer chains onto the particle surface (Ismail, et al. 2008). This confirms that PES/zeolite made by natural cooling showed lower H_2 , O_2 and N_2 permeability, but higher H_2/N_2 and O_2/N_2 selectivity. The effect of thermal treatment on the gas separation properties is also presented in Table 2.11.

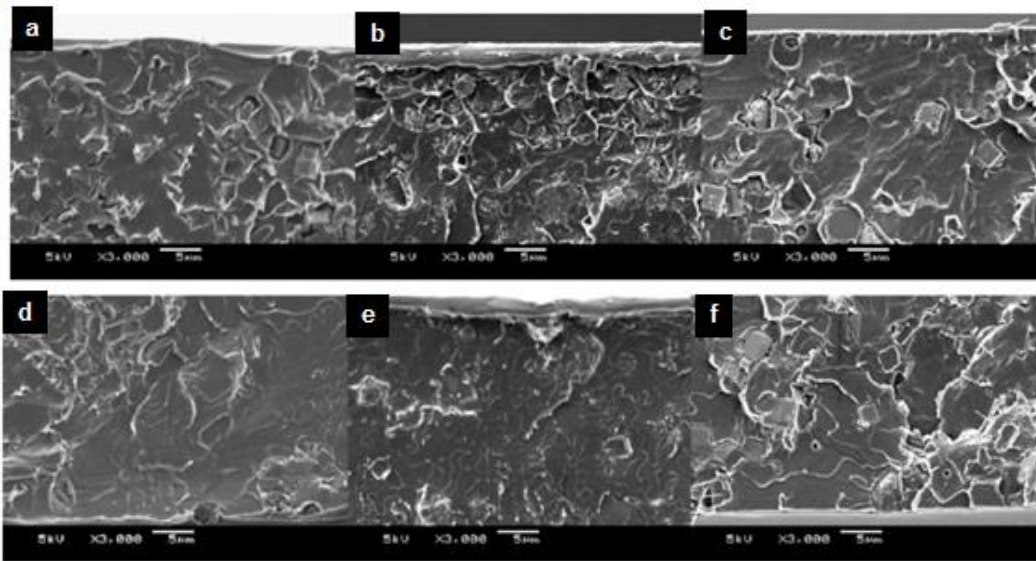


Figure 2.23 The cross section SEM images of (a, b, c) : PES/zeolite 3A, 4A and 5A MMMs with immediate cooling, respectively; (d, e, f) : PES/zeolite 3A, 4A and 5A MMMs with natural cooling, respectively (Ferreira and Trierweiler, 2009)

Surface coating is another attempt to reduce any defects or pinholes on the membrane surface (Vu *et al.*, 2003). The post-treatment coats the membrane surface with highly permeable silicone rubber polymer (PDMS) in order to fill the possible surface voids and improve membrane selectivity for gas separation (Jomekian, Pakizeh, *et al.*, 2011). Pfromm *et al.* (1993) reported the gas permeation with silicone coating substantially defect-free asymmetric polysulfone, polyester carbonate and polycarbonate membranes and compared to dense membrane from the same polymers. The asymmetric membranes exhibited higher selectivity compared to dense membrane. Chen *et al.* 1989 found that

membrane with multiple surface coating exhibited the most efficient performance due to the reduced pore size of porous sublayer with optimal dense thickness.

PDMS possesses weak intermolecular forces which results in broad distribution size of intersegmental gap, promoting high gas diffusion, but low sieving ability. The gas diffusion through PDMS layer is governed by its solubility, as listed in Table 2.12. Marchese et al. (1995) proposed an approximate representation of the coated membrane in Figure 2.24. They assumed that dense layer is partially coated by rubbery polymer and the membrane consists of five regions as follows :

- An ultrathin skin layer with thickness l (labelled 1);
- Pores in the dense layer without coating material, associated with Knudsen diffusion mechanism (labelled 2);
- Pores in the dense skin closed and filled by the coating material (labelled 3);
- Coating material with thickness d (labelled 4);
- A thick and porous sublayer region, the resistance of gas diffusion is considered to be negligible (labelled 5).

Each region is characterized by its own permeability. In order to optimize the separation properties, the pores in the surface of membrane would be completely covered by the coating material diminishing the chance of Knudsen diffusion as gas transport mechanism of the membrane.

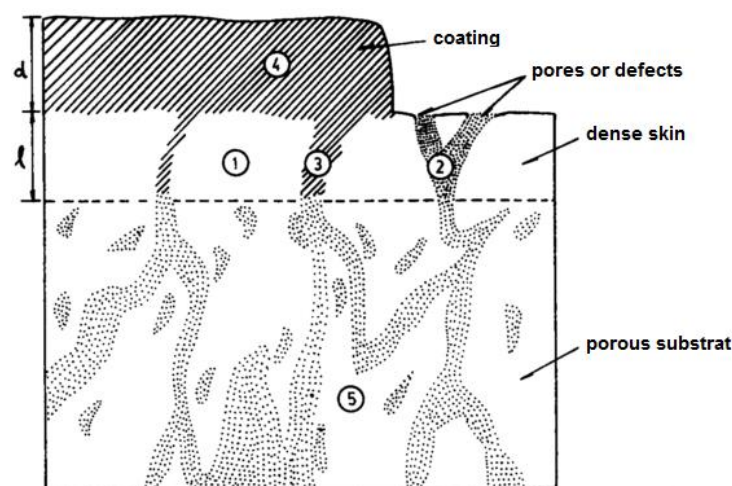


Figure 2.24 The illustration of asymmetric composite membrane partially coated by silicon rubber polymer (Marchese *et al.*, 1995)

Jomekian, Mansoori, et al. (2011) prepared PDMS-coated MCM-48/PSF MMM and the representative SEM images are shown in Figure 2.25. The figure reveals that the surface membrane is fully covered by PDMS layer that removes the possible membrane defects. Also, the cross section confirms no interfacial voids between PSF and particles. The CO_2/CH_4 and O_2/N_2 permselectivities of coated MMM are higher than selectivities for uncoated MMM with no significant reduction in permeabilities. Agustin and Sakti (2010) also investigated the effect of surface coating of polyimide/zeolite MMM on the morphology and permeation properties. The images in Figure 2.26 confirm that coated MMM has defect-free structure. Magueijo et al. (2013) showed the permeation properties of coated membranes closer to the intrinsic characteristics of the polysulfone membrane and improving the selectivity of membrane performance. The effect of surface coating on the gas separation performance is summarized in Table 2.13 and selectivities of coated MMMs significantly enhanced with acceptable permeance. It can be concluded that the introducing silicon rubber into the membrane surface is predicted to seal the defects on the membrane surface structure.

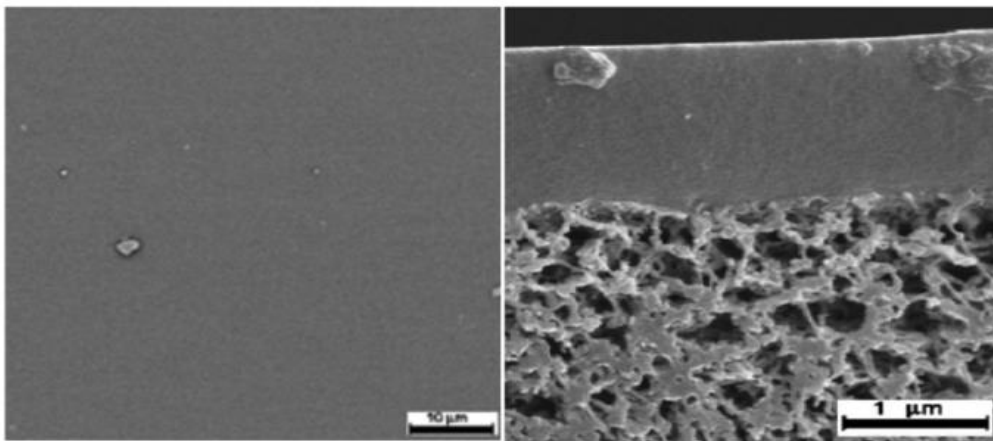


Figure 2.25 SEM images of surface (left) and cross section (right) of 20 wt% MCM-48/PSF MMM coated by 30 wt% PDMS solution (Jomekian, Mansoori, *et al.*, 2011)

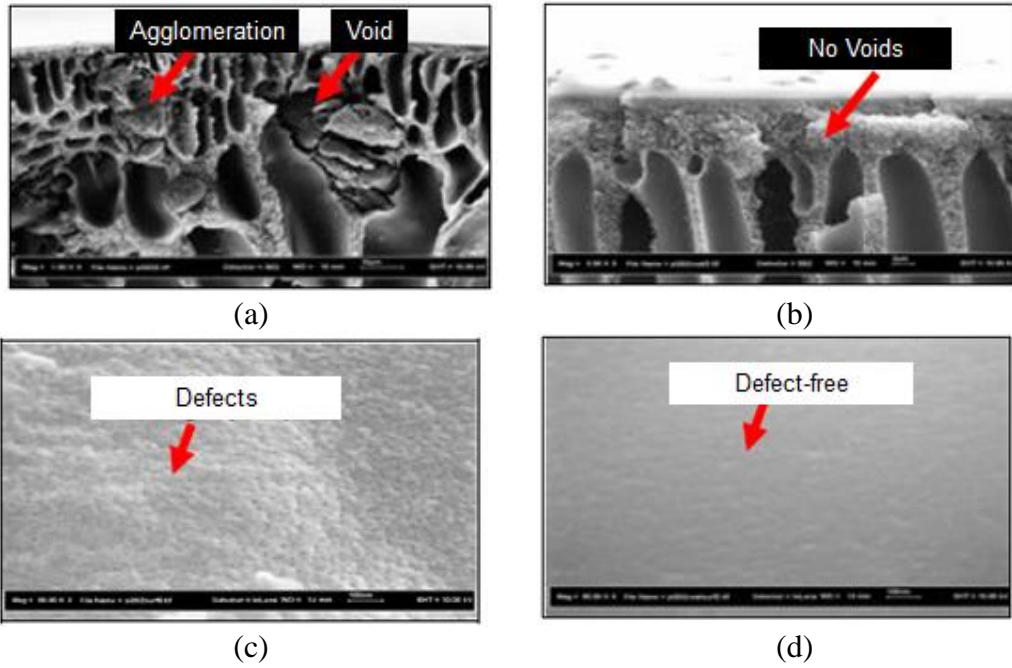


Figure 2.26 The cross section images of (a) uncoated, (b) coated polyimide/zeolite MMMs and surface images of (c) uncoated, (d) coated polyimide/zeolite MMMs (Agustin and Sakti, 2010)

Table 2.11 The Effect of Heat Treatment on the Gas Separation Properties of MMMs

| Membrane | Heat Treatment (HT) | | Gas test | Separation properties | | Ref. |
|------------------------|---------------------|---------|----------------------------------|--|---|---|
| | Temperature (°C) | Time | | Before HT | After HT | |
| PI/PES/zeolite | 280 | 20 min | CO ₂ /CH ₄ | P _{CO2} = 55 ^b α = 17.5 | P _{CO2} = 29 ^b α = 47.5 | (Kusworo <i>et al.</i> , 2013) |
| | 280 | 120 min | CO ₂ /CH ₄ | P _{CO2} = 55 ^b α = 17.5 | P _{CO2} = 25 ^b α = 58 | |
| PES/zeolite-A | 250 | 12 h | O ₂ /N ₂ | - | P _{O2} = 0.375 ^a α = 6.2 | (Li <i>et al.</i> , 2005) |
| PSF/zeolite-β/matrimid | 200 | 2 h | O ₂ /N ₂ | P _{O2} = 206 ^b α = 0.97 | P _{O2} = 0.302 ^b α = 6.1 | (Ying <i>et al.</i> , 2006) |
| PSF/zeolite-β/matrimid | 200 | 2 h | O ₂ /N ₂ | - | P _{O2} = 0.8 ^b α = 6.2 | (Ferreira and Trierweiler, 2009) |
| | 200 | 6 h | O ₂ /N ₂ | - | P _{O2} = 0.75 ^b α = 6 | |
| PES-PI/zeolite-4A | 280 | 12 h | O ₂ /N ₂ | - | P _{O2} = 5.9 ^a α = 4.5 | (A. F. Ismail, Rahim, <i>et al.</i> , 2008) |
| PES-P84/zeolite-β | 220 | 2 h | O ₂ /N ₂ | P _{O2} = 0.0611 ^b α = 6.4 | P _{O2} = 0.0612 ^b α = 6.56 | (A. F. Ismail, Rahim, <i>et al.</i> , 2008) |
| | | | CO ₂ /CH ₄ | - | P _{CO2} = 0.239 ^b α = 32.7 | |
| | 235 | 2 h | O ₂ /N ₂ | P _{O2} = 0.0569 ^b α = 6.4 | P _{O2} = 0.0572 ^b α = 6.60 | |
| | | | CO ₂ /CH ₄ | - | P _{CO2} = 0.183 ^b α = 32.6 | |

^aunit in barrer

^bunit in GPU

Table 2.12 The Solubility of Gases With PDMS (Jomekian, et al. 2011)

| Pure gases | Solubility, $S \times 10^{-2}$ (cm ³ (STP)/cm ³ (mHg)) |
|-----------------|--|
| CO ₂ | 1.75 |
| CH ₄ | 0.27 |
| O ₂ | 0.24 |
| N ₂ | 0.12 |

Table 2.13 The Effects of Surface Coating Parameter on the Gas Separation Properties of MMMs

| Membrane | PDMS concentration | Coating time | Drying time | Gas test | Separation properties (best performance) | | Ref. |
|--------------------|---------------------------|--------------|--------------|----------------------------------|--|--|---------------------------------------|
| | | | | | Uncoated membrane | Coated membrane | |
| PSF | 3 wt% in <i>n</i> -hexane | - | - | CO ₂ /CH ₄ | P _{CO2} = 187 ^a α = 1.02 | P _{CO2} = 84.9 ^a α = 40.3 | (Magueijo <i>et al.</i> , 2013) |
| | | | | O ₂ /N ₂ | P _{O2} = 135 ^a α = 1 | P _{O2} = 84.9 ^a α = 8.35 | |
| PSF/carbon xerogel | 3 wt% in <i>n</i> -hexane | - | - | CO ₂ /CH ₄ | P _{CO2} = 365 ^a α = 0.91 | P _{CO2} = 95.4 ^a α = 39.1 | |
| | | | | O ₂ /N ₂ | P _{O2} = 280 ^a α = 0.96 | P _{O2} = 15.3 ^a α = 7.03 | |
| PSF/TNTs | 3 wt% in <i>n</i> -hexane | 10 min | RT, for 48 h | CO ₂ /CH ₄ | - | P _{CO2} = 120.57 ^a α = 25.93 | (Zulhairun <i>et al.</i> , 2017) |
| | | | | O ₂ /N ₂ | - | P _{O2} = 25.97 ^a α = 6.20 | |
| | | | | CO ₂ /N ₂ | - | P _{CO2} = 120.57 ^a α = 28.76 | |
| | | | | H ₂ /CH ₄ | - | P _{H2} = 269.07 ^a α = 57.86 | |
| PSF/cloisite® 15A | 3 wt% in <i>n</i> -hexane | 10 min | RT, for 48 h | CO ₂ /CH ₄ | - | P _{CO2} = 56.25 ^a α = 40.26 | (Zulhairun, Ng, <i>et al.</i> , 2014) |

| | | | | | | | |
|------------------------|-----------------------------|-------------------|------------------------------|----------------------------------|---|--|---|
| PSF/MCM-41 | 30 wt% in <i>n</i> -hexane | 1. 5 s 2. 30 s | 1. RT, 30 min 2. RT, 12 h | CO ₂ /CH ₄ | P _{CO2} = 31.6 ^a α = 18.51 | P _{CO2} = 26 ^a α = 35 | (Jomekian, Pakizeh, <i>et al.</i> , 2011) |
| | | | | O ₂ /N ₂ | P _{O2} = 5.33 ^a α = 5.38 | P _{O2} = 5.02 ^a α = 7.1 | |
| PSF | 3 wt% in <i>n</i> -hexane | 10 min | RT, for 24 h | CO ₂ /CH ₄ | P _{CO2} = 69.66 ^a α = 2.96 | P _{CO2} = 64.54 ^a α = 28.06 | (Zulhairun <i>et al.</i> , 2015) |
| | | | | CO ₂ /N ₂ | P _{CO2} = 69.66 ^a α = 3.87 | P _{CO2} = 64.54 ^a α = 31.34 | |
| PSF/fumed silica | 3 wt% in <i>n</i> -hexane | - | - | CO ₂ /CH ₄ | - | P _{CO2} = 90.04 ^a α = 32.74 | (Wahab <i>et al.</i> , 2012) |
| | | | | O ₂ /N ₂ | - | P _{O2} = 15.83 ^a α = 6.35 | |
| PSF/zeolite-β/Matrimid | 2 wt% in <i>n</i> -hexane | 30 min | RT, for 48 h | O ₂ /N ₂ | P _{O2} = 4.03 ^a α = 1.03 | P _{O2} = 0.402 ^a α = 5.3 | (Ying <i>et al.</i> , 2006) |
| | 2 wt% in <i>iso</i> -octane | 30 min | RT, for 48 h | O ₂ /N ₂ | P _{O2} = 1.84 ^a α = 1.01 | P _{O2} = 0.0529 ^a α = 5.2 | |
| PES/modified zeolite | 3 wt% in <i>n</i> -hexane | 24 h | 60°C | CO ₂ /CH ₄ | P _{CO2} = 6.67 ^a α = 28.75 | P _{CO2} = 1.62 ^a α = 46.28 | (A. F. Ismail, Kusworo, <i>et al.</i> , 2008) |
| | | | | O ₂ /N ₂ | P _{O2} = 2.71 ^a α = 4.78 | P _{O2} = 0.574 ^a α = 7.26 | |
| PSF/ZIF-8 | 3 wt% in <i>n</i> -hexane | 10 min | 60°C, 12 h | CO ₂ /CH ₄ | - | P _{CO2} = 21.2 ^a α = 34 | (Nordin <i>et al.</i> , 2017) |

^aunit in GPU

CHAPTER 3

RESEARCH METHODOLOGY

This chapter explains the details of some experimental and analytical techniques used to achieve the goals of this research. The experimental aspects including filler preparation and membrane fabrication were conducted. The single and biner gas permeation study were studied in order to investigate the feasibility of filler materials for gas separation MMMs. To improve the MMMs performance for gas separation, some treatments of MMM were performed by surface coating and heat treatment process. The details of calculation were also described in this chapter.

3.1 Materials

Sodium aluminate powder (NaAlO_2) and sodium silicate solution (Na_2SiO_3), both provided by Sigma Aldrich, sodium hydroxide pellets (NaOH , 99% pa purchased from Merck) and deionized water were used to synthesize zeolite-Y template. The materials used for ZTC-1 synthesis were sucrose ($\text{C}_{12}\text{H}_{22}\text{O}_{11}$ 98% Fluka) as the carbon source, sulfuric acid (H_2SO_4 , 98% pa), fluoric acid (HF , 48% purchased from Merck), hydrochloric acid (HCl , 37% SAP), distilled water and nitrogen gas with purity above 99.999%. While, the ZTC-2 was synthesized using zeolite-Y template (Na-form, HSZ320NAA) supplied by Tosoh. Polysulfone (Udel-P3500) supplied by Amoco Chemicals (USA) was selected as polymer matrix. *N,N*-dimethylacetamide (DMAc, 99% provided by Merck) and tetrahydrofuran (THF, 99.8% supplied by QreC) were used as non volatile and volatile solvent, respectively. Ethanol (EtOH) was selected as non solvent additive provided by Merck. *N*-Methyl-2-pyrrolidone (NMP) chosen as bore liquid coagulant was purchased from QreC. Methanol (MeOH , 99.9% procured from Merck) was used for hollow fiber membrane post treatment. Silicon elastomer base and curing (Sylgard 184) from Dow Corning (USA) and *n*-hexane solvent from Merck were used to coat the membranes. Pure gases (O_2 , N_2 , CO_2 , CH_4 and

H₂, 99.99%) were purchased from Mega Mount Industrial Gases Sdn Bhd, Malaysia for single gas permeation test.

3.2 Preparation of Zeolite Templated Carbon (ZTC)

The zeolite-Y template was synthesized using three type of gel composition : seed gel, feedstock gel and overall gel (Zones and Yuen, 2016). The seed gel was prepared with molar composition of 10.67Na₂O:1Al₂O₃:10SiO₂:180H₂O and the molar ratio of feedstock gel to seed gel was 18. For preparing seed gel, NaOH was dissolved in deionised water followed by adding NaAlO₂ and stirring until homogeneous. The preparation of feedstock gel was conducted by similar steps. The feedstock gel was then mixed with 16.5 g seed gel to form the overall gel. Then, the mixture was poured into the stainless steel autoclave and left for 24 h at room temperature followed by hydrothermal process at 100 °C for 7 h. The wet solid product was filtered and washed using deionised water to get pH of filtrate below 9, followed by drying at 110 °C for 12 h. Prior to use, the zeolite-Y was treated at 200°C for 4 h under N₂ stream to release trapped water.

Sucrose impregnation : About 12.5 g of sucrose was dissolved in 50 mL of 0.35 M sulfuric acid and 10 g of pretreated zeolite-Y was then added to this clear solution (Kayadoe & Nurul, 2013). The zeolite-Y can maintain its structure from H₂SO₄ up to 5 M without complete dissolution (Wang et al. 2016). The solution was stirred for 72 h at room temperature. The resulted wet solid was then filtered followed by carbonization process. The carbonization was conducted in a tube furnace under N₂ flow to a fixed temperature of 800°C and 2°C/min for a heating rate for 4 h, then cooled until room temperature using N₂ stream. The material obtained is called as zeolite-carbon composite (ZCC-1). Based on our previous finding, the ZCC-1 was washed using three steps of acid treatment for template removal. Firstly, about 8 g ZCC-1 was treated by 50 mL of 5% HF solution for 1 h for silica removal from template framework. The sample was then filtered and washed with deionized water until pH of decanted solution was neutral followed by drying at 110°C for 12 h. Secondly, 5 g of composite sample was refluxed in 50 mL concentrated HCl at 60°C for 1 h to dissolve aluminium content in zeolite framework, then washed until pH 7 with deionized water followed by drying at

120°C for 12 h. Subsequently, about 3 g solid sample was soaked in 50 mL of 48% HF for 1 h to totally remove the zeolite framework, followed by washing with deionized water until neutral pH of filtrate. The solid sample called as zeolite templated carbon (ZTC-1) was then dried at 120°C for 12 h.

FA impregnation-CVD : zeolite-Y channels were first impregnated with furfuryl alcohol (FA). The dried zeolite-Y was placed in a flask and dried at 200 °C under vacuum for 6 h. Liquid FA was then put into the flask under reduced pressure. Then the pressure was returned to atmospheric pressure by flowing N₂ into the system. The mixture was stirred at room temperature for 3 h, and subsequently filtered, followed by washing with mesitylene to remove residual FA on the external zeolite surface. The washing process was repeated three times. The FA polymerization was conducted by heating at 150°C for 24 h under a N₂ flow. The obtained zeolite/PFA composite was heated at 700°C for 2 h to carbonize PFA in the zeolite channels. Then, the propylene gas (4% in N₂) was passed through the reactor and kept for 2 h. The thermal decomposition of propylene resulted in pyrolytic carbon deposition in the zeolite channels. The prepared zeolite/carbon composite was further heat treated at 900°C for 3 h under a N₂ flow and the obtained sample is referred to a ZCC-2. The zeolite framework in the composite sample was dissolved by washing with an excess amount of 46% aqueous HF solution at room temperature for 5 h. The sample was then filtered and washed with pure water three times, followed by drying. The obtained black solid is referred to a ZTC-2.

3.3 Membrane Preparation

For MMMs preparation, a certain amount of ZTC-1 was suspended in 30 g DMAc via sonication. To achieve better dispersion, the suspension was further sonicated with Q125 Micro-tip sonicator (amplitude 100%, 2s elapsed time) for a certain time, depending on the amount of filler loaded. 30 g of THF was added into the suspension and put in ultrasonic bath for 10 min for sonication process. 30 g of PSF was then added through three parts for priming purpose and the solution was further stirred to obtain homogeneity. About 10 g ethanol was added dropwise into the mixture solution with vigorously stirring. At last, the resulting

mixture was sonicated in an ultrasonic water bath for 1 h and left for 24 h at room temperature to remove microbubbles. The loading of ZTC-1 in MMMs was adjusted to 0.25, 0.4; 0.5; 0.7 and 1 wt% on the basis of Equation 3.1.

$$filler\ loading\ (wt\%) = \left(\frac{m_{filler}}{m_{filler} + m_{PSF}} \right) \times 100 \quad (3.1)$$

where m_{filler} and m_{PSF} are mass of filler and PSF in the MMMs, respectively. The dope solution for pure PSF membrane was also prepared using similar steps.

The MMMs were fabricated according to dry-jet wet spinning process using the customized machine (Figure 3.1). The dope reservoir was connected to a spinneret with outer/inner diameter dimensions of 0.8 mm/0.4 mm by a gear pump. The dope flow rate was set at 1 ml/min. Bore coagulant containing 90 vol% NMP and 10 vol% distilled water was simultaneously connected to the spinneret by a syringe pump at flow rate of 0.7 ml/min. The fibers were then extruded from the spinneret and guided into a coagulation bath of water. The dry gap distance between the water and the spinneret was controlled at 4 cm. The hollow fibers were then collected by a wind-up drum at take-up speed of 10 m/min. The obtained fibers were cut and immersed to another water bath for 48 h to remove excess solvent and the water was replaced several times. The fibers were then post treated in methanol for 4 h to reduce the pore collapse and shrinkage during drying process at room condition for 48 h. The membrane preparation is adopted from the previous literatures (Bhardwaj et al. 2003; A K Zulhairun et al. 2017; Wahab et al. 2012).

The optimum loading of ZTC-1 was used to prepare MMMs filled with different ZTC and ZCC (material prior template removal). All MMMs were prepared by same condition.

3.4 Heat Treatment of Fibers

Hollow fiber MMMs after the air drying were heated at 200 °C with a heating rate of 0.6°C/min in a vacuum furnace to reduce the surface defects. Heat treatment was performed for different durations of 30, 120 and 240 min (Ferreira

& Trierweiler 2009; Ying et al. 2006). After this, the fibers were cooled down slowly to room temperature. The treated fibers after being subjected to heat treatment were assembled into lab-scale modules, containing of ten fibers in length of 20 cm prior to testing.

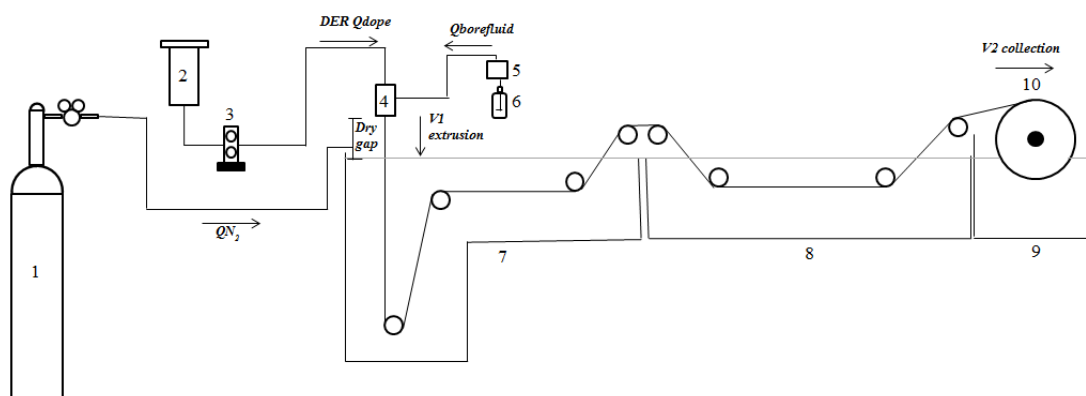


Figure 3.1 Schematic diagram of dry-wet spinning system to prepare the hollow fiber membranes for gas separation : (1) N₂ gas cylinder, (2) dope reservoir, (3) gear pump, (4) spinneret, (5) bore fluid syringe pump, (6) bore fluid reservoir, (7) coagulation bath, (8) washing bath, (9) collection bath and (10) collection drum.

3.5 Membrane Surface Coating

Before subjected to coating treatment, the fibers were potted in a laboratory-scale module containing of five fibers with length of 20 cm. One end of fibers was sealed using epoxy (Loctite E-30CL Hysol Epoxy) and the other side was potted into stainless steel tubes (1/4 in SS 316) with the lumen of fibers open. To prepare 3 wt% PDMS coating solution, 5.46 g elastomer was mixed with 194 g n-hexane. The solution was stirred for 15 min followed by adding 0.54 g hardener. The mixture solution was continuously stirred for 30 min until homogeneous. For membrane coating, the potted fibers were immersed into solution for 10 min followed by drying and curing at room temperature for 48 h.

3.6 Permeation Test

The module design has an outside-in separation configuration with feed gas permeation through the outer surface of fibers and the collected gas permeation through the fiber lumen. The gas permeation was tested for membranes before and

after heating and coating process with single gases to determine the membrane performance. The testing was conducted using customized stainless-steel housing (Figure 3.2) at room temperature with a constant operating pressure of 5 bar. When the gas has permeated through the lumen, the volumetric flow rate was determined using a soap bubble flow meter according to the Equation 3.2 :

$$\frac{P_i}{L} = \frac{Q_i}{A\Delta P} \frac{273.15}{T} \quad (3.2)$$

in which P_i/L represents the permeance of gas in GPU unit ($1 \text{ GPU} = 1 \times 10^{-6} \text{ cm}^3(\text{STP})/\text{cm}^2 \text{ s cm Hg}$), i is the gas penetrant, Q_i is the volumetric flow rate of permeation gas i across the membrane (cm^3/s), ΔP is the trans-membrane pressure gradient (cmHg), T is the temperature of permeation testing (room temperature) and A is the effective membrane surface area according to the Equation 3.3 :

$$A = 2\pi \times r \times n \times l \quad (3.3)$$

where π is the ratio of circumference of a circle to diameter ($\pi = 3.14$), r is the outer radius of fiber (cm), n is the number of fibers in the module and l is the length of fiber. The ideal selectivity was determined by taking the ratio of permeance of the fast gas i over slow gas j , as following equation :

$$\alpha_{i/j} = \frac{P_i/L}{P_j/L} \quad (3.4)$$

The gas permeation data was conducted for at least 4 replicated modules to get the accuracy and reliability of the measurement.

Mixed gas measurements were also conducted for MMMs before coating treatment by using 50/50% CO_2/CH_4 and 50/50% H_2/CH_4 gas mixture at ambient temperature. The gas was fed into the module at 5 bar and allowed to permeate through the outer surface of fibers, while the permeate gas was collected from the fiber lumen, and no sweep gas was used. The gas composition on the permeate side was analyzed by a gas chromatography (model: Shimadzu GC-8A), equipped with a thermal conductivity detector (TCD). The schematic The gas selectivity showing the ability of membrane to separate binary gas mixture was calculated according to the Equation 3.5 (Lin *et al.*, 2015) :

$$\alpha_{a,b} = \frac{y_{a,permeate}/y_{b,permeate}}{y_{a,retentate}/y_{b,retentate}} \quad (3.5)$$

where $y_{a,permeate}/y_{b,permeate}$ is the molar ratio of the components A and B in permeate, respectively, whereas $y_{a,retentate}/y_{b,retentate}$ is the molar ratio of the components A and B in retentate, respectively.

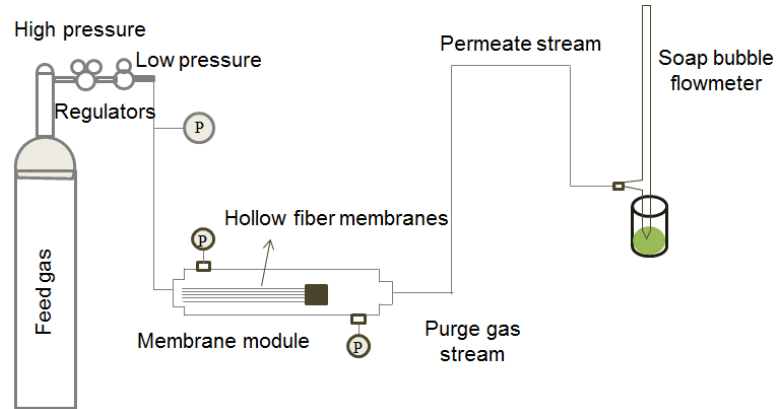


Figure 3.2 Single gas permeation testing rig

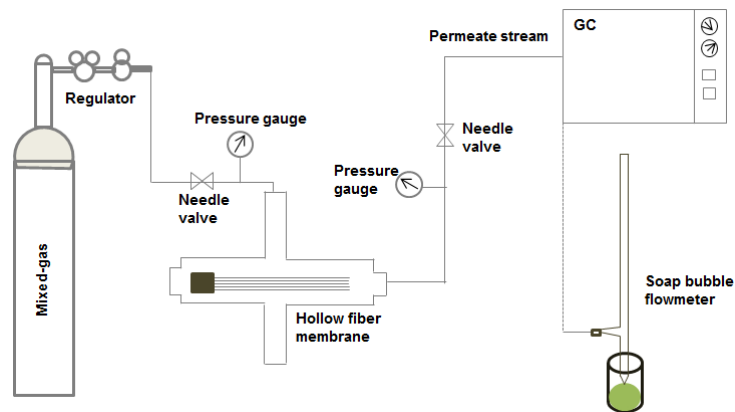


Figure 3.3 Mixed-gas permeation testing rig

Mixed-gas permeation measurement was also employed to determine the true permeation characteristics of the membranes. The non-ideal gas behavior may result the deviation of mixed-gas separation from that of pure gas measurements. The influence of non-ideal gas behavior on the gas transport across the membrane is determined by calculating the fugacity coefficient as follows (Wang *et al.*, 2002):

$$f = \phi p \quad (3.6)$$

where, f and p are the fugacity and pressure, respectively, ϕ is the fugacity coefficient. For a single component, the fugacity coefficient can be determined using the virial Equation 3.7.

$$\ln \phi = \frac{Bp}{RT} \quad (3.7)$$

where, B is obtained from

$$\frac{Bp_c}{RT_c} = f^{(0)} + \omega f^{(1)} \quad (3.8)$$

While, p_c and T_c are the critical pressure and temperature, respectively, ω is the eccentric parameter of the gas. $f^{(0)}$ and $f^{(1)}$ can be obtained from the Equation 3.9.

$$f^{(0)} = 0.1445 - \frac{0.33}{T_r} - \frac{0.1385}{T_r^2} - \frac{0.0121}{T_r^3} - \frac{0.000607}{T_r^8},$$

$$f^{(1)} = 0.0637 + \frac{0.331}{T_r^3} - \frac{0.423}{T_r^3} - \frac{0.008}{T_r^8} \quad (3.9)$$

where T_r is the relative temperature defined as $T_r = T/T_c$. For a binary mixed-gas, Equation 3.7 is rewritten as follows :

$$\ln \phi = \sum_{i=1}^2 k_i \ln \phi_i \quad (3.10)$$

where k_1 , k_2 are the fractions of component 1 and 2 in the mixture, respectively. The fugacity coefficients can be obtained by the Equation 3.11 if the interaction of two gases is considered.

$$\ln \phi_1 = (B_{11} + k_2^2 \delta_{12})p/RT,$$

$$\ln \phi_2 = (B_{22} + k_1^2 \delta_{12})p/RT,$$

$$\delta_{12} = 2B_{12} - B_{11} - B_{22} \quad (3.11)$$

where B_{11} and B_{22} refer to the single component and they can be estimated using Equations 3.8 and 3.9, while B_{12} can be calculated by Equations 3.8 and 3.9 with the empirical combination rules

$$\begin{aligned}
T_{c1,2} &= (T_{c1} \cdot T_{c2})^{1/2}, \\
\omega_{1,2} &= (\omega_1 + \omega_2)/2, \\
z_{c1,2} &= (z_{c1} + z_{c2})/2, \\
V_c &= z_c RT_{c1,2}/V_{c1,2}, \\
V_{c1,2} &= [(V_{c1}^{\frac{1}{3}} + V_{c2}^{\frac{1}{3}})/2]^3, \\
p_{c1,2} &= z_{c1,2} RT_{c1,2}/V_{c1,2} \tag{3.12}
\end{aligned}$$

where z_c and V_c are the critical compressibility and critical volume, respectively. The critical properties of some gases are listed in. These Equations is applied for the conditions below.

$$p \leq T p_c / 2 T_c \text{ for a pure gas,}$$

$$p \leq T(k_1 p_{c1} + k_2 p_{c2}) / 2(k_1 T_{c1} + k_2 T_{c2}) \text{ for binary gas} \tag{3.13}$$

Table 3.1 Critical Properties and Omega Values (Wang *et al.*, 2002)

| Component | T_c (K) | P_c (bar) | ω | Z_c |
|----------------------------------|-----------|-------------|----------|-------|
| CO ₂ | 304.19 | 73.81 | 0.228 | 0.274 |
| CH ₄ | 190.58 | 46.04 | 0.011 | 0.288 |
| CO ₂ /CH ₄ | 204.77 | 58.31 | 0.120 | 0.281 |

3.7 Material Characterizations

3.7.1 X-Ray Diffraction (XRD)

The X-ray diffractograms of zeolite-Y, ZCC, ZTC, neat PSF and MMMs were recorded with radiation of CuK α at wavelength of $\lambda = 0.154 \text{ \AA}$ at 40 kV and 30 mA by Expert PAN Analytical. The X-ray scans were determined ranging from 3-50° to identify the changes on the crystal structure and the intermolecular distances between intersegmental chains of polymer upon the filler adding. The intermolecular (dsp) spacing was calculated using the Bragg's equation.

$$n\lambda = 2d \sin \theta \tag{3.14}$$

3.7.2 Braunauer-Emmett-Teller (BET)

The nitrogen sorption was conducted at $-196\text{ }^{\circ}\text{C}$ by Micromeritics, ASAP 2020 (V4.02 E) to determine the specific surface area and pore volume of zeolite-Y, ZCC and ZTC. While the specific surface area was obtained using Braunauer-Emmett-Teller (BET) method at P/P_0 between 0.06 to 0.27, the total pore volume was determined from the amount of N_2 adsorbed. The pore size distribution (PSD) was determined from the N_2 isotherm via non-local density functional theory (NLDFT) using SAIEUS software of Micromeritics equipment. Prior to analysis, the sample was heated at $250\text{ }^{\circ}\text{C}$ under vacuum for 12 h.

3.7.3 High Resolution Transmission Electron Microscopy (HR TEM)

The microstructure of zeolite-Y, ZCC and ZTC were analyzed using HR TEM H9500 operated at 200 kV acceleration voltage.

3.7.4 Scanning Electron Microscopy (SEM)

The morphology and particle size for zeolite-Y, ZCC and ZTC were examined by SEM (model: SU-3500, Hitachi) operating at 10 kV equipped with an energy-dispersive X-ray (EDX) spectroscopy. The samples were coated with palladium prior to analysis. The particle size distribution was calculated using ImageJ software. The cross section and surface morphology of pure PSF and MMMs were performed using Hitachi TM3000. This analysis was also used to observe the compatibility between particles and matrix as well as particle distribution in MMMs. The surface morphology was further examined using field emission scanning electron microscope (FESEM), made by Carl Zeiss, on the selected MMM samples. In order to get smooth fraction, the cross section of membrane were cut inside liquid nitrogen. The fractured membranes were placed on the carbon tape and coated with platinum before scanning. To confirm the successful coating on the membrane surface and the particle distribution, the SEM equipped with EDX were also performed. The elements observed for PDMS-coated MMM mapping were C, O, S and Si. The detection of Si element can indicate the presence of PDMS layer.

3.7.5 Atomic Force Microscopy (AFM)

The surface roughness properties of all prepared MMMs were also investigated by AFM. The analysis was conducted using AIST-NT, Inc. with a silicone tip cantilever to analyze the specimen area of $2\mu\text{m} \times 2\mu\text{m}$. The membrane roughness was investigated in terms of root mean square and average roughness.

3.7.6 Fourier Transforms Infrared Spectroscopy (FTIR)

The presence of surface functional groups on the ZCC, ZTC, PSF membrane and MMM was analyzed using FTIR (model: Thermo Scientific Nicolet iS10). Powder samples were homogenised with KBr and pressed into a disc. Then, the spectra were recorded over $500\text{-}4000\text{ cm}^{-1}$ at a resolution of 4 cm^{-1} .

3.7.7 Thermogravimetric Analysis (TGA)

In order to investigate the thermal stability of all prepared MMMs, TGA analyses were obtained using a Mettler TGA/SDTA851^c. About 4-5 mg samples were cut into small pieces and loaded in sample crucible. The membranes were heated in a high purity flowing N_2 atmosphere (20 mL/min) within the temperature range $30\text{-}800\text{ }^\circ\text{C}$ at a heating rate of $10\text{ }^\circ\text{C}/\text{min}$.

3.7.8 Differential Scanning Calorimetry (DSC)

To determine the glass transition temperature (T_g) of membranes, DSC analyses were obtained by a Mettler Toledo DSC 822e. The membrane was heated in the temperature range $30\text{-}250\text{ }^\circ\text{C}$ at a heating rate of $10\text{ }^\circ\text{C}/\text{min}$ for twice heating scan. The first heating was aimed to remove the thermal history of sample and the T_g value was measured from the midpoint temperature of the transition region during the second heating.

3.8 Filler Interparticle Spacing and Size of Polymer Molecule

Knowing the weight fraction of filler (C_{filler}) in the MMM, the filler particle weight (M_{particle}), and the densities of polymer (ρ_{polymer}) and filler (ρ_{filler}), the number of filler particles per unit volume of polymer matrix and, thus the

interparticle spacing can be estimated using simple geometry and assuming uniform dispersion.

Density of polymer/filler composite :

$$\rho_{composite} = \frac{\rho_{filler}\rho_{polymer}}{\rho_{polymer}C_{filler} + \rho_{filler}(1-C_{filler})} \quad (3.15)$$

Number of particles per unit volume of membrane :

$$n_{particle} = \frac{\rho_{composite}C_{filler}}{M_{particle}} \quad (3.16)$$

Interparticle spacing :

$$X_{p-p,i} = n_{particle}^{-1/3} \quad (3.17)$$

The interparticle spacing will be compared to the diameter of the particle to determine the adjacency of the inclusions in the polymer matrix. Given the molecular weight of the polysulfone ($M_w = 66,100$), the weight ($M_{ws} = 442$) and approximate length ($X_s = 80 \text{ \AA}$) of each repeating unit in the macromolecular chain, the size of polysulfone molecules can be calculated (Magueijo *et al.*, 2013; Bhardwaj *et al.*, 2003; Hwang *et al.*, 1999).

$$X_{polymer} = X_s \left(\frac{M_w}{M_{ws}} \right)^{1/2} \quad (3.18)$$

Furthermore, in order to know the voids contribution in the membrane as the gas transport mechanism, the Knudsen selectivity was calculated as follow.

$$\alpha_{a,b} = \sqrt{\frac{M_{wb}}{M_{wa}}} \quad (3.19)$$

where M_w is gas molecular weight.

3.9 Summary the Sample Designation

In this study, there are several sample prepared using different treatment. The list of the sample designation is summarized below.

Table 3.2 Sample Designation of Membrane

| Membrane Sample (amount of filler loading, wt%) | Filler type | Membrane treatment | |
|---|---|--------------------|---------|
| | | Coating | Heating |
| PSF/ZTC-1 (0.25, 0.4, 0.5, 0.7, 1 wt%) | Zeolite templated carbon prepared by impregnation | - | - |
| Coated PSF/ZTC-1 (0.25, 0.4, 0.5, 0.7, 1 wt%) | Zeolite templated carbon prepared by impregnation | v | |
| Heated PSF/ZTC-1 (0.25, 0.4, 0.5 wt%) | Zeolite templated carbon prepared by impregnation | - | v |
| PSF/ZTC-2 (0.25 wt%) | Zeolite templated carbon prepared by impregnation- CVD | v | - |
| PSF/ZCC-2 (0.25 wt%) | Zeolite carbon composite (ZTC prior template removal) prepared by impregnation-CVD | v | - |
| PSF/ZCC-1 (0.25 wt%) | Zeolite carbon composite (ZTC prior template removal) prepared by impregnation | v | - |

This page is left blank

CHAPTER 4

SYNTHESIS AND CHARACTERISTICS OF ZEOLITE TEMPLATED CARBON AS MEMBRANE FILLER

This chapter discusses characteristics of Zeolite Templated Carbon (ZTC) that is used as filler for Mixed Matrix Membrane (MMM) in this study. High resolution transmission electron microscopy (HR-TEM), Scanning electron microscopy (SEM), X-ray diffraction (XRD), Raman spectroscopy and BET analysis were conducted for understanding the structural morphology of the synthesized ZTC. The different ZTC with distinct pore properties was also used in order to find the influence of filler structure on the membrane performance. We synthesized the ZTC through different method of carbon filling into the zeolite-Y channels. In this study, there are two types of ZTC, synthesized by impregnation method with sucrose as carbon source, named as ZTC-1, and by combination of impregnation-chemical vapor deposition (CVD), named as ZTC-2.

4.1 Characteristics of Zeolite Templated Carbons (ZTCs)

The ZTC is a structurally engineered carbon having a negative replica of zeolite template, thus its structure is different from traditional porous carbons. The use of zeolite in its synthesis increases the structure regularity of ZTC and keeps the similar morphology as the zeolite. Combined with large surface area and high pore volume, the ZTC was found to be potential in application of hydrogen (H₂) and carbon dioxide (CO₂) adsorption and the results have also exhibited to be beneficial (Stadie et al. 2012; Zhou et al. 2012). With this unique structure, the ZTC ensures higher gas adsorption capacity. Therefore, the ZTC is suited for other gas related application such as membrane gas separation.

In this study, to determine the structure of zeolite-Y template, Zeolite Carbon Composite (ZCC-1, material prior template removal) and ZTC-1, XRD analysis is performed and the results are given in Figure 4.1. Figure 4.1 provides XRD spectra that reveals all diffraction patterns and intensities for zeolite-Y were

matched with the standard data of JCPDS No. : 39-1380 (ICDD, 1997). The typical structure of zeolite-Y was characterized by many sharp peaks at $2\theta = 6.14^\circ$ (111), 15.53° (331), 23.46° (533), 27.56° (551), 31.18° (555). All diffraction peaks of zeolite-Y were still observable in the peak patterns for ZCC-1 with a slight shift to high angle position. The change in the peak direction might be due to a shrinkage of the zeolite framework after carbonization at high temperature (Su *et al.*, 2004). Also, the reduction in peak intensities was observed in the XRD patterns of ZCC-1 sample due to the coverage of zeolite particles by carbon layer (Konwar and De, 2013). Furthermore, the ZTC-1 exhibited a weak and broad XRD peak around 6.05° , indicating poor ordering structure in the carbon originated from (111) plane of zeolite-Y (Ma *et al.* 2000; Kyotani *et al.* 2003). The ZTC also showed a very broad and low intensity peak around 25° , corresponding to the (002) peak from graphitic carbon. The low intensity and broadening of these peak indicates low graphitic level and essentially an amorphous character (Cai, *et al.* 2014). This peak may be due to the presence of some disordered carbon layer at the outside surface of zeolite-Y. Sucrose can partly penetrate through the zeolite-Y channels and the suitable conformation enables to diffuse through the pore window of zeolite-Y (Figure 4.2a). Meanwhile, sucrose with diameter more than 0.74 nm (Figure 4.2b) unables to enter the zeolite channels, resulting in the formation of disordered carbon shell on the zeolite surface. Such external carbon layer could hinder the filling of carbon precursors into the zeolite-Y channels, hence, result in the incomplete carbon filling. Additionally, the disappearance of other zeolite-Y diffractions indicated that the template was successfully removed in the ZTC sample. From the XRD result indicates that ZTC-1 preserve some pore ordering structure of zeolite-Y with some external carbon deposits. These results are comparable to those reported by Cai, *et al.* (2014), who investigated the ZTC synthesis using sucrose impregnation.

The low graphitic degree of ZTC-1 as observed in XRD data is consistent with the Raman spectra (Figure 4.3). The ZTC shows bands at 1354 cm^{-1} and 1585 cm^{-1} , attributing to the D-peak (amorphous carbon) and G-peak (graphitic carbon domain), respectively (Balahmar *et al.*, 2016). The intensity ratio between D-peak and G-peak (I_D/I_G) was 1.25. These value of I_D/I_G is in the range for non

graphitic carbon, indicating the presence of some sp^3 configurations for the carbon element in amorphous carbon (Cai, et al. 2014). However, the graphitic level of sucrose-based carbon in this work is higher compared to that of sucrose-based carbon in the literature (Song et al. 2013). The formation of higher mesopores or the micropores collapse leads to the graphitisation process.

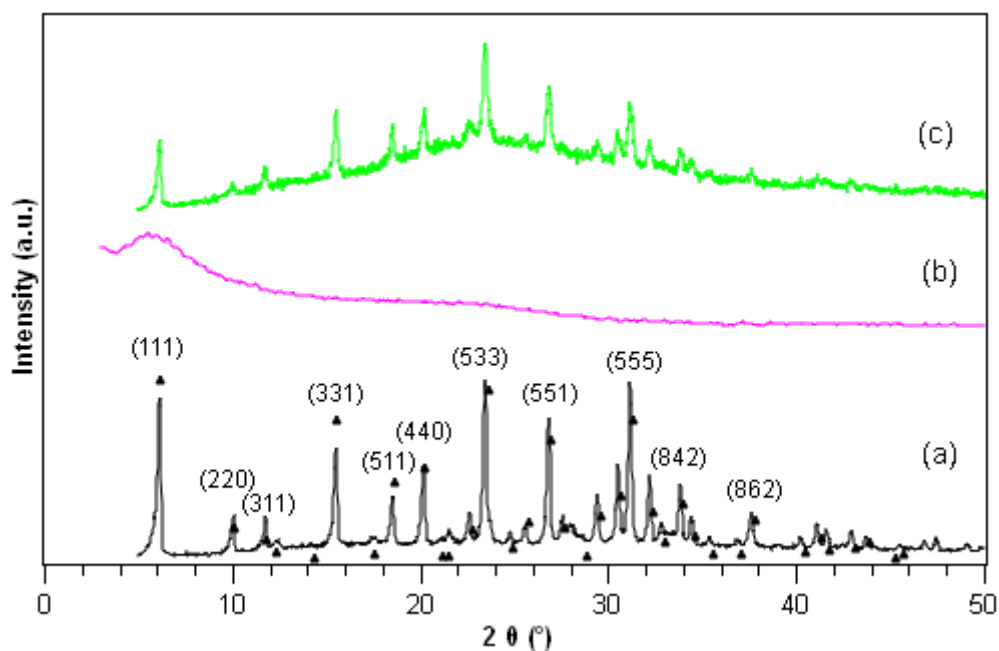


Figure 4.1 XRD spectra of (a) synthesized zeolite-Y, (b) ZCC-1 and (c) ZTC-1 (zeolite-Y standard is indicated by triangle symbol)

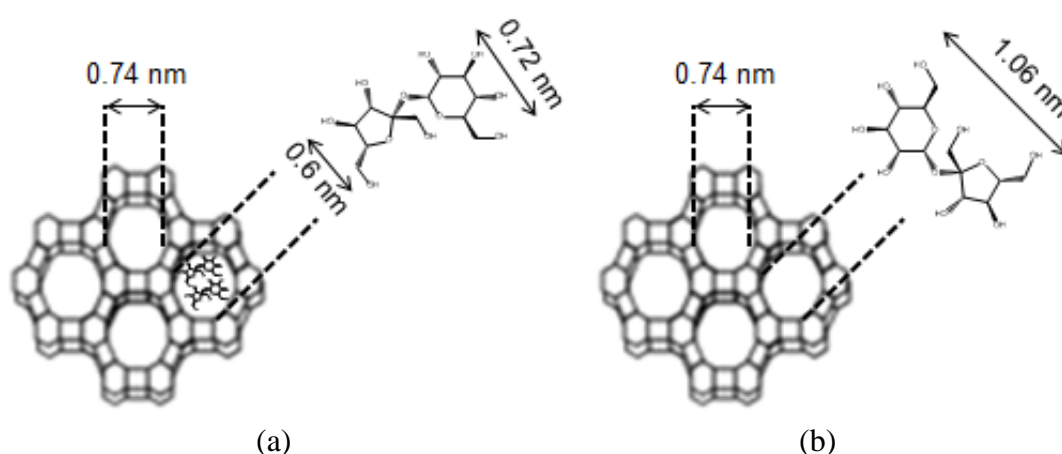


Figure 4.2 The possibility filling of sucrose molecules into the pore window of zeolite-Y

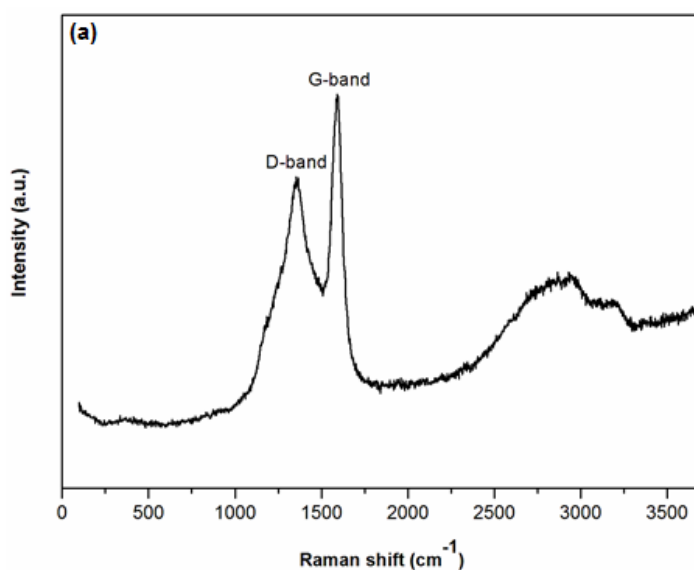


Figure 4.3 Raman spectra of ZTC-1

Figure 4.4 shows the XRD patterns of material prepared by FA impregnation and propylene-CVD over zeolite-Y. In the case of ZTC-2, the XRD pattern exhibits a sharp diffraction at $2\theta = 6.36^\circ$ and also a weak peak at $2\theta = 10.3^\circ$ with corresponding distance of 1.39 nm and 0.43 nm, respectively. These peaks are attributed from the (111) and (220) planes originating from the zeolite-Y, respectively (Nishihara and Kyotani, 2012). The sharp peak suggests that the ordering structure of the ZTC-2 is better than those of the ZTC-1. It is due to that FA possess smaller molecular dimension than the channel size of zeolite-Y template (Figure 4.5). Hence, FA molecules can diffuse and deposit into the zeolite-Y channels. Also, the ZTC-2 did not exhibit any detectable peaks at around 25° and 44° , which originated from the (002) and (100), respectively. The disappearance of these peaks supports that most of the carbon precursor is formed inside the zeolite-Y channels. As a result, the long range ordering structure of the ZTC-2 can be well formed.

The zeolite-Y, ZCC and ZTC used in this study were also characterized using SEM in order to confirm the particle morphology. The corresponding images are exhibited in Figure 4.6. SEM micrograph of the zeolite-Y shows clear octahedral crystal faces from each particles. The histogram in Figure 4.7a exhibits particle size distribution of 500 – 1300 nm with an average diameter of

about 916 nm. Furthermore, there is a different morphology between zeolite-Y and ZCC-1 as shown in Figure 4.6b. As surface coverage with carbon occurred, the particle surface looks rough than those of zeolite surface. The surface roughness was caused due to the precursor deposition on the external zeolite surface. The particle size of ZCC-1 also seems to be larger with an average particle size of approximately 1069 nm, which may be due to a higher aggregation in the presence of sucrose.

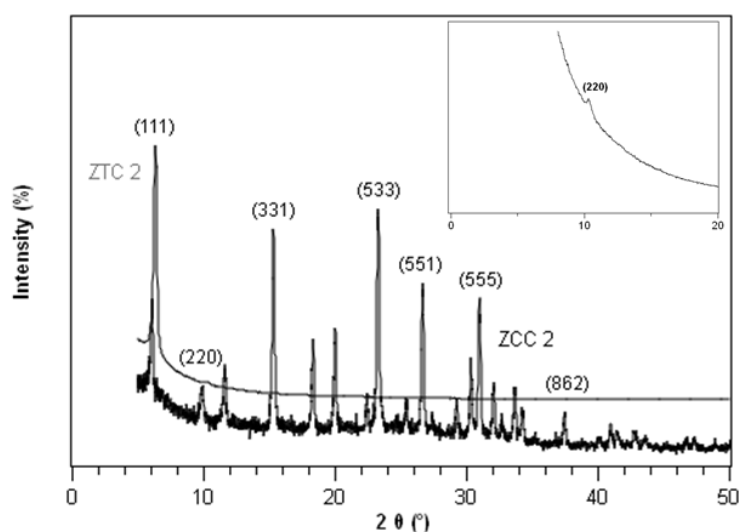


Figure 4.4 XRD spectra of ZCC-2 and ZTC-2

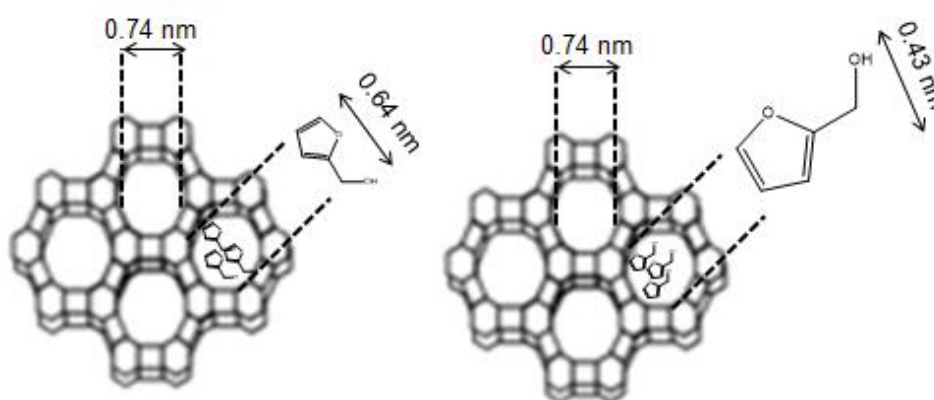


Figure 4.5 The possibility filling of FA molecules into the pore window of zeolite-Y

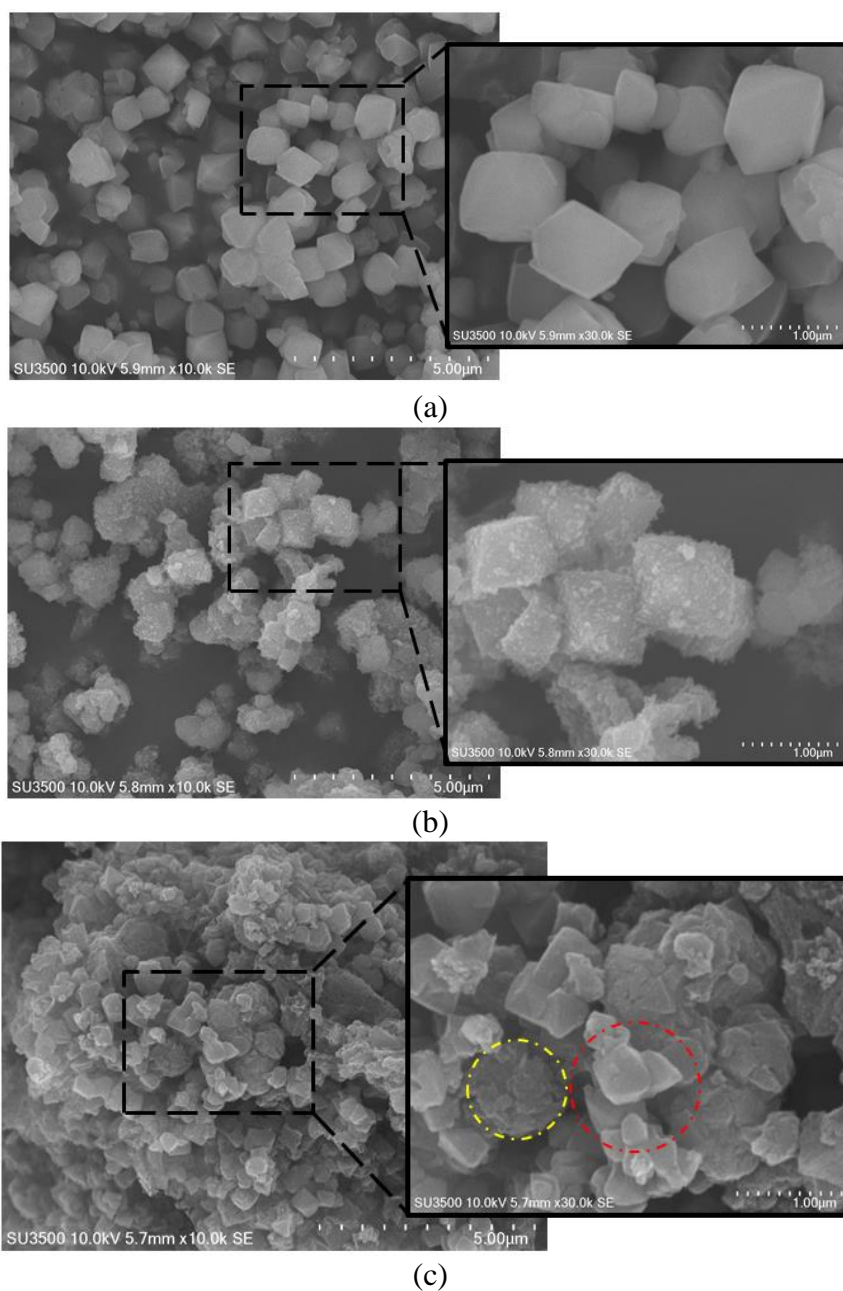


Figure 4.6 SEM images of (a) zeolite-Y, (b) ZCC-1 and (c) ZTC-1

As can be seen in Figure 4.7b, the histogram shows wider particle size distribution (600 – 1700 nm) than that of zeolite-Y. Furthermore, there is no obvious change in morphology between ZCC-1 and ZTC-1 (Figure 4.6c). The morphology of the ZTC-1 was obviously observed as smooth surface with sharp particle edges (red circle) and also accompanied by some graphitic sheets (yellow circle), indicating that a carbon deposition on the external zeolite-Y surface occurs. The formation of

stacked graphene sheets is due to the absence of spatial limitation on the external surface. The SEM image is well agreement with the XRD pattern with respect to the appearance of (111) and (002) planes. Furthermore, the particle size histogram of the ZTC-1 in Figure 4.7c is ranging from 190 to 500 nm with an average diameter of about 369 nm, smaller than those of template crystal. It may be due to the zeolite shrinkage during carbonization process, as observed by XRD data (Chen *et al.*, 2007).

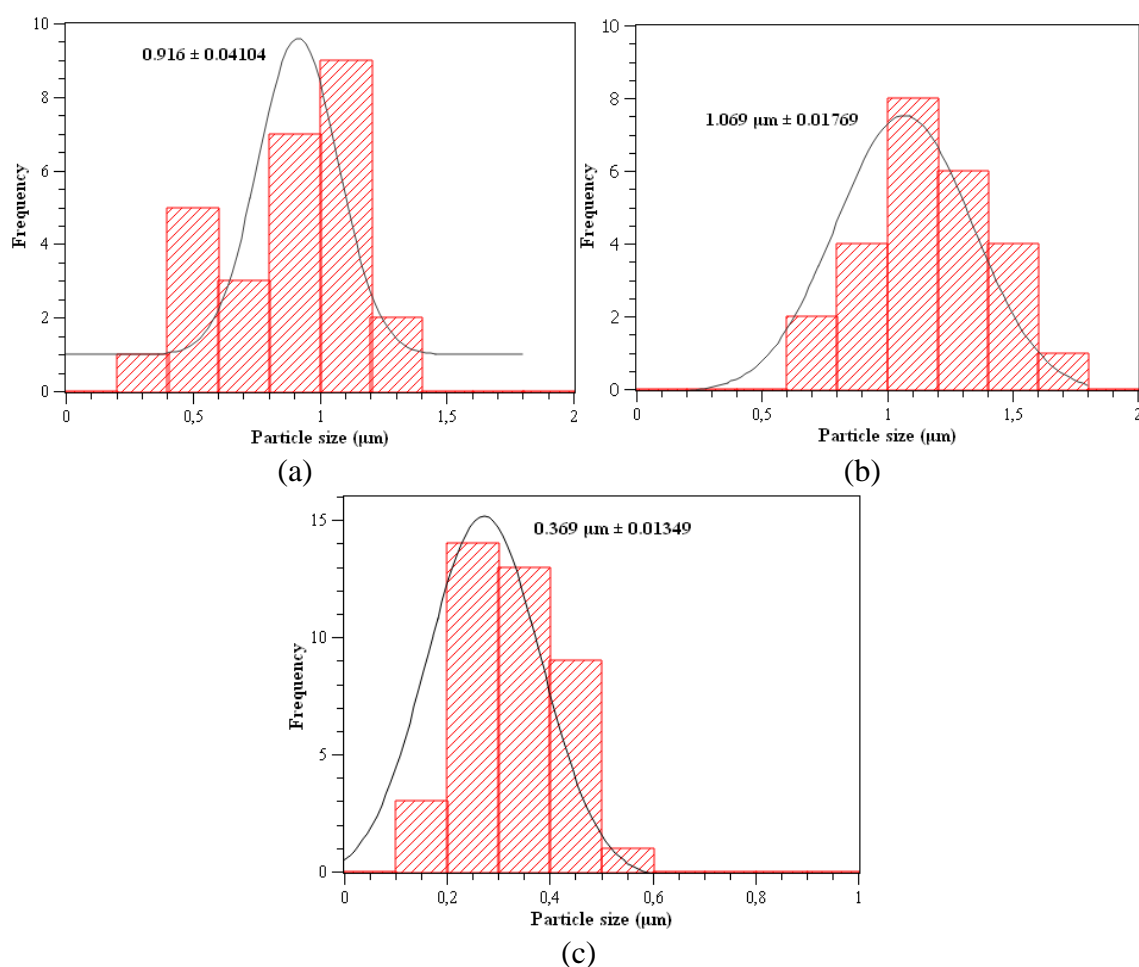


Figure 4.7 Particle size histogram of (a) zeolite-Y, (b) ZCC-1 and (c) ZTC-1 obtained from the SEM data

Figure 4.8a exhibits the TEM image of zeolite-Y depicting its morphology with octahedral configuration. In the TEM image of ZCC-1, a deposition of carbon precursor was clearly observed on the external surface of microporous

carbon region. Also, a TEM equipped with EDX analysis was conducted in order to further observe the element distribution of ZCC-1. Figure 4.8c,d exhibited the EDX scanning on the ZCC with intensities of C, O, Na, Al, Si elements. The scanning results confirmed that a high concentration of carbon was distributed inside the zeolite channels with a small amount of carbon in the outer surface of zeolite. This result supports the XRD and SEM observations as discussed above.

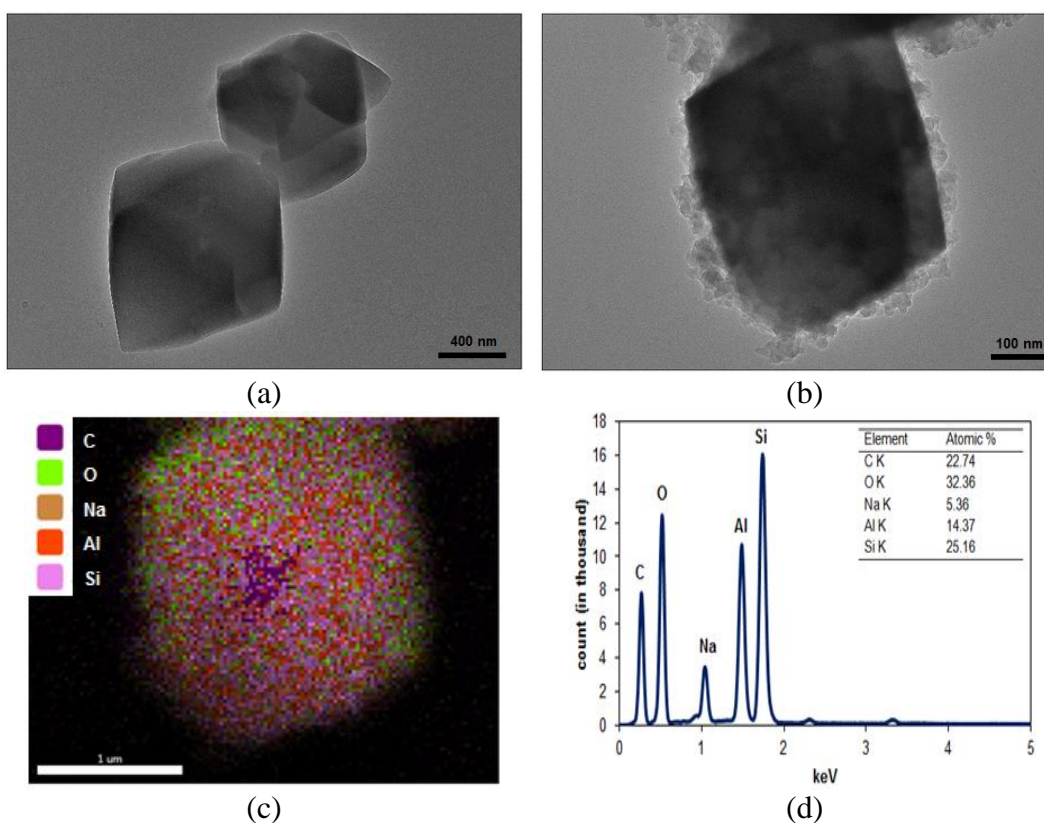


Figure 4.8 TEM images from zeolite-Y (a), ZCC-1 (b), The EDX mapping for ZCC-1 (c) and the concentration of elements represent of zeolite and carbon particles (d)

The TEM images of the ZTC-1 in Figure 4.9a further exhibited that some carbon source have deposits on the external surface of zeolite-Y, which corresponds to the (002) diffraction. Such external carbons have randomly distributed mesopores with average thickness of about 57 nm, as shown in Figure 4.9b. A little mesopore was also observed in the inner surface of zeolite-Y (Figure 4.9c), resulted from insufficient carbon filling, and the carbon could not maintain

the ordered structure of zeolite-Y during the etching process. Meanwhile, the ordered microporous structure was detected in the deep inner region of ZTC-1, corresponding to a (111) plane of zeolite-Y, as shown in Figure 4.9c. The results showed that ZTC-1 obtained possessed both micro and mesoporosity, which were in well agreement with XRD and SEM analyses.

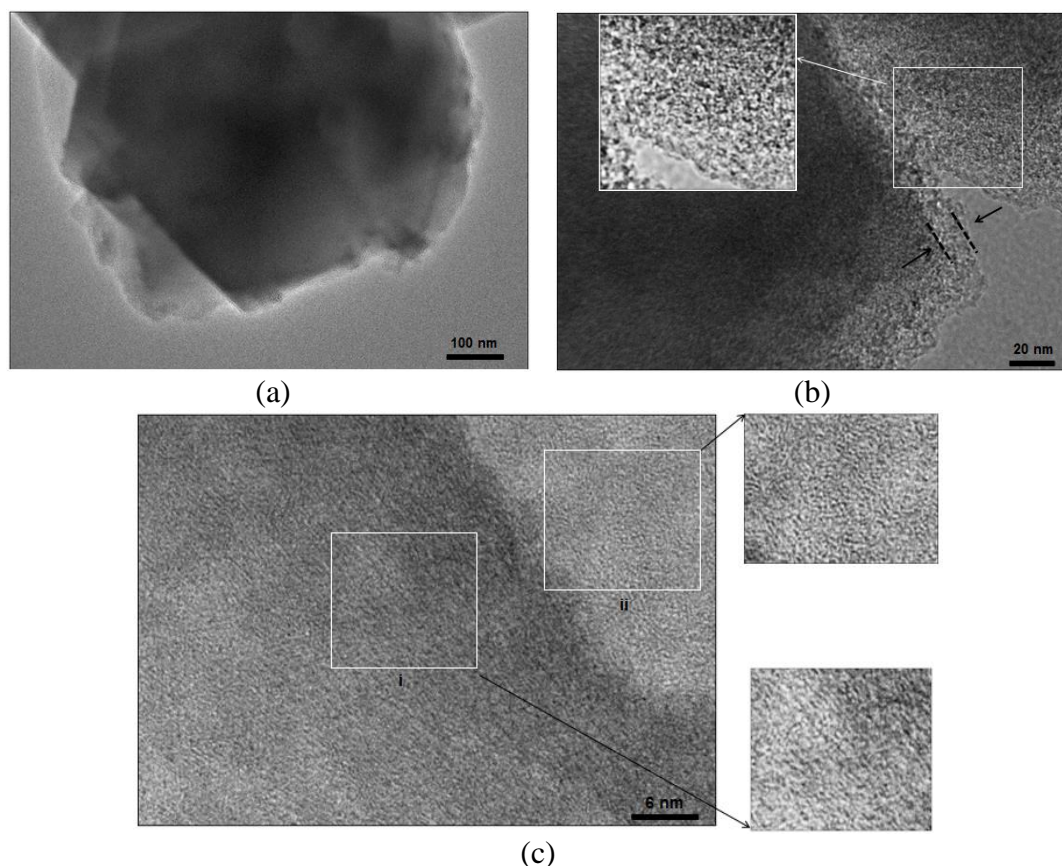


Figure 4.9 The TEM images of ZTC-1 (a), the HRTEM images for the ZTC with randomly distributed mesopores structure, the region indicated by an arrow is the carbon layers deposited in the external surface of zeolite-Y (b) the partial ordered micropores (i) and little mesopores (ii) in the inner surface of zeolite-Y (c)

The SEM images of ZCC-2 and ZTC-2 are also given in Figure 4.10. In Figure 4.10a, the image of ZCC-2 demonstrates the similar uniformity in morphology of zeolite-Y particles. The histogram in Figure 4.11a shows a narrow particle size distribution of about 200 – 550 nm with an average crystal size of 288 nm. The element distribution of the ZCC-2 was further observed by EDX analysis, as shown in Figure 4.12. It can be observed from the EDX mapping, the

carbon was uniformly deposited inside the zeolite framework, which supports the XRD and SEM results. During the zeolite removal, the ZTC-2 particles in Figure 4.10b showed obvious crystal like morphology with an average particle size of about 247 nm, showing faithful replication. This is the main reason for the appearance of a sharp peak at around 6.36° . It is also seen in Figure 4.11b that the particle size appears to be uniform with a size distribution of 200 – 410 nm. Based on these results, it can be concluded that carbon deposition method would be the key factor for the faithful replication of ZTC. The use of two step methods results in the faithfully replicated ZTC since the deposition of disordered external carbon layer is largely suppressed. Therefore, the ZTC with high structural regularity can be obtained (Choi *et al.*, 2015).

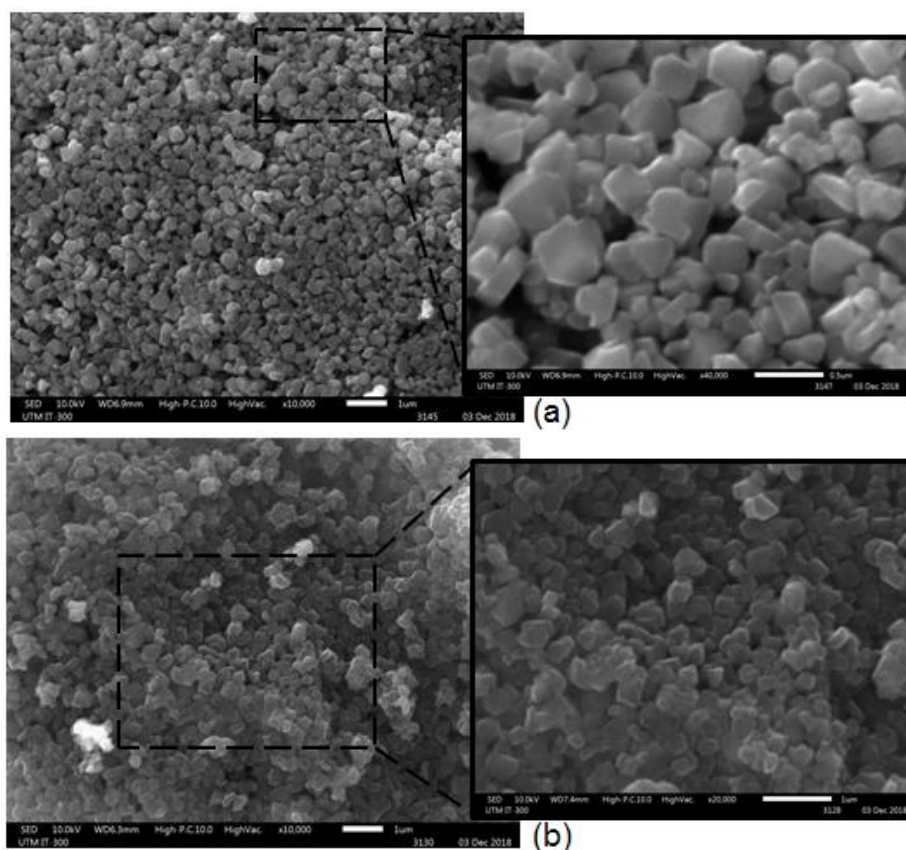


Figure 4.10 SEM images of (a) ZCC-2 and (b) ZTC-2

The HRTEM images of ZTC prepared by impregnation-CVD method was studied by Ma *et al.* (2002), as shown in Figure 2.16. The ordered microporous

structure with straight lattice fringes could be clearly observed. The periodicity of this array structure is about 1.4 nm, corresponding to the pattern from a (111) plane of zeolite-Y with $\langle 110 \rangle$ direction, and suggests microporous structural ordering replicated from the zeolite-Y. The distance of this plane was similar to the XRD result. In addition, its diffraction pattern (inset in Figure 2.16) was obviously observed as two pairs of spots, which corresponds to a (111) reflection of zeolite-Y. This observation indicates that the regular ordering of carbon originates from the zeolite-Y crystal planes, mostly from the ordering of (111) plane as observed by a strong and sharp XRD peak at 6.36° (Figure 4.4).

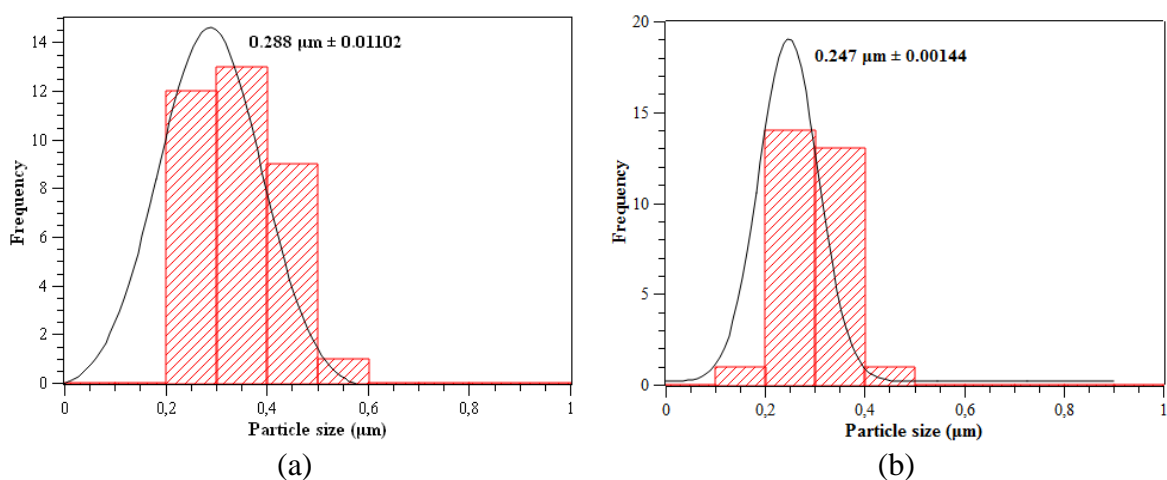


Figure 4.11 Particle size histogram of (a) ZCC-2 and (b) ZTC-2

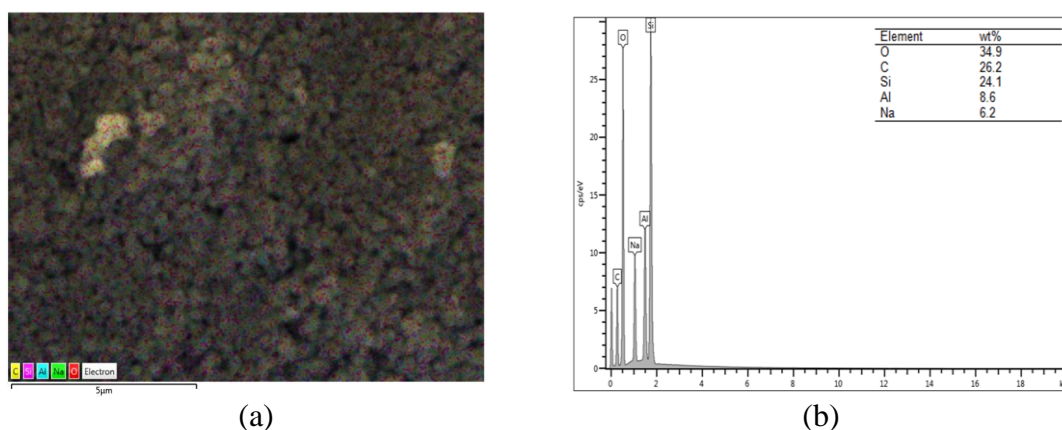


Figure 4.12 The EDX mapping for ZCC-2 (c) and the content of elements represent of zeolite and carbon particles

To understand the pore properties of the particles, the N₂ adsorption analysis of zeolite-Y, ZCC and ZTC are conducted and the corresponding N₂ sorption isotherm are presented in Figure 4.13. The adsorption isotherm of zeolite-Y was a characteristic type 1, indicating a high surface area and developed microporosity. However, a small desorption hysteresis at $P/P_0 = 0.45 - 1.0$ indicates the presence of narrow mesopores in the zeolite-Y structure due to the formation of interparticle voids (Cai, Yang, *et al.*, 2014). Furthermore, the N₂ isotherms for ZCC-1 and ZTC-1 were same to each other. Both samples exhibit type IV isotherm which indicates the multilayered adsorption on mesoporous surface (Shi *et al.*, 2015)(Khanday *et al.*, 2017). The hysteresis loops on the desorption branch ($P/P_0 = > 0.4$) is indicative of capillary condensation in mesopores, while the adsorption at low pressure corresponds to the filling of micropores. The type hysteresis loops can be categorized as H4, indicating narrow slit-like pores. Those observations show that both ZCC-1 and ZTC-1 possess not only micropores, but also some portion of mesopores with narrow slit-like pores. These mesopores are exposed to the external surface and a little portion in the inner of zeolite-Y channels as observed in HRTEM result. In the case of ZTC-2, the adsorption isotherm is largely type 1 which indicates the existence of a microporous nature. The amount of N₂ adsorbed in ZTC-2 at low pressure ($P/P_0 = 0.05$) is larger than those in ZTC-1, showing a larger proportion of microporosity for ZTC-2. The formation of micropores is perfectly consistent with the high structural ordering of ZTC-2 as observed in XRD analysis.

The results above are also reflected in the pore size distribution (PSD) curve as seen in Figure 4.14. The zeolite-Y contains micropores in the size range of 4 – 10 Å with a mean pore size of 8.04 Å that confirms a microporous character. When the carbon was deposited inside the zeolite channels, the micropore peak reduces and shifts toward a maxima pore size of 7.29 Å with an average mesopore diameter of 23.9 Å. Meanwhile, the PSD curve of ZTC-1 displays broad peaks with average micropore size at 9.23 Å, which is ascribed to the templating effect of zeolite-Y framework. Furthermore, some proportion of mesopores which correspond to the hysteresis loop in N₂ sorption isotherm of the ZTC-1 are observed in a mean pore size of 24.6 Å. The formation of mesopores is originated

from the carbon layer deposited on the external zeolite surface, as observed by HRTEM. Also, a little amount of mesopores was observed inside the zeolite-Y channels, coming from the collapse of unstable carbon framework during the etching process. On the contrary, the ZTC-2 shows a major micropore size at around 12.1 Å indicating the faithful replication of zeolite-Y, as reported in previous studies (Cai, Li, *et al.*, 2014).

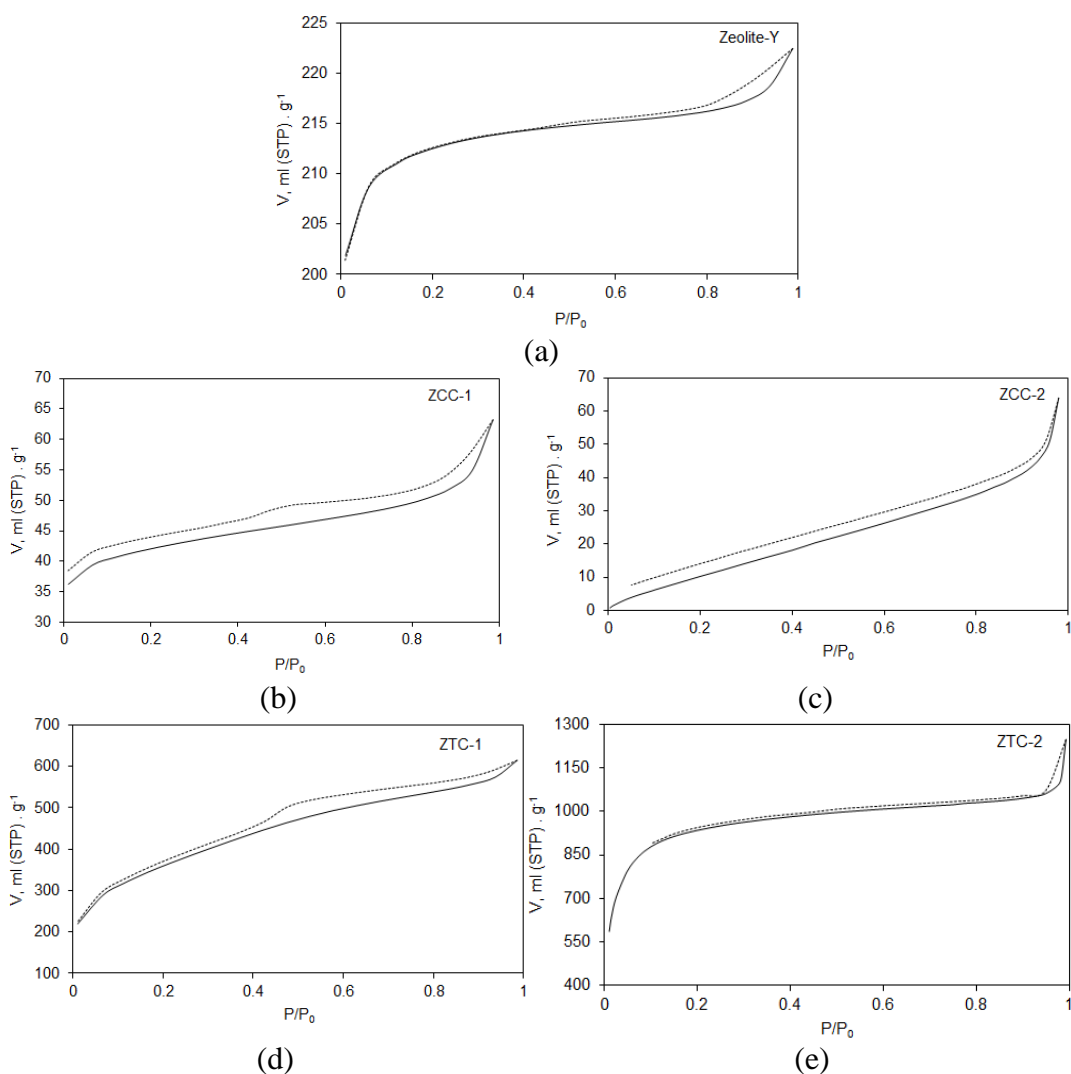


Figure 4.13 Nitrogen adsorption-desorption isotherms of (a) zeolite-Y, (b) ZCC-1 (c) ZCC-2, (d) ZTC-1 and (e) ZTC-2 (solid and dot line : adsorption and desorption branch, respectively)

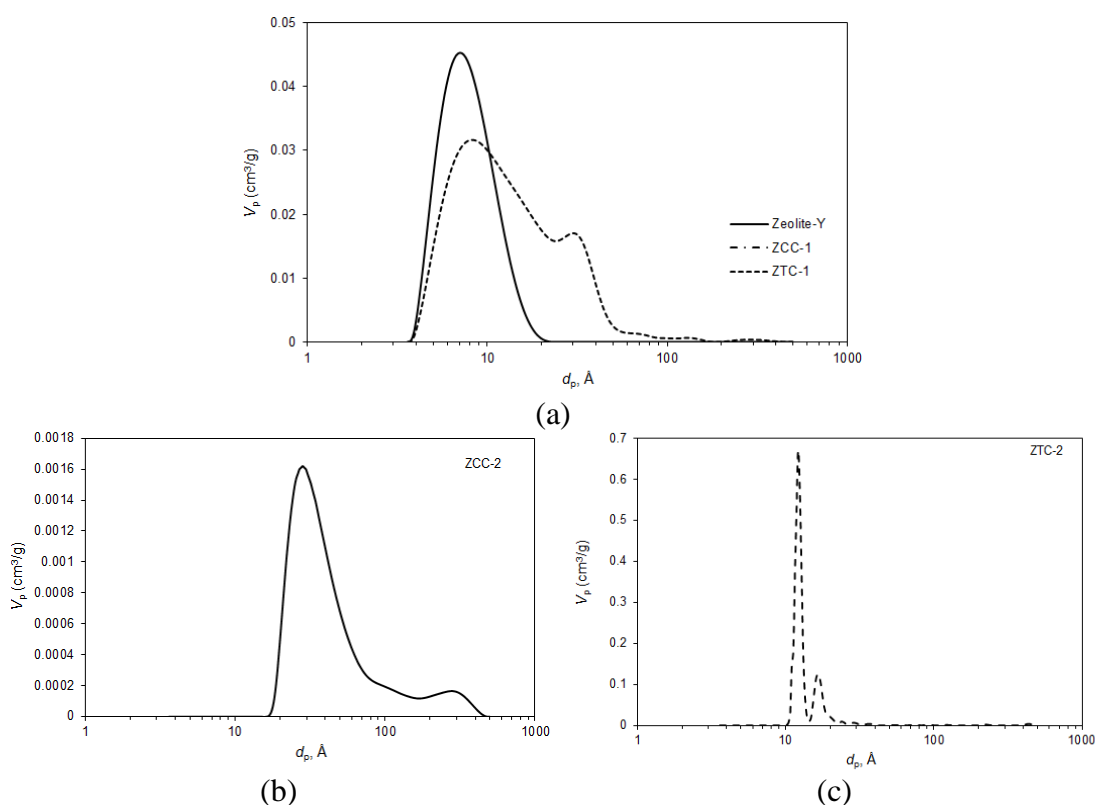


Figure 4.14 Pore size distributions of (a) zeolite-Y, ZCC-1, ZTC-1, (b) ZCC-2 and (c) ZTC-2 obtained by the 2D-NLDFT method

From the PSDs coupled with XRD results support a fact that the greatest level of zeolite-like structural ordering gives a larger contribution to a high surface area and pore volume, as listed in Table 4.1. The results show that carbon incorporation inside the zeolite-Y reduces the surface area and pore volume of ZCC-1, due to the formation of external carbon layer. Furthermore, the particle size increment may also contribute to the decrease of the surface area. For ZCC-2, the surface area decreases significantly than those of ZCC-1 due to the perfect filling of zeolite channels with carbon. Furthermore, the amount of N₂ adsorbed on the ZTC greatly increased compared to the ZCC, suggesting the formation of new pore structure and porosity after the zeolite removal. If we observed the textural properties of ZTC, the ZTC-2 exhibited higher surface area with almost no mesoporosity, while the lower surface area of ZTC-1 is due to the presence of mesoporous carbon layer. The larger surface area and pore volume indicate that the zeolite structure was well replicated by a carbon framework.

Table 4.1 Textural Properties of Zeolite-Y Template, ZCC and ZTC

| Sample | $S_{\text{BET}}^{\text{a}}$ (m^2/g) | V_{t}^{b} (cm^3/g) | $V_{\text{micro}}^{\text{c}}$ (cm^3/g) | d_{p}^{d} (\AA) |
|-----------|---|--|--|--|
| Zeolite-Y | 656 | 0.344 | 0.31 | 8.04 |
| ZCC-1 | 133 | 0.098 | 0.05 | 7.29 |
| ZCC-2 | 38 | 0.099 | 0.08 | 26.5 |
| ZTC-1 | 1254 | 0.950 | 0.86 | 15.4 |
| ZTC-2 | 2939 | 1.929 | 1.90 | 12.2 |

^aBET surface area.

^bTotal pore volume.

^cThe micropore volume

^dMean pore width size.

4.2 Summary

Based on the results presented in this chapter, it can be summarized that the carbon filling process is indispensable for preparing ZTC with highly ordered structure. The structural ordering of ZTC from the two steps routes is much higher than the ZTC from the single carbon deposition. The schematic representation of carbon deposition on the zeolite at different step is presented in Figure 4.15. In the case of sucrose-impregnation, the amount of disordered mesoporous carbon layer was deposited on the external zeolite-Y channels, indicating the (002) diffraction. This layers restricts the continuous filling of sucrose to the zeolite-Y channels. Hence, the zeolite-Y structure could not be fully replicated by the carbon. However, the broadening and low intensity of these diffraction peak suggests that the ZTC is amorphous and the carbon precursor is mostly deposited inside the zeolite-Y channels rather than on the external zeolite-Y surface. This results in the porous carbon consisted of both micropores and mesopores. Therefore, a ZTC with lower BET surface area ($1254 \text{ m}^2/\text{g}$) and pore volume ($0.950 \text{ cm}^3/\text{g}$) than the ZTC synthesized by FA-impregnation and propylene CVD. This indicates that the obtained ZTC possesses poor ordering structure as proven by a broad and low peak at $2\theta = 6.05^\circ$. By combining the carbon impregnation with CVD process, the amount of carbon filled inside the zeolite-Y channels was enough to maintain the network structure. In results, such carbon was amorphous with a very porous structure and exhibited high BET surface area up to $2939 \text{ m}^2/\text{g}$. The porosity of ZTC-2 possesses micropores with almost no mesopores, indicating high degree long

range ordering and it was also revealed by the appearance of sharp peak at $2\theta = 6.36^\circ$ and a weak peak at $2\theta = 10.3^\circ$.

The ZTC with a large surface area and porosity has a great potential as filling material in gas separation membrane. The gas adsorption capacity increased by increasing the particle surface area. Hence, a higher gas permeance is predicted for MMM filled with higher surface area of filler. Also, a high porosity and good pore size distribution of particles will ensure high gas selectivity due to the size selective property. Therefore, the simultaneous increase in permeability and selectivity is well achieved of these filler.

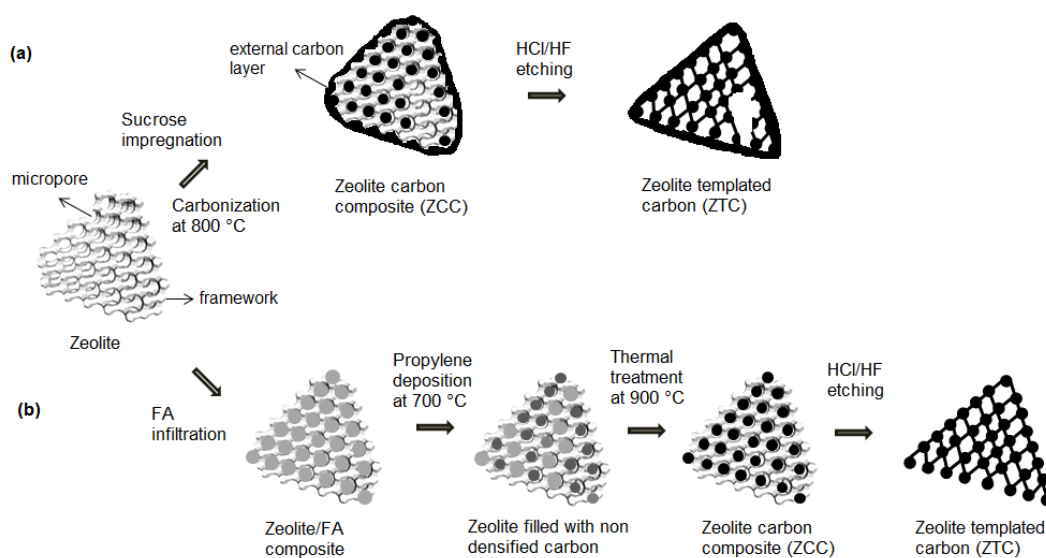


Figure 4.15 Illustration of carbon deposition at different routes (a) sucrose impregnation (ZTC-1) (b) FA-impregnation and propylene CVD (ZTC-2)

CHAPTER 5

MIXED MATRIX MEMBRANE CHARACTERISTICS AND ITS PERFORMANCE FOR GAS SEPARATION

This section describes characterisation of all prepared Mixed Matrix Membrane (MMMs) as a function of ZTC-1 loading, followed by discussion of the experimental results on the MMMs performance for gas separation. Single (CO₂, O₂, H₂, CH₄ and N₂) gas permeation through the membrane is investigated and mixed (50/50% CO₂/CH₄ and H₂/CH₄) gas is also important for the practical implementation.

5.1 Characteristics of MMM

The effects of ZTC-1 loadings on the structural, morphological and thermal properties of PSF membrane were conducted in order to investigate the effectiveness of MMM to separate gases.

To determine the changes on the intermolecular distances between intersegmental chains of polymer during the particle incorporation, X-ray diffraction (XRD) analysis was conducted and the results are given in Figure 5.1. Neat PSF membrane in Figure 5.1a exhibited an amorphous nature with a weak peak observed at $2\theta = 17.77^\circ$. For comparison, the peak positions for PSF/ZTC-1 MMMs are listed in Table 5.1. The results showed that no significant change in the diffraction angle for PSF after particles were added, indicating a slight changes on the polymer chain mobility. Also, the peak intensity slightly reduced after ZTC-1 was loaded. This results indicate that the slight increase of disorder in the sample with increasing filler loading. This might suggest that the arrangement of polymer chain packing has been disturbed by the presence of filler. Furthermore, the characteristic of pristine ZTC-1 at around $2\theta = 6.05^\circ$ was observed for MMM at higher ZTC-1 loading. Meanwhile, the disappearance of the ZTC-1 characteristic peak in some MMMs is attributed to the low contents of

ZTC-1 and indicates a good particle dispersion within PSF, as proven by Raman analysis in the following discussion (Ionita *et al.*, 2014)(N. M. Ismail *et al.*, 2015).

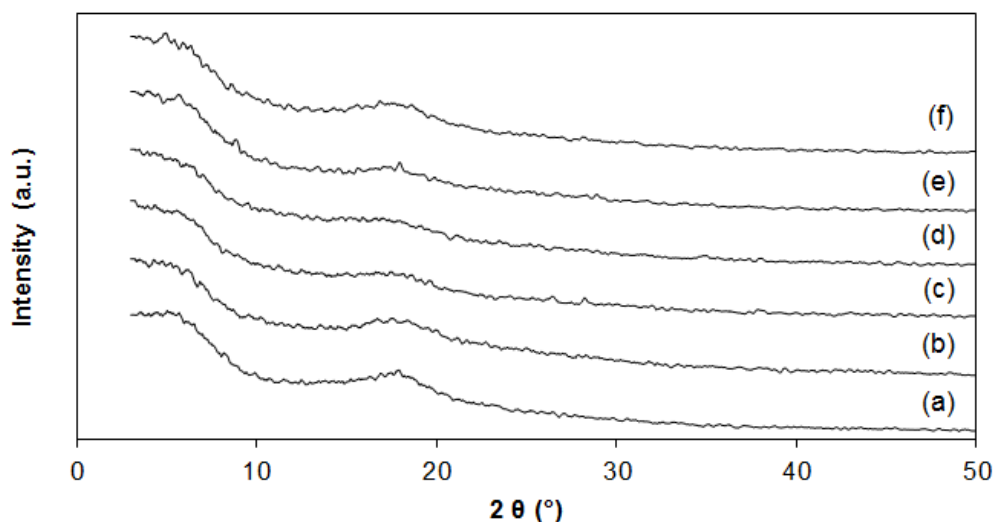


Figure 5.1 XRD spectra of PSF/ZTC mixed matrix membrane with (a) 0, (b) 0.25, (c) 0.4, (d) 0.5, (e) 0.7 and (f) 1 wt% ZTC-1 loadings.

Table 5.1 XRD Parameters for Pure PSF and PSF Based Membrane Filled with ZTC-1

| Sample | Angle (2θ) | <i>d</i> -spacing (nm) |
|--------------------|------------------------|---------------------------|
| Pristine PSF | 17.77 | 0.50 |
| 0.25% ZTC-1 in PSF | 17.88 | 0.50 |
| 0.4% ZTC-1 in PSF | 17.55 | 0.51 |
| 0.5% ZTC-1 in PSF | 17.06 | 0.52 |
| 0.7% ZTC-1 in PSF | 8.92, 17.96 | 0.99, 0.49 |
| 1% ZTC-1 in PSF | 6.27, 17.57 | 1.41, 0.50 |
| ZTC | 6.05 | 1.46 |

In order to further observe the structure of PSF/ZTC-1 MMM, Raman spectroscopy is used and the results are given in Figure 5.2. The neat PSF membrane shows four typical peaks at ~ 790 , ~ 1148 , ~ 1587 and ~ 3064 cm^{-1} , ascribed to the asymmetric C-S-C, C-O-C, aromatic ring chain and C-H vibrations, respectively (Ionita *et al.*, 2015). The Raman spectrum of PSF/ZTC-1 membrane possess both the PSF and ZTC characteristic peaks (Figure 5.2a). The G-band at approximately of 1585 cm^{-1} slightly splitted in

two peaks for MMM at lower ZTC-1 contents (0.25 and 0.5 wt%) and became one peak for 1 wt% ZTC-1 loading (Figure 5.2b). The peak broadening at higher ZTC-1 loading can be ascribed by a higher amount of ZTC aggregations due to higher ZTC-1 concentration in the membrane (Ionita *et al.*, 2014). The prominent D band is coming from the disordered carbon structure on the ZTC-1 and this indicates the presence of particles within the composite membrane (Lee *et al.*, 2013). The intensity ratio values of D to G bands are also presented in Figure 5.2b (inset). The values of I_D/I_G ratio of ZTC-1 slightly decreased after adding with PSF up to 1.1 at 0.25 wt% ZTC-1 loading. By increasing the ZTC-1 loading to 1 wt% within PSF matrix, the I_D/I_G ratio was slightly increased to about 1.12. The enhanced of the intensity ratio of D and G bands indicates the increase of disordered structure due to a higher of ZTC-1 consistent with XRD data.

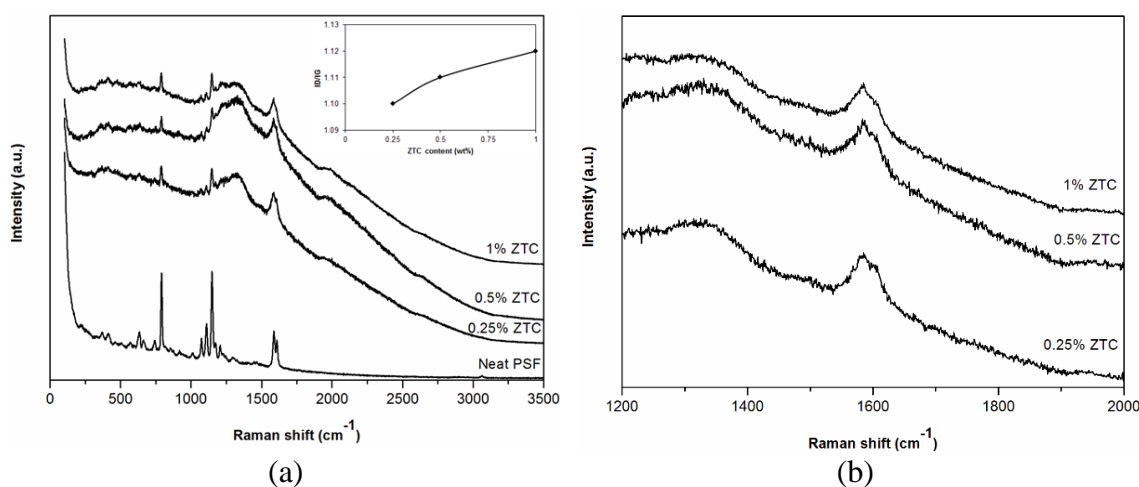


Figure 5.2 Raman spectra of (a) selected MMMs (Inset : I_D/I_G peak intensity ratio vs ZTC-1 loading) and (b) selected MMMs between 1200-2000 cm^{-1}

In order to further investigate the particle dispersion within PSF matrix and the morphology of all prepared MMMs, SEM analysis was used. The cross sectional SEM images of MMMs are shown in Figure 5.3. All MMMs revealed asymmetric structure containing dense top layer followed by finger-like structure beneath the outer layer and interconnected pores from the inner layer (lumen side). The development of dense layer was a result of the slow solvent evaporation

during the dry-phase inversion and the presence of ethanol caused rapid solidification in the surface layer, resulting the membrane with thinner surface layer. Conversely, the formation of porous sub layer is due to a faster diffusion rate of non solvent into low concentrated polymer phase during wet-phase inversion. Furthermore, the presence of volatile solvent reduced the interaction between non solvent and solvent, hence, leading to the formation of finger-like instead of large macrovoids structure. The dispersion of particles was hardly identified throughout the cross-sectional view for MMMs containing 0.25 and 0.4 wt% ZTC-1 loadings, indicating a good particle distribution within the PSF matrix. This might be due to a rigorous ultrasonication force during the dope solution preparation, hence, aiding the particle dispersion (Zulhairun and Ismail, 2014). However, the presence of particles can be observed at the top surface of membrane containing 0.5 wt% filler and the particles seem to be well embedded inside the polymer matrix. Further incorporation of 0.7 and 1 wt% of ZTC-1 into PSF matrix leads to the particle agglomeration within the pores. The fast liquid-liquid demixing obstructs the particles mobility and leads to the entrapment of the particles within the pores. The entrapment of particles within the closed pores was observed from the cross-sectional view in Figure 5.3e,f and the interfacial voids were detected for these membranes.

The surface images of PSF/ZTC-1 MMMs at different filler loadings are revealed in Figure 5.4. The surface of neat PSF membrane in Figure 5.4a is considered a dense and defect-free. Furthermore, the particles seemed to be randomly loaded on the surface and no obvious voids were observed for MMMs at 0.25 to 0.4 wt% loading, indicating good adhesion with the polymer matrix. Further increasing the particle loading to 0.5 wt% exhibited the localization of particles without voids around the particles. However, the agglomerated particles with diameter more than 1 μm were observed for MMM with 0.7 and 1 wt% ZTC-1. The particles naturally agglomerated in a viscous polymer solution and become severe aggregated at higher loadings (Zulhairun *et al.*, 2017). The particles were assembled to each other resulting large voids formation on the membrane surface.

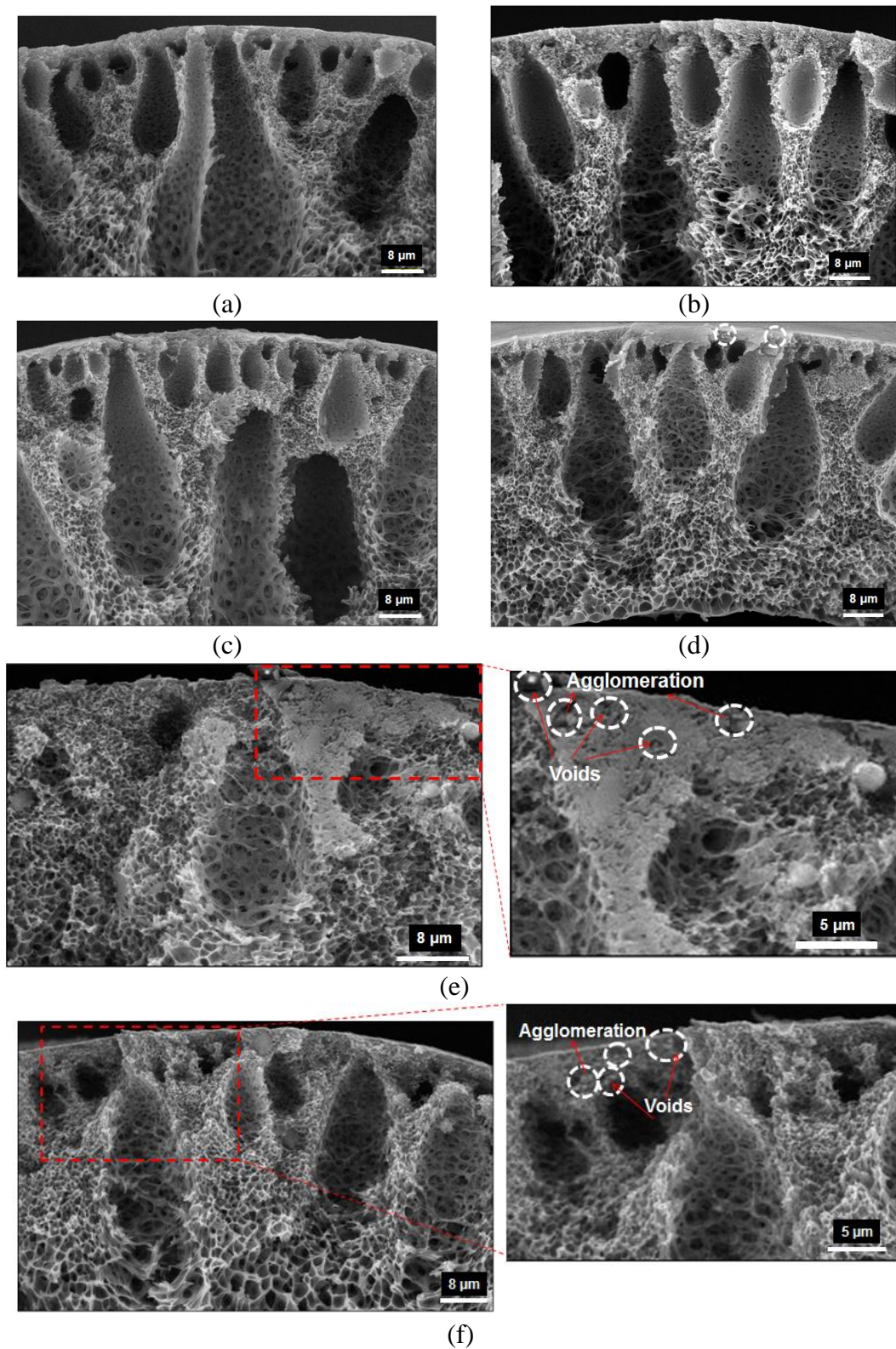


Figure 5.3 SEM micrographs of cross section of (a) neat PSF and PSF/ZTC-1 MMM with (b) 0.25 wt%, (c) 0.4 wt%, (d) 0.5 wt%, (e) 0.7 wt% and (f) 1 wt% ZTC-1 loadings

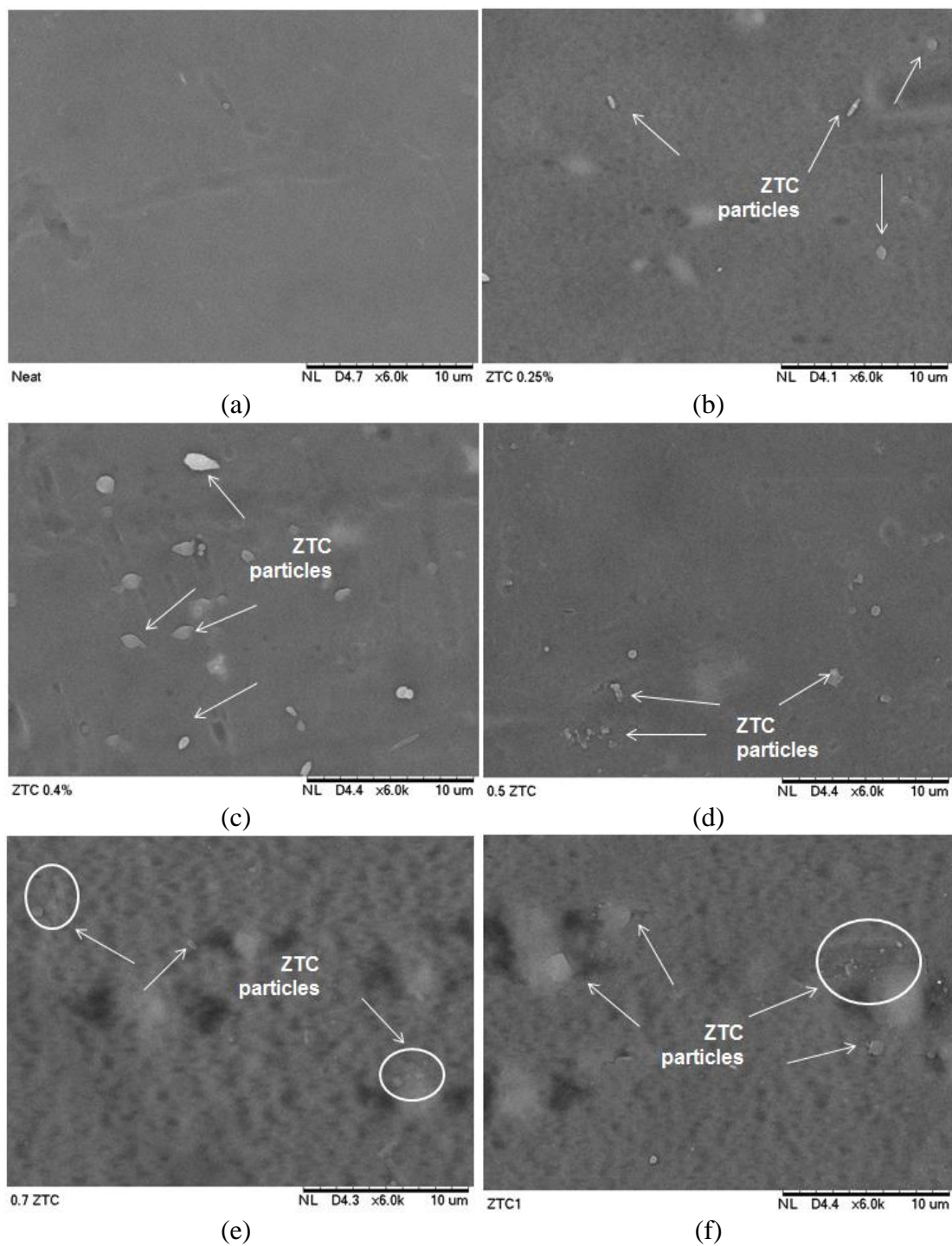
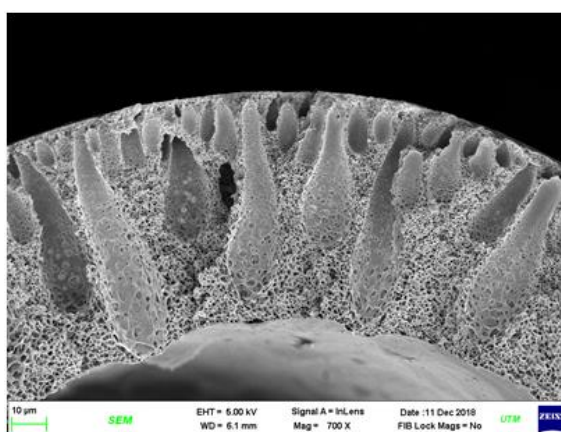


Figure 5.4 SEM micrographs of surface of (a) neat PSF and PSF/ZTC-1 MMM with (b) 0.25 wt%, (c) 0.4 wt%, (d) 0.5 wt%, (e) 0.7 wt% and (f) 1 wt% ZTC-1 contents

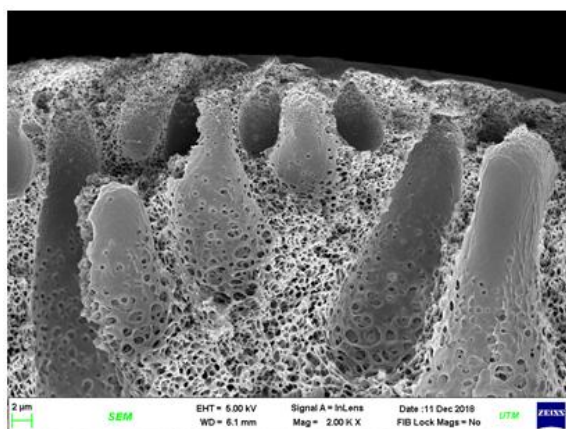
The void formation was detected from the surface view of MMM at higher ZTC-1 loading, regarded as defects. Therefore, 0.7 wt% seemed to be the threshold ZTC-

1 loading for preparing membrane in this study. The threshold limit of filler content is normally < 5 wt% for asymmetric membrane due to a thinner skin layer (Zulhairun *et al.*, 2017).

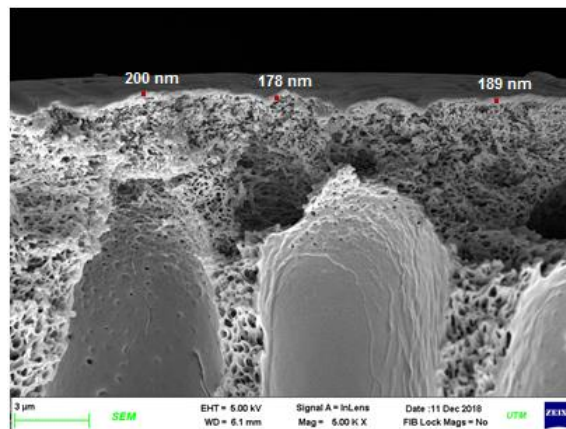
In order to further scrutinize the compatibility between the two phase, the FESEM was used on the neat PSF and the selected MMM samples and the images are shown in Figure 5.5 and Figure 5.6, respectively.



(a)



(b)



(c)

Figure 5.5 FESEM images of cross section morphology of neat PSF membrane at different magnification (a) 700x, (b) 2000x and (c) 5000x revealing the average dense selective layer of ~ 189 nm

Figure 5.5 shows a dense selective layer of about 189 nm in thickness supported by porous sub layer containing finger-like macrovoids. It also assumes that the dense layer thickness did not change by filler loading because all membranes were

fabricated by similar conditions and parameters. Furthermore, the surface morphology of PSF/ZTC-1 MMMs at different amount of ZTC-1 loadings is shown in Figure 5.6. From the image, the adding of 0.25 wt% particles into PSF membrane resulted in a homogeneous particle dispersion and seemed to be in good interfacial contact with PSF matrix. A well adhered particle within the matrix with no voids around the particles was visible for PSF/ZTC 0.5 wt%. Furthermore, a few agglomerates with diameter up to $> 1 \mu\text{m}$ can be observed for MMM with 1 wt% particle loading. Also, these membrane exhibited some voids of approximately 60 nm, hence, the higher permeance with poorer selectivity is anticipated. These observations were in well accordance with SEM results previously discussed.

Further supporting investigation on the membrane surface is conducted using AFM analysis. Both the plane and three-dimensional images are presented in Figure 5.7. A relatively smoother surface area was noticed for neat PSF membrane. According to AFM images in Figure 5.7b-f, the brighter and darker spots can be identified as filler and polymer area, respectively. The presence of filler resulted in the increase of valleys (depressions) and nodules (peaks), leading to a higher surface roughness and becoming rougher by increasing ZTC-1 in the membranes (Table 5.2). The particles well distributed on the surface layer of membrane at low concentrations (0.25 – 0.5 wt%) with a size within the range of ZTC size. Meanwhile, the particle agglomeration was observed with a size of 777 nm for 0.7 wt% loading, indicating that two particles combined to each other. Also, the particle with 1046 nm in size was clearly detected for 1 wt% loading, which is in well agreement with FESEM observation (Figure 5.6c). Therefore, a high surface roughness can be attributed to a high viscosity, more agglomeration and less dispersion of particles on the membrane surface. Referring to AFM images, the peaks with a height of about 20 - 55 nm indicated that the filler body were well incorporated on the membrane surface, thus preventing the particles to peel-off from the membrane.

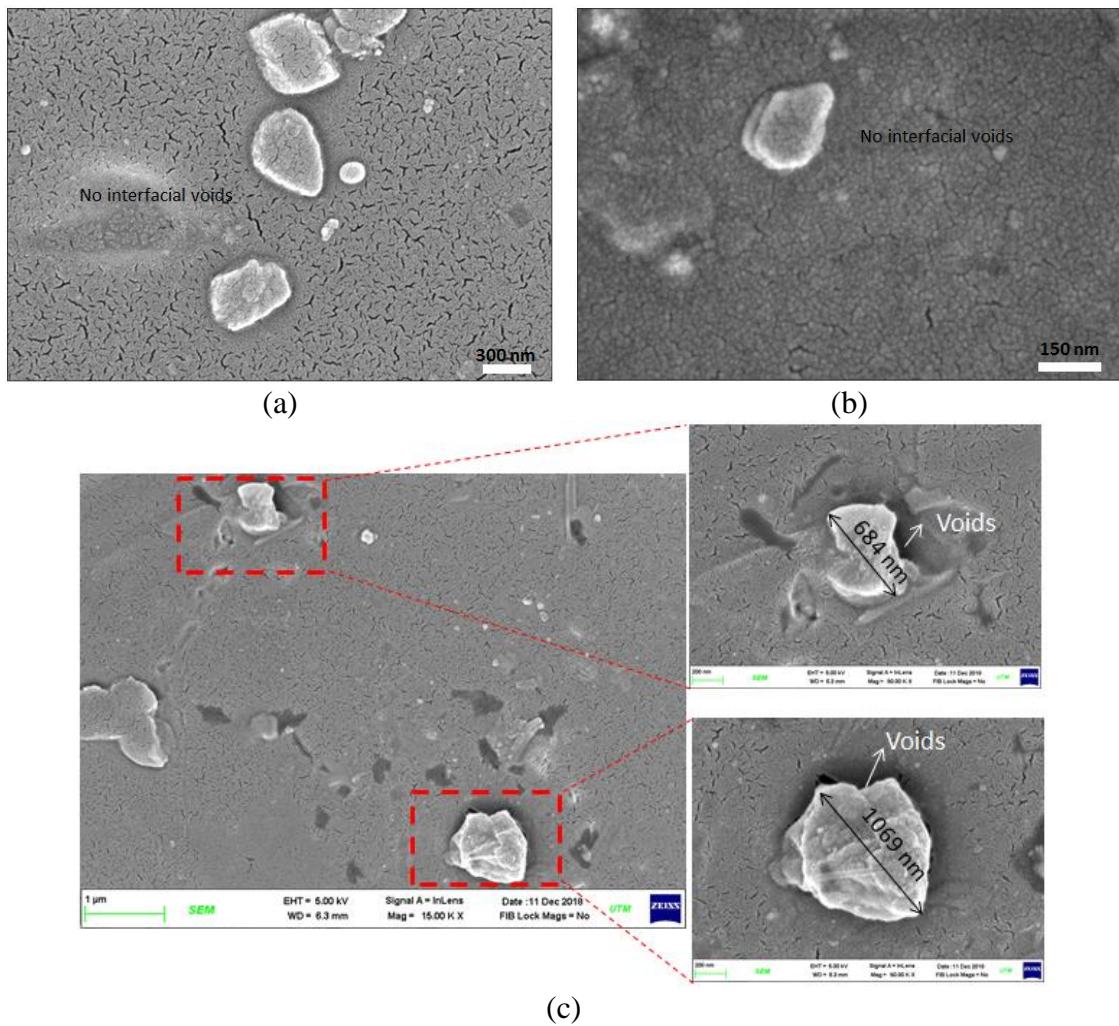
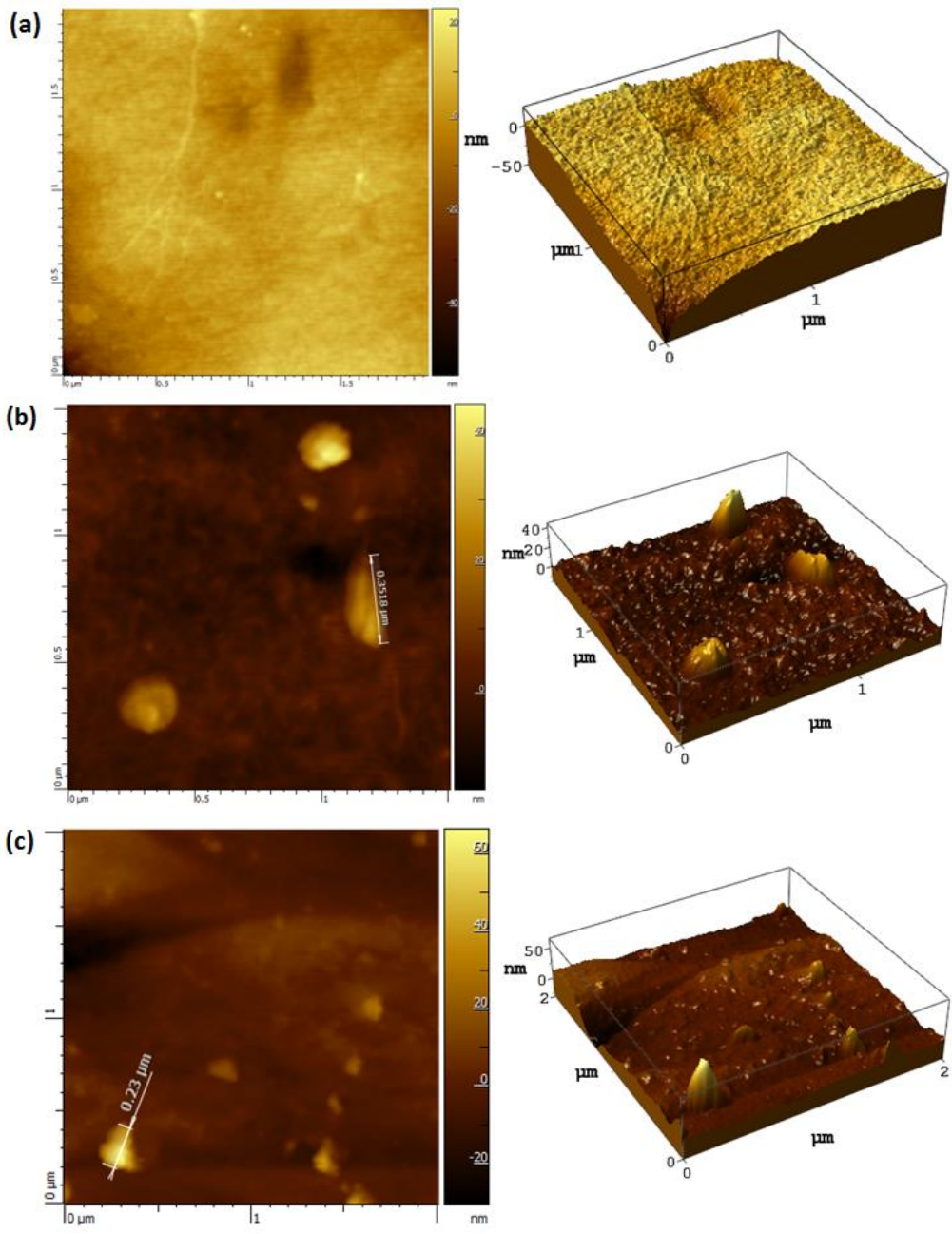


Figure 5.6 Surface FESEM images of PSF/ZTC-1 with (a) 0.25 wt%, (b) 0.5 wt% and (c) 1 wt% ZTC-1 loadings

Table 5.2 Surface Roughness Parameters of PSF/ZTC-1 MMMs

| Membranes | Roughness Parameter | |
|--------------|---------------------|----------------------------|
| | Average rough (nm) | R _{ms} rough (nm) |
| Neat PSF | 2.50 | 3.26 |
| 0.25 wt% ZTC | 3.20 | 5.40 |
| 0.4 wt% ZTC | 5.11 | 7.54 |
| 0.5 wt% ZTC | 5.22 | 7.28 |
| 0.7 wt% ZTC | 7.30 | 12.89 |
| 1 wt% ZTC | 7.09 | 11.14 |



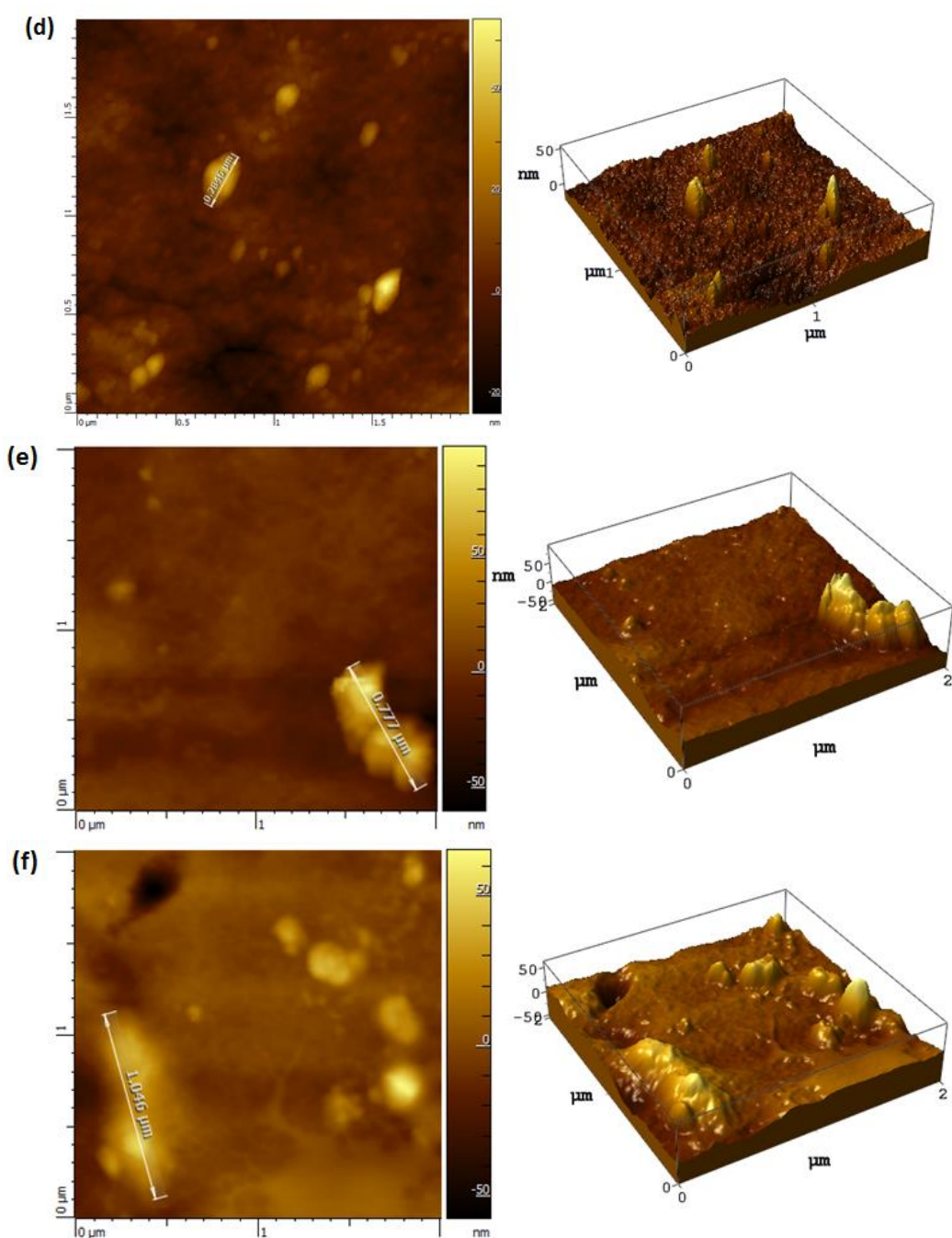


Figure 5.7 AFM images of the surface of PSF/ZTC-1 MMM : (a) 0, (b) 0.25, (c) 0.4, (d) 0.5, (e) 0.7 and (f) 1 wt% ZTC-1 loadings

In order to have fundamental understanding of the interaction of polymer with particle surface, the FTIR analysis of filler, neat PSF and MMMs was conducted and the results are shown in Figure 5.8. From Figure 5.8a, the ZTC showed several peaks at around 3341 cm^{-1} (O-H functional group stretching),

1700 cm^{-1} (C=O stretching), 1575 cm^{-1} (C=C aromatic stretching) and 1173 cm^{-1} (C-C stretching) (Nishihara *et al.*, 2008). On the other hand, neat PSF revealed several absorption peaks at around 852 and 872 cm^{-1} (C-H rocking), at 1013, 1079, 1104 and 1168 cm^{-1} (C-C stretching), at 1147 and 1322 cm^{-1} (Ar-SO₂-Ar symmetric bending), 1236 cm^{-1} (Ar-O-Ar stretching), 1293 cm^{-1} (S=O symmetric stretching) and 1583 cm^{-1} (C=C aromatic stretching). The similar peaks of neat PSF were observed in other study reported by Junaidi *et al.* (2014) and Zornoza *et al.* (2009). Similarly to PSF/ZTC MMMs in Figure 5.8b, the spectrum was noticed to be the same with that of the neat PSF. By adding ZTC, no occurrence of new peaks or wavenumber change was detected besides neat PSF spectrum. This shows no interaction between PSF molecules and ZTC functional groups, hence, it can be said that the adhesion between the two phase in all MMMs was poor. Furthermore, the intensity of all PSF peaks in MMM spectra at 0.7 and 1 wt% was observed to decrease in comparison to neat PSF spectra, indicating a high amount of ZTC-1 embedded into PSF matrix (Mahmoudi *et al.*, 2019).

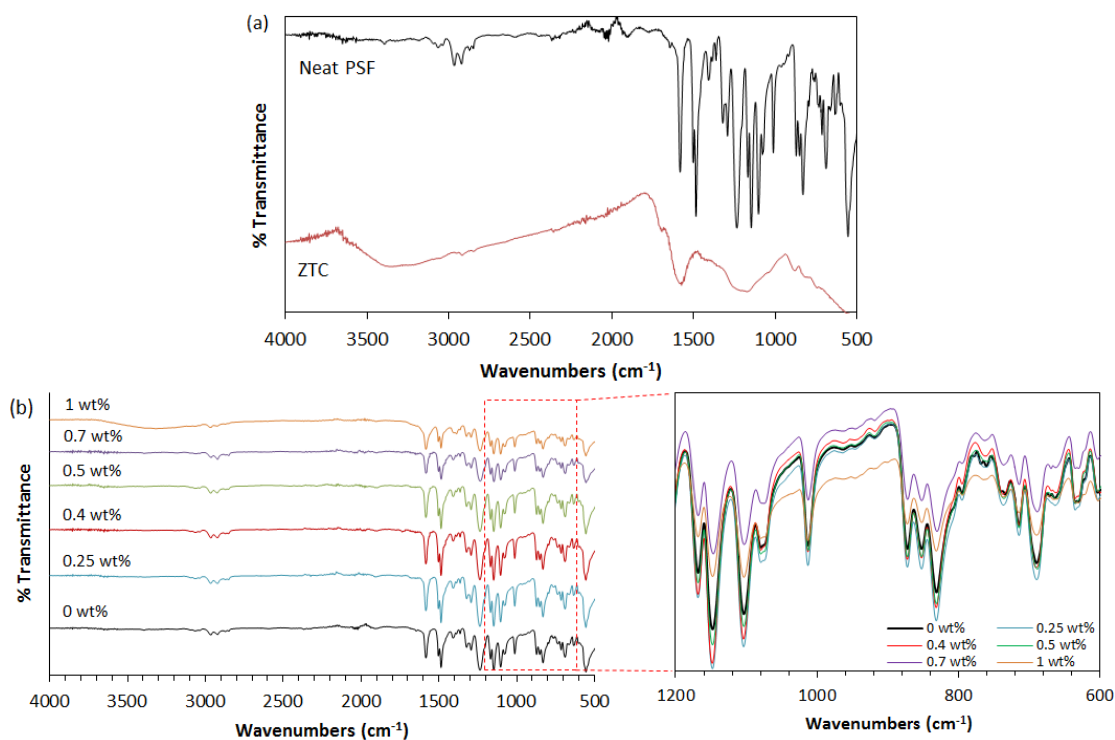


Figure 5.8 FTIR spectra of (a) neat PSF and ZTC-1 (b) all prepared MMMs

In order to support the interaction between the two phase, the glass transition temperature (T_g) is performed by DSC. The T_g value shows the flexibility of polymer chains. From the Table 5.3, the T_g of MMMs up to 0.4 wt% was higher in comparison to neat PSF. The increased T_g is caused by reducing the polymer segmental mobility. We speculated that due to the interface rigidification effect, the decreased segmental mobility resulted in higher selectivity than that of neat PSF. The good interaction between ZTC surface and the PSF might result in the formation of rigidified polymer. This examination was in well accordance with the surface observation. However, the rigidification effect at higher ZTC loading was negligible due to the unchanged T_g compared to the neat PSF.

Table 5.3 The Thermal Behavior of PSF/ZTC-1 MMMs

| Membrane | ZTC loading (wt%) | T_g (°C) | Weight loss (%) 400-600 °C | Residue (%) 800 °C |
|-------------|-------------------|------------|-------------------------------|-----------------------|
| Neat PSF | 0 | 178 | 64.18 | 27.86 |
| PSF/ZTC MMM | 0.25 | 213 | 62.59 | 33.24 |
| PSF/ZTC MMM | 0.4 | 182 | 62.45 | 36.77 |
| PSF/ZTC MMM | 0.5 | 179 | 62.53 | 34.62 |
| PSF/ZTC MMM | 0.7 | 179 | 61.92 | 36.35 |
| PSF/ZTC MMM | 1 | 178 | 62.00 | 35.28 |

All prepared MMMs were then examined using TGA to study the thermal stability. Figure 5.9 shows the TGA curve of all MMMs with different filler contents. It can be seen that neat PSF was thermally less stable than those of MMMs, while the thermal stability of MMMs was improved with increasing of filler loadings. The weight loss of neat PSF quickly started at about 120°C due to removal of residual solvent, followed by significant weight loss when the temperature reached to 500°C. The major degradation of neat PSF and MMMs are due to decomposition of PSF main chains. Moreover, the MMMs showed a lower weight loss between 400 – 600 °C and the residue at the end of temperature analysis (800°C) was higher in comparison to neat PSF (Table 5.3). The addition of ZTC-1 within PSF matrix acts as shielding effect to hinder the transport of degradation product. As a result, a higher amount of MMMs residue was obtained

compared to neat PSF. Subsequently, the final decomposition started at around 550°C was detected for all MMMs, indicating further degradation of membrane residue (Zulhairun *et al.*, 2017).

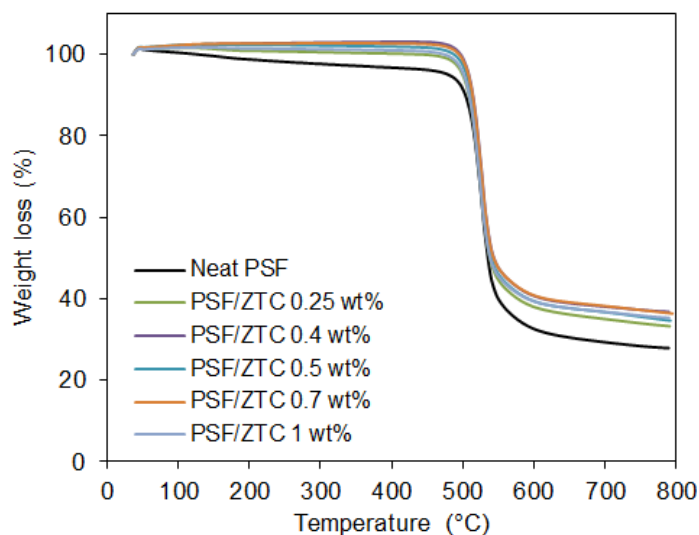


Figure 5.9 Thermal Decomposition Curve of PSF/ZTC-1 MMMs

5.2 Gas separation performance of MMM

Single gas permeation is used to evaluate the possible performance of all prepared MMMs under ideal conditions. The permeance of each membrane was measured for carbon dioxide, oxygen, hydrogen, nitrogen and methane at ambient temperature and at a pressure of 5 bar. For each membrane, the pair gas selectivities were obtained by taking the ratio of the permeances.

The permeances and selectivities of MMM are shown in Figure 5.10. The results revealed that the reduction in the gas permeance of neat PSF was proportional to the decrement kinetic diameter of gas with permeance order : N_2 (17 GPU) < O_2 (21 GPU) < CH_4 (23 GPU) < CO_2 (60) < H_2 (183 GPU). However, CH_4 (3.8 Å) had a higher permeance than O_2 and N_2 due to its higher solubility in polysulfone matrix (Ghosal *et al.* 1993). The CO_2/CH_4 , CO_2/N_2 , O_2/N_2 and H_2/CH_4 selectivity of neat PSF were 2.56, 3.64, 1.28 and 7.77, respectively, and the results were comparable with the data reported previously (Table 5.7).

When comparing to neat PSF, the selectivities of MMMs up to ZTC-1 loading of 0.5 wt% enhanced and the gas permeances varied (Figure 5.10). These

good performance indicated an ideal polymer-filler interface resulting from the formation of rigidified polymer around the ZTC particles consistent with the increased Tg. However, the rigidification effect is negligible at above 0.5 wt% loading due to the stable Tg compared to neat PSF. As the ZTC loading was further increased to 0.7 and 1 wt%, the MMMs showed significant increase of permeances with poorer selectivity for all separation. The reduced selectivity was observed due to the higher enhancement permeance of larger kinetic diameter gas (CH₄ and N₂). Such gases would take bigger advantages of Knudsen diffusion mechanism, either through the voids between particles and polymer or the pores within the particle agglomerates. It was previously showed from the surface observation, the surface defects were detected for MMMs (0.7 and 1 wt% loadings) and these unselective voids formation was believed to be related to higher permeance and selectivity loss. The voids could be formed within the particle agglomerates and the polymer chains could not be adsorbed within the voids, hence, they would act as extra channels to provide gas diffusion swiftly. The calculated values of Knudsen selectivity obtained from the Equation 2.19 are listed in Table 5.6. The obtained selectivity values for MMMs with 0.7 and 1 wt% loading were consistent with the Knudsen selectivities, indicating that the gas transport through the membranes was controlled by Knudsen diffusion mechanism. The Knudsen mechanism is the diffusion mechanism governed by interfacial voids. However, the selectivity values for other MMMs were not in accordance, hence, these high selectivity could not be attributed to a Knudsen mechanism. Also, these results could not be described by molecular sieving mechanism since the pore size of ZTC-1 (1.54 nm) is larger than molecular diameter of penetrants. These increasing selectivity might be associated to a surface flux mechanism through micro-mesoporous ZTC-1, with mechanism of more favorable surface diffusion of fast, lower kinetic diameter gases relative to slow, larger kinetic diameter gases (CH₄ and N₂), followed by gas diffusion in the ZTC-1 micropores (Magueijo *et al.*, 2013; Anson *et al.*, 2004).

Table 5.7 compares the gas performances of PSF-based MMMs with different type of porous filler for some separation. The improvement in CO₂ and O₂ permeances by using carbon xerogel filler was reported by Magueijo *et al.*

(2013), while the enhancement of CO_2/CH_4 , CO_2/N_2 and O_2/N_2 selectivities was not significant. Also, Bhardwaj et al. (2003) investigated a higher O_2 permeances of PSF-based MMMs by incorporating TiO_2 and carbon, but the selectivities of O_2/N_2 were still lower than those of value in this work. Though the slight increment in permeances was observed in this work, but it would be accompanied with sufficient selectivity enhancement. Interestingly, the low ZTC loading (0.4 wt%) could compete with the MMM utilizing larger percentage of fillers to provide higher selectivity improvement.

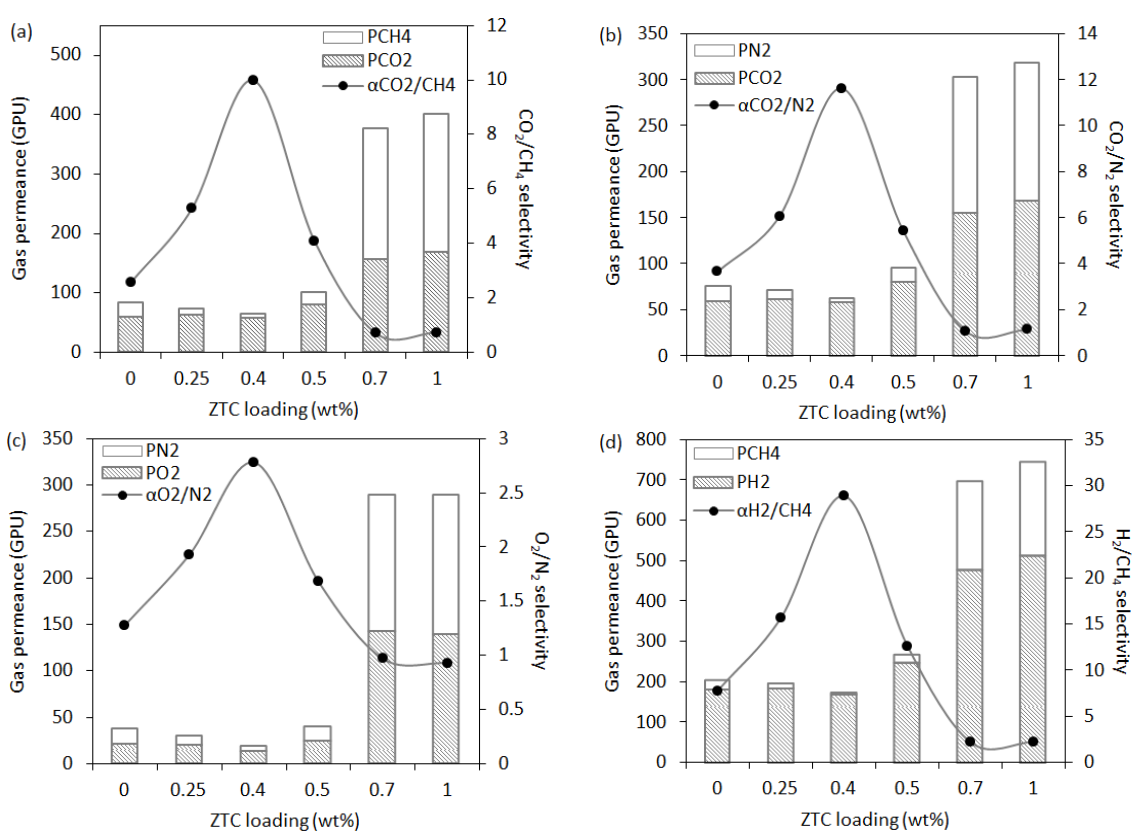


Figure 5.10 Gas permeability and selectivity of (a) CO_2/CH_4 , (b) CO_2/N_2 , (c) O_2/N_2 and (d) H_2/CH_4 of all prepared membranes

Single gas permeation is a necessary first step for new material screening process, but in reality, the transport of a component is affected by the presence of other component. Therefore, this study must be followed by gas mixture measurement in realistic condition. As seen from Table 5.6, the performances of MMMs up ZTC-1 loading of 0.5 wt% were higher compared to neat PSF and the

greater selectivity improvement was obtained for CO₂/CH₄ and H₂/CH₄ gas pairs. Therefore, the MMMs were used to separate CO₂/CH₄ and H₂/CH₄ binary gas under room temperature and total feed pressure of 5 bar. However, all the membranes showed poor mixed-gas separation performances, which was inconsistent with single gas measurement data (see Table 5.4). At the same feed pressure, it was supposed that the permeance under mixed-gas flow were almost lower than those of single gas. The diffusion of a penetrant in mixed-gas through the membrane is likely different from that in single gas measurement. This could be explained considering the presence of competition of other gas penetrant. The decreased CO₂ or H₂ permeances can be attributed to a competition with the CH₄ for the sorption sites in the membrane (Jiang *et al.*, 2007). In the case of H₂/CH₄ mixed-gas, the reduction of H₂ was higher than that of CH₄. The H₂ gas has a lower critical temperature of 33.2 K than that of CH₄ (190.55 K), leading to a larger sorption of CH₄ than H₂. Consequently, the sorption of CH₄ on the polymer matrix competitively diminished the sorption of H₂, leading to a further reduction in H₂ permeance (Kim *et al.* 2019). For CO₂/CH₄ mixed-gas, the greater critical temperature of CO₂ (304.25 K) may reduce the CH₄ sorption. Furthermore, the fast diffusion of CO₂ through the membrane would facilitate the diffusivity of CH₄ (Jiang *et al.*, 2007). The increment of CH₄ diffusion is much larger than the decrease in CH₄ sorption, leading to smaller decrement or even increment in permeance for CH₄ than for CO₂.

In addition, the non-ideal gas behaviors in the gas mixture containing CO₂ lead to the deviation performance from that of single gas measurements. As seen from Table 5.5, the fugacity coefficient of CO₂ in the mixed-gas was lower compared to that in pure CO₂. This can be explained by the existence of CH₄ in the mixture giving a contribution to the total pressure. Consequently, the thermodynamic driving force for CO₂ through the membrane decreased in a mixed-gas system, leading to a lower permeance (Wang *et al.*, 2002). As a result, the mixed-gas selectivities obtained are significantly lower than the ideal gas selectivities. The decreased performances of mixed-gas from the single gas measurement were also observed in the previous studies (Kim *et al.* 2019), (Yoshimune and Haraya, 2013b), (Khan *et al.*, 2010).

Table 5.4 Binary Gas Permeance and Selectivity

| Membrane | Mixture gas permeance (GPU) 50/50% CO ₂ /CH ₄ | | Mixture gas permeance (GPU) 50/50% H ₂ /CH ₄ | | Mixture gas selectivity | | Ideal gas selectivity (this work) | |
|--------------------|--|----------------------|---|----------------------|----------------------------------|---------------------------------|-----------------------------------|---------------------------------|
| | CO ₂ | CH ₄ | H ₂ | CH ₄ | CO ₂ /CH ₄ | H ₂ /CH ₄ | CO ₂ /CH ₄ | H ₂ /CH ₄ |
| Neat PSF | 21.66±0.32 (-177%) | 12.35±0.18 (-90%) | 44±0.41 (-315%) | 16.26±0.15 (-45%) | 1.75 | 2.71 | 2.56 | 7.77 |
| PSF/ZTC-1 0.25 wt% | 34.19±1.46 (-82%) | 15.71±0.67 (+25%) | 76±1.40 (-143%) | 9.16±0.17 (-28%) | 2.18 | 8.30 | 5.28 | 15.67 |
| PSF/ZTC-1 0.4 wt% | 17.69±0.17 (-231%) | 7.11±0.07 (+17%) | 91.95±1.87 (-84%) | 9.46±0.19 (+38%) | 2.49 | 9.72 | 9.99 | 28.88 |
| PSF/ZTC-1 0.5 wt% | 31.12±0.94 (-160%) | 17.46±0.53 (-13%) | 44.22±0.70 (-463%) | 9.62±0.15 (-106%) | 1.78 | 4.60 | 4.10 | 12.60 |

Number in parenthesis showed percentage decrement (-) and increment (+) of gas permeance with respect to pure gas permeation measurements. ± values in table are standard deviation from 4 samples.

Table 5.5 Fugacity Coefficients for Single Gases and Mixed-Gases at Equivalent Feed Pressure and Temperature of 25 °C

| Single gases | | Mixed-gas (50/50%) | |
|------------------------|------------------|------------------------------|------------------|
| Fugacity coefficients* | | Mixed fugacity coefficients* | |
| φ _{CO2} | φ _{CH4} | φ _{CO2} | φ _{CH4} |
| 0.9753 | 0.9913 | 0.9440 | 0.9839 |

Calculated using Eq.3.7 – 3.12

5.3 Summary

A series study performed on the structural, morphological properties and thermal stability of PSF-based MMMs with ZTC-1 was evaluated. The XRD investigation has demonstrated that adding ZTC-1 within PSF matrix had a slight effect on the amorphous nature of PSF and induced minor change on the polymer chain mobility. The absence of the ZTC-1 peak characteristic at 2θ of about 6.05 ° in the MMM (0.25 – 0.5 wt% loading) spectrum is attributed to a low concentrations with the possibility of good particle dispersion. Raman spectroscopy, XRD and SEM observations suggested a good interaction and dispersability with PSF matrix for MMMs at low ZTC-1 loading (0.25 – 0.5 wt%). Meanwhile, it was observed that ZTC-1 dispersion was low due to some agglomerated structures for MMMs with higher ZTC content. The particles were easily merged to each other and formed larger agglomerates at a higher ZTC-1 loading due to the lack of strong interaction between the PSF matrix and the fillers, as revealed by FTIR results. The aggregated structure was also proven by

the AFM analyses. According to AFM images, the membrane surface was rather rough by adding ZTC-1 and the roughness values enhanced by increasing ZTC-1 in the membranes. The TGA analysis presented a higher thermal stability when ZTC-1 was embedded within PSF matrix. The Tg of the membranes was found to be enhanced and the values were slightly dropped with the increase in ZTC-1 loading.

Results from permeation measurements showed that permeance and selectivity depended on the filler loadings. With increasing ZTC-1 loading up to 0.5 wt%, the permeance of all gases varied and the selectivity for all pair gases raised. When the ZTC content was further increased to 1 wt%, the higher permeances with loss selectivity were achieved. The gas transport in the membranes through the voids between ZTC-1 and polymer chains is the main reason for enhanced gas permeance due to the higher ZTC loading. Consequently, the gas selectivity dropped as the ZTC loading increased from 0.25 wt% to 1 wt%. Binary gas measurement were also performed to know the effect of other gas penetrant in the mixture. It has been revealed that there was a difference in the membrane performances between single gas and mixed-gas measurements under similar operating conditions. The results showed that permeance and selectivity in the mixture gas were significantly lower than that in single gas. This can be due to the influence of competitive sorption and the effect of non-ideal gas behavior in a mixed-gas system.

Table 5.6 Gas Permeation Properties of All Fabricated Membranes

| Sample | P/l_{CO_2} (GPU) | P/l_{CH_4} (GPU) | P/l_{O_2} (GPU) | P/l_{N_2} (GPU) | P/l_{H_2} (GPU) | α_{CO_2/CH_4} | α_{O_2/N_2} | α_{CO_2/N_2} | α_{H_2/CH_4} |
|---------------------|--------------------|--------------------|-------------------|-------------------|-------------------|----------------------|--------------------|---------------------|---------------------|
| Neat PSF | 60.13±5.17 | 23.49±1.41 | 21.17±3.11 | 16.53±1.11 | 182.57±10.59 | 2.56 | 1.28 | 3.64 | 7.77 |
| PSF/ZTC 0.25 wt% | 62.09±8.72 | 11.77±3.23 | 19.76±0.37 | 10.26±0.81 | 184.40±22.35 | 5.28 | 1.93 | 6.05 | 15.67 |
| PSF/ZTC 0.4 wt% | 58.53±4.17 | 5.86±1.96 | 13.99±1.15 | 5.04±1.07 | 169.20±5.65 | 9.99 | 2.78 | 11.62 | 28.88 |
| PSF/ZTC 0.5 wt% | 80.93±7.02 | 19.75±3.59 | 25.11±1.97 | 14.97±2.02 | 248.91±12.99 | 4.10 | 1.68 | 5.41 | 12.60 |
| PSF/ZTC 0.7 wt% | 160.19±3.14 | 224.97±9.95 | 146.26±4.89 | 150.39±8.60 | 487.93±24.82 | 0.71 | 0.97 | 1.07 | 2.17 |
| PSF/ZTC-1 wt% | 169.43±2.86 | 230.64±4.14 | 139.65±3.68 | 149.49±3.14 | 512.69±10.80 | 0.73 | 0.93 | 1.13 | 2.22 |
| Knudsen selectivity | | | | | | 0.60 | 0.94 | 0.80 | 2.82 |

1 GPU = 10^{-6} [cm³(STP) s⁻¹ cm⁻² cmHg⁻¹], ± values in table are standard deviations from 4 samples

Table 5.7 The Comparisons of Gas Separation Performances of PSF Based MMMs Loaded with Several Type of Fillers

| Membranes | Filler loading (best performance, wt%) | Operating condition | | Pristine membrane performance | | | | | MMM performance (best performance) | | | | | Ref. |
|----------------------------------|--|---------------------|---------|-------------------------------|-----------------|----------------------|---------------------|--------------------|------------------------------------|-----------------|----------------------|---------------------|--------------------|---------------------------------|
| | | T (°C) | P (bar) | P_{CO_2} (GPU) | P_{O_2} (GPU) | α_{CO_2/CH_4} | α_{CO_2/N_2} | α_{O_2/N_2} | P_{CO_2} (GPU) | P_{O_2} (GPU) | α_{CO_2/CH_4} | α_{CO_2/N_2} | α_{O_2/N_2} | |
| PSF/ZTC | 0.25-1 (0.4) | 25 | 5 | 60.13 | 21.17 | 2.56 | 3.64 | 1.28 | 58.53 | 13.99 | 9.99 | 11.62 | 2.78 | This work |
| PSF/carbon xerogel | 5-10 (5) | 25 | 5 | 187 | 135 | 1.02 | 1.40 | 1.00 | 262 | 175 | 1.20 | 1.68 | 1.13 | (Magueijo <i>et al.</i> , 2013) |
| PSF/TiO ₂ | 5 | 25 | 5 | - | 97.71 | - | - | 1.06 | - | 119.52 | - | - | 0.97 | |
| PSF/carbon black | 2-10 (2) | 25 | 5 | - | 97.71 | - | - | 1.06 | - | 292.84 | - | - | 1.76 | (Bhardwaj <i>et al.</i> , 2003) |
| PSF/vapor-grown carbon nanofiber | 5 | 25 | 5 | - | 97.71 | - | - | 1.06 | - | 119.56 | - | - | 1.78 | |

1 GPU = 10^{-6} [cm³(STP) s⁻¹ cm⁻² cmHg⁻¹]

CHAPTER 6

MEMBRANE MODIFICATION BY SURFACE COATING AND HEATING TREATMENT

Based on the results presented in Chapter 5, the obtained MMMs result in the formation of interfacial voids between the two phase, especially at higher particle loading, thereby causing the enhancement in permeance with loss selectivity. The MMM at 1 wt% showed an average of 522% permeance enhancement for all gases and 60% selectivity decrement in all separation. The results clearly exhibited that MMM possessed less ability to separate gas due to some particle aggregates at the membrane surface. These filler aggregates would be responsible for defects between the polymer matrix and particle and/or among the particles. However, such membrane can be still a promising candidate for a new membrane material with necessary modification of the membrane.

Post-treatment by surface coating can be performed to seal the pinholes (voids) on the surface of the skin layer without affecting structural integrity, thus improving gas pair selectivity. Polydimethylsiloxane (PDMS) has been used as coating material to modify the surface of hollow fiber membranes (Roslan *et al.*, 2018). In addition to surface coating, annealing process at temperature above the polymer T_g has been investigated to result a better polymer-filler adhesion. The membranes which were heated at temperature above the polymer T_g minimized the void formation when the filler loading was increased (Mahajan & Koros 2002). The annealing treatment affects the polymer chain flexibility and subsequently leads to the contact between particles and polymer matrix (A. F. Ismail, Rahim, *et al.*, 2008). As discussed in Chapter 2 Literature Review, the polymer chains become quite mobile and flexible and easily surround the particles, thus causing the increase in the adhesion of particles to the polymer matrix. However, by combining the thermal annealing with surface coating, the membrane selectivity was further improved (Ferreira and Trierweiler, 2009).

This chapter describes the single gas permeation performance of post-treated membrane as a function of ZTC-1 loading in comparison to untreated membrane. The post-treated membrane by surface coating is referred to a coated MMM, while the post-treated membrane using heating treatment is referred to a heated MMM. Scanning Electron Microscopy (SEM) was conducted for understanding the different of the treated and untreated membrane surface. The EDX measurement was also conducted to confirm the successful coating on the outer surface of the membranes. Moreover, in order to determine the effect of heat treatment on the thermal stabilities and glass transition temperature (T_g) of membrane, thermogravimetric analysis (TGA) and differential scanning calorimetry (DSC) were also conducted.

6.1 The Improvement of MMM Performance by Coating Surface

To improve the existing performance of PSF-based MMMs, polydimethyl siloxane (PDMS) solution was used to form a thin coating layer on the outer surface of membrane. This is further supported by SEM images as shown in Figure 6.1. Figure 6.1(1) shows the cross-sectional images of selected coated MMMs. This images suggest a good quality coating of membrane. Furthermore, the surface images in Figure 6.1(2) also confirm that all MMM surface is perfectly coated by PDMS layer that seals the membrane surface voids or pinholes. Consequently, the surface of coated MMMs is more defect free and smoother compared to that of uncoated MMMs in Figure 5.4.

Table 6.1 shows the EDX results on the surface of coated MMMs. The selected area for each membrane surface is presented in Figure 6.2. The presence of silicon (Si) confirms the successful formation of PDMS layer and it is well distributed on the membrane surface. As determined from Figure 6.1, the coating layer of PDMS is ranging from 83 – 112 nm. However, the EDX results could not precisely indicate the absolute amount of PDMS material on the membrane surface since the penetration depth of EDX (1000 nm) is much larger compared to the thickness of coating layer. As a result, this analysis would also cover the elements of the PSF and particles. The detection of carbon (C), oxygen (O) and

sulfur (S) on the membrane surface is the characteristics of ZTC itself and PSF matrix containing sub unit of aryl-SO₂-aryl.

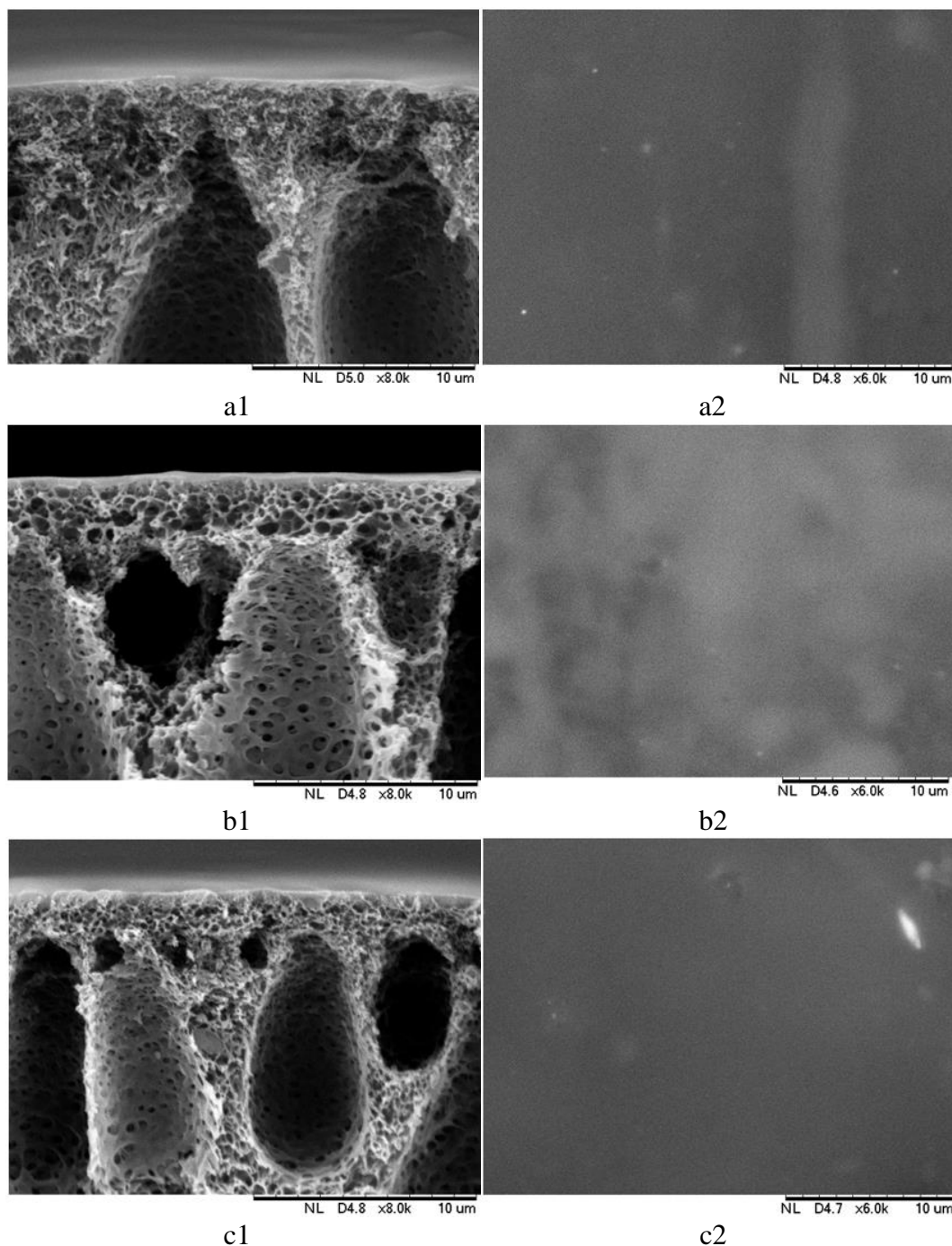


Figure 6.1 SEM images of (1) cross section and (2) surface of (a) 0.25 wt% ZTC/PSF, (b) 0.4 wt% ZTC/PSF and (c) 0.5 wt% ZTC/PSF MMMs with 3 wt% PDMS solution

Table 6.1 EDX Surface Mapping Result for the Coated MMMs

| Membrane | Element (wt%) | | | Total |
|------------------|---------------|--------|--------|-------|
| | Carbon | Oxygen | Sulfur | |
| 0.25 wt% ZTC/PSF | 46.54 | 29.49 | 9.36 | 100 |
| 0.4 wt% ZTC/PSF | 54.00 | 27.18 | 10.15 | 100 |
| 0.5 wt% ZTC/PSF | 47.03 | 31.24 | 8.65 | 100 |

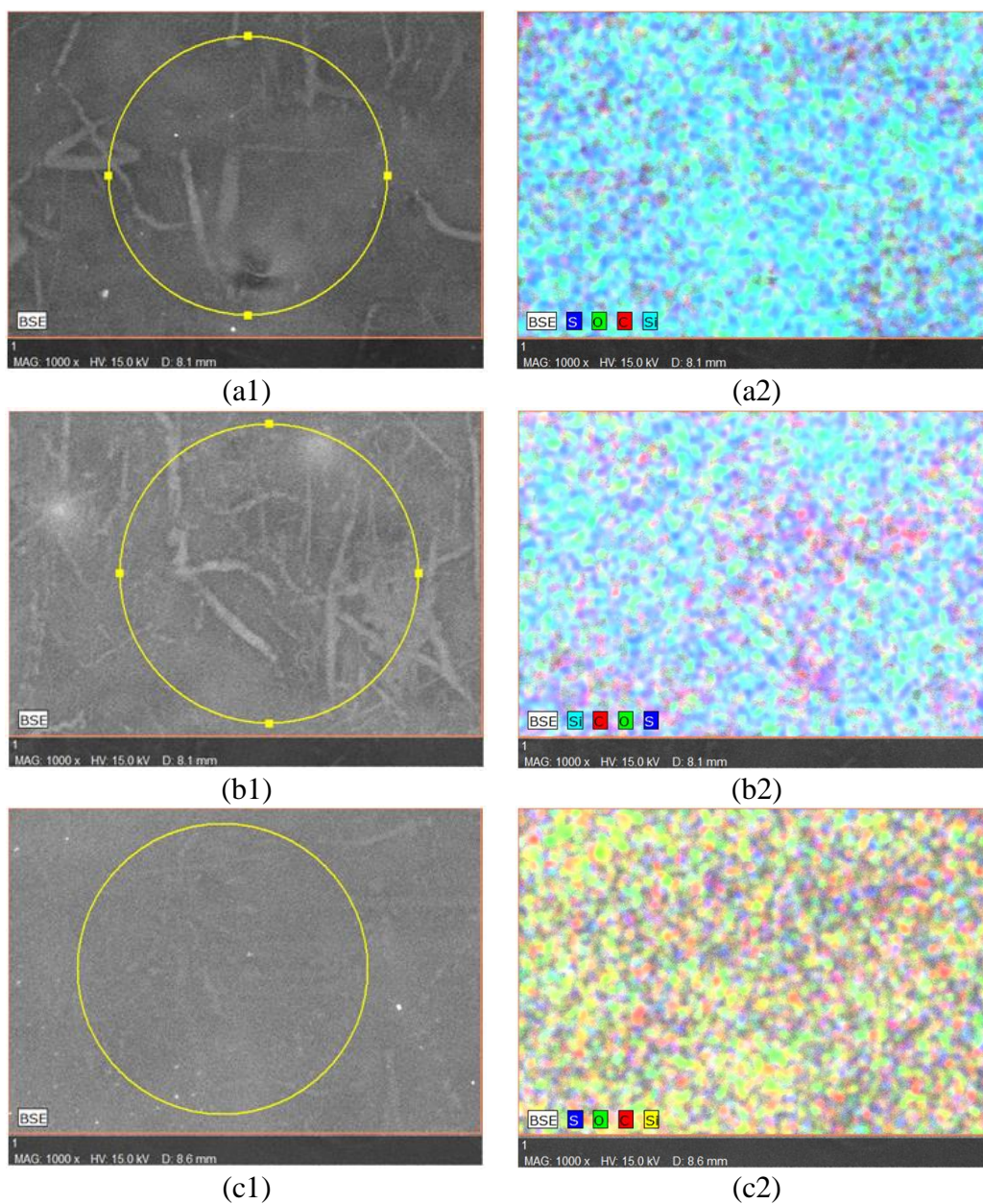


Figure 6.2 SEM EDX surface marking for (a) 0.25 wt% ZTC/PSF, (b) 0.4 wt% ZTC/PSF and (c) 0.5 wt% ZTC/PSF MMMs, respectively (1) and their representative mapping (2)

After coating treatment, the membranes were tested using single gases and the results are listed in Table 6.2. The performances of coated MMMs are more relevant since it represents the membrane performance. For instance, the CO₂/CH₄, CO₂/N₂, H₂/CH₄ and O₂/N₂ ideal gas selectivities of neat PSF were improved from 2.56, 3.64, 7.77 and 1.28 to 28.77, 32.27, 66.27 and 5.87, respectively, upon PDMS surface coating. The results revealed that neat PSF showed selectivities exceeding the intrinsic selectivity of PSF (Castro-muñoz, 2018). Fast gases (CO₂, H₂ and O₂) are now preferred compared to the slower and larger kinetic diameter gases (CH₄ and N₂). As a result, it leads to a higher selectivity. Compared to uncoated PSF, the permeances of coated neat PSF against all gases are dropped. This suggests that the presence of PDMS layer has a strong effect in the pores sealing, hence, it significantly increases gas selectivity to solution diffusion level and reduce permeance. The hydrophobic nature of PSF makes interaction with hydrophobic ZTC surface, thus perfectly sealing the voids between these two phases. Furthermore, the reduced permeance of CO₂ are reported to be lower compared to other gases since the PDMS coated membrane showed a greater affinity towards CO₂ molecules (Roslan *et al.*, 2018).

These coating process also improves all PSF/ZTC-1 MMMs selectivity and reduces permeance in comparison to uncoated MMMs. Moreover, the presence of filler improved the permeance of all gases compared to the coated PSF. The larger permeance of coated MMMs might be arise from the porosity induced by the filler. The mesopore structure in the outer layer of ZTC would assist the gases to diffuse faster into the inner micropores of the ZTC. This could be attributed to a higher permeance of MMMs. Furthermore, the ZTC also possesses strong physisorption properties for carbon dioxide (CO₂) and hydrogen (H₂) and results in higher permeance. Based on our previous study, the CO₂ and H₂ sorption on the ZTC material was up to 9.51 wt% and 1.72 wt%, respectively, at room temperature and 1 bar pressure (Gunawan, 2018)(Wijiyanti 2015). The permeances for MMMs at 0.4 wt% loading were lower than 0.25 wt% loaded filler. If filler induced voids were playing significant role for MMMs at these loadings, the greater permeance would be observed from 0.4 wt% loaded ZTC-1 due to the higher number of particles, but this was not the case. Meanwhile, the

slight enhancement in permeance with reduced selectivity was observed at 0.5 wt% loading, which can be ascribed to the decrease in polymer chain rigidity consistent with the decrease in T_g. Further increment of filler loading up to 1 wt% led to the prominent increment of slow and large kinetic diameter (CH₄ and N₂) permeances which take greater advantage of Knudsen diffusion opportunity due to severe interfacial voids in the initial membrane structure. Due to the great portion of large interface voids or pinholes, the silicon rubber which has a very high permeability will highly contribute as a third phase in the dense layer and the gas molecules will diffuse through this, leading to a very high permeance.

Furthermore, there was an improved selectivity of coated PSF membrane with the presence of ZTC-1. The highest selectivity improvement was found in 0.25 wt% loaded ZTC-1 with the permeance remained higher compared to the coated PSF, but only the modest selectivity was seen for 0.5 wt% loading. We argue that the reduced segmental mobility which consistent with the increase in T_g, 0.25 wt% loaded MMM resulted in higher selectivity improvement than that of 0.5 wt% MMM. The selectivity improvement could not be explained by molecular sieving mechanism as the average pore size of ZTC-1 (1.54 nm) is larger than molecular diameter of penetrants. Also, the enhanced selectivity might not be related to a Knudsen diffusion mechanism since the experimental selectivity was not in accordance with Knudsen selectivity value. These high selectivities could be associated to a surface flux mechanism through mesoporous ZTC-1, with mechanism of more favourable surface diffusion of fast and lower kinetic diameter gases rather than slow and larger kinetic diameter gases, subsequently followed by gas diffusion in the ZTC-1 micropores. Furthermore, the lower prevalence of inclusions in the MMM containing 0.25 wt% ZTC, as shown in the interparticle spacing (Table 6.3), might allow a higher portion of the gas flow to be solution diffusion through the polysulfone instead of diffusion through the ZTC pores. This phenomena is similar with those of previous published work (Magueijo *et al.*, 2013). However, at higher ZTC-1 loading (0.7 and 1 wt%) the selectivity can not be improved because of coating material overtake the function of the bulk mixed matrix material.

The separation performances of coated PSF/ZTC-1 MMM for CO₂/CH₄, O₂/N₂, CO₂/N₂ and H₂/CH₄ are compared with that of other PSF-based MMMs in the literature with respect to Robeson trade-off line (Figure 6.3). The diagram suggests that the permselectivity values for all MMMs are located below the 1991 and 2008 upper bound line, while the points of coated PSF/ZTC-1 MMM transcend the 1991 upper bound of polymer membrane performance for CO₂/N₂ separation. However, PSF/ZTC-1 MMM exhibited a better separation performance, approaching the upper bound line as compared to other MMMs in the literature. As shown in Table 6.4, the prepared PSF/ZTC MMM showed a higher permeance and selectivity than the reported MMM containing zeolite and other carbons. In addition, an interesting result was that the small amount of ZTC-1 content (0.25 wt%) loaded in this study can compete with MMM in other studies incorporated relatively higher percentage of filler loadings. Here, the high permeance and selectivity of MMMs in this work can be correlated to the intrinsic selectivities properties of PSF matrix, the selective gas capacity of ZTC-1 adsorption and the good compatibility between PSF matrix and particles as revealed by increasing T_g and SEM image. The results exhibited that PSF/ZTC MMM possess a great potential and favorable for carbon dioxide (CO₂), oxygen (O₂) and hydrogen (H₂) separation.

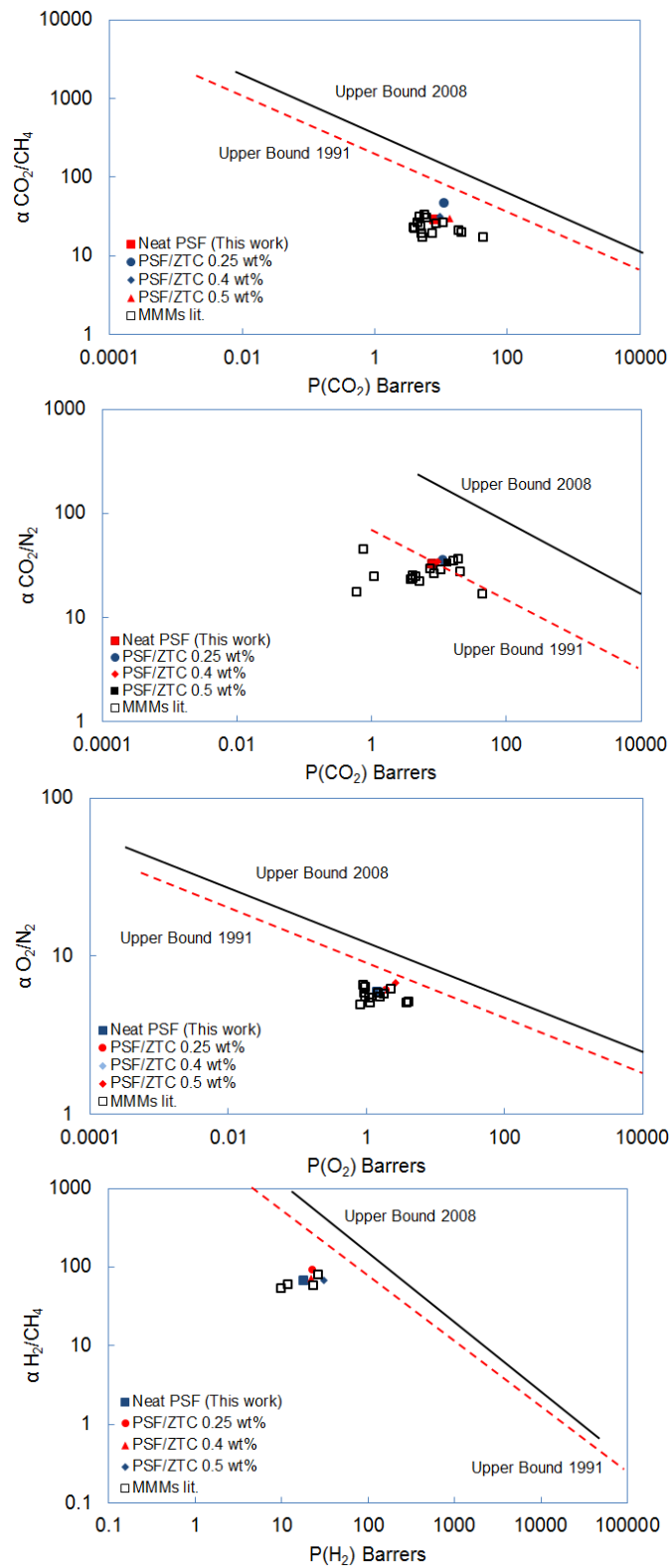


Figure 6.3 Gas separation performance of PSF/ZTC-1 MMMs for CO_2/CH_4 , CO_2/N_2 , O_2/N_2 and H_2/CH_4 gas pairs with respect to Robeson trade-off line, compared with the data on other PSF-based MMMs from literatures. The detail citations are listed in Table 6.4.

Table 6.2 Gas Separation Performance of Coated MMMs

| Sample | P/l_{CO_2} (GPU) | P/l_{CH_4} (GPU) | P/l_{O_2} (GPU) | P/l_{N_2} (GPU) | P/l_{H_2} (GPU) | α_{CO_2/CH_4} | α_{O_2/N_2} | α_{CO_2/N_2} | α_{H_2/CH_4} |
|----------|--------------------|--------------------|-------------------|-------------------|-------------------|----------------------|--------------------|---------------------|---------------------|
| Neat PSF | 41.34±3.87 | 1.44±0.19 | 7.52±0.85 | 1.28±0.12 | 95.23±10.54 | 28.77 | 5.87 | 32.27 | 66.27 |
| 0.25 wt% | 59.67±5.83 | 1.29±0.25 | 10.29±1.01 | 1.70±0.19 | 119.01±16.40 | 46.42 | 6.06 | 35.14 | 92.57 |
| 0.4 wt% | 51.51±7.96 | 1.66±0.36 | 9.03±1.20 | 1.51±0.29 | 116.49±18.31 | 30.98 | 5.99 | 34.15 | 70.07 |
| 0.5 wt% | 71.45±6.87 | 2.45±0.27 | 14.35±2.86 | 2.15±0.22 | 163.97±11.90 | 29.12 | 6.69 | 33.29 | 66.81 |
| 0.7 wt% | 45.00±5.42 | 7.52±1.45 | 10.61±1.21 | 4.72±1.16 | 98.73±15.32 | 5.99 | 2.25 | 9.53 | 13.14 |
| 1 wt% | 28.29±1.72 | 17.43±2.45 | 13.37±1.56 | 11.11±3.00 | 75.15±3.33 | 1.62 | 1.20 | 2.55 | 4.31 |

1 GPU = $1 \times 10^{-6} \text{ cm}^3 \text{ (STP)/cm}^2 \text{ s cmHg}$, \pm values in table are standard deviation from 4 samples

Table 6.3 Filler Interparticle Spacing and Size of PSF Molecule, Assuming Uniform Dispersion of Filler

| Membranes | Filler density (g/cm^3) | Filler particle diameter (nm) | Number of particles per m^3 | Interparticle spacing (nm) | Size of PSF molecule (nm) |
|-----------|---------------------------------------|----------------------------------|---|-------------------------------|------------------------------|
| 0.25 wt% | | | 1.57×10^{17} | 1854 | |
| 0.4 wt% | 0.75 | 369 | 2.51×10^{17} | 1586 | 97.8* |
| 0.5 wt% | | | 3.13×10^{17} | 1472 | |

Calculated using Eq. 3.15 – 3.18.

Table 6.4 Gas Separation Performances of Coated PSF Based MMMs from Previous Work

| Membranes | Best filler loading (wt%) | Operating condition | | | Neat Membrane performance | | | | | | MMM performance | | | | | | Ref. | |
|-----------------------|---------------------------|---------------------|---------|---------------------------|---------------------------|--------------------------|--------------------|-------------------|------------------|-------------------|---------------------------|--------------------------|--------------------------|--------------------|-------------------|------------------|-------|---|
| | | T (°C) | P (bar) | P _{CO2} (barrer) | P _{O2} (barrer) | P _{H2} (barrer) | $\alpha_{CO2/CH4}$ | $\alpha_{CO2/N2}$ | $\alpha_{O2/N2}$ | $\alpha_{H2/CH4}$ | P _{CO2} (barrer) | P _{O2} (barrer) | P _{H2} (barrer) | $\alpha_{CO2/CH4}$ | $\alpha_{CO2/N2}$ | $\alpha_{O2/N2}$ | | $\alpha_{H2/CH4}$ |
| PSF/ZTC-1 | 0.25 | 25 | 5 | 41.34* | 7.52* | 95.23* | 28.77 | 32.27 | 5.87 | 66.27 | 59.67* | 10.29* | 119.01* | 46.26 | 35.14 | 6.06 | 92.57 | This work |
| | 0.25 | 25 | 5 | 7.86 ^a | 1.43 ^a | 18.09 ^a | 28.77 | 32.27 | 5.87 | 66.27 | 11.34 ^a | 1.96 ^a | 22.61 ^a | 46.26 | 35.14 | 6.06 | 92.57 | |
| PSF/GO | 0.25 | 25 | 5 | 5.22 | - | - | 17.15 | 17.26 | - | - | 5.96 | - | - | 29.90 | 44.4 | - | - | (K. Zahri <i>et al.</i> , 2016) |
| PSF/Carbon xerogel | 5 | 25 | 5 | 84.90* | 15.0* | - | 40.30 | 43.54 | 8.35 | - | 103.3* | 17.8* | - | 32.70 | 31.21 | 5.95 | - | (Magueijo <i>et al.</i> , 2013) |
| PSF/CMS | 20 | 25 | 1 | - | 1.58 | - | - | - | 5.50 | - | - | 7.96 | - | - | - | 5.97 | - | (Ismail <i>et al.</i> , 2009) |
| PSF/SWNT | 5 | 35 | 4 | 3.90 | 0.84 | - | 22.94 | 22.94 | 4.94 | - | 5.12 | 1.16 | - | 18.96 | 22.26 | 5.04 | - | (Kim <i>et al.</i> , 2007) |
| PSF/GO | 0.25 | 25 | 5 | 64.47* | - | - | 19.20 | - | - | - | 86.80* | - | - | 25.98 | - | - | - | (K. Zahri <i>et al.</i> , 2016) |
| PSF/SAPO-34 | 10 | 25 | 3.48 | 44.02 | - | - | 17.3 | 16.5 | - | - | 471.03 | - | - | 28.2 | 26.1 | - | - | (Junaidi <i>et al.</i> , 2014) |
| PSF/MCM-41 | 30 | 25 | 2 | 7.53 | 1.50 | - | 19.40 | 29.30 | 5.84 | - | 20.50 | 3.83 | - | 19.60 | 27.22 | 5.08 | - | (Reid <i>et al.</i> , 2001) |
| PSF/TNT ₁₀ | 0.4 | 25 | 3 | 4.04 | 0.94 | 9.85 | 21.85 | 24.93 | 5.80 | 53.31 | 10.61 | 2.29 | 23.68 | 25.93 | 28.76 | 6.20 | 57.86 | (Zulhairun <i>et al.</i> , 2017) |
| PSF/Cloisite-15A | 1 | 25 | 5 | 4.97 | 1.10 | - | 23.12 | 24.54 | 5.43 | - | 18.72 | 4.09 | - | 20.98 | 23.48 | 5.13 | - | (Zulhairun, Ismail, <i>et al.</i> , 2014) |
| PSF/Fumed silica | 0.1 | 25 | 5 | 4.83 | 0.92 | - | 31.05 | 34.41 | 6.53 | - | 5.56 | 0.98 | - | 32.74 | 36.02 | 6.35 | - | (Wahab <i>et al.</i> , 2012) |
| PSF/MCM-48 | 10 | 25 | 4 | 4.46 | 0.98 | - | 25.88 | 24.78 | 5.47 | - | 8.45 | 1.84 | - | 25.47 | 26.41 | 5.75 | - | (Kim <i>et al.</i> , 2006) |
| PSF/MSS | 8 | 35 | 5 | - | - | 11.80 | - | - | - | 58.90 | - | - | 26.50 | - | - | - | 79.20 | (Zornoza <i>et al.</i> , 2009) |
| PSF/zeolite-AgA | 20 | | | 5.60 | - | - | - | 22.40 | - | - | 3.22 | - | - | - | 27.13 | - | - | (Tian-ming <i>et al.</i> , 2012) |

*unit in GPU, 1 GPU = 1 x 10⁻⁶ cm³ (STP)/cm² s cmHg

^aDense skin layer thickness of 190 nm is assumed

6.2 The Improvement of MMM Performance by Heating Treatment

Heat treatment above PSF's T_g is another attempt to compact the polymer-particle contact and densify the surface layer. Figure 6.4 and 6.5 represent the cross sectional and surface SEM images of MMMs heat treated at 200°C for 30 min and the results partially confirm the assumptions. It is noticed in Figure 6.4 that the mixed matrix structure was quite dense as compared to the untreated membranes and the particles were evenly distributed in the membrane structure. The polymer seemed to be in better attached to the particle surface, but some voids between the particles and polymer were also detected for all MMMs and the whole outer layer was rough. It can be seen in Figure 6.5 in which the polymer and particles possess a distinct boundary. Though the heat treatment can help the polymer chains to surround the ZTC-1 surface more easily, the interaction between these two phase possibly can not totally prevent the particle detachment upon the treatment (Ferreira and Trierweiler, 2009). In addition, the surface layer is formerly porous and some particles loosely adhere to the polymer (Figure 5.3). It possibly occurs since the soaking time (30 min) may not be adequate enough to compact the polymer and particle contact.

Figure 6.6 shows the permeability and selectivity of the heated MMMs. With heating, the permeances of all gases significantly dropped as compared to the untreated MMMs. This was due to decrement of void spaces between the polymer chains and particles (A. F. Ismail, Rahim, *et al.*, 2008). The flexible chains of polymer are thermodynamically easier to be reoriented during the heat treatment process. As a result, the membrane possess better chain packing. The segmental mobility of polymer is decreased by the heat treatment as revealed by an increase in T_g (see Table 6.5) and this has contributed to the permeance reduction. Because of the thicker dense layer at higher filler loading (Figure 6.4), the diffusion rate of big molecules increased compared to small gases, thus leading to a lower selectivity.

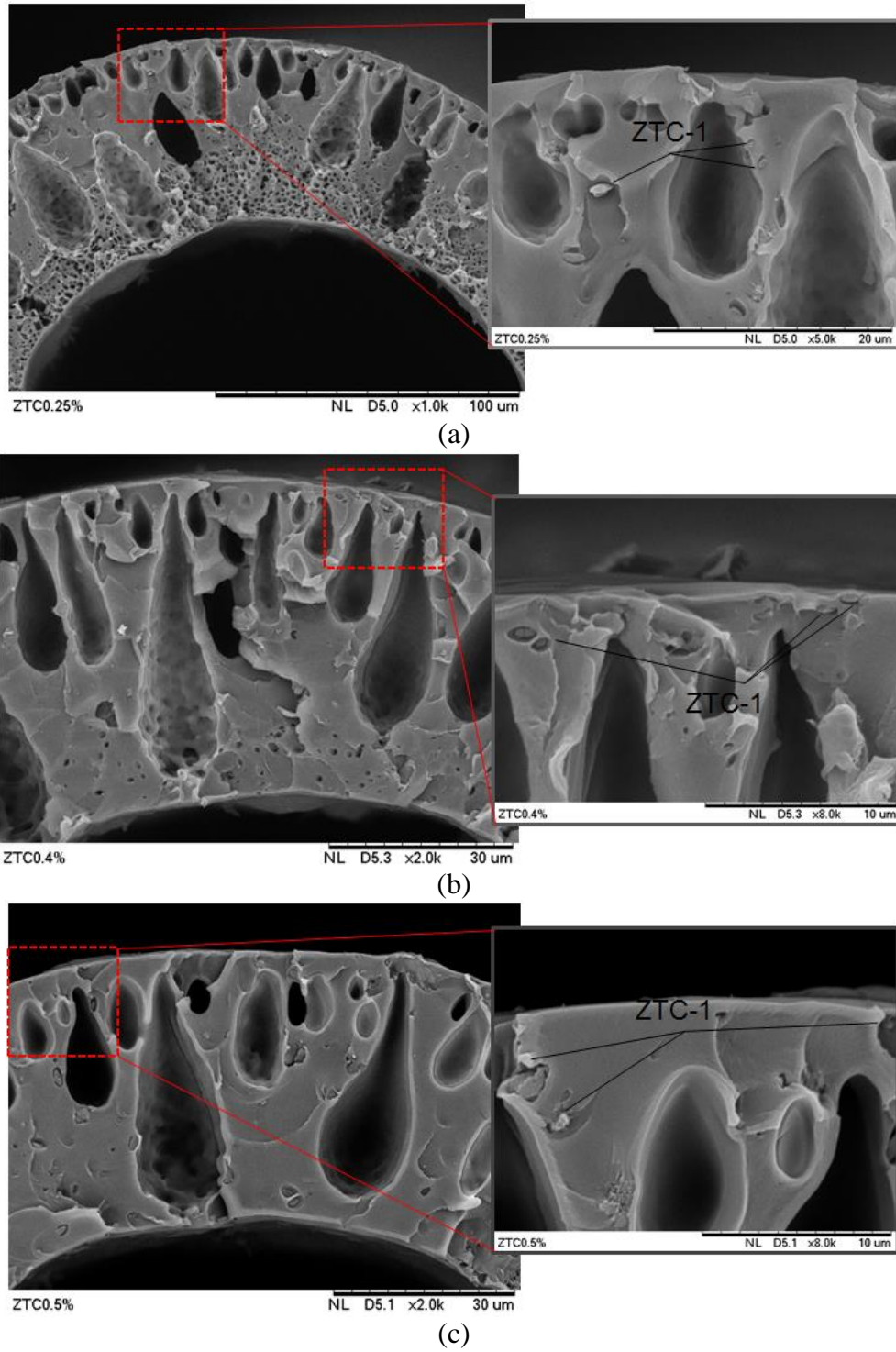


Figure 6.4 SEM micrograph of the cross-sectional view of the (a) 0.25 wt%, (b) 0.4 wt% and (c) 0.5 wt% ZTC-1 loaded MMMs after heat treated at 200°C

Table 6.5 The Glass Transition Temperature of MMMs at Various Heating Period

| Membrane | T _g (°C) |
|------------------------------|---------------------|
| 0.25 wt% ZTC-1 MMM (30 min) | 480 |
| 0.4 wt% ZTC-1 MMM (30 min) | 480 |
| 0.5 wt% ZTC-1 MMM (30 min) | 484 |
| 0.25 wt% ZTC-1 MMM (120 min) | 483 |
| 0.4 wt% ZTC-1 MMM (120 min) | 490 |
| 0.5 wt% ZTC-1 MMM (120 min) | 477 |
| 0.25 wt% ZTC-1 MMM (240 min) | 486 |

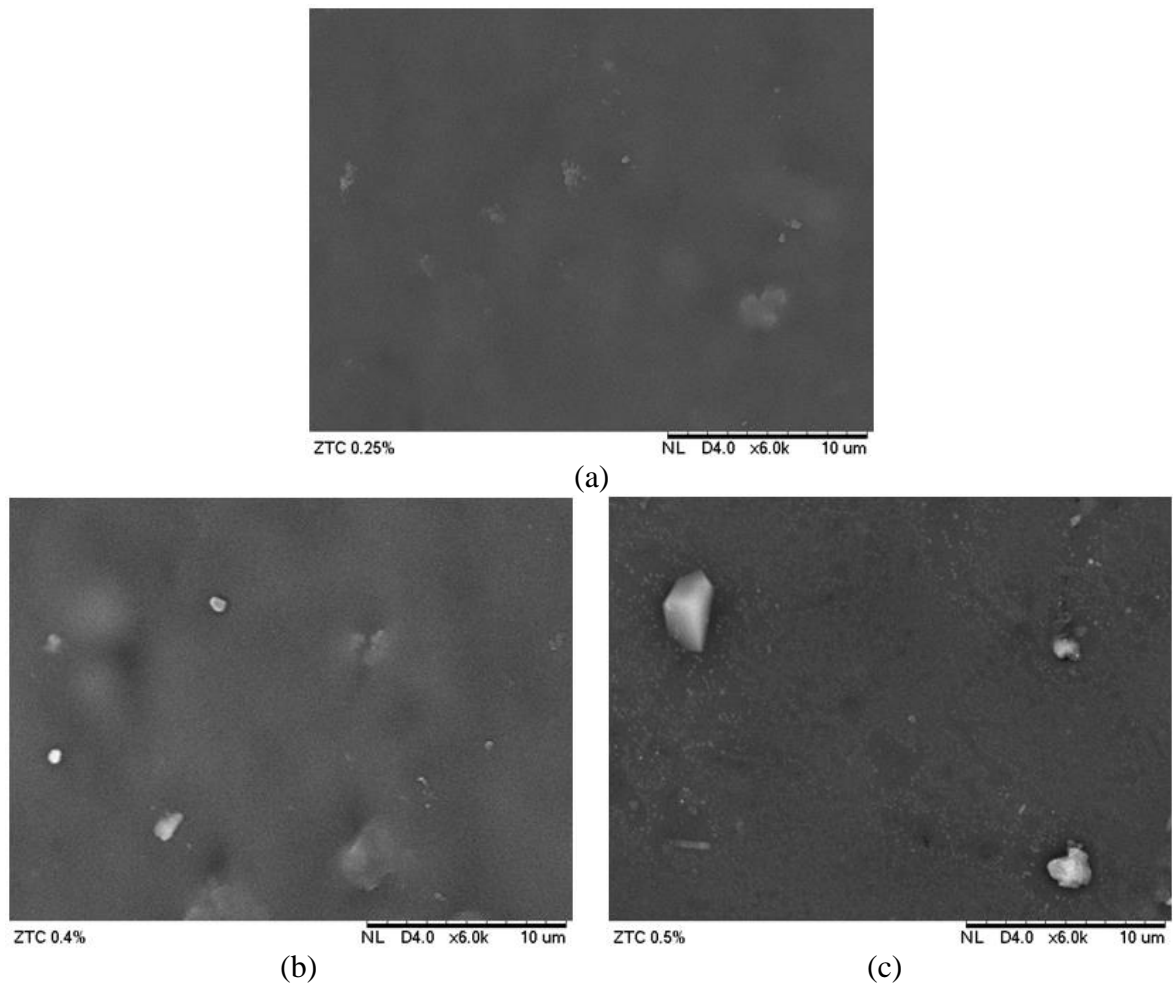


Figure 6.5 Surface morphology of the (a) 0.25 wt%, (b) 0.4 wt% and (c) 0.5 wt% ZTC-1 loaded MMMs with heat treatment at 200°C

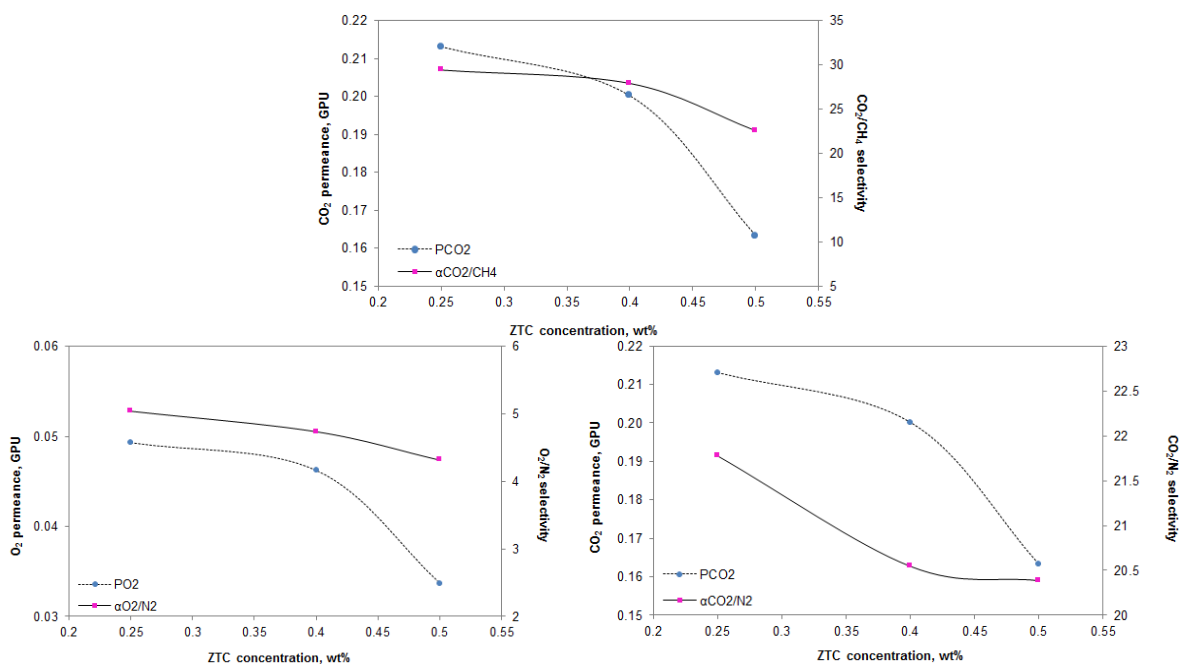


Figure 6.6 The permeance and selectivity of membrane as a function of ZTC-1 loading after heat treated at 200 °C for 30 min.

To demonstrate whether the long thermal soaking time is effective in achieving a less defective polymer-ZTC-1 structure, the membranes are heated at 200°C for 120 min. The SEM micrographs in Figure 6.7 and Figure 6.8 exhibit the morphology of the heated membrane. The cross-sectional images showed that the outer layer became denser in contrast with that in Figure 6.4. Also, the prolonged heating treatment suppressed the free volume in the polymer matrix. Both surface and cross-sectional images showed that the voids has been reduced by increasing heating period, but some nanosized polymer-particle interface voids still existed for all MMMs and the surface layer was still rough (see in Figure 6.7). It can be concluded that the increase in soaking period to 120 min is still not enough to totally blend the polymers with particle.

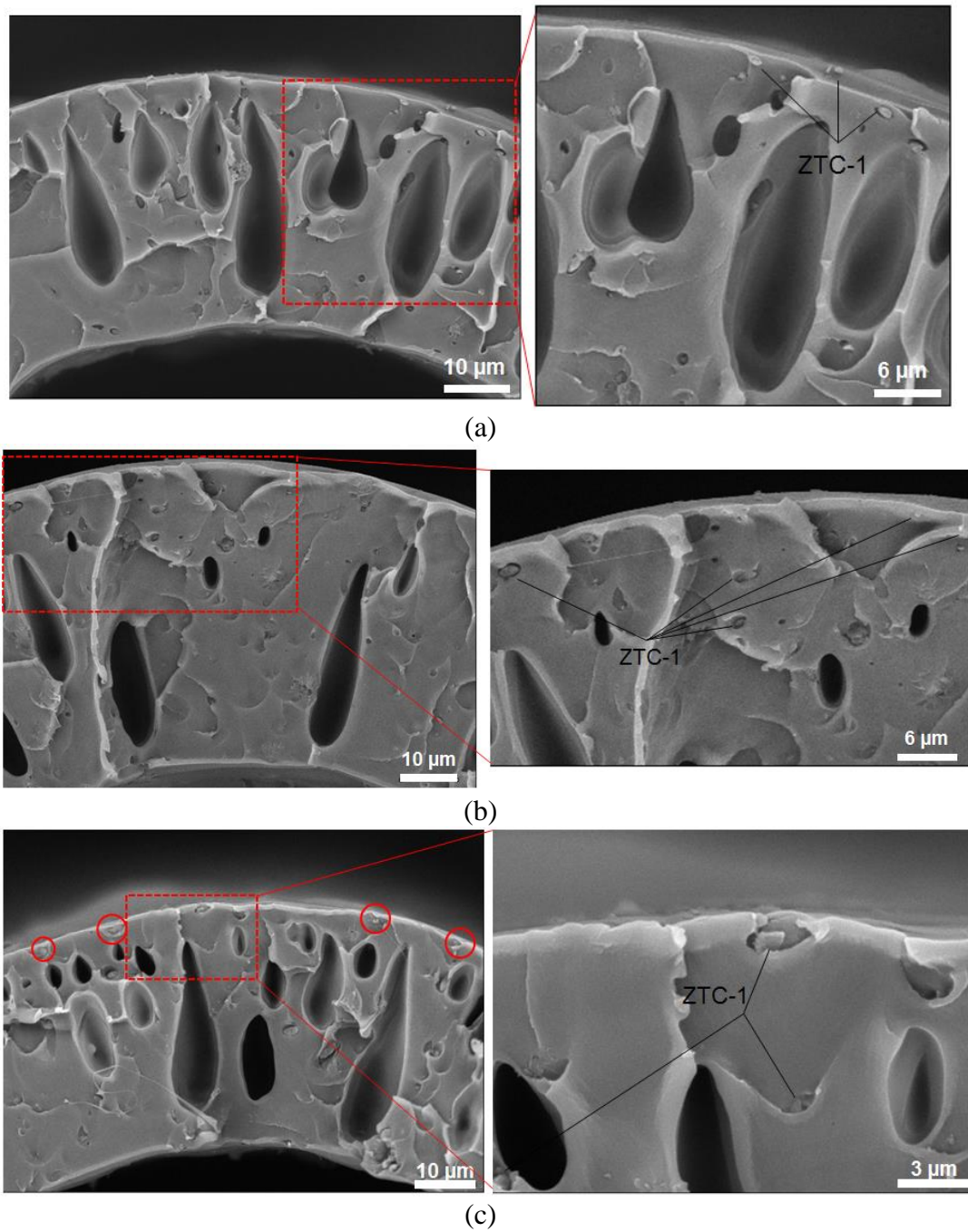


Figure 6.7 SEM micrograph of the cross-sectional view of the (a) 0.25 wt%, (b) 0.4 wt% and (c) 0.5 wt% ZTC-1 loaded MMMs after heat treated at 200°C

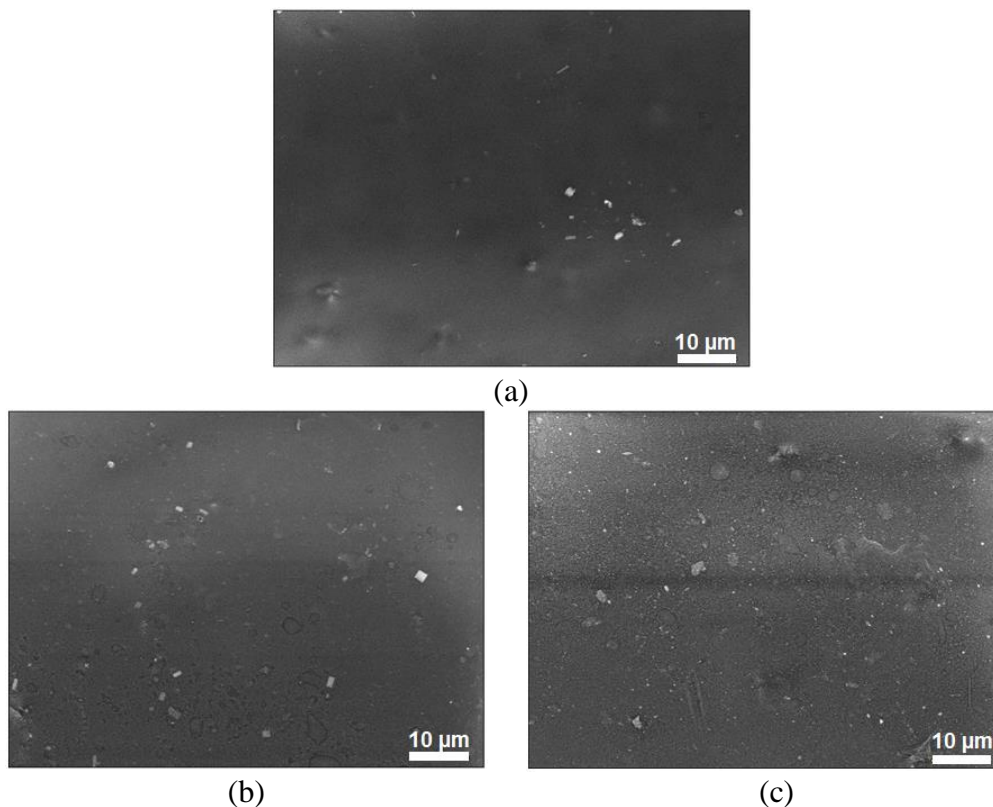


Figure 6.8 Surface morphology of the (a) 0.25 wt%, (b) 0.4 wt% and (c) 0.5 wt% ZTC-1 loaded MMMs with heat treatment at 200°C

Figure 6.9 shows the single gas permeation data (permeance and selectivity) of the heat treated membranes. The permeances of the membranes generally dropped with increasing ZTC-1 loading. However, up to 0.4 wt% loading, the lowest permeance for all gases was observed. This would be associated to the increase of polymer chain rigidity consistent with the T_g increment (Table 6.5). As the filler loading was further increased to 0.5 wt%, the permeances rose due to the increase in T_g . These values of permeance of the heat treated membranes were significantly lower compared to that of untreated membranes due to the relatively thicker selective layer and the denser substructure. Furthermore, it can be observed that all the heated MMMs exhibited sensible CO_2/CH_4 , CO_2/N_2 and O_2/N_2 selectivities and the values dropped with increasing ZTC-1 loading for three separations. Note that 0.4 wt% MMM showed simultaneous permeance and selectivity loss, which might be due to the blockage of ZTC pores as a result of severe interface rigidification. However, the decrement selectivity with increasing

ZTC-1 loading could also be associated to the the interface voids, which were still exist even in small amount and the gas transport through the voids is assumed to be Knudsen diffusion. This phenomena can be explained by the mechanism of gas transport through the polymer matrix, pore network of the particles and through non selective voids between the matrix and particles.

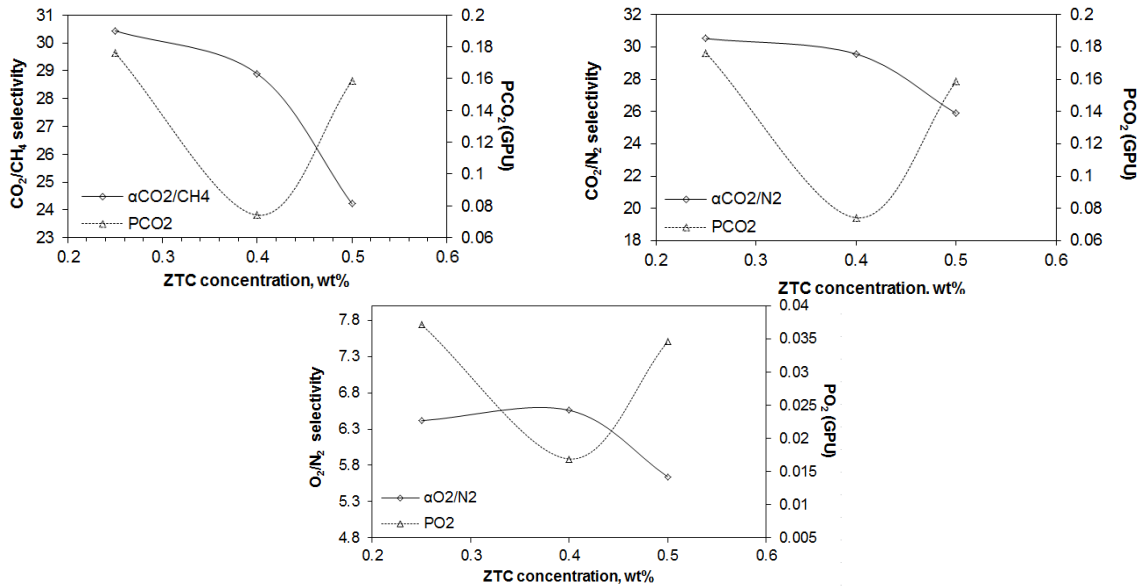


Figure 6.9 The permeance and selectivity of membrane as a function of ZTC-1 loading after heat treated at 200 °C for 120 min.

The optimum membrane (0.25 wt% loading) is further heated at 200°C for 240 min to investigate the possibility of reducing the voids. The obtaining morphology is exhibited in Figure 6.10. The prolonged heat treatment highly suppressed the pore structure in the polymer matrix and the outer layer became denser and more homogeneous (Figure 6.10). The compact packed chains in the substructure and the outer layer provide a high degree of size discrimination between the gas penetrants and this leads to undesirable resistance to gas transport. Another effect after the prolonged heat treatment was made the better adherence of ZTC-1 particles with polymer matrix and no obvious voids between two phases were observed. The defects on the fiber surface due to the poor interaction between polymer and particles could be minimized as shown in Figure 6.10b. The good compatibility between these two phases may have resulted in the

formation of rigidified polymer around the particles as revealed by the increase in T_g . After prolonged heat treatment, the permeance showed the average decrement of 138% for all gases and recorded average of 45% selectivity enhancement (Table 6.6). Consequently, it was no surprise that the permeance was lower but higher selectivity, as a result of the densification of substructure and the outer layer as well as the rigidification effect.

Table 6.6 Single Gas Permeation Data of 0.25 wt% ZTC Loaded MMM Heat Treated at 200° C for 240 Min

| Soaking period (min) | Permeance (GPU) | | | | Selectivity | | |
|----------------------|-----------------|----------------|-----------------|----------------|----------------------------------|---------------------------------|--------------------------------|
| | CO ₂ | O ₂ | CH ₄ | N ₂ | CO ₂ /CH ₄ | CO ₂ /N ₂ | O ₂ /N ₂ |
| 240 | 0.1403 ± | 0.0277 ± | 0.0035 ± | 0.0042 ± | 39.65 | 33.79 | 6.66 |
| | 0.0063 | 0.0048 | 0.0014 | 0.0005 | | | |

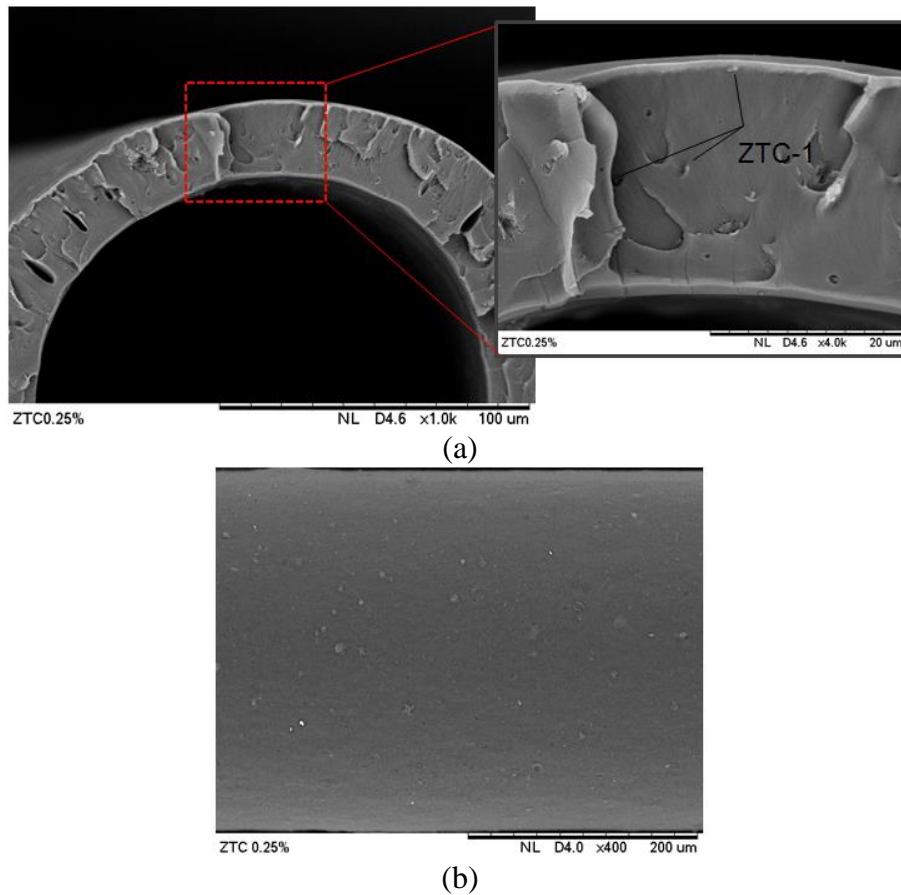


Figure 6.10 SEM images of (a) cross sectional and (b) surface of 0.25 wt% ZTC-1 heat treated at 200 °C for 4 h.

6.3 Summary

Based on the results presented in this section, it can be concluded that both coating and thermal treatment can be used as effective methods to improve adhesion of ZTC-1 particles with polymer matrix. It can reduce the interfacial void formation in hollow fiber mixed matrix membrane. As a result, the membrane selectivity can be improved.

After surface coating, the initial structure with observable interfacial voids becomes more defect free and smoother, resulting in a higher selectivity. The change in structure suggests that the surface coating treatment can effectively fill the voids. Nevertheless, the separation characteristic of coating material as a third phase in MMM will contribute in the whole performance of the membrane. Since the great amount of voids were observed for 0.7 and 1 wt% ZTC loaded MMMs, the silicon rubber (PDMS) dominates as a third phase in the surface layer and the gas will diffuse through this instead of mixed matrix. Since PDMS has no molecular sieving properties and possesses broad distribution of intersegmental gap size, the selectivity can not be improved and very high permeance was observed for all gases. Due to the small portion of existing defects at lower ZTC-1 loading, the selectivity of CO_2/CH_4 , O_2/N_2 , CO_2/N_2 and H_2/CH_4 enhanced up to 780%, 215%, 481% and 491%, respectively, with a slight change in permeance compared to uncoated MMM. These selectivity improvement was observed for MMM at 0.25 wt% ZTC-1 loading.

Because of the thermal effect the packed chains in the polymer matrix and the packed structure in the surface layer and substructure became denser. Consequently, the membrane became more compact as compared to the untreated membrane. In addition, the heat treatment increased the glass transition temperature (T_g) of the fibers. The increase in T_g suggests the reduced segmental mobility, and hence lower permeance than untreated membrane. The permeance of heated membrane was significantly low depending on the thermal soaking period. Thermal treatment at shorter period (30 min) produces a less defective membrane in the surface layer since the voids were still observed. However, the selectivity of CO_2/CH_4 , O_2/N_2 and CO_2/N_2 was found to be improved up to 457%, 162% and 277%, respectively as compared to that of untreated membrane. The

membrane selectivity with prolonged heat treatment (120 min) was further improved, but the permeance was severely diminished, as a result of the more densification of the substructure. However, some interfacial voids and the surface roughness were still observable. Obviously, at the prolonged soaking period (240 min) these voids have been removed and it seriously densify the polymer layer structure. As a result, the selectivity improvement of CO_2/CH_4 , O_2/N_2 and CO_2/N_2 was recorded up to 652%, 246% and 458%, respectively. The selectivity was enhanced by the prolonged heat treatment, the permeance was significantly dropped and this lead to undesirable resistance to gas transport.

For both treatments, the highest selectivity improvement was obtained at lower ZTC-1 loading (0.25 wt%). Also, it is found that surface coating can more effectively improve the performance of mixed matrix membrane with increasing selectivity without compromising the permeance.

CHAPTER 7

GAS SEPARATION PROPERTIES OF POLYSULFONE BASED MMMs

In Chapter 6, post-treatment to the PSF/ZTC-1 MMM by surface coating with PDMS and heat treatment above the PSF's T_g were investigated to obtain high performance membranes for gas separation. The results show that membrane with the most efficient performance can be produced by blocking the defects or pores with silicone coating. From the gas permeation results presented in the previous chapter, we considered that 0.25 wt% was the optimum loading to fabricate PSF/ZTC MMMs with the highest selectivities and acceptable permeances. In this study, we have used two types of ZTC prepared by different methods of carbon filling and we succeed to produce ZTC of distinctive structures. Another interesting material that obtained during the ZTC synthesis is zeolite carbon composite (ZCC), a material prior template removal. This composite substantially differs from those zeolite-carbon composite normally used since its pore is covered by carbon material. This material would be suitable as membrane filler due to the surface characteristic of zeolite with the presence of carbon inside, as explained in Chapter 2. Therefore, the polysulfone membrane filled with this type of material was extensively characterized and CO_2/CH_4 , CO_2/N_2 , H_2/CH_4 and O_2/N_2 gas separation properties were discussed in this chapter.

7.1 Characteristics of Polysulfone (PSF) Based MMMs

Three different fillers (ZTC-2, ZCC-1 and ZCC-2) were used in order to find the effect of filler structure on the membrane characteristics. To determine the stability of particles in MMMs, XRD was conducted on the MMMs and the results are shown in Figure 7.1. Due to the amorphous structure of PSF, the XRD pattern of PSF membrane shows a broad peak from 2θ of 15° to 20° . The diffraction patterns of MMMs confirmed the presence of both PSF and filler phases. The XRD patterns of MMMs (see Figure 7.1c and d) appeared of any

zeolite characteristic peak in the range of 5° - 35° , which indicate the presence of ZCC particles. Furthermore, coated PSF/ZTC-2 exhibited no characteristic peaks induced by the integration of ZTC-2 particles, suggesting that good particle dispersion through polymer matrix has occurred. We can also see that the characteristic peak of amorphous PSF was slightly shifted to the lower angle from $2\theta = 17.77^{\circ}$ to 16.38° . This slightly shift is related to the low interaction between the filler and polymer, leading to an increase of the distance between polymer chains. These increase is expected to affect the gas permeation rate since a higher d -spacing provides a faster diffusion and therefore larger permeances (Boroglu *et al.*, 2017). Furthermore, the integration of filler reduces the peak intensity and results in peak broadening, indicating the changes in PSF structure (Ionita *et al.*, 2014).

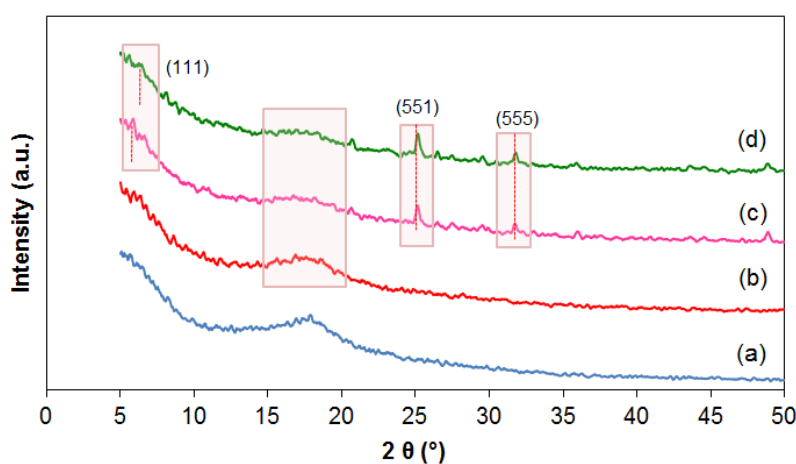


Figure 7.1 XRD patterns of (a) neat PSF, (b) PSF/ZTC-2, (c) PSF/ZCC-2 and (d) PSF/ZCC-1 at 0.25 wt% filler loading

Table 7.1 XRD Parameters for Neat PSF and PSF Based MMMs

| Sample | Angle (2θ) | d -spacing (nm) |
|--------------|---------------------|-------------------|
| Pristine PSF | 17.77 | 0.50 |
| ZTC-2 in PSF | 17.40 | 0.51 |
| ZCC-2 in PSF | 17.23 | 0.51 |
| ZCC-1 in PSF | 16.38 | 0.54 |

SEM is conducted to understand the different morphology of the neat PSF and PSF MMM embedded with filler, which is used to support the XRD and their results are represented in Figure 7.2. All membranes show a dense skin supported by small to large macrovoids finger-like substructure beneath the outer layer and interconnected pores from the inner layer (lumen side). These micrographs exhibit no considerable changes in cross sectional membrane morphology between neat PSF (Figure 5.3a). However, it was hard in spotting the fillers through hollow fiber samples, except for PSF/ZCC-1. The disappearance of filler particles confirm that particle might be homogeneously dispersed throughout the polymer matrix which possibly obtained due to sonication filler dispersion technique used during the dope solution preparation (Zulhairun, Ng, *et al.*, 2014). The bulk particle might be segregated to its smallest form by the aid of rigorous ultrasonication force. On the other hand, the ZCC-1 particles were observed locating in the in the sub layer region of the membrane since the ZCC-1 possessed larger particle size compared to other fillers. The agglomerate of particle with a more than 3 μm diameter in the porous sub layer may be due to fast liquid-liquid demixing, which restricts the particle mobility (N. M. Ismail *et al.*, 2015). These particle agglomerates in the pore probably give insignificant influence on permeability and selectivity.

Furthermore, the surface images of the MMMs were considered smooth and almost defect free representing the active dense layer. The existence of particles can be clearly detected on the dense layer and well distributed throughout the membrane surface. Moreover, the particle size was below 0.3 μm , which was in the range of the ZTC-2 (0.247 μm) and ZCC-2 (0.288 μm) average particles size. Nevertheless, membrane with ZCC-1 loading showed some particle agglomerates which may not be completely segregated due to its large bulk particle size. Thus, an increase in permeance with lower selectivity is expected.

The EDX scanning on the ZCC embedding MMMs cross sectional images is shown in Figure 7.4. The images confirmed relatively homogeneous dispersion in depth of PSF matrix. The results of elemental analysis for the area selected in Figure 7.4(a and b) are shown in Table 7.2. This exhibited a larger intensity of carbon (C) element, which represent the PSF matrix and the composite carbon

filler. The existence of zeolite in the composite filler was identified by low contents of aluminium (Al) and silica (Si) elements due to a small concentration of filler. In addition, the intensity of oxygen (O) content was also high, representing the presence of O element in the structure of ZCC particle (AlO_4 and SiO_4).

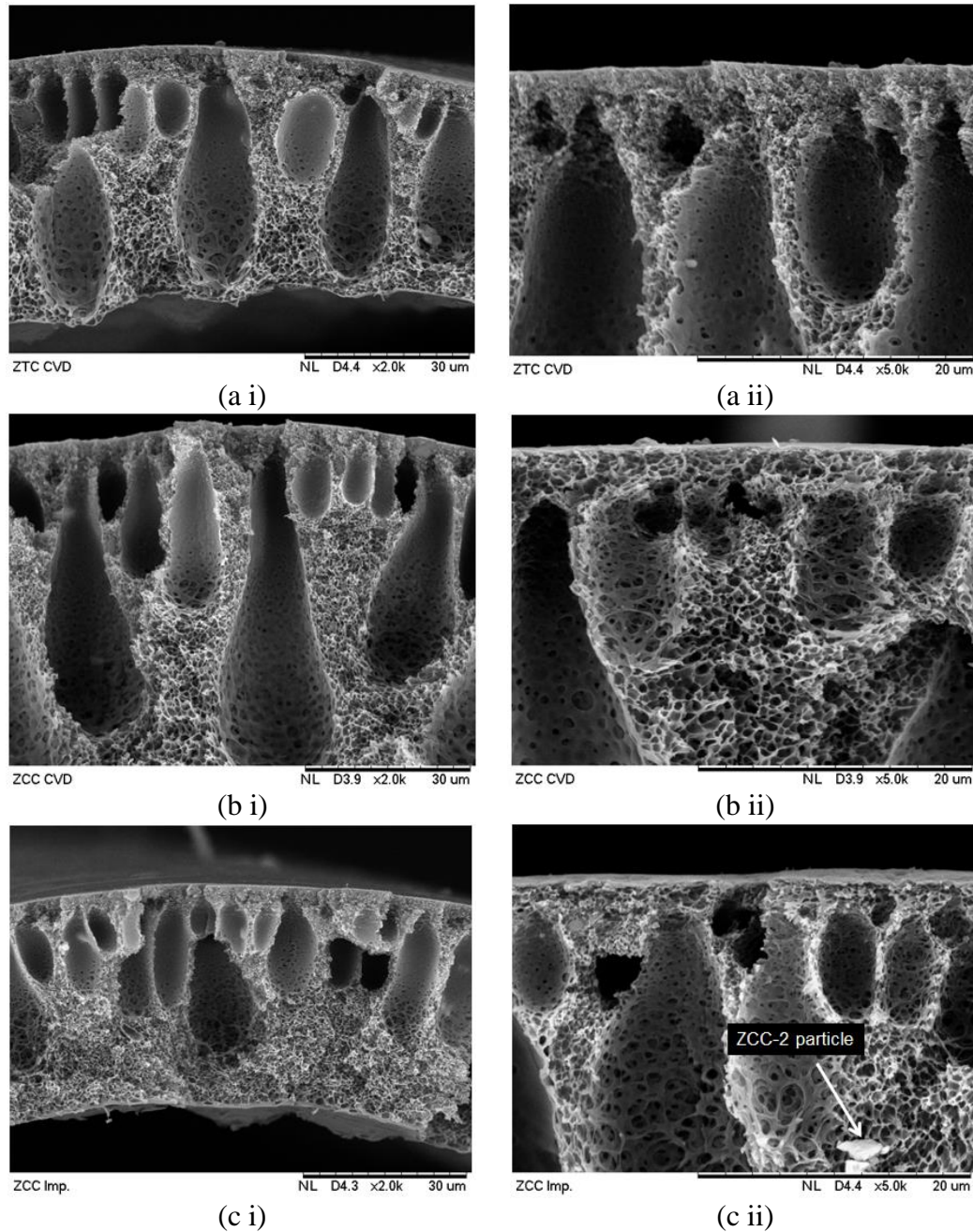


Figure 7.2 Cross section view of PSF membrane incorporating (a) ZTC-2, (b) ZCC-2 and (c) ZCC-1 particles at (i) low and (ii) high magnification

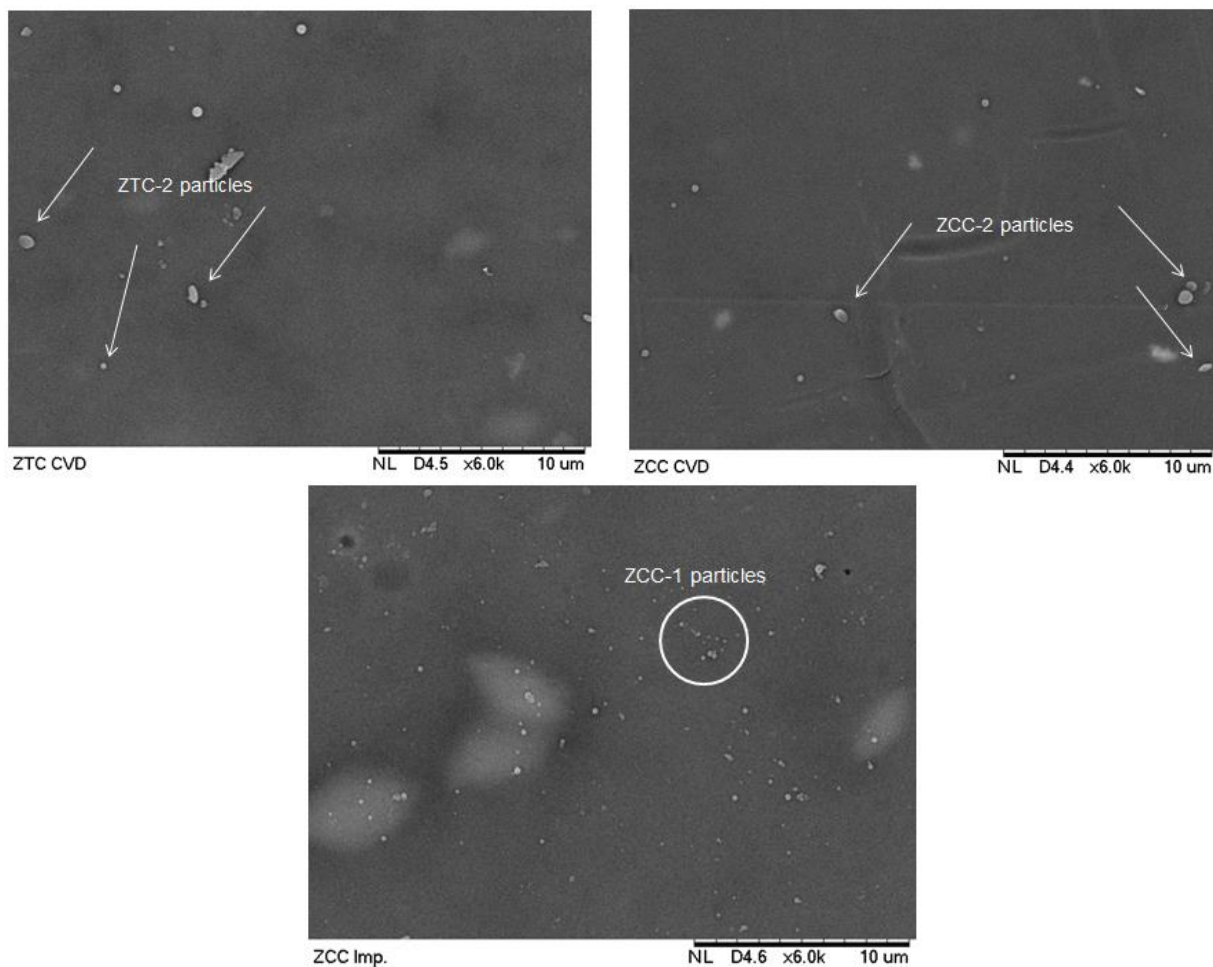


Figure 7.3 Surface view of PSF membrane incorporating (a) ZTC-2, (b) ZCC-2 and (c) ZCC-1 particles

Table 7.2 SEM-EDX Cross Sectional Elemental Analysis Results for 0.25 wt% Filler Embedding MMMs

| Membrane | C content (at.%) | O content (at.%) | Al content (at.%) | Si content (at.%) |
|-----------|------------------|------------------|-------------------|-------------------|
| PSF/ZCC-2 | 74.5 | 23.2 | 2.2 | 0.1 |
| PSF/ZCC-1 | 73.9 | 23.2 | 2.6 | 0.3 |

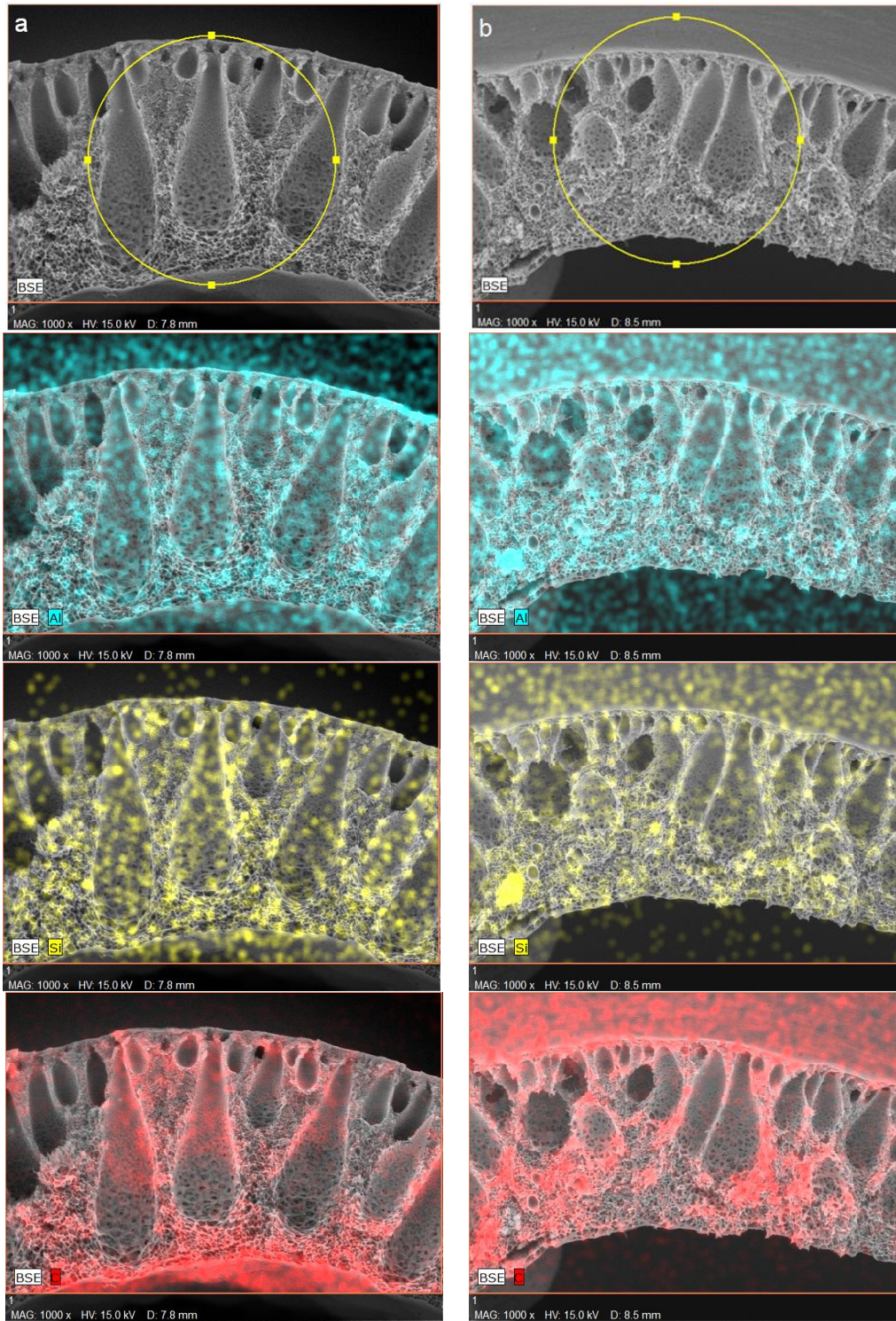


Figure 7.4 Cross sectional X-ray mapping of (a) PSF/ZCC-2 and (b) PSF/ZCC-1 MMMs containing 0.25 wt% ZCC (blue, yellow and red represent to Al, Si and C elements, respectively)

To further investigate the nature of the interaction between filler particles and polymer, FTIR spectroscopy was performed on the selected MMMs and the result are given in Figure 7.5. ZCC particles showed a band at 572 cm^{-1} , which is attributed to the deformation vibration of Al-O-Si group (Khanday *et al.*, 2017). The bands at 706 and 980 cm^{-1} are assigned to the symmetric and asymmetric stretching vibrations, which respectively related to the AlO_4 and SiO_4 structure. On the other hand, the bands at 1618 and 2049 cm^{-1} correspond to the O-H stretching vibrations occurring due to proton vibrations in water molecules. The strong and broad peak between 3300 to 3700 cm^{-1} is related to the stretching vibration of surface hydroxyl group of the zeolite structure (Wongcharee *et al.*, 2018). As shown in Figure 7.5b, the PSF/ZCC MMM demonstrated similar FTIR patterns to the neat PSF membrane. However, the MMM showed the band in the wavelength range of $500 - 750\text{ cm}^{-1}$, indicating the vibration of Al-O-Si and Al-O tetrahedral in zeolite structure, which were not appeared in the neat PSF (Figure 7.5c). Furthermore, the band in the wavelength range of $750 - 800\text{ cm}^{-1}$ appear to form Si-C aliphatic arising owing to the bond between zeolite and carbon (Velayudhan and Yameni, 2012). However, there were no observable peaks indicating the interaction between ZCC and PSF in the MMM. Hence, poor adhesion of ZCC in the PSF matrix occurred which was consistent with XRD data. Also, comparing the spectra of the PSF/ZTC-2 MMM (Figure 7.5d) with neat PSF, slight changes in the wavenumber peaks and a new peak with very low intensity at around 3650 cm^{-1} were observed. The new peak can be assigned to hydroxyls in phenols from ZTC. Further, peaks at 1236 and 1293 cm^{-1} related to the absorption of Ar-O-Ar and S=O groups, respectively, are slightly shifted to 1238 and 1295 cm^{-1} . These slightly changes suggests that there probably occurs a low degree of hydrogen bonding interaction between aryl ether and sulfonyl groups of PSF and the surface hydroxyl group of the ZTC.

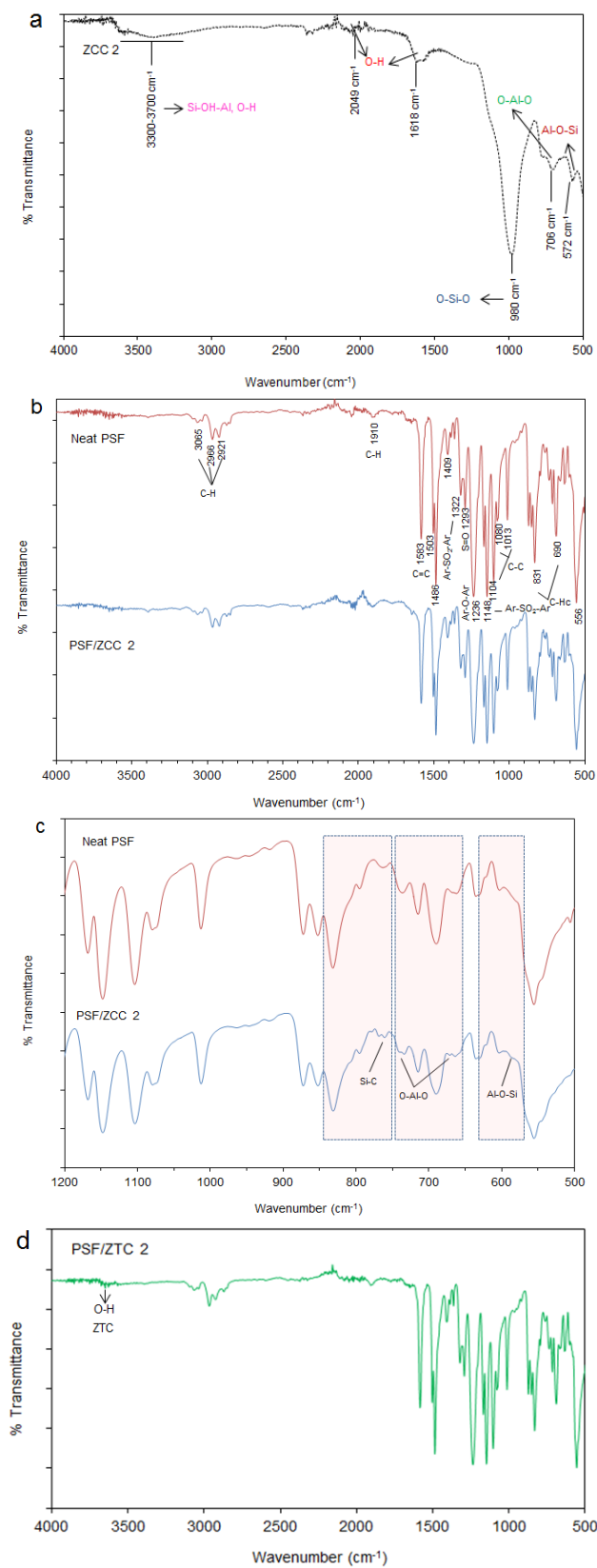


Figure 7.5 FTIR patterns of (a) ZCC-2, (b) neat PSF with PSF/ZCC-2, (c) neat PSF with PSF/ZCC-2 between 1200-500 cm^{-1} and (d) PSF/ZTC-2

To determine the effect of filler on the thermal properties of PSF membrane, the glass transition temperature (T_g) and degradation temperature were determined using DSC and TGA analysis. The interaction of filler inside PSF matrix was shown by means of T_g value. Table 7.3 showed that the measured T_g of MMMs increased than those of neat PSF. This is a typical of reduced polymer chain mobility due to particle stiffening and/or decrease in the amorphous PSF structure as proven by XRD. Nevertheless, PSF/ZCC-1 demonstrated lower improvement in T_g . From SEM images, we have observed some assembled particles, locating in between polymer chains, thus decreasing the surface area and reducing the effect on polymer chain flexibility (Zulhairun *et al.*, 2017).

Furthermore, the TGA curves of neat PSF and MMMs are shown in Figure 7.6. The thermal stability of PSF membrane was enhanced with the presence of filler particle. The initial weight loss of neat PSF membrane occurred at about 120 °C indicating the removal of residual solvents and this was not observed in the PSF-based MMMs. Furthermore, major degradation of neat PSF and MMMs occurred at about 500 °C, corresponding to the decomposition of PSF main chains. However, the MMMs showed lower weight loss than those of neat PSF membrane. The major weight loss at temperature between 400 and 600 °C and the percent residue at 800 °C are presented in Table 7.3. A lower weight loss of MMMs indicated that a good thermal properties of particles could maintain higher heat adsorbed and thus, the decomposition of MMMs become slower. Moreover, the final degradation occurred for all membranes at around 550 °C indicating the decomposition of membrane residue and the increase in the mass residue was observed for MMMs.

Table 7.3 Summary of Thermal Properties for Neat PSF and MMMs Filled with Different Fillers

| Membrane | ZTC loading (wt%) | T_g (°C) | Weight loss (%) | Residue (%) |
|-----------|-------------------|------------|-----------------|-------------|
| | | | 400-600 °C | 800 °C |
| Neat PSF | 0 | 178 | 64.18 | 27.86 |
| PSF/ZTC-2 | 0.25 | 186 | 63.86 | 34.02 |
| PSF/ZCC-2 | 0.25 | 185 | 64.14 | 30.07 |
| PSF/ZCC-1 | 0.25 | 180 | 63.59 | 33.78 |

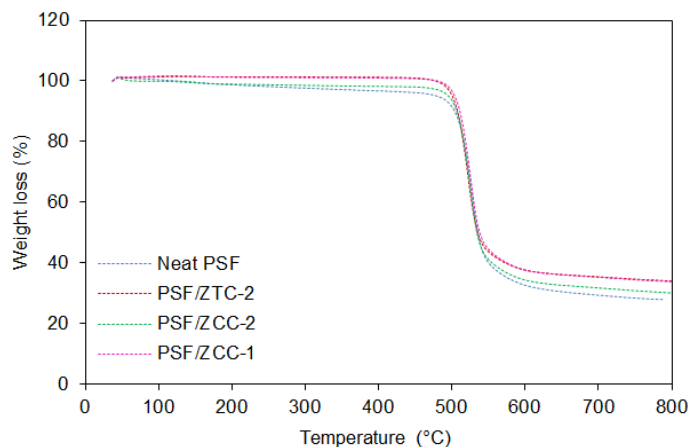


Figure 7.6 Thermogravimetric analysis for different MMMs

7.2 Comparison of ZTC and ZCC as a Filler Toward The Improvement of MMM Performance

Gas permeation experiment on ZTC-1 exhibited good improvement in selectivity of fast gas over the slow gas as the filler contents were reduced. In order to ensure the influence of these filler on gas permeation properties, especially the selectivity improvement at extremely low loading, MMMs containing different type of filler with low amount of particle loading were tested by single gases. Figure 7.7 and Table 7.5 compare the gas permeance and selectivity of ZTC and ZCC loaded MMM of same loading. The MMMs containing ZTC filler exhibited enhanced gas pair selectivities as well as gas permeances. The selectivities were higher for ZTC-2 filled fibres than for the ZTC-1 loaded fibers. This is not surprising given the lack of mesoporosity, prevalence microporosity, and hence small pore size in the ZTC-2 inclusions (Table 4.1). The highly microporous of ZTC-2 inclusions would also significantly increase the flow of the fast, low kinetic diameter, solution diffusion dependent gases (CO_2 , O_2 and H_2) and slightly improve the larger kinetic diameter, but lower molecular weight gas (CH_4 and N_2) through these sample. The presence of inclusions containing more micropores is more favourable for gas separation MMM than the presence of inclusions with more mesopores, suggesting the favourability of sub-Knudsen micropores over larger mesopores (Magueijo *et al.*, 2013). Furthermore, the specific surface area and pore volume of ZTC-2 were

2939 m²/g and 1.929 cm³/g, respectively. As opposed to ZTC-1, its specific surface area and pore volume were greatly lower, 1254 m²/g and 0.950 cm³/g, respectively. The higher gas permeance of MMM embedded with ZTC-2 can be attributed to its higher ZTC-2 specific surface area, leading to a higher adsorption capacity for gases. In addition to specific surface area, higher permeance enhancement can be ascribed to its higher pore volume with a good pore size distribution (Figure 4.14), providing a highway for molecular transmission (Dong *et al.*, 2013).

The high selectivities of PSF/ZTC-2 membrane could be associated to a surface flux mechanism through microporous ZTC, with mechanism of more favourable surface diffusion of fast gases rather than slow gases. However, a low ZTC-2 inclusions in the MMM, as reflected in the particle spacing (Table 7.4), possibly allow the dominant gas transmission to be solution diffusion through the matrix rather than diffusion through the pore network of ZTC-2. It can be said that high productivity and selectivity of membrane can be attributed in part to the intrinsic properties of PSF matrix, the selective gas capacity of ZTC-2 adsorption correlated with its good textural properties and the good interfacial contact between polymer matrix and filler phase.

Similar to ZTC loaded MMMs, ZCC-2 MMM exhibited enhanced gas permeance as well as selectivity. However, it was no surprise to find that ZCC-2 MMM had lower permeance since the specific surface area of ZCC-2 was found to be lower than ZCC-1. Also, the selectivity of ZCC-2 MMM was better due to a higher micropore portion of particles. Furthermore, the lower prevalence of ZCC-2 inclusions in the membrane, as observed in the interparticle spacings, should permit the gas transmission through the polymer matrix than through the ZCC-2 pores. Though the polymer dominating the gas transmission, the filler still give some contribution to the gas diffusion. In addition to surface area, the lower permeance of ZCC-2 than ZTC-2 filled MMM can also be attributed to the presence of zeolite enveloping the carbon in the composite filler. The heat of adsorption for the high quadrupole moment of gas (CO₂) on zeolite is higher than on carbon (Ma *et al.*, 2012). The presence of Na⁺ ions with CO₂ gas results in the strong interactions between the gas and zeolite surface, and hence lower gas

permeance (Shao *et al.*, 2009). As observed from Table 7.5, a tremendous increase in the gas permeance can be achieved when the ZCC-1 particles are loaded into the PSF membrane due to the particle agglomeration in the membrane surface. These agglomerates lead to the formation of channels surrounding the particles, providing a path for the gas to bypass the particles. If particles induced defects were significant, increased Knudsen diffusion of bigger gases, and hence lower selectivity.

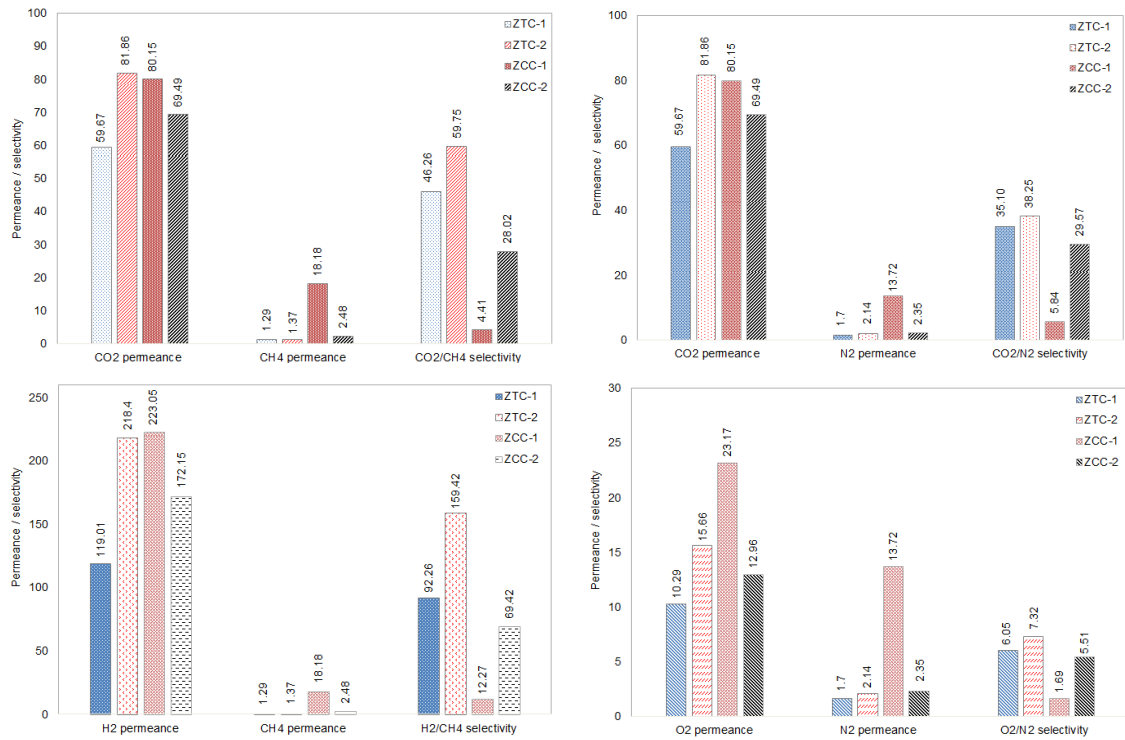


Figure 7.7 Gas permeation results for coated PSF-based MMM containing different filler types

We can see variations of the gas transport performance of MMMs upon the addition of different fillers. As shown in Table 6.4, the ZTC filled MMMs showed a higher selectivity with good permeance than the reported MMMs containing zeolite and carbon alone, indicating potential for CO₂, O₂ and H₂ separation. K. Zahri *et al.* (2016) demonstrated an improvement on the selectivity, but the CO₂ permeance were slightly improved by incorporating GO. By contrast, Ismail *et al.* (2009) and Junaidi *et al.* (2014) showed significant enhancement on

the O₂ dan CO₂ permeances by incorporating CMS and zeolite, respectively, but the improvement on selectivity was minimal. In this work, the selectivity of all gas pairs was found to be relatively higher with good permeance compared to neat PSF and other MMMs. It was interesting to note that the use of very low loading of ZTC was sufficiently considered to provide high improvement to those for a high percentage of loading with different filler. Figure 7.8 shows comparison of the gas separation properties for the PSF based MMMs with other types of filler in the literature (Table 6.4) with respect to Robeson trade-off line. The performance of PSF/ZTC-2 MMM is located below the 2008 upper bound line, but it clearly lies on the 1991 upper bound for polymeric membrane performance. Specifically, these membrane transcends the 1991 upper bound for CO₂/N₂ gas pairs.

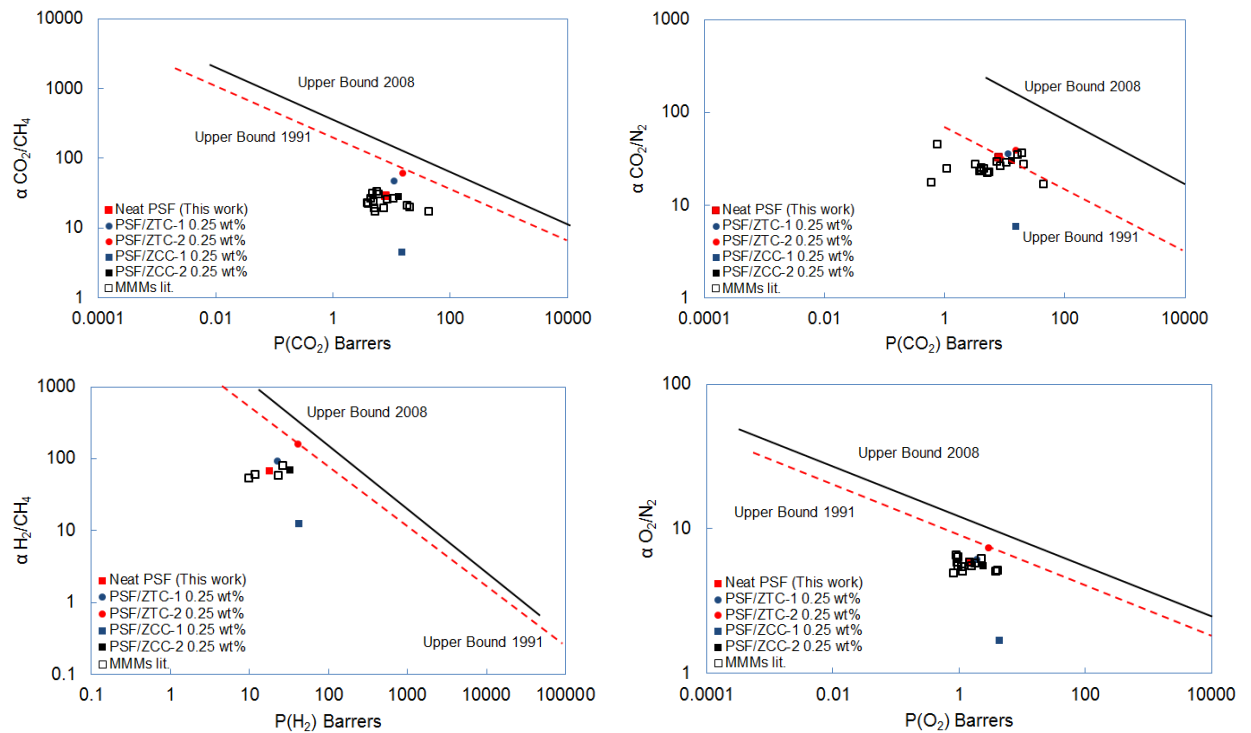


Figure 7.8 Gas separation performance of the MMM at 0.25 wt% filler loading with respect to Robeson trade-off line, compared with the data on other MMMs in the references. Detailed citations of MMMs are listed in Table 6.4

Table 7.4 Filler Interparticle Spacing and Size of PSF Molecule, Assuming Uniform Dispersion of Filler

| Membranes | Filler density (g/cm ³) | Filler particle diameter (nm) | Number of particles per m ³ | Interparticle spacing (nm) | Size of PSF molecule (nm) |
|-----------|-------------------------------------|-------------------------------|--|----------------------------|---------------------------|
| ZTC-2 | 0.45 | 247 | 8.70×10^{17} | 1048 | 97.8* |
| ZCC-2 | 0.44 | 288 | 5.61×10^{17} | 1212 | |

Calculated using Eq. 3.15 – 3.18.

7.3 Summary

The different fillers, ZTC and ZCC prepared using different method of carbon filling were used in this study in order to find the influence of filler structure on the membrane properties. The adding of ZTC-2, ZCC-2 and ZCC-1 fillers had a slight change on the amorphous structure of the PSF and induced slight change on the polymer chain packing. No substantial of interfacial voids indicates a good interfacial adhesion of particles with the PSF even without surface modification, except for PSF/ZCC-1. In addition, the thermal stability and the Tg of MMMs were also shown to be improved. A very interesting result was that all four types of MMM gave higher permeance of the fast and solution diffusion dependent gases, such as carbon dioxide, oxygen and hydrogen than neat PSF. ZTC filled MMMs showed selectivity improvement for all separation, but no selectivity increment was observed for ZCC filled MMMs. Most importantly, the MMM filled with ZTC-2 (ZTC where microporosity dominates) showed appreciable enhancement in permeance and selectivity when compared to the ZTC-1 filled MMM. By contrast, the MMM filled with ZCC-1 exhibited a strong increase in the permeation of slow gases with high kinetic diameter, such as methane and nitrogen, leading to a decline in the selectivity. The selectivity loss can be attributed to particle aggregates in the PSF polymer matrix, which generate interfacial voids between the particles due to bigger size of filler particles. Based on the results presented in this chapter, the effect of porous filler on the gas separation characteristics will depend on its properties, such as the particle size, porous structure (micropore and mesopore) and the surface chemistry.

Table 7.5 Gas Separation Performance of Coated MMM Containing Different Filler Types

| Sample | P/l_{CO_2} (GPU) | P/l_{CH_4} (GPU) | P/l_{O_2} (GPU) | P/l_{N_2} (GPU) | P/l_{H_2} (GPU) | α_{CO_2/CH_4} | α_{O_2/N_2} | α_{CO_2/N_2} | α_{H_2/CH_4} |
|----------|--------------------|--------------------|-------------------|-------------------|-------------------|----------------------|--------------------|---------------------|---------------------|
| Neat PSF | 41.34±3.87 | 1.44±0.19 | 7.52±0.85 | 1.28±0.12 | 95.23±10.54 | 28.77 | 5.87 | 32.27 | 66.27 |
| | 7.86* | 0.27* | 1.43* | 0.24* | 18.09* | - | - | - | - |
| ZTC-2 | 81.86±33.87 | 1.37±0.59 | 15.66±7.11 | 2.14±2.74 | 218.40±2.58 | 59.75 | 7.32 | 38.25 | 159.42 |
| | 15.55* | 0.26* | 2.98* | 0.41* | 41.50* | - | - | - | - |
| ZTC-1 | 59.67±5.83 | 1.29±0.25 | 10.29±1.01 | 1.70±0.19 | 119.01±16.40 | 46.42 | 6.06 | 35.14 | 92.57 |
| | 11.34* | 0.24* | 1.96* | 0.32* | 22.61* | - | - | - | - |
| ZCC-2 | 69.49±8.27 | 2.48±0.98 | 12.96±2.19 | 2.35±0.51 | 172.15±16.38 | 28.02 | 5.51 | 29.57 | 69.42 |
| | 13.20* | 0.47* | 2.46* | 0.45* | 32.71* | - | - | - | - |
| ZCC-1 | 80.15±22.06 | 18.18±4.96 | 23.17±1.43 | 13.72±3.19 | 223.05±94.29 | 4.41 | 1.69 | 5.84 | 12.27 |
| | 15.23* | 3.45* | 4.40* | 2.61* | 42.38* | - | - | - | - |

1 GPU = $1 \times 10^{-6} \text{ cm}^3 \text{ (STP)/cm}^2 \text{ s cmHg}$, \pm values in table are standard deviation from 3 samples

*Dense skin layer thickness of 190 nm is assumed

This page is left blank

CHAPTER 8

CONCLUSIONS AND RECOMMENDATIONS

8.1 Conclusions

This thesis has aimed to investigate the feasibility of separating gas using ZTC filler inside the PSF matrix, including an efforts to enhance the membrane performance by post treatment with surface coating and heat treatment. The present research has focussed on the application for CO₂, O₂ and H₂ separation. The following conclusions have been drawn from the current research.

8.1.1 Synthesis and Characteristics of Zeolite Templated Carbon (ZTC) as Membrane Filler

In this research, the ZTC and its zeolite-Y template has characterized using XRD, SEM, HRTEM and BET analysis. The zeolite-Y has successfully prepared which matched with the standard data of JCPDS No. : 39-1380. The octahedral zeolite-Y possessed BET surface area of 656 m²/g and total pore volume of 0.344 cm³/g with major micropore content. The average pore size of zeolite-Y was 0.804 nm. When the carbon (sucrose) was deposited on the zeolite channels by impregnation, the reduced pore of zeolite-Y (0.729 nm) with the formation of mesopores (2.39 nm) was attained. In this case, the surface area and total pore volume of ZCC-1 significantly decreased. After template removal, the ZTC-1 could not fully replicate the zeolite-Y structure and it was nongraphitic as reflected by a broad and low XRD peak at $2\theta = 25^\circ$. These peak suggests (002) diffraction from a few carbon deposited on the external surface, as observed by HRTEM. In addition, an XRD peak was observed at $2\theta = 6.05^\circ$, originating from the ordering of (111) plane of zeolite-Y. The broadness and low intensity of this peak indicates the low structure regularity of the resulting carbon. The specific surface area of ZTC-1 was 1254 m²/g and 90% of its total pore was micropore content. The formation of mesopores with average pore size of 2.46 nm is originated from the carbon on the external zeolite surface and the carbon inside

the zeolite-Y channels coming from the collapse of unstable carbon framework. Meanwhile, the ordered microporous structure was observed in the deep inner region of ZTC-1 with a mean pore size of 0.923 nm. On the contrary, when the carbon source was filled by two step routes (FA impregnation and propylene CVD), the surface area and porosity of ZCC-2 significantly decreased than that of ZCC-1 due to the perfect filling of zeolite channels with carbon source. After zeolite removal, the ZTC-2 showed higher surface area (2939 m²/g) with almost no mesoporosity and the major micropore size was observed at 0.121 nm. Its XRD pattern showed a sharp peak at $2\theta = 6.36^\circ$ and also a weak peak at $2\theta = 10.3^\circ$ with corresponding distance of 1.39 nm and 0.43 nm, respectively. These peaks has revealed the long ordering structure of ZTC-2. The use of two step method of carbon filling results in a better ordering of the carbon because the carbon can totally deposit on the zeolite channels. Having a high surface area with microporous structure (ZTC where microporosity dominates) is more favourable as filler material for gas separation membrane since mesopore leads to a poor selectivity.

8.1.2 Mixed Matrix Membranes Embedded with ZTC-1 for Gas Separation

The effectiveness of ZTC-1 to separate gas was then examined as a function of ZTC-1 loading. Results indicated that a slight changes on the amorphous nature of MMMs as the ZTC-1 loading increased. Also, irregular shift in diffraction angle was observed during addition of the ZTC-1, suggesting a changes on the polymer chain packing. However, addition of the ZTC-1 did not alter the microscopic structure containing dense top layer, followed by finger-like structure beneath the outer layer and interconnected pores from the lumen side. The thermal stability was also found to be improved with increasing of filler loadings, but the glass transition temperature (T_g) was dropped by increasing loadings. By adding ZTC, no occurrence of new peak and wavenumber change was observed beside neat PSF spectrum since no functionalizatiois regarding the surface chemistry of ZTC-1 were done. Membrane with no severe interfacial voids were achieved up to 0.5 wt% addition of ZTC-1. The selectivity for all separation increased with the addition up to a ZTC-1 loading of 0.5 wt%. PSF/ZTC-1 0.4 wt% MMM showed

the highest selectivity enhancement up to 290% for CO₂/CH₄, with CO₂/CH₄, CO₂/N₂, O₂/N₂, H₂/CH₄ selectivity of 9.99, 11.62, 2.78, 28.88, respectively, with acceptable permeances. Unlike low ZTC loading, the loss selectivity with very high permeance shown by 0.7 and 1 wt% ZTC loadings indicated that interfacial voids plays a key role in the overall performance of MMMs. The observable agglomeration with some interfacial voids were revealed by surface observation (FESEM and AFM). Furthermore, all new materials are initially characterized by single gas measurements, but must be followed by mixed-gas measurements. Therefore, in this thesis MMMs were conducted to separate CO₂/CH₄ and H₂/CH₄ mixed-gas. However, the separation performance under mixed-gas system was almost lower than those of single gas due to the competition between the gas penetrants and the effect of non-ideal gas behaviors particularly for separation containing condensable gas. Moreover, the increase in CO₂/CH₄ and H₂/CH₄ mixed-gas selectivity compared with neat PSF was attained for all ZTC-1 loadings.

8.1.3 Membrane Post-treatment using Heat Treatment and Surface Coating

To improve the existing performance of MMMs, surface modification was conducted in this research by surface coating, and hence, repairing any surface defects. This treatment allows the membrane to achieve permeation properties closer to the intrinsic characteristics of the PSF membrane. The coating process was conducted by dip-coating method with 3 wt% PDMS solution. Thus, this research investigated the influence of surface coating on the gas separation performance of MMMs.

The SEM images showed defect-free and smoother membrane and the existing voids were blocked by the coating solution. The coating markedly increased selectivity and reduced permeances. After coating treatment, note that even the smallest amount of ZTC-1 loading (0.25 wt%) resulted the highest selectivity improvement (up to 780% for CO₂/CH₄), with CO₂/CH₄, CO₂/N₂, O₂/N₂, H₂/CH₄ selectivity of 46.42, 35.14, 6.06 and 92.57, respectively, without sacrificing the permeances. These high selectivities could be explained by a surface flux mechanism through mesoporous carbon surface, with mechanism of

more favourable surface diffusion of fast gases instead of slow penetrants, subsequently followed by gas diffusion in the ZTC micropores. Moreover, the lower prevalence of filler in the 0.25 wt% ZTC-1 loaded MMM, as shown by interparticle spacing, permitted a higher portion of the gas diffusion to be solution diffusion through polysulfone matrix rather than diffusion through the ZTC pore network. The highest permeance with poor selectivity were found in the MMMs at higher ZTC-1 loading (0.7 and 1 wt%). It was no surprise the lower performance of higher ZTC-1 loaded MMMs than the other MMMs, considering the formation of severe interfacial voids. As a result, highly permeable silicone rubber dominated as a third phase and the gas molecules would diffuse through this easily, unselectively.

Other approach have been proposed in this thesis in order to fabricate void-free MMMs by employing high processing temperature higher than the T_g of PSF. Due to the thermal effect, the polymer packed chains in the surface layer and substructure became more compact as compared to untreated MMMs, depending on the thermal soaking period. At shorter period (30 min), some voids in the surface layer were still detected. The selectivity was improved compared to that of untreated MMM, with CO_2/CH_4 , O_2/N_2 and CO_2/N_2 selectivity up to 29.41, 5.04 and 21.78, respectively. However, the permeances of all gases tested were severely diminished, as a result of membrane densification. Further selectivity improvement was attained by the prolonged heat treatment (120 min), with CO_2/CH_4 , O_2/N_2 and CO_2/N_2 selectivity of 30.43, 6.42 and 30.39, respectively. These highest selectivity was attained at 0.25 wt% addition of ZTC-1, while the selectivity enhancement was lower as the ZTC-1 loading increased. Obviously, the prolonged soaking period (240 min) totally removed the voids in the membrane surface and seriously densified the polymer structure. A better compatibility of polymer with particles was revealed by increasing T_g and its value enhanced with the longer thermal soaking period. As a result, the CO_2/CH_4 , O_2/N_2 and CO_2/N_2 selectivity was recorded up to 39.65, 6.66 and 33.79, respectively.

Based on those approaches, surface coating is considered simple and effective way to improve membrane selectivity with acceptable permeance, but

without affecting structural integrity. Unlike to surface coating, heat treatment produced a high selectivity membrane, but very low fluxes which lead to undesirable resistance to gas transport.

8.1.4 Gas Separation Properties of Polysulfone Based MMMs

From the gas permeation results, we have considered that 0.25 wt% was the optimum loading to fabricate PSF/ZTC-1 MMMs with acceptable permeances, but highest selectivities. In this thesis, we synthesized PSF based MMMs with different fillers (ZTC and ZCC) and the effects on the membrane structural, morphological, thermal stability and gas permeation properties were compared with ZTC-1 filled MMM of same loading. Similar to ZTC-1 MMM, addition of ZTC-2, ZCC-2 and ZCC-1 had a minor change on the amorphous structure and the polymer chain packing. In addition, the same microscopic structure (thin dense layer, finger-like structure beneath the outer layer and interconnected pores from inside layer) was noticed for all MMMs. The particles were well dispersed inside the matrix with no observable voids, except for PSF/ZCC-1 MMM. The formation of agglomerations in ZCC-1 filled MMM was due to a bigger size ZCC-1 particles. However, the thermal stability and the glass transition temperature of MMMs were also found to be improved. Prior to test, the MMMs were silicone-coated and all ZTC loaded MMMs recorded higher selectivity and permeance of fast gases (CO_2 , O_2 and H_2) compared to neat PSF. The significant improvement in permeances (up to 98% for CO_2 , 108% for O_2 and 129% for H_2), with CO_2/CH_4 , O_2/N_2 , CO_2/N_2 and H_2/CH_4 selectivity of 59.75, 7.32, 38.25 and 159.42, respectively, were attained for MMM filled with ZTC-2. The permeance and selectivity improvement of PSF/ZTC-2 were higher than PSF/ZTC-1 which ascribed to its higher surface area, total pore volume and narrower pore size distribution. Furthermore, the high selectivity of ZTC-2 filled PSF could be explained with a surface flux mechanism through microporous ZTC, with mechanism of more favourable surface diffusion of fast gases instead of slow gases. The performance of PSF/ZTC-2 MMM transcends the 1991 upper bound for polymeric membrane performance. The high permeance and selectivity improvement could be attained even at 0.25 wt% loading and the ZTC filler could

be a potential candidate for a new filler for CO₂, O₂ and H₂ separation. Compared to ZTC-2, the lower permeance of PSF/ZCC-2 could be ascribed to the presence of zeolite outside the carbon. The adsorption heat of high quadrupole moment of gas on zeolite is higher than on carbon, leading to strong interaction between the zeolite surface and gas, and hence lower permeance. Smaller surface area of ZCC-2 also contributes to the lower permeance. On the contrary, strong increase in the permeation of slow gases (CH₄ and N₂) for PSF/ZCC-1 lead to poor selectivity. The selectivity decrement of CO₂/CH₄, O₂/N₂, CO₂/N₂ and H₂/CH₄ was 85%, 71%, 82% and 81%, respectively. This was no surprise that Knudsen diffusion opportunity for the slow gases increased due to the presence of agglomerations in the PSF matrix resulting voids between the particles.

8.2 Recommendations

This thesis has focussed on the feasibility of gas separation using ZTC filler inside the PSF matrix including an attempt to improve the membrane performance through silicone-coated and heat treatment. Results of this present work have exhibited good potential of all ZTC types as filler inside PSF membrane for CO₂, O₂ and H₂ separation and provided a significant improvement of the MMM through modification with surface coating and heat treatment. In comparison to heat treatment, surface modification through silicone-coated have demonstrated better membrane performance without affecting the membrane integrity. However, several issues regarding to a further understanding on the scientific level and the practical applications should be addressed in future work.

Further understanding regarding to the PDMS coating treatment should be conducted. For instance, the distribution of PDMS solution in the membrane structure should be further analyzed. FESEM combined with EDX analysis could be performed in order to confirm the presence of PDMS inside the membrane. PDMS concentration and the coating time should be also studied to ensure the PDMS only sealing in the outer surface of membrane.

A better understanding on the transport mechanism through PSF-based MMMs could be attained by performing single gas sorption isotherm on the pure filler (ZTC and ZCC), neat PSF and composite membrane. By carrying out the

gas sorption on the solid particles, the adsorption selectivity of gas on the solid surface can be determined. Meanwhile, the permeation mechanism inside the polymer can be described by the dual sorption model and the sorption parameter can be achieved from the isotherm experiments through the neat PSF and MMM.

Single gas experiments are a necessary to give an indication of possible performance of membranes under ideal conditions. But in reality, the transport of a gas is affected by the presence of other penetrants. Future work could include gas mixture measurements for membrane after coating in realistic conditions. Furthermore, studies of several parameters such as feed concentration, permeation temperature and total feed pressure, would also be important for practical application. The results of single gas measurements are usually far higher from what is found with mixed-gas measurements.

In addition, chemical modification on ZTC should be conducted in order to improve interfacial adhesion with polymer matrix. The ZTC could be oxidized using mixture of $\text{H}_2\text{SO}_4/\text{HNO}_3$ to form carboxylic acid group. Also, chemical treatment on the membrane would be performed using xylenediamine or other molecules containing amine groups before subjected to silicone coating. It is predicted that $-\text{NH}_2$ of the molecules containing amine groups forms hydrogen bonding with aryl ether or sulfonyl oxygen groups in the PSF and the $-\text{OH}$ groups on the ZTC surface simultaneously, thus enhancing the contact between the two phase and improving the membrane separation performance.

This page is left blank

REFERENCES

- Abdul, N., Nordin, H., Racha, S. M., Matsuura, T., Misdan, N., Aimie, N., Sani, A., Ismail, A. F. and Mustafa, A. (2015), "Facile Modification of ZIF-8 Mixed Matrix Membrane for CO₂/CH₄ Separation : Synthesis and Preparation", *RSC Advances*, Vol. 5, pp.43110–43120.
- Adewole, J. K., Ahmad, A. L., Ismail, S. and Leo, C. P. (2013), "Current Challenges in Membrane Separation of CO₂ from Natural Gas : A Review", *International Journal of Greenhouse Gas Control*, Vol. 17, pp. 46–65.
- Agustin, N.C.S. and Sakti, O.P. (2010), "The Effect of Membrane Heating, Gradient Pressure and Permeation Time of CO₂/CH₄ Separation for Biogas Treatment using Polyimide Membrane and Polyimide-Zeolite Composite Membrane", Undergraduate Thesis, Department of Chemical Engineering, Diponegoro University, Semarang, Indonesia
- Ahmad, A. L., Jawad, Z. A., Low, S. C. and Zein, S. H. S. (2014), "A Cellulose Acetate/Multi-Walled Carbon Nanotube Mixed Matrix Membrane for CO₂/N₂ Separation", *Journal of Membrane Science*, Vol. 451, pp. 55–66.
- Ansaloni, L. and Deng, L. (2016), "Advances in Polymer-Inorganic Hybrids as Membrane Materials", *Recent Developments in Polymer Macro, Micro and Nano Blends*, Elsevier Ltd.
- Anson, M., Marchese, J., Garis, E., Ochoa, N. and Pagliero, C. (2004), "ABS Copolymer-Activated Carbon Mixed Matrix Membranes for CO₂/CH₄ separation", *Journal of Membrane Science*, Vol. 243, pp. 19–28.
- Antoniou, M. K., Diamanti, E. K., Enotiadis, A., Policicchio, A., Dimos, K., Ciuchi, F., Maccallini, E., Gournis, D. and Agostino, R.G. (2014), "Methane Storage in Zeolite-Like Carbon Materials", *Microporous and Mesoporous Materials*, Vol. 188, pp. 16–22.
- Aroon, M. A. and Ismail, A. F. (2010), "Performance Studies of Mixed Matrix Membranes for Gas Separation: A Review", *Separation and Purification Technology*, Vol. 75, pp. 229–242.
- Aroon, M. A., Ismail, A. F., Montazer-Rahmati, M. M. and Matsuura, T. (2010), "Morphology and Permeation Properties of Polysulfone Membranes for Gas Separation: Effects of Non-Solvent Additives and Co-Solvent", *Separation and Purification Technology*, Vol. 72, pp. 194–202.
- Baker, R. W. and Low, B. T. (2014), "Gas Separation Membrane Materials: A Perspective", *Macromolecules*, Vol. 47, pp. 6999-7013.
- Bakhtiari, O., Mosleh, S., Khosravi, T. and Mohammadi, T. (2011), "Preparation, Characterization and Gas Permeation of Polyimide Mixed Matrix Membranes", *Journal of Membrane Science & Technology*, Vol. 1, pp. 1–6.

- Balahmar, N., Lowbridge, A. M. and Mokaya, R. (2016), "Templating of Carbon in Zeolites under Pressure: Synthesis of Pelletized Zeolite Templated Carbons with Improved Porosity and Packing Density for Superior Gas (CO₂ and H₂) Uptake Properties", *Journal of Material Chemistry A*", Vol. 4, pp. 14254–14266.
- Bastani, D., Esmaeili, N. and Asadollahi, M. (2013), "Polymeric Mixed Matrix Membranes Containing Zeolites as A Filler for Gas Separation Applications : A Review", *Journal of Industrial and Engineering Chemistry*, Vol. 19, pp. 375–393.
- Bhardwaj, V., Macintosh, A., Sharpe, I. D., Gordeyev, S. A. and Shilton, S. J. (2003), "Membranes Filled with Submicron Particles", *New York Academy of Sciences*, Vol. 328, pp. 318–328.
- Boroglu, M. S., Ugur, M. and Boz, I. (2017), "Enhanced Gas Transport Properties of Mixed Matrix Membranes Consisting of Matrimid and RHO Type ZIF-12 Particles", *Chemical Engineering Research and Design*, Vol. 123, pp. 201–213.
- Cai, J., Li, L., Lv, X., Yang, C. and Zhao, X. (2014), "Large Surface Area Ordered Porous Carbons via Nanocasting Zeolite 10x and High Performance for Hydrogen Storage Application", *ACS Applied Materials and Interfaces*, Vol. 6, pp. 167–175.
- Cai, J., Yang, M., Xing, Y. and Zhao, X. (2014), "Large Surface Area Sucrose-Based Carbons via Template-Assisted Routes : Preparation , Microstructure, and Hydrogen Adsorption Properties, *Colloids and Surfaces A: Physicochemical and Engineering Aspects*, Vol. 444, pp. 240–245.
- Castro-muñoz, R. and Fíla, V. (2018), "Progress on Incorporating Zeolites in Matrimid@5218 Mixed Matrix Membranes towards Gas Separation", Vol. 8, pp 30.
- Chen, H. Z., Li, P. and Chung, T. (2012), "PVDF / Ionic Liquid Polymer Blends with Superior Separation Performance for Removing CO₂ from Hydrogen and Flue Gas", *International Journal of Hydrogen Energy*, Vol. 37, pp. 11796–11804.
- Chen, L., Singh, R. K. and Webley, P. (2007), "Synthesis, Characterization and Hydrogen Storage Properties of Microporous Carbons Templated by Cation Exchanged Forms of Zeolite Y with Propylene and Butylene as Carbon Precursors", *Microporous and Mesoporous Materials*, Vol. 102, pp. 159–170.
- Choi, S., Kim, H., Lee, S., Wang, Y., Ercan, C., Othman, R. and Choi, M. (2015), "Large-scale Synthesis of High-quality Zeolite-templated Carbons without Depositing External Carbon Layers", *Chemical Engineering Journal*, Vol. 280, pp. 597–605.

- Chung, T. S., Jiang, L. Y., Li, Y. and Kulprathipanja, S. (2007), "Mixed Matrix Membranes (MMMs) Comprising Organic Polymers with Dispersed Inorganic Fillers for Gas Separation", *Progress in Polymer Science*, Vol. 32, pp. 483–507.
- Compañ, V., Del Castillo, L. F., Hernández, S. I., Mar López-González, M. and Riande, E. (2010), "Crystallinity Effect on the Gas Transport in Semicrystalline Coextruded Films Based on Linear Low Density Polyethylene", *Journal of Polymer Science, Part B: Polymer Physics*, Vol. 48, pp. 634–642.
- Cong, H., Zhang, J., Radosz, M. and Shen, Y. (2007), "Carbon Nanotube Composite Membranes of Brominated Poly(2,6-diphenyl-1,4-phenylene oxide) for Gas Separation", *Journal of Membrane Science*, Vol. 294, pp. 178–185.
- Daufin, G., Escudier, J.-P., Carrère, H., Bérot, S., Fillaudeau, L. and Decloux, M. (2001), "Recent and Emerging Applications of Membrane Processes in the Food and Dairy Industry", *Food and Bioproducts Processing*, Vol. 79, pp. 89–102.
- Dechnik, J., Gascon, J., Doonan, C. J., Janiak, C. and Sumbly, C. J. (2017), "Mixed-Matrix Membranes", *Angewandte Chemie*, Vol. 56, pp. 9292–9310.
- Deng, H., Yi, H., Tang, X., Yu, Q., Ning, P. and Yang, L. (2012), "Adsorption Equilibrium for Sulfur Dioxide, Nitric Oxide, Carbon Dioxide, Nitrogen on 13X and 5A Zeolites", *Chemical Engineering Journal*, Vol. 188, 77–85.
- Ding, X., Cao, Y., Zhao, H. and Wang, L. (2013), "Interfacial Morphology Between the Two Layers of the Dual-layer Asymmetric Hollow Fiber Membranes Fabricated by Co-extrusion and Dry-jet Wet-spinning Phase-inversion Techniques", *Journal of Membrane Science*, Vol. 444, pp. 482–492.
- Ding, X., Cao, Y., Zhao, H., Wang, L. and Yuan, Q. (2008), "Fabrication of High Performance Matrimid/Polysulfone Dual-layer Hollow Fiber Membranes for O₂/N₂ Separation", Vol. 323, pp. 352–361.
- Dong, G., Li, H. and Chen, V. (2013), "Challenges and Opportunities for Mixed-Matrix Membranes for Gas Separation", *Journal of Materials Chemistry A*, Vol. 1, pp. 4610–4630.
- Duval, J. M., Folkers, B., Mulder, M. H. V, Desgrandchamps, G. and Smolders, C. A. (1993), "Adsorbent Filled Membranes for Gas Separation. Part 1. Improvement of the Gas Separation Properties of Polymeric Membranes by Incorporation of Microporous Adsorbents", *Journal of Membrane Science*, Vol. 80, pp. 189–198.
- Enzel, P. and Bein, T. (1992), "Poly(acrylonitrile) Chains in Zeolite Channels: Polymerization and Pyrolysis", *Chemistry of Materials*, Vol. 4, pp. 819–824.

- Fang, M., Okamoto, Y., Koike, Y., He, Z. and Merkel, T. C. (2016), "Gas Separation Membranes Prepared with Copolymers of Perfluoro(2-Methylene-4,5-Dimethyl-1,3-Dioxlane) and Chlorotri Fluoroethylene", Vol. 188, pp. 18–22.
- Farnam, M., Mukhtar, H. and Shariff, A. (2016), "Analysis of the Influence of CMS Variable Percentages on Pure PES Membrane Gas Separation Performance", *Procedia Engineering*, Vol. 148, pp. 1206–1212.
- Jiang L.Y. and Chung T.S. (2009), "Fabrication of Mixed Matrix Hollow Fibers with Intimate Polymer - Zeolite Interface for Gas Separation", *AIChE Journal*, Vol. 52, No. 8, pp. 2898-2908.
- Ismail, A.F, Rana, D, Matsuura, T and Foley, HC, (2014), *Carbon-based Membranes for Separation Processes*, Springer, New York.
- Ge, L., Zhu, Z. and Rudolph, V. (2011), "Enhanced Gas Permeability by Fabricating Functionalized Multi-Walled Carbon Nanotubes and Polyethersulfone Nanocomposite Membrane", *Separation and Purification Technology*, Vol. 78, pp. 76–82.
- Geng, Z., Zhang, C., Wang, D., Zhou, X., and Cai, M. (2015), "Pore Size Effects of Nanoporous Carbons with Ultra-High Surface Area on High-Pressure Hydrogen Storage", *Journal of Energy Chemistry*, Vol. 24, pp. 1–8.
- Giel, V., Kredatusová, J., Trchová, M., Brus, J., Žitka, J. and Peter, J. (2016), "Polyaniline/Polybenzimidazole Blends: Characterisation of Its Physico-Chemical Properties and Gas Separation Behaviour", *European Polymer Journal*, Vol. 77, pp. 98-113.
- Goh, P.S., Ismail, A.F., Sanip, S.M., Ng, B.C. and Aziz, M. (2011), "Recent Advances of Inorganic Fillers in Mixed Matrix Membrane for Gas Separation", Vol. 81, pp. 243–264.
- Goh, P. S., Ng, B. C., Ismail, a. F., Sanip, S. M., Aziz, M., dan Kassim, M.A. (2011), "Effect of Dispersed Multi-Walled Carbon Nanotubes on Mixed Matrix Membrane for O₂/N₂ Separation", *Separation Science and Technology*, Vol. 46, 1250–1261.
- Guan, C., Wang, K., Yang, C. and Zhao, X.S. (2009), "Characterization of a Zeolite-Templated Carbon for H₂ Storage Application, *Microporous and Mesoporous Materials*, Vol. 118, pp. 503–507.
- Gunawan, T., Wijiyanti R., and Widiastuti N. (2018), "Adsorption - Desorption of CO₂ on Zeolite-Y Templated Carbon at Various Temperatures", *RSC Advances*, Vol. 8, pp. 41594–41602.
- He, X., Lie, J. A., Sheridan, E. and Hagg, M. B. (2011), "Preparation and Characterization of Hollow Fiber Carbon Membranes from Cellulose Acetate Precursors", *Industrial and Engineering Chemistry Research*, Vol. 50, pp.

2080–2087.

- Heck, R., Qahtani, M. S., Yahaya, G. O., Tanis, I., Brown, D., Bahamdan, A. A., Ameen, A. W., Vaidya, M. M., Ballaguet, J. R., Alhajry, R. H., Espuche, E. and Mercier, R. (2017), "Block Copolyimide Membranes for Pure and Mixed Gas Separation", *Separation and Purification Technology*, Vol. 173, pp. 183–192.
- Hwang, J.W., Cho, K., Yoon, T.H. and Park, C.E. (1999), "Effects of Molecular Weight of Polysulfone on Phase Separation Behavior for Cyanate Ester/Polysulfone Blends", Vol. 77, pp. 921–927.
- ICDD (1997), "JCPDS-International Centre for Diffraction Data", USA.
- Ionita, M., Pandele, A.M., Crica, L.E., dan Obreja, A.C. (2015), "Preparation and Characterization of Graphene Oxide Composite Membrane Material", *High Performance Polymers*, Vol. 28, pp. 1-8.
- Ionita, M., Pandele, A.M., Crica, L., dan Pilan, L. (2014), "Improving the Thermal and Mechanical Properties of Polysulfone by Incorporation of Graphene Oxide, *Composites Part B: Engineering*, Vol. 59, pp. 133–139.
- Ismail, A.F., Khulbe, K.C. and Matsuura, T. (2015), *Gas Separation Membranes: Polymeric and Inorganic*, Springer, Switzerland.
- Ismail, A.F., Kusworo, T.D., dan Mustafa, A. (2008), "Enhanced Gas Permeation Performance of Polyethersulfone Mixed Matrix Hollow Fiber Membranes using Novel Dynasylan Amino Silane Agent", *Journal of Membrane Science*, Vol. 319, pp. 306–312.
- Ismail, A.F., Rahim, N.H., Mustafa, A., Matsuura, T., Ng, B.C., Abdullah, S. and Hashemifard, S.A. (2011), Gas Separation Performance of Polyethersulfone/Multi-Walled Carbon Nanotubes Mixed Matrix Membranes, *Separation and Purification Technology*, Vol. 80, pp. 20–31.
- Ismail, A.F., Rahim, R.A. and Rahman, W.A.W.A. (2008), "Characterization of Polyethersulfone/Matrimid®5218 Miscible Blend Mixed Matrix Membranes for O₂/N₂ Gas Separation", *Separation and Purification Technology*, Vol. 63, pp. 200–206.
- Ismail, A. F., Rahman, W. R. and Aziz, F. (2009), "Development of Polysulfone (PSF)-Carbon Molecular Sieve (CMS) Mixed Matrix Membrane (MMM) for O₂/N₂ Gas Separation", *Proceedings of International Conference on Nanoscience and Nanotechnology (NANO-Sci-Tech 2008)*, Eds : Rusop, M. et al., Selangor, Malaysia, pp. 201–206.
- Ismail, A.F., Goh, P.S., Tee, J.C., Sanip, S.M. and Aziz, M. (2008), "A Review of Purification Techniques for Carbon Nanotubes", *Nano*, Vol. 3, pp. 127–143.
- Ismail, N.M., Ismail, A.F., Mustafa, A. and Zulhairun, A.K. (2015), "Enhanced

- Carbon Dioxide Separation by Polyethersulfone (PES) Mixed Matrix Membranes Deposited with Clay", *Journal of Polymer Engineering*, Vol. 36, pp. 65-78.
- Ismail, N.M., Jakariah, N.R., Bolong, N., Anissuzaman, S.M., Nordin, N.A.H.M., Razali, A.R. (2017), "Effect of Polymer Concentration on the Morphology and Mechanical Properties of Asymmetric Polysulfone (PSf) Membrane", *Journal of Applied Membrane Science & Technology*, Vol. 21, pp. 33–41.
- Jang, K.S., Kim, H. J., Johnson, J.R., Kim, W.G., Koros, W. J., Jones, C.W. and Nair, S. (2011), "Modified Mesoporous Silica Gas Separation Membranes on Polymeric Hollow Fibers", *Chemistry of Materials*, Vol. 23, pp. 3025–3028.
- Jeazet, H.B.T., Koschine, T., Staudt, C., Raetzke, K. and Janiak, C. (2013), "Correlation of Gas Permeability in a Metal-Organic Framework MIL-101(Cr)–Polysulfone Mixed-Matrix Membrane with Free Volume Measurements by Positron Annihilation Lifetime Spectroscopy (PALS)", Vol. 3, pp. 331–353.
- Jiang, L.Y., Chung, T.S. Rajagopalan, R. (2007), "Dual-layer Hollow Carbon Fiber Membranes for Gas Separation Consisting of Carbon and Mixed Matrix Layers", *Carbon*, Vol. 45, pp. 166–172.
- Jin, H., Lee, Y.S. and Hong, I. (2007), "Hydrogen Adsorption Characteristics of Activated Carbon", *Catalysis Today*, Vol. 120, pp. 399–406.
- Jomekian, A., Mansoori, S. A. A., Monirimanesh, N. and Shafiee, A. (2011), "Gas Transport Behavior of DMDCS Modified MCM-48/Polysulfone Mixed Matrix Membrane Coated by PDMS", *Korean Journal of Chemical Engineering*, Vol. 28, pp. 2069–2075.
- Jomekian, A., Pakizeh, M., Reza, A., Ali, S. and Mansoori, A. (2011), "Fabrication or Preparation and Characterization of New Modified MCM-41 /PSf Nanocomposite Membrane Coated by PDMS", *Separation and Purification Technology*, Vol. 80, pp. 556–565.
- Julian, H. and Wenten, I.G. (2012), "Polysulfone Membranes for CO₂/CH₄ Separation: State of the Art", *IOSR Journal of Engineering*, Vol. 2, pp. 484–495.
- Junaidi, M.U.M., Leo, C.P., Ahmad, A.L., Kamal, S.N.M. and Chew, T.L. (2014), "Carbon Dioxide Separation using Asymmetric Polysulfone Mixed Matrix Membranes Incorporated with SAPO-34 Zeolite", *Fuel Processing Technology*, Vol. 118, pp. 125–132.
- Khan, A. L., Cano-Odena, A., Gutiérrez, B., Minguillón, C. and Vankelecom, I. F. J. (2010), "Hydrogen Separation and Purification using Polysulfone Acrylate-Zeolite Mixed Matrix Membranes", *Journal of Membrane Science*, Vol. 350, pp. 340–346.

- Khanday, W.A., Marrakchi, F., Asif, M. and Hameed, B.H. (2017), "Mesoporous Zeolite–Activated Carbon Composite from Oil Palm Ash as An Effective Adsorbent for Methylene Blue", *Journal of the Taiwan Institute of Chemical Engineers*, Vol. 70, pp. 32–41.
- Kiadehi, A.D., Rahimpour, A., Jahanshahi, M. and Ghoreyshi, A.A. (2015), "Novel Carbon Nano-fibers (CNF) / Polysulfone (PSf) Mixed Matrix Membranes for Gas Separation", *Journal of Industrial and Engineering Chemistry*, Vol. 22, pp. 199–207.
- Kim, S., Chen, L., Johnson, J. K. and Marand, E. (2007), "Polysulfone and Functionalized Carbon Nanotube Mixed Matrix Membranes for Gas Separation : Theory and Experiment", Vol. 294, pp. 147–158.
- Kim, S., Marand, E., Ida, J. and Guliants, V.V. (2006), "Polysulfone and Mesoporous Molecular Sieve MCM-48 Mixed Matrix Membranes for Gas Separation", *Chemistry of Materials*, Vol. 18, pp. 1149–1155.
- Konwar, R.J. and De, M. (2013), "Effects of Synthesis Parameters on Zeolite Templated Carbon for Hydrogen Storage Application", *Microporous and Mesoporous Materials*, Vol. 175, pp. 16–24.
- Konwar, R.J. and De, M. (2015), "Development of Templated Carbon by Carbonisation of Sucrose-Zeolite Composite for Hydrogen Storage", *International Journal of Energy Research*, Vol. 39, pp. 223–233.
- Kusworo, T.D., Ismail, A.F. and Mustafa, A. (2013), "Studies of Thermal Annealing on Suppression of Plasticization of the Asymmetric Hollow Fiber Mixed Matrix Membranes", *World Applied Sciences Journal*, Vol. 28, pp. 9–19.
- Kyotani, T., Ma, Z., dan Tomita, A. (2003), "Template Synthesis of Novel Porous Carbons using Various Types of Zeolites", *Carbon*, Vol. 41, pp. 1451–1459.
- Laksmono, J.A., Sudibandriyo, M., Saputra, A.H. and Haryono, A. (2017), "Development of Porous Structured Polyvinyl Alcohol/Zeolite/Carbon Composites as Adsorbent", *Proceedings of 7th International Conference on Key Engineering Materials*, Penang, Malaysia.
- Lee, J., Chae, H., June, Y., Lee, K., Lee, C., Lee, H. H., Kim, I. and Lee, J. (2013), "Graphene Oxide Nanoplatelets Composite Membrane with Hydrophilic and Antifouling Properties for Wastewater Treatment", *Journal of Membrane Science*, Vol. 448, pp. 223–230.
- Li, Y., Chung, T.S., Cao, C. and Kulprathipanja, S. (2005), "The Effects of Polymer Chain Rigidification, Zeolite Pore Size and Pore Blockage on Polyethersulfone (PES)-Zeolite A Mixed Matrix Membranes", *Journal of Membrane Science*, Vol. 260, pp. 45–55.
- Kim, E.Y., Kim, H.S., Kim, D., Kim, J. and Lee, P.S. (2019), "Preparation of

- Mixed Matrix Membranes Containing ZIF-8 and UiO-66 for Multicomponent Light Gas Separation", *Crystals*, Vol. 9, pp. 15.
- Lin, R., Ge, L., Liu, S., Rudolph, V. and Zhu, Z. (2015), "Mixed-Matrix Membranes with Metal-Organic Framework-Decorated CNT Fillers for Efficient CO₂ Separation", *ACS Applied Materials and Interfaces*, Vol. 7, pp. 14750–14757.
- Ma, J., Si, C., Li, Y. and Li, R. (2012), "CO₂ Adsorption on Zeolite X / Activated Carbon Composites", *Adsorption*, Vol. 18, pp. 503–510.
- Ma, Z., Kyotani, T. and Tomita, A. (2000), "Preparation of a High Surface Area Microporous Carbon Having the Structural Regularity of Y Zeolite", *Chemical Communications*, Vol. 2000, pp. 2365–2366.
- Ma, Z., Kyotani, T., dan Tomita, A. (2002), "Synthesis Methods for Preparing Microporous Carbons with a Structural Regularity of Zeolite Y", *Carbon*, Vol. 40, pp. 2367–2374.
- Magueijo, V.M., Anderson, L.G., Fletcher, A.J. and Shilton, S.J. (2013), "Polysulfone Mixed Matrix Gas Separation Hollow Fibre Membranes Filled with Polymer and Carbon Xerogels", *Chemical Engineering Science*, Vol. 92, pp. 13–20.
- Mahajan, R. and Koros, W.J. (2000), "Factors Controlling Successful Formation of Mixed Matrix Gas Separation Materials", *Industrial & Engineering Chemistry Research*, Vol. 39, No. 8, pp. 2692–2696.
- Mahajan, R. and Koros, W.J. (2002a), "Mixed Matrix Membrane Materials with Glassy Polymers. Part 1", *Polymer Engineering & Science*, Vol. 42, No. 7, pp. 1420–1431.
- Mahajan, R. and Koros, W.J. (2002b), "Mixed Matrix Membrane Materials with Glassy Polymers. Part 2", *Polymer Engineering & Science*, Vol. 42, No. 7, pp. 1432–1441.
- Mahmoudi, E., Ng, L.Y., Ang, W.L., Chung, Y.T., Rohani, R. and Mohammad A.W. (2019), "Enhancing Morphology and Separation Performance of Polyamide 6,6 Membranes By Minimal Incorporation of Silver Decorated Graphene Oxide Nanoparticles", *Nature*, Vol. 9, pp. 1216.
- Marchese, J., Ochoa, N. and Pagliero, C. (1995), "Preparation and Gas Separation Performance of Silicone-Coated Polysulfone Membranes", *Journal of Chemical Technology & Biotechnology*, Vol. 63, pp. 329–336.
- Marosfoi, B. B., Szabó, A., Marosi, G., Tabuani, D., Camino, G. and Pagliari, S. (2006), "Thermal and Spectroscopic Characterization of Polypropylene-Carbon Nanotube Composites", *Journal of Thermal Analysis and Calorimetry*, Vol. 86, No. 3, pp. 669–673.

- Mirfendereski, S. M., Mazaheri, T., Sadrzadeh, M. and Mohammadi, T. (2008), "CO₂ and CH₄ Permeation Through T-type Zeolite Membranes: Effect of Synthesis Parameters and Feed Pressure", *Separation and Purification Technology*, Vol. 61, No. 3, pp. 317–323.
- Mohamad, M. B., Fong, Y. Y. and Shariff, A. (2016): Gas Separation of Carbon Dioxide from Methane Using Polysulfone Membrane Incorporated with Zeolite-T, *Procedia Engineering*, Vol. 148, pp. 621–629.
- Moon, J.S., Kim, H., Lee, D.C., Lee, J.T. and Yushin, G. (2015), "Increasing Capacitance of Zeolite-Templated Carbons in Electric Double Layer Capacitors", *Journal of the Electrochemical Society*, Vol. 162, No. 5, pp. A5070–A5076.
- Moore, T.T., Mahajan, R., Vu, D.Q. and Koros, W. J. (2004), "Hybrid Membrane Materials Comprising Organic Polymers with Rigid Dispersed Phases", *AIChE Journal*, Vol. 50, No. 2, pp. 311–321.
- Nejad, M. N., Asghari, M. and Afsari, M. (2016), "Investigation of Carbon Nanotubes in Mixed Matrix Membranes for Gas Separation: A Review", *ChemBioEng Reviews*, Vol. 3, No. 6, pp. 1–24.
- Nishihara, H., Hou, P. X., Li, L. X., Ito, M., Uchiyama, M., Kaburagi, T., Ikura, A., Katamura, J., Kawarada, T., Mizuuchi, K. and Kyotani, T. (2009), "High-Pressure Hydrogen Storage in Zeolite-Templated Carbon", *Journal of Physical Chemistry C*, Vol. 113, No. 8, pp. 3189–3196.
- Nishihara, H. and Kyotani, T. (2012), *Zeolite-Templated Carbon – Its Unique Characteristics and Applications*, Elsevier Ltd.
- Nishihara, H., Yang, Q.H, Hou, P.X, Unno, M., Yamauchi, S., Saito, R., Paredes, J.I., Martínez-Alonso, A., Tascón, J.M.D., Sato, Y., Terauchi, M. and Kyotani, T. (2008), "A Possible Buckybowl-like Structure of Zeolite Templated Carbon", Vol. 47, pp. 1220-1230.
- Nordin, N.A.H. M., Ismail, A.F., Misdan, N. and Nazri, N.A.M. (2017), "Modified ZIF-8 Mixed Matrix Membrane for CO₂/CH₄ Separation", *Proceeding of 2nd International Conference on Applied Science and Technology*, Eds : Nifa, F.A.A. et al., Kedah, Malaysia, hal. 0200911-0200916.
- Kayadoe, V. (2013), *Synthesis and Characterization of Zeolite-NaY Templated Carbon with Sucrose Precursor as Hydrogen Storage Material*, Master Thesis, Institut Teknologi Sepuluh Nopember, Surabaya, Indonesia.
- Perez, E.V., Balkus, K.J., Ferraris, J.P. and Musselman, I.H. (2009), "Mixed-Matrix Membranes Containing MOF-5 for Gas Separations", *Journal of Membrane Science*, Vol. 328, pp. 165–173.
- Ghosal, K., Chern, R.T. and Freeman, B.D. (1993), "Gas Permeability of Radel A

- Polysulfone", *Journal of Polymer Science : Part B : Polymer Physics*, Vol. 31, pp.891-893.
- Pesek, S. C. and Koros, W. J. (1993), "Aqueous Quenched Asymmetric Polysulfone Membranes Prepared by Dry / Wet Phase Separation", *Journal of Membrane Science*, Vol. 81, pp. 71–88.
- Pfromm, P.H., Pinnau, I. and Koros, W.J. (1993), "Gas Transport Through Integral-Asymmetric Membranes: A Comparison to Isotropic Film Transport Properties", *Journal of Applied Polymer Science*, Vol. 48, pp. 2161–2171.
- Ranjbaran, F., Omidkhah, M.R. and Ebadi Amooghin, A. (2015), "The Novel Elvaloy4170 / Functionalized Multi-Walled Carbon Nanotubes Mixed Matrix Membranes: Fabrication, Characterization and Gas Separation Study", *Journal of the Taiwan Institute of Chemical Engineers*, Vol. 49, pp. 220–228.
- Reid, B.D., Ruiz-Trevino, A., Musselman, I.H., Balkus, K.J. and Ferraris, J.P. (2001), "Gas Permeability Properties of Polysulfone Membranes Containing the Mesoporous Molecular Sieve MCM-41", *Chemistry of Materials*, Vol. 13, pp. 2366–2373.
- Reif, O.W. (2006), "Microfiltration Membranes: Characteristics and Manufacturing", *Advances in Biochemical Engineering/Biotechnology*, Vol. 98, pp. 73–103.
- Robeson, L.M. (2008), "The Upper Bound Revisited", *Journal of Membrane Science*, Vol. 320, pp. 390–400.
- Roland, C. M. (2014), *PES (Poly(ether sulfone)), Polysulfone*, Encyclopedia of Polymeric Nanomaterials, Springer-Verlag, Berlin.
- Roslan, R.A., Lau, W.J., Sakthivel, D.B., Khademi, S., Zulhairun, A.K., Goh, P.S., Ismail, A.F., Chong, K.C. and Lai, S.O. (2018), "Separation of CO₂/CH₄ and O₂/N₂ by Polysulfone Hollow Fiber Membranes: Effects of Membrane Support Properties and Surface Coating Materials", *Journal of Polymer Engineering*.
- Shao, W., Zhang, L., Li, L. and Lee, R.L. (2009), "Adsorption of CO₂ and N₂ on Synthesized NaY Zeolite at High Temperatures", *Adsorption*, Vol. 15, pp. 497–505.
- Shekhawat, D., Luebke, D.R. and Pennline, H.W. (2003), *A Review of Carbon Dioxide Selective Membranes*, A topical Report, National Energy Technology Laboratory, US Department of Energy, America.
- Shi, J., Li, W. and Li, D. (2015), "Rapidly Reversible Adsorption of Methane with A High Storage Capacity on the Zeolite Templated Carbons with Glucose as Carbon Precursors", *Colloids and Surfaces A: Physicochemical and Engineering Aspects*, Vol. 485, pp. 11–17.

- Sidek, N. M. and Nora, A. (2011), "Polysulfone Nanofiltration Membrane Separation Process Performance : Effect of Polymer Concentration", *Proceeding of 1st International Conference and Exhibition of Women Engineer*, University Malaysia Pahang, Malaysia.
- Song, X.H., Xu, R. and Wang, K. (2013), "The Structural Development of Zeolite-Templated Carbon under Pyrolysis", *Journal of Analytical and Applied Pyrolysis*, Vol. 100, pp. 153–157.
- Sridhar, S., Bee, S. and Bhargava, S.K. (2014), "Membrane-Based Gas Separation: Principle, Applications and Future Potential", *Chemical Engineering Digest*.
- Stadie, N.P., Vajo, J.J., Cumberland, R.W., Wilson, A.A., Ahn, C.C. and Fultz, B. (2012), "Zeolite-Templated Carbon Materials for High-Pressure Hydrogen Storage", *Langmuir*, Vol. 28, pp. 10057-10063.
- Stadie, N.P., Wang, S., Kravchyk, K.V. and Kovalenko, M.V. (2017), "Zeolite-Templated Carbon as an Ordered Microporous Electrode for Aluminum Batteries", *ACS Nano*, Vol. 11, pp. 1911–1919.
- Su, F., Zhao, X.S., Lv, L. and Zhou, Z. (2004), "Synthesis and Characterization of Microporous Carbons Templated by Ammonium-Form Zeolite Y", *Carbon*, Vol. 42, pp. 2821–2831.
- Suleman, M.S., Lau, K.K. and Yeong, Y.F. (2016), "Plasticization and Swelling in Polymeric Membranes in CO₂ Removal from Natural Gas", *Chemical Engineering & Technology*, Vol. 39, No. 9, pp. 1604-1616.
- Teoh, S.H., Tang, Z.G. and Hastings, G.W. (2016), "Thermoplastic Polymers In Biomedical Applications: Structures, Properties and Processing", in *Handbook of Biomaterial Properties*, eds. Murphy, W. et al., New York.
- Tian-ming, Z., Zhen, H., Xiao-hong, Z. and Li-ying, G.U.O. (2012), "Preparation and Characterization of AgA Zeolite/Polysulfone Membranes", Vol 549, pp. 401–405.
- Tirafferri, A. and Elimelech, M. (2012), "Preparation and Gas Permeation Properties of Silicone-Coated Dry Polyethersulfone Membranes", *Journal of Membrane Science*, Vol. 48, pp. 203-219.
- Vinoba, M., Bhagiyalakshmi, M., Alqaheem, Y., Alomair, A.A., Pérez, A. and Rana, M.S. (2017), "Recent Progress of Fillers in Mixed Matrix Membranes for CO₂ Separation: A Review", *Separation and Purification Technology*, Vol. 188, pp. 431–450.
- Vu, D.Q., Koros, W.J. and Miller, S.J. (2003), "Mixed Matrix Membranes using Carbon Molecular Sieves I. Preparation and Experimental Results, Vol. 211, pp. 311–334.

- Wahab, M.F.A., Ismail, A.F. and Shilton, S.J. (2012), "Studies on Gas Permeation Performance of Asymmetric Polysulfone Hollow Fiber Mixed Matrix Membranes using Nanosized Fumed Silica as Fillers", *Separation and Purification Technology*, Vol. 86, pp, 41–48.
- Wahab, M.F., Rahim, R.A. and Ismail, A.F. (2004), "Latest Development of Mixed Matrix Membrane using Glassy Polymer as Continuous Phase for Gas Separation", Membrane Research Unit, Universiti Teknologi Malaysia, Johor.
- Wang X., Wang, K., Plackowski, C.A. and Nguyen, A.V. (2016), "Sulfuric Acid Dissolution of 4A and Na-Y Synthetic Zeolites and Effects on Na-Y Surface and Particle Properties", *Applied Surface Science*, Vol. 367, pp. 281-290.
- Wang, D., Li, K. and Teo, W.K. (1995), "Relationship Between Mass Ratio of Nonsolvent-Additive to Solvent in Membrane Casting Solution and Its Coagulation Value", *Journal of Membrane Science*, Vol. 98, pp. 233–240.
- Wang, R., Liu, S.L., Lin, T.T. and Chung, T.S. (2002), "Characterization of Hollow Fiber Membranes in A Permeator using Binary Gas Mixtures", *Chemical Engineering Science*, Vol. 57, pp. 967–976.
- Weigelt, F., Georgopoulos, P., Shishatskiy, S., Filiz, V., Brinkmann, T. and Abetz, V. (2018), "Development and Characterization of Defect-Free Matrimid® Mixed-Matrix Membranes Containing Activated Carbon Particles for Gas Separation", *Polymers*, Vol. 10, No. 51.
- Weng, T., Tseng, H. and Wey, M. (2009), "Preparation and Characterization of Multi-Walled Carbon Nanotube / PBNPI Nanocomposite Membrane for H₂/CH₄ Separation, *International Journal of Hydrogen Energy*, Vol. 34, pp. 8707–8715.
- Wenten, I.G., Aryanti, P.T.P., Hakim, A.N. and Himma, N.F. (2016), "Advances in Polysulfone-Based Membranes for Hemodialysis - Review Paper, *Journal of Membrane Science and Research*, Vol. 2, pp. 78–89.
- Wijiyanti, R. (2015), *Adsorption-Desorption of Hydrogen on Zeolite-Y Templated Carbon Materials at Various of Temperature*, Undergraduate Thesis, Institut Teknologi Sepuluh Nopember, Surabaya.
- Wongcharee, S., Aravinthan, V. and Erdei, L. (2018), "Mesoporous Activated Carbon-Zeolite Composite Prepared From Waste Macadamia Nut Shell and Synthetic Faujasite, *Chinese Journal of Chemical Engineering*, Vol. 27, pp. 226-236.
- Yabushita, M., Techikawara, K., Kobayashi, H., Fukuoka, A. and Katz, A. (2016), "Zeolite-Templated Carbon Catalysts for Adsorption and Hydrolysis of Cellulose-Derived Long-Chain Glucans: Effect of Post-Synthetic Surface Functionalization", *ACS Sustainable Chemistry and Engineering*, Vol. 4, pp. 6844–6851.

- Yeo, Z.Y., Chew, T.L., Zhu, P.W., Mohamed, A.R. and Chai, S. (2012), Conventional Processes and Membrane Technology for Carbon Dioxide Removal from Natural Gas : A Review, *Journal of Natural Gas Chemistry*, Vol. 21, pp. 282–298.
- Yin, X., Chu, N., Yang, J., Wang, J. and Li, Z. (2013), "Thin Zeolite T / Carbon Composite Membranes Supported on the Porous Alumina Tubes for CO₂ Separation", *International Journal of Greenhouse Gas Control*, Vol. 15, pp. 55–64.
- Ying, L., Shung, T. and Kulprathipanja, S. (2006), "An Investigation to Revitalize The Separation Performance of Hollow Fibers With A Thin Mixed Matrix Composite Skin for Gas Separation", Vol. 276, pp. 113–125.
- Yoshimune, M. and Haraya, K. (2013a), "CO₂/CH₄ Mixed Gas Separation Using Carbon Hollow Fiber Membranes", *Energy Procedia*, Vol. 37, pp. 1109–1116.
- Zahri, K., Goh, P.S. and Ismail, A.F. (2016), "The Incorporation of Graphene Oxide Into Polysulfone Mixed Matrix Membrane for CO₂/CH₄ Separation", *Proceedings of International Conference on Chemical Engineering and Bioprocess Engineering*, Kinabalu, Malaysia, pp. 012007.
- Zahri, K., Wong, K.C., Goh, P.S. and Ismail, A.F. (2016), "Graphene Oxide/Polysulfone Hollow Fiber Mixed Matrix Membranes for Gas Separation", *RSC Advances*, Vol. 6, pp. 89130–89139.
- Zhang, L., Hu, Z. and Jiang, J. (2012), "Metal – Organic Framework / Polymer Mixed-Matrix Membranes for H₂/CO₂ Separation: A Fully Atomistic Simulation Study", *The Journal of Physical Chemistry C*, Vol. 116, pp. 19268-19277.
- Zhou, J., Li, W., Zhang, Z., Xing, W. and Zhuo, S. (2012), "Carbon Dioxide Adsorption Performance of N-Doped Zeolite Y Templated Carbons", *RSC Advances*, Vol. 2, pp. 161–167.
- Mintova, S and Barrier, N, (2016), *Verified Syntheses of Zeolitic Materials*, 3rd Edition, The Synthesis Commission of the International Zeolite Association, France.
- Zornoza, B., Esekile, O., Koros, W.J., Téllez, C. and Coronas, J. (2011), "Hollow Silicalite-1 Sphere-Polymer Mixed Matrix Membranes for Gas Separation, *Separation and Purification Technology*, Vol. 77, pp. 137–145.
- Zornoza, B., Irusta, S., Téllez, C. and Coronas, J. (2009), "Mesoporous Silica Sphere-Polysulfone Mixed Matrix Membranes for Gas Separation", *Langmuir*, Vol. 25, pp. 5903–5909.
- Zornoza, B., Téllez, C. and Coronas, J. (2011), "Mixed Matrix Membranes Comprising Glassy Polymers and Dispersed Mesoporous Silica Spheres for

- Gas Separation", *Journal of Membrane Science*, Vol. 368, pp. 100–109.
- Zulhairun, A.K., Fachrurrazi, Z.G., Nur Izwanne, M. and Ismail, A. F. (2015), "Asymmetric Hollow Fiber Membrane Coated With Polydimethylsiloxane-Metal Organic Framework Hybrid Layer for Gas Separation", *Separation and Purification Technology*, Vol. 146, pp. 85–93.
- Zulhairun, A.K. and Ismail, A.F. (2014), "The Role of Layered Silicate Loadings and Their Dispersion States on The Gas Separation Performance of Mixed Matrix Membrane", *Journal of Membrane Science*, Vol. 468, pp. 20–30.
- Zulhairun, A.K., Ismail, A.F., Matsuura, T., Abdullah, M.S. and Mustafa, A. (2014), "Asymmetric Mixed Matrix Membrane Incorporating Organically Modified Clay Particle for Gas Separation", *Chemical Engineering Journal*, Vol. 241, pp. 495–503.
- Zulhairun, A.K., Ng, B.C., Ismail, A.F., Surya Murali, R. and Abdullah, M.S. (2014), "Production of Mixed Matrix Hollow Fiber Membrane for CO₂/CH₄ Separation", *Separation and Purification Technology*, Vol. 137, pp. 1–12.
- Zulhairun, A.K., Subramaniam, M.N., Samavati, A., Ramli, M.K.N., Krishparao, M., Goh, P.S. and Ismail, A. F. (2017), "High-Flux Polysulfone Mixed Matrix Hollow Fiber Membrane Incorporating Mesoporous Titania Nanotubes for Gas Separation", *Separation and Purification Technology*, Vol. 180, pp. 13–22.

PUBLICATIONS

Journal

1. **R. Wijiyanti**, A.N. Ubaidillah, T. Gunawan, Z.A. Karim, A.F. Ismail, S. Smart, R. Lin and N. Widiastuti, Polysulfone mixed matrix hollow fiber membranes using zeolite templated carbon as a performance enhancement filler for gas separation, *Chemical Engineering Research and Design*, Vol. 150, pp. 274-288 (2019).
2. **R. Wijiyanti**, A.R.K. Wardhani, R.A. Roslan, T. Gunawan, Z.A. Karim, A.F. Ismail and N. Widiastuti, Enhanced gas separation performance of polysulfone membrane by incorporation of zeolite templated carbon, *Malaysian Journal of Fundamental and Applied Sciences*, Vol. 16, No. 2, (2020).
3. **R. Wijiyanti**, T. Gunawan, N.S. Nasri, Z.A. Karim, A.F. Ismail and N. Widiastuti, Hydrogen adsorption characteristics for zeolite-Y templated carbon, *Indonesian Journal of Chemistry*, **In Press**.
4. T. Gunawan, R.P. Rahayu, **R. Wijiyanti**, W.N.W. Salleh and N. Widiastuti, P84/zeolite carbon composite mixed matrix membrane for CO₂/CH₄ separation, *Indonesian Journal of Chemistry*, Vol. 19, No. 3, pp. 650-659 (2019).
5. T. Gunawan, T.Q. Romadiansyah, **R. Wijiyanti**, W.N.W. Salleh and N. Widiastuti, Zeolite templated carbon : preparation, characterization and performance as filler material in co-polyimide membranes for CO₂/CH₄ separation, *Malaysian Journal of Fundamental and Applied Sciences*, Vol. 15, No. 3, pp. 407-413 (2019).
6. T. Gunawan, **R. Wijiyanti** and N. Widiastuti, Adsorption-desorption of CO₂ on zeolite-Y templated carbon at various temperatures, *RSC Advances*, Vol. 8, pp. 41594-41602 (2019).
7. Z.S. Larasti, **R. Wijiyanti**, Z.A. Karim, A.F. Ismail and N. Widiastuti, Fabrication of Mixed Matrix Membrane Polysulfone-Zeolite Carbon Composites (ZCC) for Gas Separation, Vol. 546, *IOP Conference Series: Materials Science and Engineering*, Vol. 546, 042020 (2019).

BOOK CHAPTER

A.K. Zulhairun, **Rika Wijiyanti**, Nurul Widiastuti, P.S. Goh and A.F. Ismail, Prospect of nanocomposite membranes for natural gas treatment, Edited by M. Sadrzadeh and T. Mohammad, Elsevier Science, Published on 1st November 2019.

CONFERENCES

1. **R. Wijiyanti**, U. Anggarini, W.P. Utomo, H. Fansuri and N. Widiastuti, Adsorption-desorption of hydrogen on zeolite-Y templated carbon materials at various of temperature, The 3rd Euro-Asia Zeolite Conference, Bali Indonesia, 22-25 January 2017.
2. **R. Wijiyanti**, Z.A. Karim and N. Widiastuti, Fabrication of polysulfone hollow fiber mixed matrix membranes using zeolite templated carbon as filler for gas separation, 6th International Conference on Engineering and Innovative Materials, 3-5 September 2017.
3. **R. Wijiyanti**, A.N. Ubaidillah, T. Gunawan, Z.A. Karim, A.F. Ismail and N. Widiastuti, Polysulfone mixed matrix hollow fiber membranes using zeolite templated carbon as performance enhancement filler for gas separation, The 11th Conference of the Aseanian Membrane Society, Brisbane, Queensland, Australia, 3-6 July 2018.
4. **R. Wijiyanti**, A.R.K. Wardhani, R.A. Roslan, T. Gunawan, Z.A. Karim, A.F. Ismail and N. Widiastuti, Enhanced gas separation performance of polysulfone membrane by incorporation of zeolite templated carbon, National Congress on Membrane Technology, Johor Bahru, Malaysia, 30-31 October 2018.
5. **R. Wijiyanti**, T. Gunawan, Z.A. Karim, A.F. Ismail and N. Widiastuti, Preparation, characterization and performance of zeolite templated carbon as filler in polysulfone membrane, Membrane Science & Technology, Singapore, 13-14 Juni 2019.

